ΕΘΝΙΚΟ ΜΕΤΣΟΒΙΟ ΠΟΛΥΤΕΧΝΕΙΟ

ΣΧΟΛΗ ΠΟΛΙΤΙΚΩΝ ΜΗΧΑΝΙΚΩΝ

ΕΡΓΑΣΤΗΡΙΟ ΣΤΑΤΙΚΗΣ & ΑΝΤΙΣΕΙΣΜΙΚΩΝ ΕΡΕΥΝΩΝ

ΥΣΤΕΡΗΤΙΚΑ ΠΕΠΕΡΑΣΜΕΝΑ ΣΤΟΙΧΕΙΑ ΚΑΙ ΜΑΚΡΟΣΤΟΙΧΕΙΑ ΓΙΑ ΤΗ ΜΗ ΓΡΑΜΜΙΚΗ ΔΥΝΑΜΙΚΗ ΑΝΑΛΥΣΗ ΤΩΝ ΚΑΤΑΣΚΕΥΩΝ

HYSTERETIC FINITE ELEMENTS AND MACRO-ELEMENTS FOR NONLINEAR DYNAMIC ANALYSIS OF STRUCTURES

ΔΙΔΑΚΤΟΡΙΚΗ ΔΙΑΤΡΙΒΗ

για τον Επιστημονικό Τίτλο του Διδάκτορα Μηχανικού υποβληθείσα στη Σχολή Πολιτικών Μηχανικών του Εθνικού Μετσόβιου Πολυτεχνείου

ΣΑΒΒΑ Π. ΤΡΙΑΝΤΑΦΥΛΛΟΥ

Διπλωματούχου Πολιτικού Μηχανικού Ε.Μ.Π.

ΑΘΗΝΑ 2011

This doctoral thesis was financially supported by the National Technical University of Athens

To my parents…

It is through science that we prove, but through intuition that we discover.

Henri Poincare

Abstract

Hysteretic Finite Elements and Macro-Elements for Nonlinear Dynamic Analysis of Structures

By Savvas P. Triantafyllou

National Technical University of Athens

School of Civil Engineering

Institute of Structural Analysis and Aseismic Research

A problem of significant importance in structural engineering deals with the response of elastoplastic structures subjected to either static or dynamic loading. This dissertation focuses on the derivation of computational tools that facilitate both the development and the application of nonlinear solution methods. Attention is drawn on the definition of a generalized hysteretic model that accounts for any type of yield function and kinematic hardening rule. This is accomplished on the basis of the classical plasticity theory and the mathematical theory of hysteresis.

Based on the phenomenological approach of classical plasticity the relations derived in stress space are projected onto the stress-resultant space. Within this framework, a novel three dimensional truss element that also accounts for geometrical nonlinear effects is presented. Additionally, a novel three-dimensional hysteretic Timoshenko beam element with torsional

warping is derived. These elements are macro-elements in the sense that the corresponding constitutive relations are defined in terms of stress resultants and generalized deformation measures. Moreover, a generic procedure for the derivation of finite elements is presented. The stiffness matrix of the generic element is established as a smooth function of the current stress state through the proposed Bouc-Wen formulation.

The classical second order solution schemes, namely the central difference method and the Newmark family of solvers are reformulated to account for the hysteretic equations in rate form. Moreover, the state-space approach is implemented for the solution of the equations of motion. A predictor corrector differential solver is used which demonstrates certain advantages when stiff problems are accounted for. Finally, a formulation of the equations of motion is proposed, that renders computational advantages compared to standard solution schemes, since the state matrices of the structure are evaluated only once in the beginning of the analysis and remain constant throughout the analysis procedure.

A general purpose finite element code is developed that accounts for the hysteretic finite elements and macro-elements as well as the solution procedures introduced in this work. The proposed formulations are verified through illustrative examples that demonstrate the validity and accuracy of the proposed formulations. Furthermore, the advantages of the proposed set of elements are examined in terms of accuracy and computational cost as compared to standard nonlinear FEM derivations adopted both in academic and commercial source codes.

CONTENTS

LIST OF FIGURES

LIST OF TABLES

ACKNOWLEDGEMENTS

I wish to express my most sincere gratitude to my advisor, Professor Vlasis Koumousis, for his continued guidance and support throughout the course of this research. His formidable reach and outstanding scholarship have been a constant source of motivation. His contribution extends beyond his academic role and for this I will be grateful for all my life.

I would also like to thank Professor Manolis Papadrakakis and Associate Professor Charis Gantes for serving on my doctoral committee and for contributing valuable insight to my thesis work both through their individual comments and their lessons taught at the Department of Civil Engineering of the National Technical University of Athens. Special thanks are also due to Professor George Gazetas, Associate Professor Vasilleios Panoskaltsis, Associate Professor Kostas Spiliopoulos and Associate Professor Panos Tsopelas for serving on the defense committee of my dissertation. Their individual comments essentially improved this dissertation and their support is much appreciated.

Many thanks to the research group, namely Myrtw Manola, Nikolaos Peppas, Aristotelis Charalampakis and Christos Dimou for all the comments provided throughout the course of my PhD.

This work was accomplished through the financial support from the National Technical University of Athens. This support is greatly acknowledged.

Special thanks are due to the “family” Eleni and Manolis Chatzis. There is a certain amount of disputing, controverting and partying involved in this acknowledgement I will carry along in the years to come. My sincere gratitude goes to the “Tuesday Club” for releasing the pressure when the pressure kept building up and for letting me realize that flight is impossible unless there is a crane involved in the argument. I would also like to thank my special friends, Lena, Kostis and Spyros for constantly reminding me that limits are there only to be surpassed. In their terminology, the ultimo will never come. My sincere gratitude goes

to my schoolmates EF, GT, GT, GH, PO, DP, DS, (aka, the “Zanneio Club”) that have been near me for nearly half my life.

I wish to express my gratitude to my late friend and co-worker Panos Dimizas who urged me to enroll as PhD student. His academic qualities will always be an example for me.

To the very special person in my life, my companion Eleni, I will always be grateful for her love, support and patience and the mere fact that she always stood by my side in times of total “PhD disorder”.

Most of all, I would like to thank my parents Eleni and Pavlos. This work would not have been accomplished without their selfless support, continuous encouragement and personal sacrifices, throughout my life.

Chapter 1

INTRODUCTION

1.1 Background and motivation

A problem of significant importance in structural engineering deals with the response of elastoplastic structures subjected to either static or dynamic loading. For load factored linear elastic analysis, predominantly suggested by the codes, the results are acceptable, but do not reveal the characteristics of the true behaviour of the structure. If inelastic response is taken into account, more refined models are needed to achieve a realistic behaviour. In recent years, significant research has been carried out in order to overcome the difficulties arising in such an analysis. Difficulties emanate not only from the inherent complexity of structures, but also from the uncertainties related to terms such as dynamical loading, material nonlinearity and hysteresis.

Modern design codes such as the Greek pre-norm for the Seismic Retrofit of existing buildings (ΟΑΣΠ, 2010 in Greek), the European norm for the design of structures for earthquake resistance (EN, 1998) and the ASCE standard for the Seismic Rehabilitation of Existing Buildings (ASCE, 2007) offer specific guidelines for the evaluation of the nonlinear properties of structural components and the estimation of the nonlinear structural response. Concepts such as the displacement based design and the performance based design are therefore essential in the estimation of structural integrity (Priestley et al., 2007, Fardis, 2010).

On practice, nonlinear static analysis is favoured as opposed to the nonlinear dynamic analysis procedure due to the inherent complexity of the dynamic behaviour of structures and the severe computational cost of the dynamic analysis numerical schemes. Nevertheless, the advantages of a nonlinear dynamic analysis as opposed to a nonlinear static analysis are well documented (Bozorgnia and Bertero, 2004).

Another significant drawback of the nonlinear dynamic analysis is the vast amount of output data needed to be processed in order to evaluate the necessary design quantities. Eurocode 8 explicitly states that *"The number of the accelerograms to be used shall be such as to give a stable statistical measure (mean and variance) of the response quantities of interest. The amplitude and the frequency content of the accelerograms shall be chosen such that their use results in an overall level of reliability commensurate with that implied by the use of the elastic response spectrum of 4.2.2"*. Recent advantages in this area have also been documented such as the IDA method (Vamvatsikos D. and Cornell C.A., 2004).

Nonlinearities in a structural system can have a profound effect on its transient structural response. Trusses usually have higher natural frequencies compared to relevant solid structures, because of their high stiffness-to-mass ratio. The nonlinearity of trusses under dynamic loading can stem from various origins: (i) geometrical-due to the variations in the geometrical properties of the structure as the load progresses; (ii) material-due to the inherent nonlinear behaviour of the materials under load; (iii) inertia-depending on the dynamic motion and the structural deformations; and (iv) damping depending on the structural joints and material.

In structures with non-symmetric plan configuration, structural members such as columns and walls may undergo severe torsional deformation. Existing beam element formulations tend to underestimate the importance of such deformations in the nonlinear regime.

Thus, sophisticated models are needed such as fibre beam element models or surface finite element models in order to accurately account for such behaviour. In this context, various beam elements have been proposed either displacement based (Bathe, 2007) or force based, (Sivaselvan and Reinhorn, 2003). Material nonlinearity is introduced at the section level, either macroscopically through a plastic-hinge approach (Gerolymos and Gazetas, 2005, Mazza and Mazza, 2010) or through a fibre-based formulation at the element level (Saritas

and Filippou, 2009, Papachristidis et al., 2010). In the latter, the Timoshenko beam theory is implemented within the framework of a force based distributed plasticity formulation.

Although more accurate, the fibre based formulation comes at the cost of requiring numerical integrations at the section level. At least three points of integration are needed to achieve a linear distribution of the curvature along the element's length with the most efficient Lobatto rule (Sivaselvan and Reinhorn, 2003). Thus, in a time marching-process as a nonlinear dynamic analysis, the computational advantage of concentrated plasticity, displacement based schemes remains significant.

The Timoshenko beam theory has not been addressed in such problems, mainly due to the shear locking problem (Rakowski, 1990, Stolarski & Belytschko, 1983) of the displacement based isoparametric formulation that can lead to inaccurate results both in the linear and nonlinear case. The Timoshenko beam theory leads to increased structural displacements. This increase can be even greater under dynamical excitation since the dynamic characteristics of the structure are altered. Such deviations from the standard Euler based approach can have significant influence on the displacement based design of structures (Eurocode 8, Part 3). In structural members that are subjected to high shear forces, as in shear links of eccentrically braced frames (Kasai and Popov,1986), shear effects are very important both in the elastic and inelastic regime.

Dissipation phenomena are of the utmost importance when studying the dynamic behavior of nonlinear systems. As such, hysteretic damping needs to be addressed directly by incorporating a hysteretic rule to model the cyclic response of the structure. A great number of hysteretic models have been proposed for different kind of materials and/ or structural components. Hysteretic models are either multilinear or smooth. Multilinear hysteretic models are defined as a set of linear segments together with a set of hysteretic rules to account for the various cyclic induced hysteretic phenomena, such as stiffness degradation, strength

deterioration and pinching (Reinhorn and Sivaselvan, 2000, Naeim et al, 2000). Different models exist depending on the material and the structural component such as the Takeda model (Takeda et al., 1970), the Q-hyst model (Saidi and Sozen, 1979) and the Roufaiel and Meyer model (Roufaiel and Meyer, 1987). A thorough presentation of multilinear models can be found on Fardis et al. (1996). It is important to mention that the set of rules accompanying each multilinear hysteretic model is based on observations made upon specific materials and concern force-displacement relations. Thus, a generalization of such models either on the stress-strain regime or in different materials is neither easy nor suggested.

Smooth models are defined as a set of nonlinear equations often expressed in rate form. Stiffness degradation and strength deterioration are also implemented in the form of additional rate equations. This allows for the simulation of all the available hysteretic behaviours with a single smooth model, the parameters of which are varying, to match the desired behaviour. Such smooth models are the Dahl model of hysteresis (Dahl, 1978), the Preishach family of hysteretic models (Visintin, 2003) the Kuhn model of hysteresis |(Papoulia et al., 2007) and the Bouc-Wen family of hysteretic models. The Bouc model of hysteresis was first introduced in Bouc, 1967 followed by several modifications introduced, such as the Bouc-Wen model, (Wen et al. 1976), the Baber-Noori model, (Baber et. al., 1985) and the Reinhorn model (Sivaselvan & Reinhorn, 2000). The advantages of the Bouc-Wen model as compared to other smooth rate independent hysteretic models, either smooth such as the Ozdemir model (Ozdemir, 1976) and the Ramberg–Osgood model (Ramberg and Osgood 1943) have been extensively commented in the literature (Ismail et al., 2010).

A trend, not only in the seismic retrofit of existing buildings but also on the design of new ones, is the implementation of either active, semi-active or passive seismic isolation components. Devices such as, magneto-rheological dampers (Bitaraf et al., 2010), friction devices (Mokha et al., 1991), buckling-restrained braces (Black et al., 2004) demonstrate a

well-defined and distinct hysteretic behaviour. The Bouc-Wen model has been frequently to simulation the hysteretic response of such devices as in Tsopelaset al., 2009. Shape memory alloys have been examined as a means of retrofitting damaged steel connections (DesRoches et al., 2001, Panoskaltsis et al., 2004, Auricchio et al. 2008). Such materials also demonstrate an interesting hysteretic behaviour.

So far, considerable effort has been made in introducing the Bouc-Wen model into the inelastic analysis of skeletal structures and joint behaviour, (Foliente, 1995). In Guggenberger and Grundmann, 2005, a force based concentrated plasticity beam element is derived, within the framework of Euler assumption, that accounts only for plastic bending deformations. Symeonov et al. (2000), introduce an Euler, force based, element formulation were interaction between the axial force and the bending moment is considered. This formulation leads to a non-constant flexibility matrix which depends on both the moment and the curvature of a given cross section. Although exact, especially in the case of members of variable cross sections, this approach leads to an increased computational cost due to the fact that state matrices do not remain constant and need updating, as the solution evolves. Though considerable effort has been made into introducing the Bouc-Wen model into the inelastic analysis of skeletal structures and joint behavior little has been done towards the development of surface and three-dimensional elements. This is also the case for soil-structure interaction problems, where efforts by Gerolymos and Gazetas, (2006, 2007), concentrated towards the proper use of the one dimensional Bouc-Wen model.

1.2 Research objectives

The prime objective of this research work is the description of the hysteretic response of materials and structural components within a unified and theoretically sound framework. The specific research objectives are:

- To accurately describe the hysteresis phenomenon based on both, the mathematical theory of hysteresis and a sound phenomenological background as the classical theory of plasticity
- To enhance the existing hysteretic models so as to simulate the majority of the observed hysteretic behaviors
- To introduce this hysteretic formulation into the finite element scheme, thus enhancing its applicability
- To derive simple but accurate macro-elements that account for the nonlinear hysteretic behavior of skeletal structures. The effect of geometrical nonlinearities on the hysteretic response of skeletal structures is also considered
- To examine whether the existing numerical procedures of nonlinear dynamic analysis are enhanced, in terms of computational cost, through the application of numerical solvers appropriate for the solution of stiff mathematical problems

1.3 Organization of the dissertation

This dissertation is organized as follows. In Chapter 2, the basic concepts of the theory of classical plasticity are presented. Attention is drawn to the phenomenological nature of classical plasticity. This chapter serves as a point of reference for subsequent chapters.

Chapter 3 describes the theory of smooth hysteretic operators. Commencing from the mathematical theory of hysteresis, the initial uniaxial formulation of the Bouc-Wen model is presented. Based on the governing equations of classical plasticity, a novel derivation of the Bouc-Wen model in tensorial form is presented that accounts for any combination of yield function and hardening law. By introducing appropriate operators, stiffness degradation and strength deterioration are also implemented in the proposed hysteretic model.

Chapter 4 deals with the concept of macro-modeling. Based on the phenomenological approach of classical plasticity the relations derived in stress space are projected onto the stress-resultant space. Within this framework, a novel 3 dimensional truss element that also accounts for geometrical nonlinear effects is presented. Additionally, a novel three-dimensional hysteretic Timoshenko beam element with torsional warping is derived. Simplified examples are presented to demonstrate the validity of the proposed formulations. To facilitate and clarify the presentation certain aspects of the solution approach implemented in this work are also presented.

In Chapter 5 a generic procedure for the derivation of finite elements is presented. The stiffness matrix of the generic element is established as a smooth and continuous function of the current stress state through the proposed Bouc-Wen formulation. As an example, the triangular constant strain triangle formulation is presented and the validity of the method is established through benchmark tests.

In Chapter 6 the solutions methods implemented in the present work are presented. The classical second order solution schemes, namely the central difference method and the Newmark family of solvers are reformulated to account for the hysteretic equations in rate form. Additionally, the state-space approach in the solution of the equations of motion is presented, that is adopted for the solution of the governing equations, since it is prone to certain advantages when stiff problems are accounted for. Furthermore, a formulation of the equations of motion is proposed, that renders computational advantages compared to standard solution schemes, since the state matrices of the structure are evaluated only once in the beginning of the analysis and remain constant throughout the analysis procedure.

In Chapter 7, examples are presented that demonstrate the validity and accuracy of the proposed formulations. Furthermore, the advantages of the proposed set of elements are

examined in terms of accuracy and computational cost as compared to standard nonlinear FEM derivations.

In Chapter 8 the conclusions drawn in this work are summarized. Some important results obtained are highlighted while at the same time the necessary areas requiring some further investigation are identified.

Chapter 2

CONTINUUM MECHANICS AND CLASSICAL PLASTICITY

2.1 Introduction

In this chapter, the fundamental concepts of continuum mechanics and classical plasticity are briefly presented, to form the basis of the subsequent analysis. At first, the notion of a material body is strictly defined and the associated compatibility conditions are stated. Next, the strain and stress measures used throughout this work are defined.

Finally, the theory of classical plasticity is briefly discussed, by stating its main principles, namely the additive decomposition of the strain rates, the flow rule, the normality assumption and the hardening law. In addition, specific yield functions and hardening laws are presented, that are going to be used in the examples of the subsequent chapters.

2.1.1 Basic concepts of continuum mechanics

In this work, presentation is limited to the three-dimensional Euclidean space. Within this framework, a simple body $B \subset R^3$ is formally described as an open set of continuously distributed material points P that span a region within the Euclidean space (Marsden and Hughes, 1994). Each point is uniquely defined by a set of Cartesian coordinates denoted herein as $\{X\} = \{X_1 \quad X_2 \quad X_3\}^T$. Under the influence of an arbitrary force, B translates, rotates and deforms. If t_0 is the time instant at which B is considered undeformed, then for each $t_i > t_0, i = 1,..n$ a series of deformed states or configurations of B are defined, denoted herein as C^i. A motion of the body is a one to one mapping $\phi : B \rightarrow R^3$ that maps B from the initial configuration C^0 to the current configuration C^i. Thus, for every time instance $t_i > t_0$:

$$\{x\}^i = \phi^i(\{X\}, t_i) \tag{2.1}$$

where $\{x\}^i = \{x_1 \quad x_2 \quad x_3\}^T$ is the position vector of the point $\{X\}$ at the configuration C^i.

Accordingly, the displacement vector is defined as the difference of the position vectors at each configuration thus:

$$\{u\}^i = \phi^i(\{X\},t) - \{X\} = \{x\}^i - \{X\} \tag{2.2}$$

The deformation gradient of the current configuration C^i is defined by differentiating equation (2.1) at a specific $t_i > t_0$:

$$\{dx\}^i = d\phi^i(\{X\},t_i)\{dX\} \Rightarrow [F^i] = Grad\left(\phi^i(\{X\},t_i)\right) = \frac{\{dx\}^i}{\{dX\}} \tag{2.3}$$

Replacing equation (2.1) into (2.3) the deformation gradient assumes the following form:

$$[F^i] = \begin{bmatrix} x_{1,1} & x_{1,2} & x_{1,3} \\ x_{2,1} & x_{2,2} & x_{2,3} \\ x_{3,1} & x_{3,2} & x_{3,3} \end{bmatrix} \tag{2.4}$$

with $J = \det F > 0$ (Lubliner, 2008). The deformation gradient is defined with respect to the displacement vector by substituting relation (2.2) into relation (2.3) yielding:

$$[F^i] = Grad\left(\{X\} + \{u\}^i\right) = [I] + [\Omega] \tag{2.5}$$

where $[\Omega] = Grad\left(\{u\}^i\right)$ is the displacement gradient.

2.1.2 Strain measures and accompanying stress measures

In this work, the Green-Lagrange strain measure is introduced that is commonly implemented in engineering applications (Zienkiewicz and Taylor, 2005). The Green-Lagrange strain tensor is defined by the following relation:

$$\left[E\right]=\frac{1}{2}\left(\left[F\right]^{T}\left[F\right]-\left[I\right]\right) \tag{2.6}$$

where the product $\left[F\right]^{T}\left[F\right]$ is referred to as the right Cauchy-Green tensor. Replacing equation (2.5) into relation (2.6) the strain tensor is evaluated with respect to the displacement gradient:

$$\left[E\right]=\frac{1}{2}\left(\left[\Omega\right]+\left[\Omega\right]^{T}+\left[\Omega\right]^{T}\left[\Omega\right]\right) \tag{2.7}$$

or, expressed in component form:

$$E_{IJ}^{i}=\frac{1}{2}\left(\frac{\partial u_{I}}{\partial X_{J}}+\frac{\partial u_{J}}{\partial X_{I}}+\frac{\partial u_{M}}{\partial X_{I}}\frac{\partial u_{M}}{\partial X_{J}}\right),I,J=1..3 \tag{2.8}$$

where the Einstein convention of summation is implemented. The Green-Lagrange strain tensor thus consists of two parts. The linear part coincides with the small strain approximation strain tensor:

$$e_{IJ}=\frac{1}{2}\left(\frac{\partial u_{I}}{\partial X_{J}}+\frac{\partial u_{J}}{\partial X_{I}}\right),\ I,J=1..3 \tag{2.9}$$

while the nonlinear part is given by the following relation:

$$\eta_{IJ}=\frac{1}{2}\left(\frac{\partial u_{M}}{\partial X_{I}}\frac{\partial u_{M}}{\partial X_{J}}\right),\ I,J=1,..3 \tag{2.10}$$

It is proved through proper manipulation of the energy conservation laws (Belytschko et al., 2000) that the energy conjugate stress measure of the Green-Lagrange strain tensor is the second Piola-Kirchhoff stress tensor defined as:

$$\left[S\right]^{i}=J\left[F\right]^{-1}\left[\sigma\right]^{i}\left[F\right]^{-T} \tag{2.11}$$

which refers to the area of the initial configuration, while $\left[\sigma\right]$ is the Cauchy stress or true stress that refers to the area of the current configuration.

To this point, the tensorial notation has been implemented for the derivation of the stress and strains relations. In the derivation of finite elements, the matrix notation of the stress and strain tensors is preferred since it leads to compact relations (Zienkiewicz and Taylor, 2005). In this work, the matrix notation is adopted, thus the stress and strain tensors are arranged in the following vectorial form:

$$\left\{S\right\} = \left\{S_{11} \quad S_{22} \quad S_{33} \quad S_{12} \quad S_{23} \quad S_{31}\right\}^T \tag{2.12}$$

and

$$\left\{E\right\} = \left\{E_{11} \quad E_{22} \quad E_{33} \quad 2E_{12} \quad 2E_{23} \quad 2E_{31}\right\}^T \tag{2.13}$$

If the small displacement assumption is adopted, then the nonlinear term of relation (2.10) becomes significantly smaller than unity and is therefore omitted from the definition of the strain. Furthermore, to comply with standard FEM nomenclature, when reference is made to the special case of small displacements the stress and strain tensors will be denoted as $\left\{\sigma\right\}$ and $\left\{\varepsilon\right\}$ respectively, (Cook et al., 2002).

2.2 Sources of nonlinearities in structures

2.2.1 Geometric nonlinearities

The concept of geometric-nonlinearity is directly related but not limited to the definition of the strain measure described in section 2.1.1. By considering the nonlinear strain-displacement equations (2.7) the equilibrium and constitutive equations of the continuum are formulated taking into account the change in shape (or volume) of the material body. Such

changes affect the distribution of stresses through the material volume (Marsden and Hughes, 1994). Phenomena that are also treated as geometric nonlinearities are:

- Large displacement and large strain behaviors, met in foam and rubber like materials
- Time or load varying boundary conditions
- Non-conservative loading, i.e. direction varying loading
- Contact problems

For an exhaustive description on the subject the reader is referred to Wriggers, 2008. The analysis presented in this work is mainly referred to the case of small displacements and strains. However some formulations, namely the derivation of the hysteretic truss element and the hysteretic Euler beam element, are extended to the large displacement regime proving that the extension to the large displacement regime is straightforward, though not trivial.

2.2.2 Material nonlinearities

The theory of linear elasticity is a simplified approximation, valid within a certain level of load intensity. Beyond that level, materials demonstrate a non-linear behavior that is mathematically expressed through a nonlinear stress-strain constitutive equation. Material nonlinearity is a generic term that embodies various phenomena i.e.

- Non-linear elasticity
- Rate-Independent plasticity
- Thermo-plasticity
- Rate-dependent plasticity or visco-plasticity
- Nonliner creep

In this work, the nonlinear behavior of materials under dynamic excitation is examined within the frame-work of rate-independent plasticity. Numerous experiments on structural

members such as wood joints (Foliente, 1995), steel members (Popov and Stephen, 1970) or R/C piers have demonstrated that the hysteretic energy accumulated due to irreversible plastic deformations is rate-independent.

2.3 Concepts of plasticity theory

2.3.1 A phenomenological approach to material behavior

The mathematical theory of plasticity (Hill 1998, Kachanov 2004) is based on the mere observation that materials tend to demonstrate some common behavioral properties in spite of their different actual responses. This statement has been verified with numerous experimental results on materials as diverge as metals and soils (Hill, 1998).

These common material properties can be summarized as follows:

I. There exists an elastic domain within which any deformation imposed onto the material is purely reversible.

II. If this domain of behavior is surpassed then the material undergoes permanent deformations. These deformations are called plastic and the material behavior is considered as that of a flow.

III. Under consecutive cycles of loading unloading and reloading past the elastic domain the material exhibit a hardening or softening behavior. That is, the rate of accumulation of plastic deformations tends to decrease or increase cycle after cycle.

The observations described above give rise to the three main principles of the small strain theory of plasticity that is the additive decomposition of the strain rate, the existence of a yield surface and the establishment of a hardening rule. Within this framework, and on the basis of the theory of continuum mechanics (Irgens, 2008, Reddy, 2008) a series of mathematical tools have been developed that adequately describe the inelastic material

behavior that is macroscopically observed without having to describe the microscopic mechanisms (crystal structure etc.) that give rise to such macroscopic behavior. A brief introduction on the concepts of micro-plasticity can be found in Dunne and Petrinic, 2005.

2.3.2 The classical theory of plasticity

The small strain classical plasticity theory is based on the following set of governing equations, stemming from three principles described in the previous paragraph.

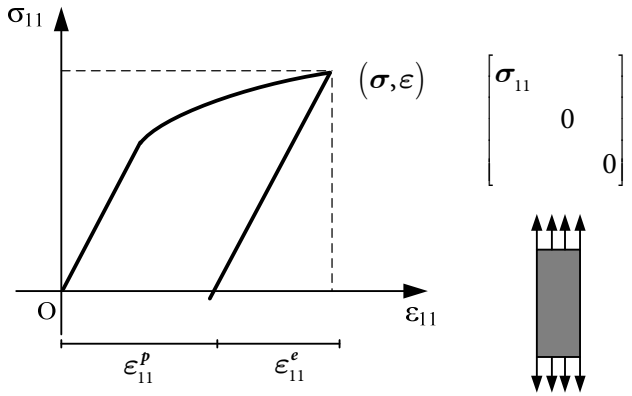

Fig.2.1 Additive decomposition of the strain, uniaxial tension test

Based on observations I and II the resulting total strain is decomposed into an elastic and a plastic part, where unloading from a stressed configuration beyond the elastic limit of the material is implied. Thus, the total strain $\{\varepsilon\}$ is decomposed into an elastic deformation $\{\varepsilon^e\}$ and a plastic deformation component $\{\varepsilon^p\}$.

$$\{\varepsilon\} = \{\varepsilon^e\} + \{\varepsilon^p\} \tag{2.14}$$

Relation (2.14) is more conveniently expressed in rate form as:

$$\{\dot{\varepsilon}\} = \{\dot{\varepsilon}^e\} + \{\dot{\varepsilon}^p\} \tag{2.15}$$

The additive decomposition of the strain tensor is schematically represented in Fig.2.1 for the case of a uniaxial tension test. The elastic deformation component accounts for the fully

reversible deformation while the plastic component accounts for the permanent deformations asserted onto the body.

Plasticity is best described with respect to the components of the stress tensor at a given material point. Taking advantage of the symmetry of the stress tensor, its components define a 6-dimensional Euclidean space. Since such a space is difficult to visualize, the problem is further simplified by referring to the 3-dimensional space defined by the principal stresses of the stress tensor. A point on the three-dimensional stress tensor defines a load point P_L.

Observation II leads to the definition of an evolution equation for the rate of the plastic deformation

$$\left\{\dot{\varepsilon}^p\right\} = \lambda \frac{\partial \Phi}{\partial \left\{\sigma\right\}} \tag{2.16}$$

where λ called the plastic multiplier and Φ is a yield function dependent on the components of the stress tensor, thus defining a hyper-surface in $\mathbb{R}^6$. Since plastic deformations are not reversible, the plastic multiplier is a non-negative quantity. As long as the stress remains within the elastic domain, the plastic multiplier is by definition equal to zero, thus:

$$\lambda = \begin{cases} 0, \text{elastic domain} \\ > 0, \text{ plastic domain} \end{cases} \tag{2.17}$$

The elastic domain is defined by the yield function, that is, any given stress tensor lying within the surface defined by the yield function stands for an elastic state, while any stress tensor lying on the boundary of the yield surface defines the plastic state. Since a direct relations exists between the stress tensor and the principal stress tensor (Marsden and Hughes, 1994), the yield function is usually reformulated in terms of the principal stresses σ_1, σ_2, σ_3 (Lubliner, 2008). Thus, its representation on the principal stress space yields a three dimensional surface.

By defining equation (2.16) another assumption of the theory is implied, that is the normality rule, stating that the direction of the evolution of the plastic strain is normal to the tangent of the yield surface at the load point.

Finally, observation III leads to the definition of the hardening rule. Two main types of hardening are observed namely the isotropic and the kinematic hardening concept. Isotropic hardening is defined as the uniform expansion of the yield surface on the stress-space as presented in Fig.2.2(a).

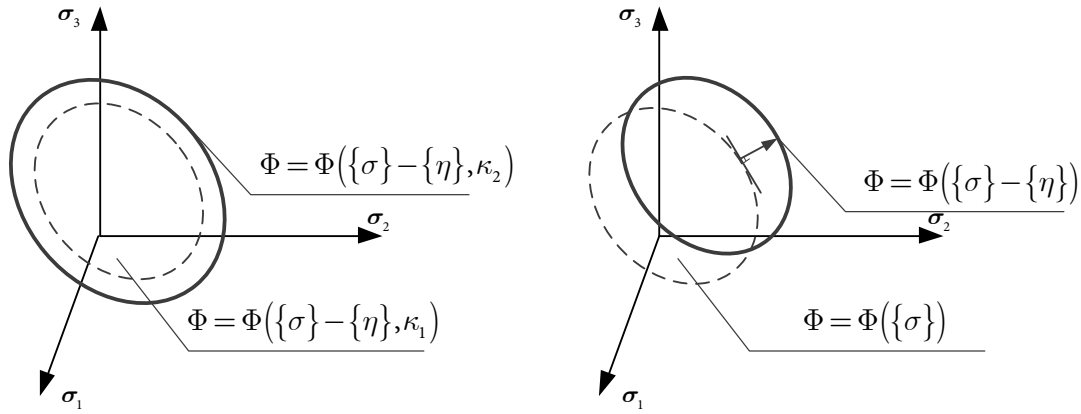

(a) (b)

Fig.2.2(a) Isotropic hardening - uniform expansion of the yield surface (b) Kinematic hardening-relative displacement of the yield surface, parallel to the direction of the plastic deformation

Kinematic hardening is defined by the displacement of the yield surface towards the direction of the plastic strain as presented in Fig.2.2(b). Both are expressed with the help of two model parameters, namely the isotropic hardening parameter $\kappa = \kappa\left(\{\sigma\}\right)$ and the kinematic hardening parameter, or back-stress η. Thus, the yield surface in its most general form is a function of the load point, the isotropic hardening parameter and the back-stress

$$\Phi = \Phi\left(\{\sigma\} - \{\eta\}, \kappa\right) \tag{2.18}$$

The kinematic hardening rule is defined as an evolution equation of the back-stress, which assumes the following form:

$$\{\dot{\eta}\} = \lambda G\left(\{\eta\},\{\dot{\eta}\},\{\dot{\varepsilon}^p\},...\right) \tag{2.19}$$

Equations (2.14) - (2.19) do not suffice to evaluate the plastic multiplier. To do so, another assumption needs to be made concerning the incremental behavior of the load point that is bound to remain on the yield surface for any further increment of the plastic multiplier. This is the consistency condition of classical plasticity that is expressed as:

$$d\Phi = 0 \Rightarrow \left(\frac{\partial \Phi}{\partial \{\sigma\}}\right)^T d\{\sigma\} + \left(\frac{\partial \Phi}{\partial \kappa}\right)^T d\kappa + \left(\frac{\partial \Phi}{\partial \{\eta\}}\right)^T d\{\eta\} = 0 \tag{2.20}$$

The introduction of the consistency condition finally leads to the evaluation of plastic multiplier at a given load point. This procedure will be described in detail in Chapter III as it will be the basis for the development of a generalized hysteretic model. The normality rule and the derived consistency condition are key concepts of the associative plasticity framework that states that the yield surface coincides with the plastic potential from which the plastic deformations are derived (Lubliner, 2008). The theoretical foundations of associative plasticity stem from the mere observation that in many materials (mainly polycrystalline metals) the direction of the principal strains coincides with the direction of principal stresses (Dunne & Petrinic, 2005).

2.3.3 Yield surfaces

In this section, the expressions of typical yield surfaces are presented, that will be used in subsequent Chapters. Historically, the concept of plasticity was first applied to metals in which the influence of the hydrostatic stress on yielding has been macroscopically observed to be negligible (Lubliner, 2008). The Tresca and von Mises yield criteria have been defined with respect to such observations. Furthermore, the Tresca and von-Mises yield criteria satisfy, by definition, symmetry properties based on the isotropy assumption (Lubliner, 2008).

This allows for the evaluation of the necessary model parameters through simple uniaxial tests.

Tresca yield surface

Tresca yield is based on the assumption that plastic deformation initiates when the maximum shear stress, over all planes, asserts a critical value. The Tresca yield criterion is defined by the following non-smooth equation:

$$\Phi_{TR} = \frac{\left|\sigma_{11} - \sigma_{22}\right| + \left|\sigma_{22} - \sigma_{33}\right| + \left|\sigma_{33} - \sigma_{11}\right|}{4\kappa} - 1 \tag{2.21}$$

where κ is a critical value where yielding initiates. The value of κ can be derived from a uniaxial tension test, where the stress tensor is $\left\{\sigma\right\} = \left\{\sigma_y \quad 0 \quad 0 \quad 0 \quad 0 \quad 0\right\}^T$ where σ_y is the yield stress in uniaxial tension. Substituting into the definition of the Tresca yield the following expression is derived:

$$\frac{2\sigma_y}{4\kappa} - 1 = 0 \Rightarrow \kappa = \frac{\sigma_y}{2} \tag{2.22}$$

Expressing the yield surface Φ_{TR} in terms of the principal stresses σ_1, σ_2, σ_3 the following relation is derived

$$\Phi_{TR} = \frac{\left|\sigma_1 - \sigma_2\right| + \left|\sigma_2 - \sigma_3\right| + \left|\sigma_3 - \sigma_1\right|}{\sigma_y} - 1 \tag{2.23}$$

Equation (2.23) represents a hexagonal prism on the principal stress space as presented in Fig.2.3(a). The prism is inclined so that its directrices are parallel to the hydrostatic pressure line defined as $\sigma_1 = \sigma_2 = \sigma_3$.

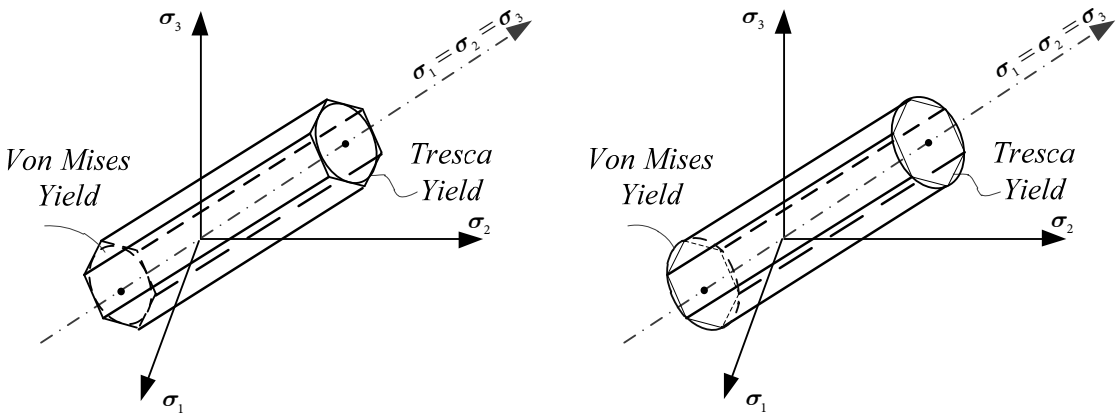

(a) (b)

Fig.2.3(a) Tresca yield surface (b) von Mises yield surface

von Mises yield surface

Von Mises yield is derived through the hypothesis that plastic deformation initiates when the distortional part of the complementary energy of a material assumes a critical value. The von-Mises yield surface is defined as the locus of points in the stress space expressed by the following relation, (Lubliner, 2008):

$$\Phi_{VM} = 0 \tag{2.24}$$

where:

$$\Phi_{VM} = \frac{\left(\sigma_{11}-\sigma_{22}\right)^2+\left(\sigma_{22}-\sigma_{33}\right)^2+\left(\sigma_{11}-\sigma_{33}\right)^2+6\left[\left(\sigma_{12}\right)^2+\left(\sigma_{23}\right)^2+\left(\sigma_{13}\right)^2\right]}{\kappa^2}-1 \tag{2.25}$$

The critical value κ is again defined through a uniaxial test and the following value is derived:

$$\frac{2\sigma_y^2}{\kappa^2}-1=0 \Rightarrow \kappa^2 = 2\sigma_y^2 \Rightarrow \kappa = \sqrt{2}\sigma_y \tag{2.26}$$

Writing equation (2.25) in terms of the second invariant of the deviatoric stress tensor (J_2), the following relation is derived:

$$\Phi_{VM} = \frac{J_2}{2\left(\sigma_y\right)^2} - 1 \tag{2.27}$$

Thus, von Mises yielding initiates when J_2 assumes a critical value. For this reason, plasticity models incorporating the von Mises yield criterion are often referred to as J_2-plasticity models (Simo & Hughes, 1998). If plotted on the principal stress space, equation (2.27) represents an inclined cylinder as presented in Fig.2.3(b). Comparing expressions (2.21) and (2.25) it is proved that if the two models are calibrated to predict the same yield stress in uniaxial tension, then the Tresca yield surface is circumscribed by the von Mises surface. Equivalently, if the two models are calibrated to predict the same yield stress in shear, the von Mises yield surface is inscribed in the Tresca one (Neto et al., 2008).

Bresler-Pister yied surface

When it comes to describing the plastic behavior of materials like soil, rock or concrete a yield criterion depending on the mean stress is needed. In this work, the Bresler-Pister yield criterion is used (Deder & Ayvaz, 2010). The Bresler-Pister yield criterion is a three parameter model that is used to simulate concrete plasticity. It is perceived as an extension of the Drucker - Prager yield criterion (Lubliner, 2008). The corresponding yield surface is defined by equation:

$$\Phi_{BP} = 0 \tag{2.28}$$

where

$$\Phi_{BP} = \frac{\frac{1}{\sqrt{6}}\sqrt{J_2} - c_1\left(\sigma_{11} + \sigma_{22} + \sigma_{33}\right) - c_2\left(\sigma_{11} + \sigma_{22} + \sigma_{33}\right)^2}{c_0} - 1 \tag{2.29}$$

where c_0, c_1, c_2 are material dependent coefficients and J_2 is the second invariant of the stress tensor. The choice of the parameter values needs to be made with care to derive a reasonably shaped yield surface. For the case of concrete, the following set of parameters is derived

$$\begin{aligned} c_1 &= \left(\frac{\sigma_t - \sigma_c}{\sqrt{3}\left(\sigma_t + \sigma_c\right)}\right)\left(\frac{4\sigma_b^2 - \sigma_b\left(\sigma_c + \sigma_t\right) + \sigma_c\sigma_t}{4\sigma_b^2 + 2\sigma_b\left(\sigma_t - \sigma_c\right) - \sigma_c\sigma_t}\right) \\ c_2 &= \left(\frac{1}{\sqrt{3}\left(\sigma_t + \sigma_c\right)}\right)\left(\frac{\sigma_b\left(3\sigma_t - \sigma_c\right) - 2\sigma_c\sigma_t}{4\sigma_b^2 + 2\sigma_b\left(\sigma_t - \sigma_c\right) - \sigma_c\sigma_t}\right) \\ c_0 &= \frac{\sigma_c}{\sqrt{3}} + c_1\sigma_c - c_2\sigma_c^2 \end{aligned} \tag{2.30}$$

In relations (2.30), σ_t, σ_c are the yield stresses in uniaxial tension and compression respectively while σ_b is the yield stress in biaxial compression. The Bresler-Pister yield criterion is part of a general family of three-parameter models for concrete constitutive behavior. Further details can be found on Zhang (1993). In Fig.2.4, the Bresler-Pister yield surface is presented for the case of biaxial loading, considering $\sigma_c = 20MPa$, $\sigma_b = 23MPa$ and $\sigma_t = 2MPa$

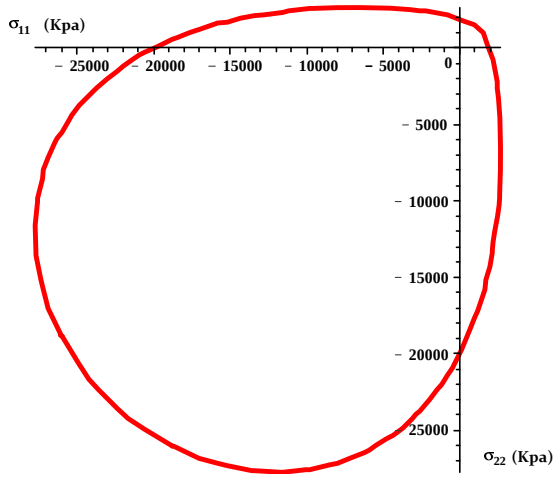

Fig.2.4 Bresler-Pister Yield Surface

2.3.4 Kinematic hardening rules

The Melan-Prager model

The Melan - Prager hardening model (Lubliner, 2008) is defined by the following relation:

$$\{\dot{\eta}\} = c(\{\eta\})\{\dot{\varepsilon}^p\} \tag{2.31}$$

where $c(\{\eta\})$ is an arbitrary function of the back-stress. When $c(\{\eta\})$ is constant, equation (2.31) stands for the linear kinematic hardening model that is schematically presented in Fig.2.5(a) and (b) for the case of a uniaxial tensile test. To demonstrate the notion of back-stress a von Mises material with linear kinematic hardening is considered. In Fig.2.5(a)the stress-strain path OAB is plotted where E is the elastic modulus and $\alpha E, \alpha \in \begin{bmatrix} 0 & 1 \end{bmatrix}$ is the post-yield modulus of the material.

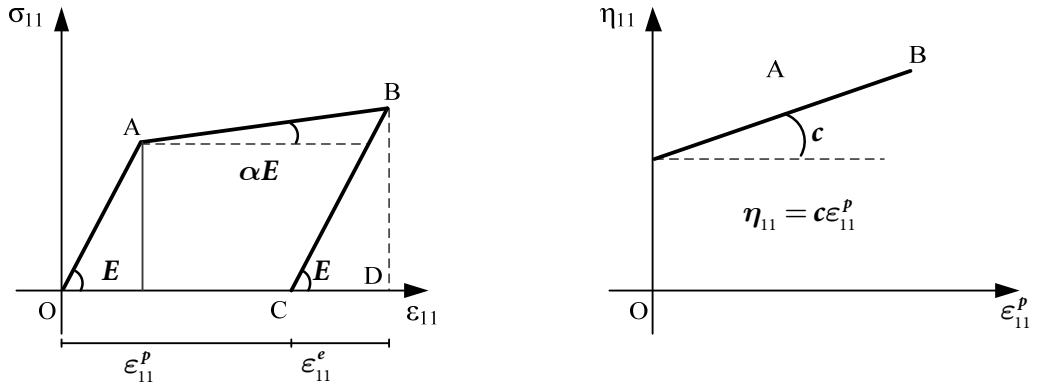

$$\Phi = (\sigma_{11} - \eta_{11}) - \sigma_y$$

Fig.2.5 Material with linear kinematic hardening

Upon unloading from point B to C, well beyond the yield stress of the material, the elastic part ε_{11}^e of the total strain ε_{11} is reversed while the residual part of the deformation is denoted as ε_{11}^p. The elastic part of the strain rate is derived as:

$$\dot{\sigma}_{11} = E\dot{\varepsilon}_{11} \tag{2.32}$$

If reloading occurs, the stress increases following the path CB. The material does not yield until point B is reached while at point B the stress assumes the following value:

$$\sigma = \alpha E\left(\varepsilon - \frac{\sigma_y}{E}\right) \tag{2.33}$$

Differentiating equation (2.33) with respect to time, the following relation is derived:

$$\dot{\sigma} = \alpha E\dot{\varepsilon} \tag{2.34}$$

Since yield occurs at point B, the yield criterion is fulfilled and the following relation holds:

$$\Phi = 0 \Rightarrow \left(\sigma_{11} - \eta_{11}\right) - \sigma_y = 0 \Rightarrow \eta_{11} = \sigma_{11} - \sigma_y \tag{2.35}$$

Therefore, the back-stress expresses the additional stress that needs to be attained beyond the initial yield stress σ_y in order for the material to yield again. Differentiating (2.35) with respect to time the following relation is derived:

$$\dot{\eta}_{11} = \dot{\sigma}_{11} \tag{2.36}$$

Thus the rate of evolution of the back-stress and the actual stress is the same. Substituting relation (2.36) into (2.31), considering equation (2.32) and implementing the additive decomposition of the strain rates (equation (2.15)), the following relation is established:

$$\frac{\dot{\sigma}}{\alpha E} = \frac{\dot{\sigma}}{E} + \frac{\dot{\sigma}}{c} \Rightarrow \frac{1}{\alpha E} = \frac{1}{E} + \frac{1}{c} \Rightarrow c = \frac{\alpha E}{\left(1-\alpha\right)} \tag{2.37}$$

Thus a direct relation exist between the kinematic hardening coefficient, the elastic modulus and the post-elastic to elastic ratio α.

The Armstrong-Frederick kinematic hardening model

The Armstrong-Frederick (AF) kinematic hardening model, which will be denoted as AF model for brevity, (Armstrong and Frederick, 1966) is expressed as:

$$\{\dot{\eta}\} = \frac{2}{3} h \{\dot{\varepsilon}^p\} - c\dot{\varepsilon}^p_{eq} \{\eta\} \tag{2.38}$$

where h, c are model parameters and $\dot{\varepsilon}^p_{eq} = \sqrt{\left(2/3\right)\{\dot{\varepsilon}^p\}^T \{\dot{\varepsilon}^p\}}$ is the equivalent plastic strain. Substituting equation (2.16) into (2.38) the following expression is derived:

$$\{\dot{\eta}\} = \frac{2}{3} h \langle\lambda\rangle \frac{\partial \Phi}{\partial \{\sigma\}} - c\sqrt{\frac{2}{3}} \langle\lambda\rangle \{\eta\} = \langle\lambda\rangle c\sqrt{\frac{2}{3}} \left(\sqrt{\frac{2}{3}} \frac{h}{c} \frac{\partial \Phi}{\partial \{\sigma\}} - \{\eta\} \right) \tag{2.39}$$

Thus, the kinematic hardening function is defined as:

$$G = \sqrt{\frac{2}{3}} \left(\sqrt{\frac{2}{3}} h \frac{\partial \Phi}{\partial \{\sigma\}} - c\{\eta\} \right) \tag{2.40}$$

The second part of equation (2.40) reveals an interesting feature of the AF model. When the back-stress assumes a constant value, that is $\{\dot{\eta}\} = 0$, equation (2.39) yields:

$$\sqrt{\frac{2}{3}} \left(\sqrt{\frac{2}{3}} h \frac{\partial \Phi}{\partial \{\sigma\}} - c\{\eta\} \right) = 0 \Rightarrow \{\eta\} = \sqrt{\frac{2}{3}} \frac{h}{c} \frac{\partial \Phi}{\partial \{\sigma\}} \tag{2.41}$$

Thus, the ratio h/c determines the maximum value of the back-stress, while from relation (2.39) it is derived that parameter c controls the speed by which this maximum value is reached. The AF model is known to overestimate the ratcheting effect observed in cyclic tests of metals under non-zero mean stress (Kyriakides, 1994). For this reason, various modifications have been proposed (Chaboche, 1991, Dafalias, 2008).

2.4 Plasticity in terms of stress resultants

The general framework of three-dimensional plasticity, though mathematically rigorous, is difficult to implement in real life applications due to the great number of the implicated unknowns, i.e. stresses, strains and displacements, and their corresponding equations. To cope with such problems various engineering theories have been proposed and used such as the Euler/Bernoulli theory of bending, the Timoshenko theory of bending or the St-Venant theory of torsion for prismatic beams. Relevant theories have been implemented for the solution of plane problems such as the Kirchhoff-Love and the Reissner-Mindlin theory of bending.

Such theories are macroscopic, in the sense that their assumptions are based on observations over macroscopic properties e.g. plane sections remain plane and perpendicular to the neutral axis for the case of Euler/Bernoulli theory of bending. Moreover, the mathematical derivations are based on stress-resultants, i.e. forces and moments rather than stresses. The stress-resultants are integral quantities of stresses over a finite space quantity and as such they also constitute macroscopical quantities. Thus, contrary to stress-strain formulations where behavior is monitored at discrete points, macro-formulations describe the behavior over a finite space, e.g. a cross-section. Based on the same reasoning and considering predetermined patterns of plastic deformation the basic constituents of the phenomenological theory of plasticity can be also established in terms of stress resultants and corresponding generalized deformation measures. In this work, the theory of stress-resultant plasticity is implemented in the derivation of new hysteretic truss and beam-column elements.

In general, stress-resultant plasticity models for skeletal structures involve adaptations of classical stress-space plasticity rules to model inelastic cross-section deformations under the combined application of axial and shear forces and moments.

Formal stress-resultant plasticity formulations for skeletal structures have been under development for about three decades. Such derivations can be found in Nigam (1970), Song Argyris et al. (1982), and Powell (1982), Orbison et al. (1982), Zhao (1993) and recently Skordeli and Bisbos (2010).These formulations are based on the assumption of plastic hinge formation where member ends are assumed to yield abruptly from elastic to perfectly plastic when a prescribed yield criterion is met. Stress-resultant plasticity models have been applied to reinforced concrete members (e.g., Takizawa and Aoyama 1976) and more recently to steel tubes (Mohareb, 2002).

Yield criteria functions usually take the form of continuous or piecewise linear surfaces representing the fully yielded strength of members under the combined action of stress resultants. Flow rules, corresponding to these yield surfaces are also established as in the stress-strain representation. The main disadvantage of the stress-resultant scheme is that no analytical relation exists for members of arbitrary cross-section. However, a yield boundary can be numerically derived using appropriate software for the case of axial-bending interaction as in Charalampakis and Koumousis (2008b).

2.4.1 Definition of stress resultants

Denoting stress resultants by $\mathcal{F}$ the corresponding generalized strains e are defined as conjugate energy measures, such that:

$$\delta W = \int_V \mathcal{F} \delta e dV \tag{2.42}$$

where δW is the variation in the internal work produced by a variation in the generalized strain measure e over a reference volume V. Considering a prismatic beam element and neglecting the work produced from shear stresses over shear strains, the vector of stress resultants is defined as:

$$\mathcal{F} = \begin{pmatrix} P & M_y & M_z \end{pmatrix}^T \tag{2.43}$$

where P is the axial force, while M_y and M_z are bending moments with respect to the strong and weak axis of the cross-section respectively. The generalized strain vector corresponding to equation (2.43) is defined as:

$$e = \begin{pmatrix} \varepsilon & \phi_y & \phi_z \end{pmatrix}^T \tag{2.44}$$

where e is the centerline axial deformation, ϕ_y is the curvature with respect to the strong axis and ϕ_z is the curvature with respect to the weak axis of the cross-section.

2.4.2 Yield surfaces in stress-resultant space

Exponential yield surface for steel sections

The exponential yield criterion concerning axial-biaxial bending interaction assumes the following form:

$$\Phi = n + \left(m_y\right)^{\alpha_x} + \left(m_z\right)^{\alpha_x} \tag{2.45}$$

where $n = P/P_u$, $m_y = M_y/M_{yu}$, $m_z = M_z/M_{zu}$, while α_x, α_y are shape factors. Relation (2.45) is also implemented for the simulation of composite sections as described in Iu et al. (2009). In the trivial case where $\alpha_x = \alpha_y = 1$, equation (2.45) reduces to the linear interaction scheme implemented in EC3. The linear scheme constitutes a lower bound solution of the plasticity problem (Lubliner, 2008) thus yielding a conservative predictor for the true cross-sectional behavior.

The Orbison yield surface

The Orbison criterion (Orbison et al., 1982) is defined by the following relation:

$$\Phi = 1.15n^2 + m_y^2 + m_z^4 + 3.67n^2m_y^2 + 3.0n^6m_z^2 + 4.65m_y^4m_z^2 \tag{2.46}$$

where $n = P/P_u$, $m_y = M_y/M_{yu}$, $m_z = M_z/M_{zu}$. In equation (2.46) y refers to the strong axis of the cross section while z refers to the weak axis of the cross-section. Equation (2.46) has been developed by curve-fitting over actual experimental data and is suited for interaction patterns observed in steel I-beams.

The Heyman-Dutton yield surface

In Heyman and Dutton (1954) the following yield criterion has been proposed for the moment-shear interaction of I-beams

$$m + m_{web}\left(1 - \sqrt{1 - \left(q\right)^2}\right) = 1 \tag{2.47}$$

where $m = M/M_p$ is the bending ratio M_p being the fully plastic moment of the cross-section, $m_{web} = M_{web}/M_p$ is the ratio of moment retrieved by the web over M_p and $q = Q/Q_p$ is the shear ration, Q_p being the fully plastic shear force. In Fig. 2.6, the Heyman-Dutton yield criterion is presented for three distinct cases of m_{web} namely 0.1, 0.2 and 0.4. The case $m_{web} = 0.4$ is an extreme scenario not accounted for in standard steel section profiles.

The bending moment is not severely reduced for values of the shear ratio smaller than 0.25. The reduction increases significantly for values of the shear ratio greater than 0.25. The reduction rate increases for increasing values of m_{web}. For standard cross-sectional profiles the overall reduction in the bending strength is not greater than 20% of the initial value.

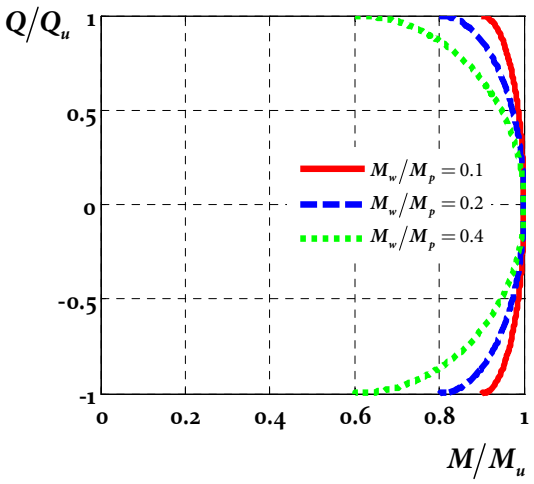

Fig. 2.6 The Heyman-Dutton yield criterion

The Simo et al. yield surface

Simo et al. (1983) analytically evaluated the following relation for the plastic interaction between axial, shear forces and bending moment for a rectangular cross-section

$$\Phi = \left|\frac{M}{M_u}\right| + \left(\frac{P}{P_u}\right)^2 \left[1 + \left(\frac{Q}{Q_u}\right)^2\right] + \left(\frac{Q}{Q_u}\right)^4 \tag{2.48}$$

Relation (2.48) is analytical, depending only on the shape of the cross-section and thus can be implemented both on steel and reinforced concrete sections, provided that the uniaxial strength components P_u, M_u, Q_u have been accurately evaluated. Fig. 2.7(a), the 3d interaction surface is presented while in Fig. 2.7(b) the corresponding iso-axial interaction curves are plotted. The bending strength of the cross-section reduces significantly for values of the axial ratio larger than 0.25.

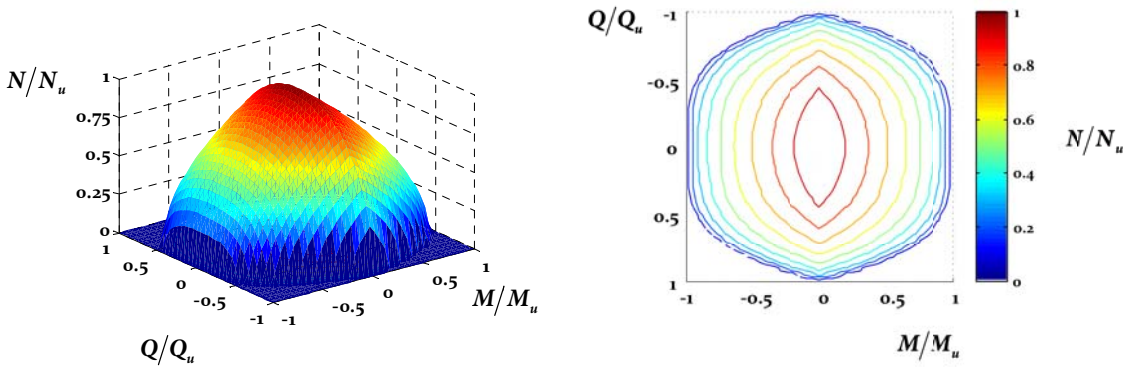

(a) (b)

Fig. 2.7(a) Simo et al. yield criterion (b) Iso-axial moment shear interaction curves

Generalized Gendy-Saleeb yield surface

Gendy and Saleeb (1992) propose the following generalized yield surface for the rectangular and wide flange sections

$$\Phi = \eta^2 + q_y^2 + q_z^2 + \frac{1}{\lambda_y} m_y^2 + \frac{1}{\lambda_z} m_z^2 + m_w^2 + t_{sv}^2 \tag{2.49}$$

where $n = P/P_u$, $q_y = Q_y/Q_p$, $q_z = Q_z/Q_p$, $m_y = M_y/M_{yu}$, $m_z = M_z/M_{zu}$ while $m_w = M_w/M_{pw}$ is the ratio of the warping bimoment over the fully plastic warping bimoment and $t_{sv} = M_{sv}/M_{svp}$ is the ratio of the pure torsional moment over the fully plastic torsional moment. Parameters λ_y and λ_z are shape dependent. For rectangular cross-sections they assume the following form

$$\lambda_y = \lambda_z = 1 - \eta^2 \tag{2.50}$$

while for I-beams the corresponding expressions are:

$$\lambda_y = 1 - \eta, \quad \lambda_z = 1 - 1.1\eta \tag{2.51}$$

The advantage of the expressions described above, rest in the fact that they are analytical and thus facilitate the evaluation of corresponding flow rates.

Chapter 3

BOUC-WEN HYSTERESIS

3.1 Introduction

An issue of major importance, for a nonlinear analysis, is the hysteretic rule needed to model the cyclic response of structures. Over the last twenty years, significant development has occurred in the so-called phenomenological approach of hysteresis. Following Massing (1925), Preisac (1935) and Valanis (1971), Bouc presented his formulation (1967) of the single degree degrading hysteresis model with pinching. Subsequently, many modifications have been introduced, such as the Bouc-Wen model (Wen, 1976, 1980), the Baber-Noori model (Baber and Wen 1980, Baber et al. 1986) and the Reinhorn model (Sivaselvan and Reinhorn, 2000). These hysteresis models –also known as smooth hysteretic models- are capable of simulating different types of hysteretic behavior using a single smooth hysteretic function affected by a set of user-defined parameters.

The last decades Bouc-Wen hysteretic model is proven very versatile in expressing a wide range of hysteretic response including stiffness degradation, strength deterioration as well as pinching phenomena in reinforced concrete, steel members and connections, wood etc., (Foliente G. C, 1995). In addition, considerable effort has been devoted to alleviate Bouc-Wen model from inconsistencies regarding thermodynamic admissibility, (Erlicher and Point 2004, Erlicher and Bursi, 2009) and violation of plasticity postulates, (Charalampakis and Koumousis, 2009). The rate form of evolution equations, derived also on the basis of endochronic theories of plasticity (Valanis, 1971), is capable of expressing in an integrated way the phenomenological hysteretic behavior at the component level. This facilitates direct incorporation of identified model parameters for various members and/or connections leading to a more effective and controllable analysis, as compared to the pointwise stress-strain relations required in standard Finite Element Analysis. These features are revealed at the cost

of extending the elastic finite elements by introducing additional stiffness matrices that account for inelastic behavior and the inherent interaction of different components of stress.

During the last decade, Bouc-Wen model has been adopted by many researchers, (Pires, 1993, Choi and Lee, 2001) as a robust and accurate tool, to simulate the hysteretic behavior of various materials. At the same time, techniques were developed for the identification of the Bouc-Wen model parameters utilizing among others, advanced analytical techniques, as in Chatzi and Smyth (2008), evolutionary identification approaches, (Charalampakis and Koumousis, 2008a) and more recently in Chang et al. (2010) using wavelet analysis.

3.1.1 The concept of hysteresis

Consider the single degree of freedom (s.d.o.f.) oscillator presented in Fig.3.1. The oscillator exhibits an elastic-perfectly plastic material behavior with a yield stress σ_y.

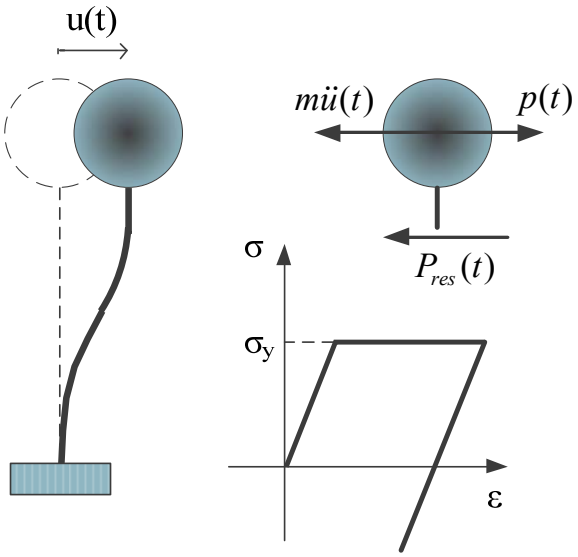

Fig.3.1 Single degree of freedom oscillator under cyclic excitation

The response of the nonlinear oscillator is depicted in more detail in Fig.3.2. For stresses smaller than the yield stress, material behavior is defined by Hooke's law, so that the elastic range of the response is evaluated as:

$$\sigma(\varepsilon) = E\varepsilon, \ \ |\sigma| \le \sigma_y \tag{3.1}$$

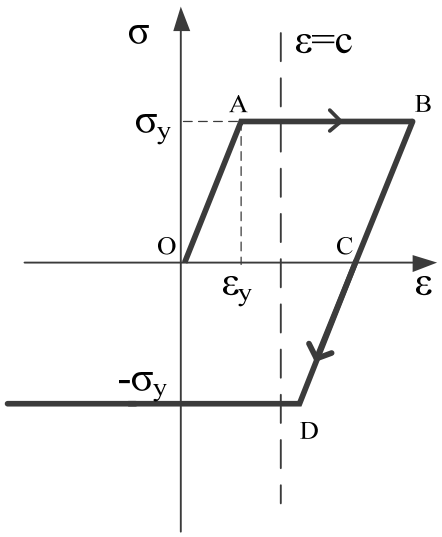

Fig.3.2 Hysteretic loop

and there is 1:1 correspondence between the input and the output.

However, there are at least two possible stress states $\sigma \in [-\sigma_y, \sigma_y]$ that correspond to an arbitrary strain level $\varepsilon = c, c \in [\varepsilon_y, +\infty)$, larger than the yield strain ε_y.Thus, there does not exist a function $\sigma(\varepsilon)$ that can uniquely map the current level of strain to the current level of stress even for the trivial case of an elastic-perfectly plastic material. The mathematical theory of hysteresis tries to define a proper output function $\sigma = \sigma(t) : [0,T] \to \mathbb{R}$ given an input function $\varepsilon = \varepsilon(t) : [0,T] \to \mathbb{R}$ such that the derived vector phase space $(\sigma(t), \varepsilon(t))$ coincides with the curve presented in Fig.3.2.

Thus, the mechanical problem of hysteresis is translated into the mathematical problem of defining an operator, denoted herein as the hysteresis operator $B[In](t)$ where $In : [0,T] \to \mathbb{R}$, is an arbitrary input time history such as displacement, strain e.t.c. From physical point of view, the functional has to be rate independent since the hysteretic energy accumulated over consequent loading and unloading cycles does not depend on the rate of the

input or output functions. Moreover, the hysteretic operator must be piecewise monotone, as the shape of the hysteretic loops implies (e.g. with respect to Fig.3.2, monotonically increasing in path OAB and monotonically decreasing in path BCD). Finally, the operator must have some property of memory which in mathematical terms is covered by the notion of causality (Logemann and Mawby, 2003).

It is evident from the approach presented in this paragraph that the notion of hysteresis is coped with mathematical tools that are indifferent to the input and output functions describing the hysteretic loop. For this reason, the theory presented herein constitutes a phenomenological approach. Nevertheless, there are aspects that are directly connected to the mechanical properties of hysteresis such as energy dissipation mechanisms and hardening effects that will be addressed through this theory in a consistent way.

3.2 The initial derivation of the Bouc-Wen model

Bouc (1967) studied the response of a single degree of freedom oscillator with mass m and a hysteretic restoring force $P_{res}(t)$. According to the notions described in paragraph 2.1, the hysteretic restoring force is considered to be the result of a hysteretic operator B over the displacement $u(t)$:

$$P_{res}(t) = B[u](t) \tag{3.2}$$

The equation of motion of the s.d.o.f oscillator is then expressed as:

$$m\frac{d^2u}{dt^2} + B\big[u\big]\big(t\big) = p\big(t\big) \tag{3.3}$$

where $p\big(t\big)$ is the external force. Based on the initial work of Volterra (1928) for an internal restoring force with hysteretic properties, Bouc defined operator B as an integral scheme:

$$B[u](t) = \int_{t_0}^{t} \mu(t,t')du(t') \tag{3.4}$$

where μ is an intrinsic kernel and $t' > t$. Furthermore, the following assumption is adopted for the kernel:

$$\mu(t,t') = \mu(t-t') \tag{3.5}$$

that is, the evolution of μ is irrelevant to the velocity of the oscillator. The property of piecewise monotony is met by requiring that the kernel is a bounded, continuous and decreasing function of the time increment $\Delta t = t - t'$. Thus the following relations hold:

$$0 \le \mu(\Delta t) \le \infty, \quad \frac{d\mu(\Delta t)}{d\Delta t} \le 0 \tag{3.6}$$

The condition of causality is met since the upper limit of the integral in equation (3.4) is the current time t and the current value of the operator is the cumulative sum of the kernel over the displacement. Since the kernel depends on the time-step Δt, the derived hysteretic restoring force depends on the rate of the imposed load, yielding a formulation not eligible for a rate-independent plasticity formulation. To overcome this deficiency, Bouc introduced the following transformation:

$$\Delta t \to \Delta u(t,t') \Rightarrow \mu(\Delta t) \to \mu(\Delta u(t,t')) \tag{3.7}$$

mapping the time increment Δt to the corresponding displacement increment Δu. Thus, the hysteretic force is expressed as:

$$B[u](t) \equiv P_{res}(t) = \int_{t_0}^{t} \mu(\Delta u(t,t'))du(t') \tag{3.8}$$

where the kernel μ is now a bounded, positive and non-decreasing function of Δu:

$$0 \le \mu\left(\Delta u\right) \le \infty, \quad \frac{d\mu\left(\Delta u\right)}{d\Delta u} \le 0 \tag{3.9}$$

Similarly, the intrinsic time step Δu is a positive, increasing function, since time t' is larger than t. Different definitions of the intrinsic time step lead to different hysteresis formulations, given that they all comply to equations (3.9). A typical example that is consistent with the above remarks is the following:

$$d\Delta u = \left|du\right| = \left|\frac{du}{dt}\right|dt = \left|\frac{du}{d\tilde{t}}\right|d\tilde{t} := d\theta,\ \tilde{t} = \varphi(\mathrm{t}) \tag{3.10}$$

The mathematical expression of the restoring force introduced in equation (3.8)though rigorous, fails to clarify the key parts of the restoring force in terms of mechanics. Trying to clarify the physical properties of the hysteretic operator B, Bouc introduced two arbitrary continuous scalar functions f, Φ with the following properties:

$$\begin{aligned} f : R \to R;\ \mathrm{f}(0){=}0;\ \left|f(u_1) - f(u_2)\right| \le K_1(A)\left|u_1 - u_2\right| \\ \Phi : R \to R; \Phi(0){=}0;\ \left|\Phi(u_1) - \Phi(u_2)\right| \le K_2(A)\left|u_1 - u_2\right| \end{aligned} \tag{3.11}$$

where K_1,K_2 constants, for every A, u_1, u_2. A generalization of the Volterra expression (equation (3.8)) is then established, such that:

$$\begin{aligned} P_{res}(t) &= f(u(t)) + z(t) \\ z(t) &= \Phi\left(u\left(t'\right)\right)\int_{t_0}^{t} \mu\left(\Delta_u\left(t,t'\right)\right)du \end{aligned} \tag{3.12}$$

Since relations (3.12) hold for every function f, Φ, they also hold for:

$$f\left(u\left(t\right)\right) = ku\left(t\right) + \tilde{f}\left(u\left(t\right)\right) \tag{3.13}$$

where $\tilde{f}\left(.\right)$ is also a continuous scalar function.

Thus, substituting relation (3.13) into (3.12) a clear distinction is made between the linear elastic component of the restoring force $ku\left(t\right)$, the nonlinear elastic term $f\left(u\left(t\right)\right)$ and the nonlinear, history dependent, component $z\left(t\right)$. Operator Φ depends on the displacement time history u, so that the expression of the nonlinear component is irrelevant to the displacement rate. The integral of the second of relations (3.12) is a Lebesgue – Stieltjes integral (Halmos, 1974) that can be cast in the following Riemannian form:

$$z\left(t\right)=z\left(\theta\left(t\right)\right)=\int_{0}^{\theta\left(t\right)}\mu\left(\theta\left(t\right)-\theta'\right)\frac{d\Phi}{du}\frac{du}{d\theta'}d\theta' \tag{3.14}$$

where $\theta\left(t\right)$ is an intrinsic time complying to (3.10).The integral of equation (3.14) is the "memory" of the dynamical system, since $z\left(t\right)$ is an integral over the time period $t-t_0$. As such, it adheres, by definition, to the Volterra property. Furthermore, since the kernel of the integral does not explicitly depend on t, the hysteretic parameter $z\left(t\right)$ is by definition rate-independent. Thus, the formulation proposed by Bouc is a formal, continuous and stable hysteretic operator (Brokate et al., 1993).

Thus, the single degree of freedom equation of motion is evaluated as:

$$\begin{cases} m\dfrac{d^2w}{dt^2}+P_{res}(t)=p\left(t\right) \\ P_{res}(t)=ku(t)+\tilde{f}(u(t))+z(t) \\ z\left(t\right)=\displaystyle\int_{0}^{\theta\left(t\right)}\mu\left(\theta\left(t\right)-\theta'\right)\frac{d\Phi}{du}\frac{du}{d\theta'}d\theta' \end{cases} \tag{3.15}$$

Bouc imposed the following relation on the variation of u:

$$\Delta_u\left(t,t'\right)=\theta\left(t\right)-\theta\left(t'\right)=\theta-\theta'=\int_{t}^{t'}d\theta(\tau)=\int_{t}^{t'}\left|\frac{du}{d\tau}\right|d\tau:=V_{t'}^{t}u \tag{3.16}$$

where $V_{t'}^{t}u$ is defined as the total variation of u on $\left[t', t\right]$. It is easily proven that the following relation holds:

$$d\theta(\tau) = \left|du(\tau)\right| \tag{3.17}$$

Any type of function can serve as a kernel. However, it can be proven that the differential equation of the nonlinear component can be derived always for an exponential kernel.

3.2.1 The exponential kernel case

Consider the following case where:

$$f\left(t\right) = 0, \Phi\left(u\right) = u \tag{3.18}$$

Equations (3.18) fulfill the properties set on relation (3.11).

Substituting into the second of relations (3.15), the following expression for the restoring force is derived:

$$P_{res}(t) = ku(t) + z(t) = ku(t) + \int_{0}^{\theta(t)} \mu\left(\theta(t) - \theta'\right)\frac{du}{d\theta'}d\theta' \tag{3.19}$$

The kernel in the integral of relation (3.19) is considered to be an exponent of the following form:

$$\mu(\theta) = \mathrm{A}e^{-\beta\theta}, \qquad \mathrm{A},\ \beta>0 \tag{3.20}$$

that complies with relations (3.9). Differentiating relation (3.19):

$$dP_{res} = kdu + dz(\theta) \tag{3.21}$$

Substituting the integral form of $z(t)$ into (3.21), the following relation is derived:

$$\begin{aligned} dP_{res} &= kdu + \left[\mathrm{A}e^{-\beta(\theta-\theta')}du(\theta') \right]_{\theta'=\theta} - \left[\int_{\theta_0}^{\theta} \frac{\partial\left(\mathrm{A}e^{-\beta(\theta-\theta')} \right)}{\partial\theta} \frac{du(\theta')}{d\theta'} d\theta' \right] d\theta \\ &= kdu + \mathrm{A}du(\theta) - \beta \left[\int_{\theta_0}^{\theta} \mathrm{A}e^{-\beta(\theta-\theta')} \frac{du(\theta')}{d\theta'} d\theta' \right] d\theta \end{aligned} \tag{3.22}$$

Finally, taking into account the definition of the kernel introduced into (3.20) the following equation is derived:

$$dP_{res} = kdu + dz = Kdu + Adu - \beta z d\theta \tag{3.23}$$

Or equivalently in rate form:

$$\frac{dP_{res}}{dt} = k\frac{du}{dt} + \frac{dz}{dt} = k\frac{du}{dt} + A\frac{du}{dt} - \beta z\frac{d\theta}{dt} \tag{3.24}$$

Combining the first and second of equations (3.24) , the following rate form is derived for the hysteretic parameter $z(t)$:

$$\frac{dz}{dt} = A\frac{du}{dt} - \beta z\frac{d\theta}{dt} \tag{3.25}$$

Finally, substituting equation (3.17) into (3.25), the following, trivial equation of the Bouc-Wen model is derived:

$$\frac{dz}{dt} = \left[A - \beta z\,\mathrm{sgn}(du) \right]\frac{du}{dt} \qquad \mathrm{A},\beta>0 \tag{3.26}$$

and relation (3.15) is rewritten as:

$$\begin{cases} \dfrac{d^2u}{dt^2} + P_{res}^{B}(t) = p\left(t\right) \\ \dfrac{dP_{res}^{B}}{dt} = \dfrac{dz}{dt} = \left[A - \beta z\,\mathrm{sgn}(du) \right]\dfrac{du}{dt} \end{cases} \tag{3.27}$$

Equations (3.27) correspond to the simple case of a perfectly nonlinear s.d.o.f oscillator. The second of equations (3.27) can be solved by quadratures and the restoring force is established as a function of the displacement u:

$$P_{res}\left(u\right)=z\left(u\right)=\frac{A}{\beta sign\left(du\right)}\left(1-e^{-\beta sign\left(du\right)u}\right)=\frac{A}{\beta}sign\left(du\right)\left(1-e^{-\beta sign\left(du\right)u}\right) \quad (3.28)$$

Referring to equation (3.20) one can assume without loss of generality that $A=C\beta$. Thus, equation (3.28) is rewritten as:

$$P_{res}\left(u\right)=Csign\left(du\right)\left(1-e^{-\beta sign\left(du\right)u}\right) \quad (3.29)$$

Different values of C and β give rise to different hysteretic loops with the rigid plastic body being an upper limit. In the limit case where $\beta\to\infty$ the restoring force coincides with the expression of the perfect slider with unit threshold.

$$\begin{aligned}\lim_{\beta\to\infty}P_{res}&=Csign\left(du\right)\\ F_s&=\mu Nsign\left(du\right)\end{aligned} \quad (3.30)$$

where F_s is the friction force, μ the coefficient of friction and N the normal force. Thus, the trivial case of Bouc-Wen hysteresis smooths the standard expression of the friction force by merely relying on the mathematical expression of hysteresis as established by the pioneering work of Volterra (1928).

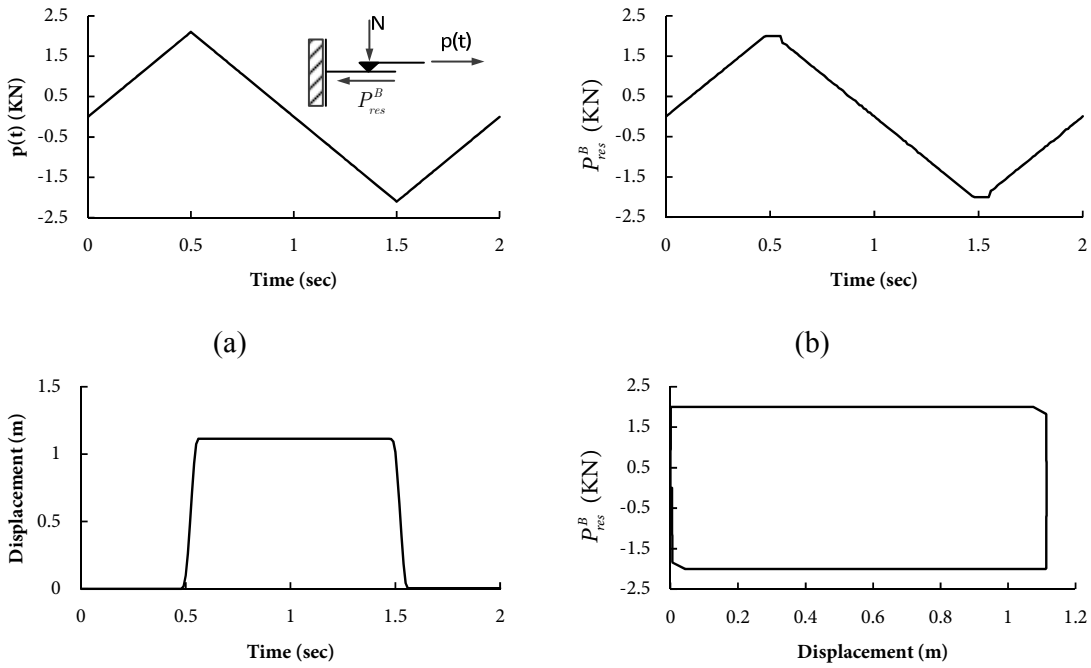

Fig.3.3(a) External Force (b) Friction Force (c) Displacement on slider (d) Friction Force-Displacement hysteretic loop

As an example, the response of the dynamic system presented in equations (3.27) is examined with constants $C = 2$ KN and $\beta = 10000$ under cyclic loading. The excitation is presented in Fig.3.3(a). In Fig.3.3(b) and (c) the time-history of the friction force and the displacement are presented respectively. As predicted by equations (3.30), the system evolves as a perfect slider, with zero displacement until the external force reaches the sliding threshold defined by the constant C. The corresponding hysteresis loop is presented in Fig.3.3(d). As expected, a permanent displacement is observed after full unloading due to the dissipative nature of the friction force.

3.3 From classical plasticity to Bouc-Wen hysteresis

3.3.1 Decomposing the Bouc-Wen hysteretic model

Modifications of the initial Bouc formulation (relation (3.27)) have been subsequently introduced such as the Bouc-Wen model (Wen, 1976, 1980), the Baber-Noori model (Baber

and Wen 1980, Baber et al. 1986) and the Reinhorn model (Sivaselvan and Reinhorn, 2000). In this work, the Bouc-Wen model as introduced in Wen, (1980) and later modified by is used as the basis for every subsequent step of analysis:

$$\begin{cases} \ddot{u} + c\dot{u} + P_{res}^{BW} = p(t) \\ P_{res}^{BW} = \alpha K u + z \\ \dot{z} = (1-\alpha)\mathrm{K}\left[A - |z|^{n}(\beta + \gamma\,\mathrm{sgn}(z\dot{u})\right]\dot{u} \end{cases} \tag{3.31}$$

where c is the viscous damping coefficient, P_{res}^{BW} is the Bouc-Wen restoring force, α is the post-elastic to elastic stiffness ratio, K is the elastic stiffness of the oscillator while A, β, γ are model parameters. Parameter A has been proven to be redundant in subsequent works (Ma et al, 2004) and will be considered to be equal to unity throughout this work. As implied by the first of equations (3.31), the restoring force is split into two parts. The first part is linear with an effective stiffness equal to the plastic stiffness of the material and a hysteretic one with z being the restoring force that bares the memory of the nonlinear system. In this work, a variant of this formulation is considered where z is considered to be the hysteretic displacement of the system and thus:

$$\begin{cases} \ddot{u} + c\dot{u} + P_{res}^{BW} = p(t) \\ P_{res}^{BW} = \alpha K u + (1-\alpha)\mathrm{K}z \\ \dot{z} = \left[1 - \left|\dfrac{z}{z_y}\right|^{n}(\beta + \gamma\,\mathrm{sgn}(z\dot{u})\right]\dot{u} \end{cases} \tag{3.32}$$

where z_y is the maximum value of the hysteretic parameter.

The formulations presented in equations (3.31) and (3.32) are based on mechanical insight rather than the mathematical theory of hysteresis. Thus, the derivation of relation (3.31) from the mathematical background established in section 3.2 is not straightforward. However, a mechanical representation of the model can be established that allows for the decomposition of relation (3.31).

This decomposition is schematically represented in Fig.3.4. Considering $c = 0$ for the sake of presentation, the model can be visualized as a parallel combination of a linear spring (Spring #1) and a nonlinear element, as shown inFig.3.4(a). The nonlinear element consists of a linear spring (Spring #2) and a slider connected in series. Thus, a two degree of freedom system is introduced, u, being the total displacement and z, being the relative displacement of Spring 2. From compatibility considerations, the sliding displacement, if any, is determined by the difference $\left(x = u - z\right)$.

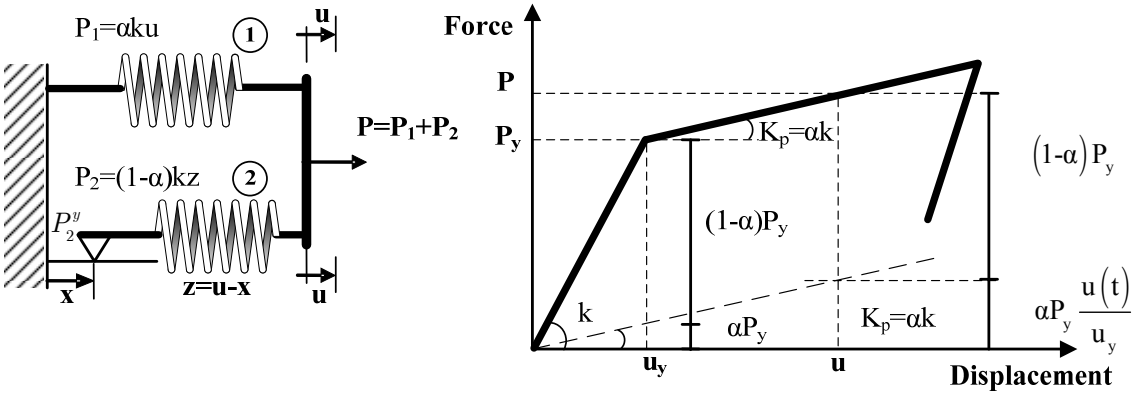

(a) (b)

Fig.3.4 (a) Bouc-Wen model components (b) Force-displacement relation

As long as the force acting on the slider is smaller than a threshold $\left(x_y\right)$, sliding does not occur, thus $x = 0$ and the relative displacement on Spring #2 is equal to the total imposed displacement. In such a case, the system behaves elastically with combined stiffness k, since

springs #1 and #2 are given an elastic stiffness of αk and $\left(1-\alpha\right)k$ respectively, α being the inelastic to elastic stiffness ratio.

When the slider threshold is overcome, sliding occurs and the relative displacement in spring #2 remains constant, denoted herein as z_y. All these phases are summarized in the following force-displacement relationship:

$$P_{res}^{BW} = P_1 + P_2 = \alpha k u + \left(1-\alpha\right)kz \tag{3.33}$$

where z is:

$$z = \begin{cases} u, & x \le x_y \\ z_y, & x > x_y \end{cases} \tag{3.34}$$

As in engineering applications, the internal variable x is neither easy to measure, nor derive theoretically, the total displacement at which sliding occurs is used instead. This can be easily derived (from a uniaxial tension experiment or implementing a specific yield criterion) and thus relation (3.34) is treated equivalently as:

$$z = \begin{cases} u, & u \le u_y \\ u_y, & u > u_y \end{cases} \tag{3.35}$$

Wen (1980) proposed the following relation in order to smooth the transition from the elastic (no sliding) to the inelastic response (sliding) of the system:

$$\dot{z}(t) = f(\dot{u}(t), z(t)) = \dot{u}\left[\mathrm{A} - h_1 h_2\right] \tag{3.36}$$

where:

$$h_1 = \left|\frac{z}{z_y}\right|^n, \qquad h_2 = \left(\beta + \gamma\,\mathrm{sgn}\left(z\dot{u}\right)\right) \tag{3.37}$$

h_1 can be regarded as a uniaxial flow rule and h_2 as the corresponding cyclic loading rate, while in the above relation, dot $(\cdot)$ denotes differentiation with respect to time. Parameter n controls the smoothness of the transition from the elastic to the inelastic regime, while the terms β and γ introduced in relation (3.37) are shape factors that affect the shape of the hysteresis loop (Sivaselvan & Reinhorn, 2000). In Fig.3.5 the results from a strain controlled numerical experiment on a D18 rebar are presented for different values of the model parameters n, β and γ. Material parameters are S500 and E=200 GPa, while the length of the bar is considered to be 2m.

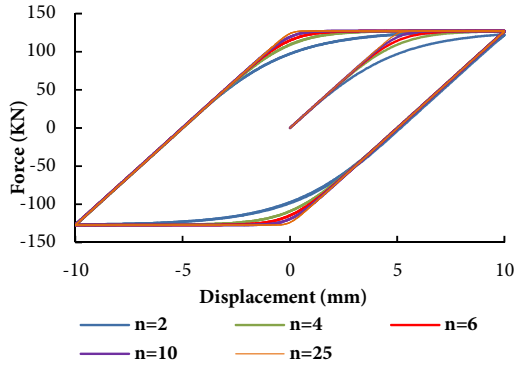

(a)

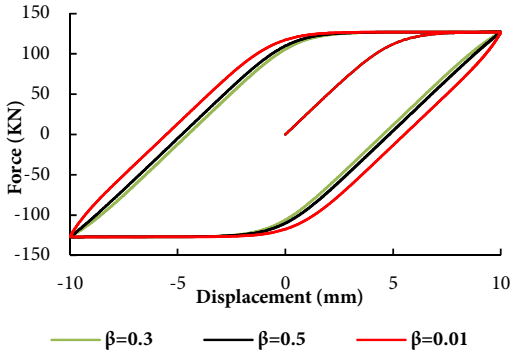

(b)

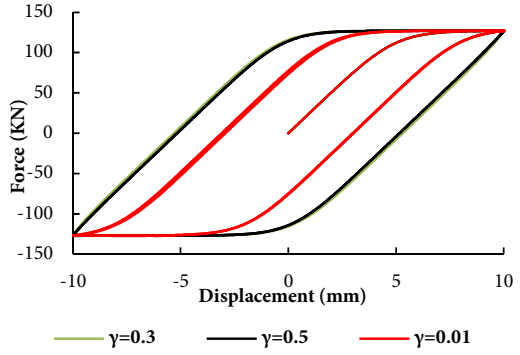

(c)

Fig.3.5 Strain controlled numerical experiment (a) Variation in hysteretic loop with respect to n (b) Variation in hysteretic loop with respect to parameter β ($\gamma = 0.2$, n =5) (c) Variation in hysteretic loop with respect to parameter γ ($\beta = 0.2$, n =5)

3.3.2 Remarks on Bouc-Wen modelling

An immediate consequence of equations (3.33)and (3.36), is the fact that a small value of the smoothness parameter n, results on sliding even before the yield displacement z_y is reached. This is evident by considering, without loss of generality, that $sign(z\dot{u}) = 1$ (state of loading on the positive half plane), and thus relation (3.36) becomes:

$$\dot{z}(t) = \dot{u}\left[1 - \left|\frac{z}{z_y}\right|^n \left(\beta + \gamma\right)\right] \tag{3.38}$$

Due to the physical considerations as described above, in the elastic case, it must hold that, with respect toFig.3.4, the relative displacement in spring 2 equals the displacement in spring 1 and thus:

$$z = u \Rightarrow \dot{z}(t) = \dot{u} \Rightarrow \left[1 - \left|\frac{z}{z_y}\right|^n \left(\beta + \gamma\right)\right] = 1 \overset{(\beta+\gamma)=1}{\Rightarrow} z = 0 \tag{3.39}$$

It is evident that relation (3.39) cannot hold since this would mean that the imposed displacement is also zero. What the normalized smoothing function does, is that it holds the term $\left|z/z_y\right|^n \left(\beta + \gamma\right)$ sufficiently low, as long as $z < z_y$, so that the following relation holds.

$$1 - \left|\frac{z}{z_y}\right|^n \left(\beta + \gamma\right) \overset{(\beta+\gamma)=1}{\rightarrow} 1 \tag{3.40}$$

The effectiveness of the smoothing function with respect to parameter n is presented inFig.3.6.The arithmetic performance of this function increases as parameter n retains a large value, but is somewhat reduced as the n value reduces. As a result, equation (3.39) slightly deviates from equality and micro sliding occurs even before the yield displacement is reached.

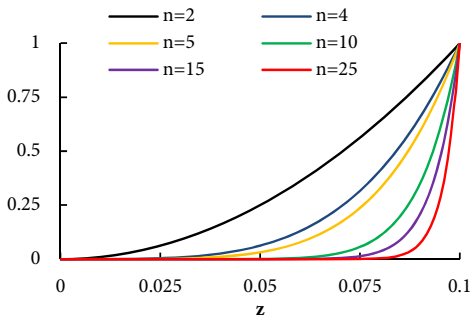

Fig.3.6Variation of the smoothing function with respect to n

Nevertheless, it is evident that such a formulation is able to model any uniaxial behavior introduced in the context of classical plasticity, by incorporating in a single equation the yield criterion, the flow rule and the loading rate. It is noted that the term defined herein as yield displacement, is a phenomenological quantity which stands for the displacement by which plastic deformation commences. This quantity together with the terms β, γ and n can be evaluated by various identification techniques. However, as Erlicher and Bursi (2004) proved, the identified parameters should comply to the following restriction, to yield a thermodynamic admissible model:

$$-\beta \leq \gamma \leq \beta \tag{3.41}$$

Up to this point, the presentation of the Bouc-Wen model is based on the grounds of force-displacement relations. Though versatile, this formulation limits the applicability of these relations where the Finite Element Method is concerned. In the next paragraphs, a general formulation is presented, within the framework of classical plasticity, that allows for the implementation of these smooth-hysteretic operators, thus avoiding the need for piece-wise linear hysteretic models.

3.4 The generalized triaxial Bouc-Wen model

Though the derivation of the Bouc-Wen model presented in section 3.2 was based on mathematical grounds, it can be proven that the same relations can be deducted considering

the physics of classical plasticity. The advantage of this approach is the fact that smoothed plasticity relations are deducted in terms of tensorial stress-strain relations. This leads to a versatile material model both from computational and experimental perspective.

Classical plasticity is based on a set of governing equations, namely the flow rule, the yield condition, the consistency condition and the hardening rule. In the work presented herein, the case of associative plasticity is addressed where the plastic potential coincides with the flow rule. Denoting the flow rule as Φ, the rate of plastic deformation is defined as:

$$\left\{\dot{\varepsilon}^p\right\} = \dot{\lambda}\frac{\partial\Phi\left(\left\{\sigma\right\}\right)}{\partial\left\{\sigma\right\}} \tag{3.42}$$

where $\left\{\dot{\varepsilon}^p\right\}$ is the plastic strain tensor, $\dot{\lambda}$ the plastic multiplier, $\left\{\sigma\right\}$ the stress tensor and (.) denotes differentiation with respect to time. The plastic multiplier and the yield function are found to comply with the Kuhn-Tucker optimality conditions:

$$\dot{\lambda} \geq 0, \quad \Phi \leq 0, \quad \dot{\lambda}\Phi = 0 \tag{3.43}$$

The consistency condition is an immediate consequence of relation (3.43) stating that when at yield:

$$\dot{\lambda}\dot{\Phi} = 0 \tag{3.44}$$

A typical isotropic yield criterion (or plasticity model for brevity) is the von-Mises yield criterion defined as:

$$\Phi = \left\|\left\{\sigma\right\} - \left\{\eta\right\}\right\| - \sigma_M \leq 0 \tag{3.45}$$

where $\left\{\sigma\right\}$ is the deviatoric stress tensor and $\left\{\eta\right\}$ the deviatoric back-stress tensor. The evolution of the back-stress, determines the type of hardening introduced in the material model during subsequent cycles of loading and unloading. A commonly used type of

hardening is the linear kinematic hardening assumption which dictates a constant plastic modulus during plastic loading. This is accomplished by demanding:

$$\{\dot{\eta}\} = C\{\dot{\varepsilon}^p\} \tag{3.46}$$

where C is defined as the hardening material constant.

A key concept of classical plasticity is the additive decomposition of the strain into reversible elastic and irreversible plastic components. Consequently, the additive decomposition of the strain rate is established as:

$$\{\dot{\varepsilon}\} = \{\dot{\varepsilon}^{el}\} + \{\dot{\varepsilon}^{p}\} \Rightarrow \{\dot{\varepsilon}^{el}\} = \{\dot{\varepsilon}\} - \{\dot{\varepsilon}^{p}\} \tag{3.47}$$

where $\{\dot{\varepsilon}\}$ is the rate of the total deformation tensor, while $\{\dot{\varepsilon}^{el}\}$ is the rate of the elastic part of the total deformation vector. Based on observations, the unloading stiffness of a plastified material is considered equal to the elastic and thus the following relation holds between the total stress tensor and the elastic part of the strain rate:

$$\{\dot{\sigma}\} = [D]\{\dot{\varepsilon}^{el}\} \tag{3.48}$$

where $[D]$ is the elastic constitutive matrix. Substituting equation (3.42) into relation (3.47) and using relation (3.48) the following equation is derived:

$$\{\dot{\sigma}\} = [D]\left(\{\dot{\varepsilon}\} - \dot{\lambda}\frac{\partial\Phi(\{\sigma\})}{\partial\{\sigma\}}\right) \tag{3.49}$$

By means of the consistency condition (equation (3.44)) and relation (3.49) the value of the plastic multiplier $\dot{\lambda}$ is evaluated as:

$$\dot{\lambda}\dot{\Phi} = 0 \Rightarrow \dot{\lambda}\left(\left(\frac{\partial\Phi}{\partial\{\sigma\}}\right)^T\{\dot{\sigma}\} + \left(\frac{\partial\Phi}{\partial\{\eta\}}\right)^T\{\dot{\eta}\}\right) = 0 \tag{3.50}$$

When at yield, Φ=0 and $\dot{\lambda}$>0 and thus relation (3.50) can be written as:

$$\left(\frac{\partial\Phi}{\partial\{\sigma\}}\right)^T\{\dot{\sigma}\}+\left(\frac{\partial\Phi}{\partial\{\eta\}}\right)^T\{\dot{\eta}\}=0\Rightarrow\left(\frac{\partial\Phi}{\partial\{\sigma\}}\right)^T\{\dot{\sigma}\}=-\left(\frac{\partial\Phi}{\partial\{\eta\}}\right)^T\{\dot{\eta}\} \quad (3.51)$$

Premultiplying relation (3.49) with $\partial\Phi/\partial\{\sigma\}$ the following equation is derived:

$$\left(\frac{\partial\Phi}{\partial\{\sigma\}}\right)^T\{\dot{\sigma}\}=\left(\frac{\partial\Phi}{\partial\{\sigma\}}\right)^T[D]\left(\{\dot{\varepsilon}\}-\dot{\lambda}\frac{\partial\Phi(\{\sigma\})}{\partial\{\sigma\}}\right) \quad (3.52)$$

Substituting equation (3.51) into equation (3.52) the following relation is established:

$$-\left(\frac{\partial\Phi}{\partial\{\eta\}}\right)^T\{\dot{\eta}\}=\left(\frac{\partial\Phi}{\partial\{\sigma\}}\right)^T[D]\left(\{\dot{\varepsilon}\}-\dot{\lambda}\frac{\partial\Phi(\{\sigma\})}{\partial\{\sigma\}}\right) \quad (3.53)$$

In classical plasticity the hardening law is defined as a relation between the back-stress tensor and the plastic strain tensor. This relation can be either rate dependent or rate independent. In any case, the back-stress is finally derived as a function of the plastic multiplier $\dot{\lambda}$ and one can write:

$$\{\dot{\eta}\}=\dot{\lambda}G(\{\eta\},\Phi) \quad (3.54)$$

Substituting relation (3.54) into equation (3.53) the following relation is derived:

$$-\left(\frac{\partial\Phi}{\partial\{\eta\}}\right)^T\dot{\lambda}G(\{\eta\},\Phi)=\left(\frac{\partial\Phi}{\partial\{\sigma\}}\right)^T[D]\left(\{\dot{\varepsilon}\}-\dot{\lambda}\frac{\partial\Phi(\{\sigma\})}{\partial\{\sigma\}}\right) \quad (3.55)$$

Rearranging and solving for the plastic multiplier the following expression is derived:

$$\dot{\lambda}=\left(-\left(\frac{\partial\Phi}{\partial\{\eta\}}\right)^T G(\{\eta\},\Phi)+\left(\frac{\partial\Phi}{\partial\{\sigma\}}\right)^T[D]\frac{\partial\Phi(\{\sigma\})}{\partial\{\sigma\}}\right)^{-1}\left(\frac{\partial\Phi}{\partial\{\sigma\}}\right)^T[D]\{\dot{\varepsilon}\} \quad (3.56)$$

In the case of the elastic perfectly plastic material G=0, and relation (3.56) coincides with the one proposed by Casciati, 2006. Equations (3.51) to (3.56) hold when yielding has occurred, either in the positive or in the negative semi-plane and thus by introducing the following Heaviside functions:

$$H_1\left(\Phi\right)=\begin{cases}1, & \Phi=0\\ 0, & \Phi<0\end{cases}\qquad H_2\left(\dot{\Phi}\right)=\begin{cases}1, & \dot{\Phi}>0\\ 0, & \dot{\Phi}<0\end{cases} \tag{3.57}$$

a single relation is established for the plastic multiplier, in the whole domain of the strain tensor:

$$\dot{\lambda}=H_1H_2\left(-\left(\frac{\partial\Phi}{\partial\{\eta\}}\right)^T G\left(\{\eta\},\Phi\right)+\left(\frac{\partial\Phi}{\partial\{\sigma\}}\right)^T[D]\frac{\partial\Phi\left(\{\sigma\}\right)}{\partial\{\sigma\}}\right)^{-1}\left(\frac{\partial\Phi}{\partial\{\sigma\}}\right)^T[D]\{\dot{\varepsilon}\} \tag{3.58}$$

Instead of describing the cyclic behavior of a material in a step-wise approach considering the domains of the Kuhn-Tucker conditions (Fig.3.7(a)) or of the correspondent Heaviside functions (Fig.3.7(b)), Casciati, proposed the smoothening of the latter, introducing additional material parameters.

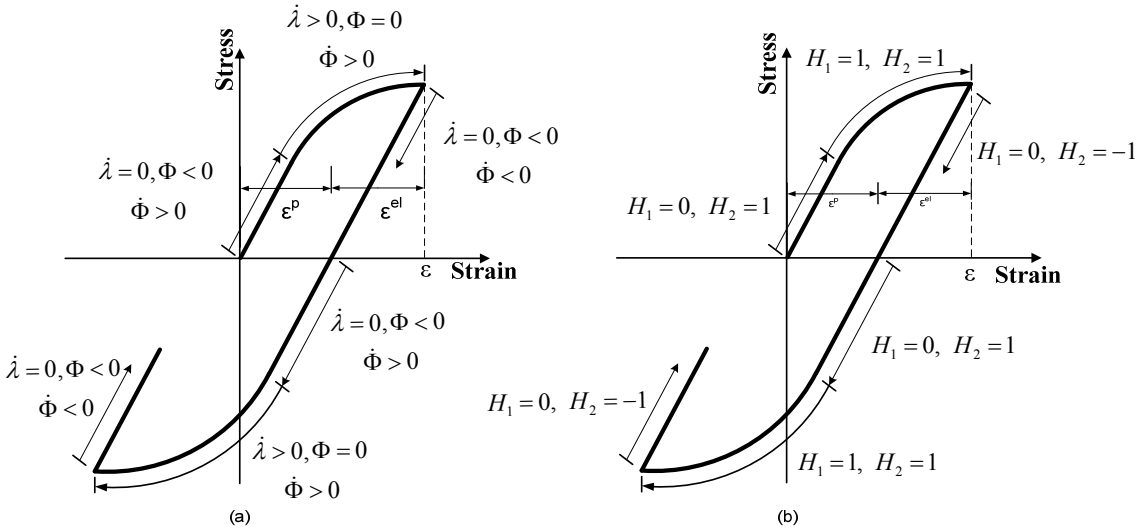

Fig.3.7 (a) Inelastic Cyclic Response (b) Heaviside Functions

According to this approach, the two Heaviside functions are smoothened using the following expressions:

$$H_1 = \left|\frac{\Phi}{\Phi_0}\right|^N, \quad N \geq 2 \tag{3.59}$$

and:

$$H_2 = H\left(\left(\frac{\partial \Phi}{\partial \sigma}\right)^T \{\dot{\sigma}\}\right) = \frac{1+\operatorname{sgn}\left(\left(\frac{\partial \Phi}{\partial \sigma}\right)^T \{\dot{\sigma}\}\right)}{2} \approx \beta + \gamma \operatorname{sgn}\left(\{\varepsilon\}^T \{\dot{\sigma}\}\right) \tag{3.60}$$

where N, β and γ are model parameters and Φ_0 is the maximum value of the yield function or yield point. In the special case where $\beta = \gamma = 0.5$, the unloading stiffness is equal to the elastic one. The model proposed by Baber-Noori is thermodynamically admissible as long as relation (3.41) is satisfied. An immediate consequence of equation (3.59) is that the material is allowed to yield even before the theoretical yield point is reached $\left(\Phi_0\right)$. Rearranging equation (3.49) and substituting the definition of the plastic multiplier, the following Bouc-Wen model is derived:

$$\{\dot{\sigma}\} = [D]\left([I] - \left|\frac{\Phi}{\Phi_0}\right|^N \left(\beta + \gamma \operatorname{sgn}\left(\{\varepsilon\}^T \{\dot{\sigma}\}\right)\right)[R]\right)\{\dot{\varepsilon}\} \tag{3.61}$$

where the matrix [R] is evaluated as:

$$[R] = \left(-\left(\frac{\partial \Phi}{\partial \{\eta\}}\right)^T G(\{\eta\}, \Phi) + \left(\frac{\partial \Phi}{\partial \{\sigma\}}\right)^T [D] \frac{\partial \Phi(\{\sigma\})}{\partial \{\sigma\}}\right)^{-1} \left(\frac{\partial \Phi}{\partial \{\sigma\}}\right)\left(\frac{\partial \Phi}{\partial \{\sigma\}}\right)^T [D] \tag{3.62}$$

and defines the interaction relation between the components of the stress tensor at yield. Thus, the step-wise plasticity equations of relation (3.43) are replaced by a continuous stress-strain relation. In the uniaxial case, the von Mises yield criterion is reduced to the following form:

$$\Phi_{VM} = \frac{\left(\sigma_{11} - \eta_{11}\right)^2}{\left(\sigma_y\right)^2} - 1$$

and accordingly, relation (3.61) becomes:

$$\dot{\sigma}_{11} = E\left(1 - \frac{E}{c+E}\left|\frac{\sigma_{11} - \eta_{11}}{\sigma_y}\right|^{2N}\left(\beta + \gamma\,\mathrm{sgn}\left(\varepsilon_{11}\dot{\sigma}_{11}\right)\right)\right)\dot{\varepsilon}_{11} \tag{3.63}$$

The similarities between equation (3.63) and Bouc's derivation of the hysteretic parameter z in equation (3.32) are evident.

3.4.1 A subcase – the parallel generalized model of hysteresis

The generalized parallel model of Bouc-Wen introduced by Karray and Bouc (Wen, 1980, Casciati, 2006) is a subcase of the formulation presented in the previous Section. Generalizing the parallel spring concept introduced in Fig.3.4(a), the stress tensor is decomposed into an elastic and hysteretic part as follows:

$$\left\{\sigma\right\} = \left[\alpha\right]\left\{\sigma^e\right\} + \left(\left[I\right] - \left[\alpha\right]\right)\left\{\sigma^h\right\} \tag{3.64}$$

where $\left[\alpha\right]$ denotes a square diagonal matrix with post yield to elastic stiffness ratios, which for an isotropic material is considered constant in every direction, $\left[I\right]$ is the identity matrix, while the elastic part $\left\{\sigma^e\right\} = \left\{\sigma^e_{11} \quad \sigma^e_{22} \quad \sigma^e_{12}\right\}^T$ is expressed by the following relation:

$$\left\{\sigma^e\right\} = \left[D\right]\left\{\varepsilon\right\} \tag{3.65}$$

where $\left[D\right]$ is the elastic constitutive matrix. The hysteretic part $\left\{\sigma^h\right\} = \left\{\sigma_{11}^h \quad \sigma_{22}^h \quad \sigma_{12}^h\right\}^T$ evolves according to the following Bouc-Wen hysteretic rule (Sivaselvan and Reinhorn, 2003):

$$\begin{Bmatrix} \dot{\sigma}_{11}^h \\ \dot{\sigma}_{22}^h \\ \dot{\sigma}_{12}^h \end{Bmatrix} = \left[D\right]\left([I] - H_1 H_2\left[\tilde{R}\right]\right)\begin{Bmatrix} \dot{\varepsilon}_{11} \\ \dot{\varepsilon}_{22} \\ \dot{\varepsilon}_{12} \end{Bmatrix} \tag{3.66}$$

where H_1, H_2 and are smoothed Heaviside functions defined in equations (3.59) and (3.60) respectively while $\left[\tilde{R}\right]$ is the interaction matrix defined in equation (3.62) setting $G \equiv 0$. However, equations (3.64) to (3.66) are capable of simulating hysteretic systems with linear kinematic hardening. Clearly this limits the applicability of the model.

Writing equation (3.64) in rate form and substituting relation (3.66) the following equation is derived:

$$\left\{\dot{\sigma}\right\} = \left[\alpha\right]\left[D\right]\left\{\dot{\varepsilon}\right\} + \left(\left[I\right] - \left[\alpha\right]\right)\left[D\right]\left([I] - H_1 H_2\left[\tilde{R}\right]\right)\left\{\dot{\varepsilon}\right\} \tag{3.67}$$

Matrix $\left[\alpha\right]$ is diagonal, thus relation (3.67) can be cast on the following form:

$$\left\{\dot{\sigma}\right\} = \left[D\right]\left(\left[\alpha\right] + \left[I\right] - \left[\alpha\right]\left([I] - H_1 H_2\left[\tilde{R}\right]\right)\right)\left\{\dot{\varepsilon}\right\} \tag{3.68}$$

Comparing equations (3.61) and (3.68) the following generalized relation can be derived:

$$\left\{\dot{\sigma}\right\} = \left[D\right]\left(\left[\mathrm{Z}_1\right] + \left[\mathrm{Z}_2\right]\left([I] - H_1 H_2\left[R\right]\right)\right)\left\{\dot{\varepsilon}\right\} \tag{3.69}$$

where in the case of the generalized model:

$$\begin{aligned} \left[\mathrm{Z}_1\right] &= \left[I\right] \\ \left[\mathrm{Z}_2\right] &= -\left[I\right] \end{aligned} \tag{3.70}$$

while in the case of the parallel model:

$$\begin{aligned} \left[\mathrm{Z}_1\right] &= \left[\alpha\right] \\ \left[\mathrm{Z}_2\right] &= \left[I\right] - \left[\alpha\right] \\ \left[R\right] &= \left[R\right]\big|_{G=0} \end{aligned} \tag{3.71}$$

3.4.2 Numerical experiments

A steel von Mises type specimen $dxdydz$ under uniaxial cyclic tension is examined. Two loading-unloading cycles are considered with a peak value of tensile stress equal to $p = 1.20\sigma_y$ (Fig. 3.8). The material parameters are $\sigma_y = 235\,\mathrm{MPa}$, $E = 210\,\mathrm{GPa}$, $\nu = 0.3$. Linear kinematic hardening of the Melan-Prager type (Section 1.4.4) is considered with a constant hardening parameter $c = 4117647\,\mathrm{KPa}$.

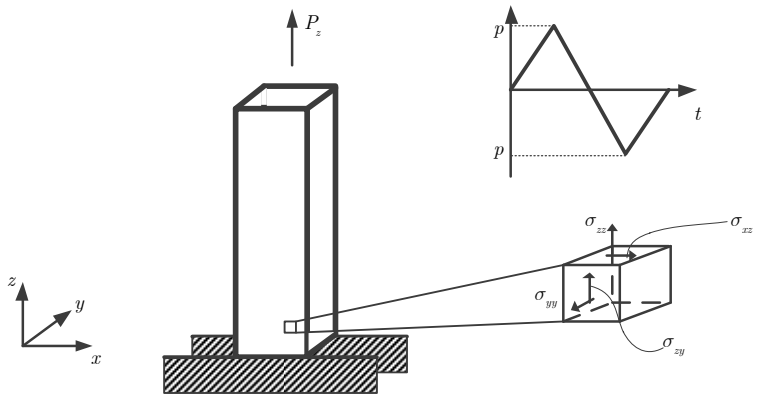

Fig. 3.8 Cyclic uniaxial tensile test

In Fig.3.9, the normal stress component σ_{11} is plotted with respect to the corresponding strain ε_{11} for different values of the model parameters n, β, γ .The discrepancies are not as striking as in the uniaxial formulation presented in Fig.3.5 due to the effects of kinematic hardening. However, the same qualitative conclusions are drawn. In Fig.3.9(a) the stress-strain plot is presented for different values of parameter n considering linear unloading branches with $\beta = \gamma = 0.5$. Again, as the value of parameter n increases, the stress-strain plot tends

towards the sharp bilinear curve. In Fig.3.9(b), the evolution of the Von Mises equivalent stress ($\sigma_{VM} = \left|\sigma_{11} - \eta_{11}\right|$) for different values of the smoothening parameter n is presented.

In Fig.3.9(c) the influence of parameter β is examined, fixing the values of $n = 2$ and $\gamma = 0.5$. As the value of β decreases the hysteretic loop bulges while an increasing value of β results in a narrower hysteretic loop. However, when $\beta < -\gamma$, the hysteretic loop degenerates into an S type of curve with increasing stiffness at the nonlinear regime. In Fig.3.9(d) the effect of parameter γ is examined, setting $n = 2, \beta = 0.5$. As γ decreases the unloading branches tend to bend inwards. A negative value of parameter γ results in instabilities (Ikhouane & Rodellar, 2007) and thus is not considered in this work.

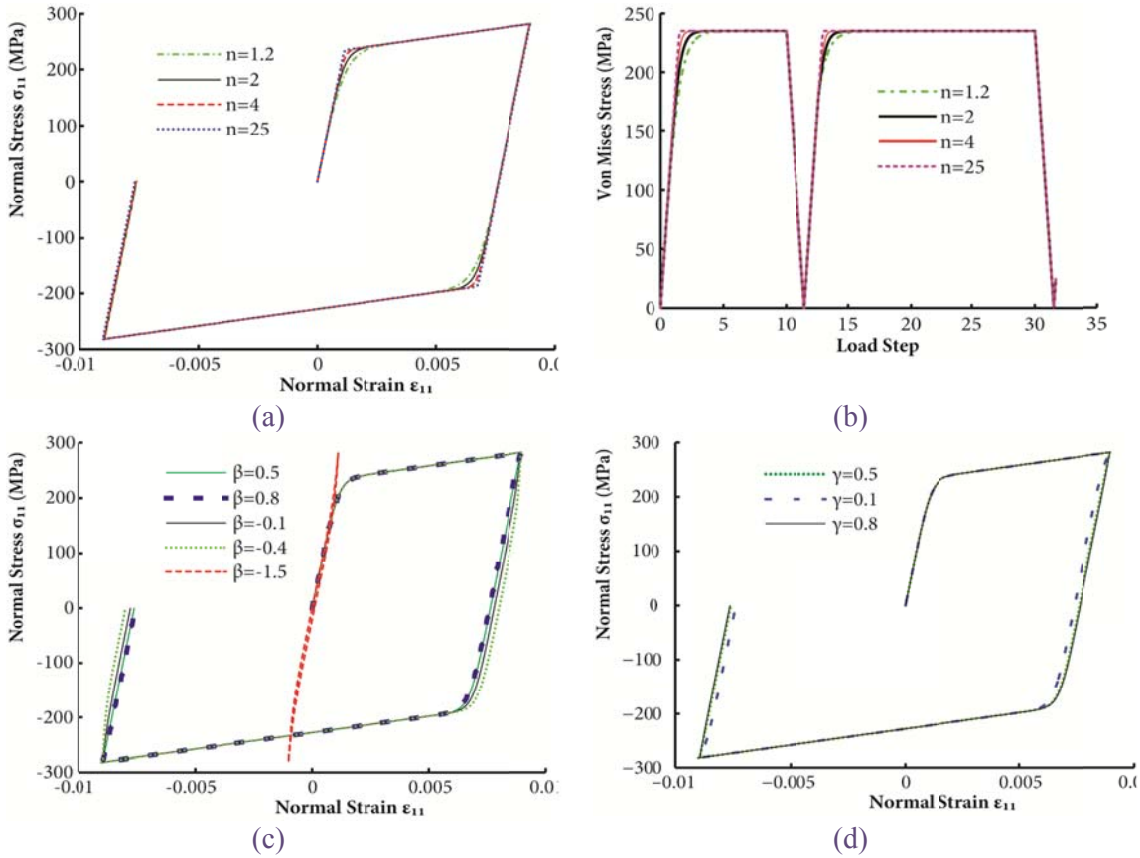

Fig.3.9 Cyclic Tension experiment stress- strain plots (a) Variation of parameter n for $\beta = \gamma = 0.5$ (b) Evolution of the Von Misses Stress for different values of parameter n (c) Variation of parameter β for n =2, γ =0.5 (d) Variation of parameter γ for n =2, β =0.5

Next, a concrete specimen is considered with the following set of properties, namely $\sigma_c = 25MPa$, $\sigma_t = 1.8MPa$ while the concrete strength under biaxial compression is estimated at $\sigma_b = 1.15\sigma_c = 28.75MPa$ (Newman and Choo, 2003). The Bresler-Pister yield criterion is implemented (equation 1.27). The elastic modulus and Poisson's ratio are $E = 30.5GPa$ and $\nu = 0.2$ respectively. The set of Bouc-Wen parameters utilized in this simulation is $\beta = \gamma = 0.5$ and $n = 2$. Since plain concrete does not demonstrate a significant hardening behavior, a small kinematic hardening constant is considered $c = 9000$ KPa.

A cyclic imposed strain experiment is simulated with a maximum imposed strain $\varepsilon_{11} = 0.003$. The strain envelop is presented in Fig.3.10(a).

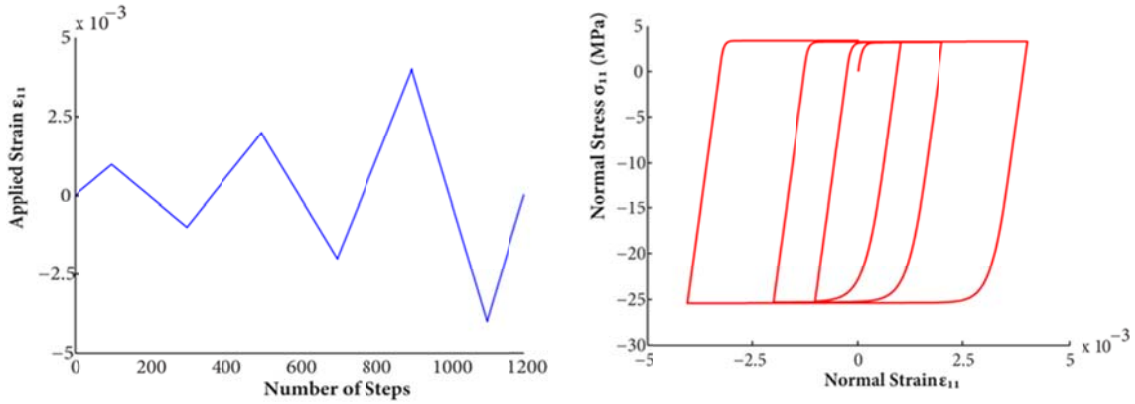

(a) (b)

Fig.3.10(a) Imposed Strain envelop (b) Stress-Strain plot

The derived stress-strain plot is presented in Fig.3.10(b). As dictated by the yield criterion implemented, the hysteretic loops are non-symmetric since the tensile strength of the specimen is significantly smaller than the compressive one. Thus, the proposed formulation is able of simulating both symmetric and non-symmetric hysteresis by choosing appropriate yield criteria without reverting to mathematical formulations without a clear physical interpretation.

3.5 Cyclic loading induced phenomena

The hysteretic loops presented in Fig.3.10(b) fail to correctly simulate the real behavior of concrete under cyclic loading. Two main mechanisms are observed in concrete cyclic behavior, namely the stiffness degradation and strength deterioration mechanism. Both are related to the damage sustained by the solid due to propagating micro-cracks and are mainly treated within the framework of Damage Mechanics (Krajcinovic, 1996, Voyiadjis and Kattan, 2005). The main aspect of Damage Mechanics is the definition of the fourth-rank damage tensor whose evolution is determined through phenomenological damage flow rules. This derivation, though accurate and robust, leads to cumbersome formulations when implemented into the finite element scheme. An exhaustive presentation on the subject can be found on Kattan and Voyiadjis, 2001. In this work, attention is drawn towards the derivation of appropriate smooth operators that account for stiffness degradation and strength deterioration when applied onto the Bouc-Wen evolution equations, expressed in stress-strain form. This idea has been successfully implemented in uniaxial piece-wise linear stress-strain relations (Cope et al., 2005) but not in the general, three-dimensional, case.

In the uniaxial case, Baber and Wen (1981) introduced two additional model parameters to account for stiffness degradation and strength deterioration phenomena. Relation (3.36) was modified as follows:

$$\dot{z}(t) = \frac{\dot{u}}{n_s}\left[1 - \nu_s \left|\frac{z}{z_y}\right|^n \left(\beta + \gamma\,\mathrm{sgn}\left(z\dot{u}\right)\right)\right] \tag{3.72}$$

where n_s is related to stiffness degradation and v_s to strength deterioration. Both parameters depend on the hysteretic energy density e^h (i.e. energy per unit volume) dissipated by the model and are defined as:

$$n_s = 1 + c_{n,s} e^h, \qquad v_s = 1 + c_{v,s} e^h, \qquad c_{n,s} \geq 0, \qquad c_{v,s} \geq 0 \tag{3.73}$$

The energy density accumulated into the hysteretic spring(Fig.3.4) due to plastic dissipation is evaluated, using relation as:

$$e^h = \oint (1-\alpha) Ez(t) d\varepsilon \tag{3.74}$$

Analytical expressions for the amount of hysteretic energy accumulated under T – periodic excitations, were derived by Charalampakis & Koumousis (2008b) using hyper-geometric functions. The introduced material constants $c_{n,s}$ and $c_{v,s}$ can be identified by various identification techniques.

Erlicher and Bursi (2009) proved the thermodynamic admissibility of Bouc-Wen models with stiffness degradation and strength deterioration based on a similarity approach to endochronic plasticity models of Valanis (1971). According to their results a degradation rule is thermodynamically admissible, provided that the following condition is satisfied:

$$\dot{\eta} \leq \eta \nu \dot{\xi} \tag{3.75}$$

where η is a given degradation function, ν is a given deterioration function and ξ the model's intrinsic time in the context of endochronic theory. In the present work, the following functions are considered for stiffness degradation and strength deterioration modelling respectively:

$$\dot{\eta}_s = c_\beta \left(\frac{1}{n_s} \right)^{m_u} \beta \nu_s \dot{\xi}, \quad v_s = 1 + c_{v,s} e^h \tag{3.76}$$

where $m > 0$ and $c_\beta > 0$. The rate $\dot{\xi}$ is the intrinsic time of the Bouc-Wen model as defined in Erlicher and Bursi (2009), given by the following relation:

$$\dot{\xi} = \left(1 + \frac{\gamma}{\beta}\operatorname{sgn}\left(z\dot{u}\right)\right)\left|\dot{u}\right|\left(\frac{z}{z_y}\right)^{n-1} \tag{3.77}$$

Relations (3.76) and (3.77) constitute a thermodynamically admissible set of degradation functions that can be used to model a specific material given the proper set of model parameters. Both the stiffness degradation parameter n_s and the strength deterioration parameter v_s are analogous to the hysteretic energy accumulated, and thus increasing functions of time.

3.5.1 A pure-shear test

To reveal the interesting and compact features of the Bouc-Wen hysteretic model, a generic case is presented that corresponds to a pure- shear test under sinusoidal excitation $p\left(t\right) = \sin\left(\pi/6\, t\right)$. In Fig.3.11**,** the shear stress is plotted against shear strain. A bilinear material law is considered with a yield stress equal to 117.5 MPa and an elastic shear modulus equal to 81 GPa. The following set of Bouc-Wen parameters is selected: $\alpha = 0.002$, $n = 2$, $\beta = \gamma = 0.5$, $m_u = 2$, $c_\beta = 25$ and $c_v = 0.0001$ while the yield shear strain is $\gamma_y = 0.00145$.

The resulting shear stress-shear strain plot is presented in Fig.3.11(a). The unloading stiffness is repeatedly decreasing as the accumulated hysteretic energy increases. At the same time the yield strength of the specimen is decreasing.

In Fig.3.11(b) the evolution of the stiffness degradation parameter is presented with respect to time. As expected η_s is a constantly increasing function of time. The value of the stiffness degradation parameter remains constant during elastic loading and unloading where no hysteretic energy is being accumulated. This corresponds to the hysteretic energy time history presented in Fig.3.11(c).

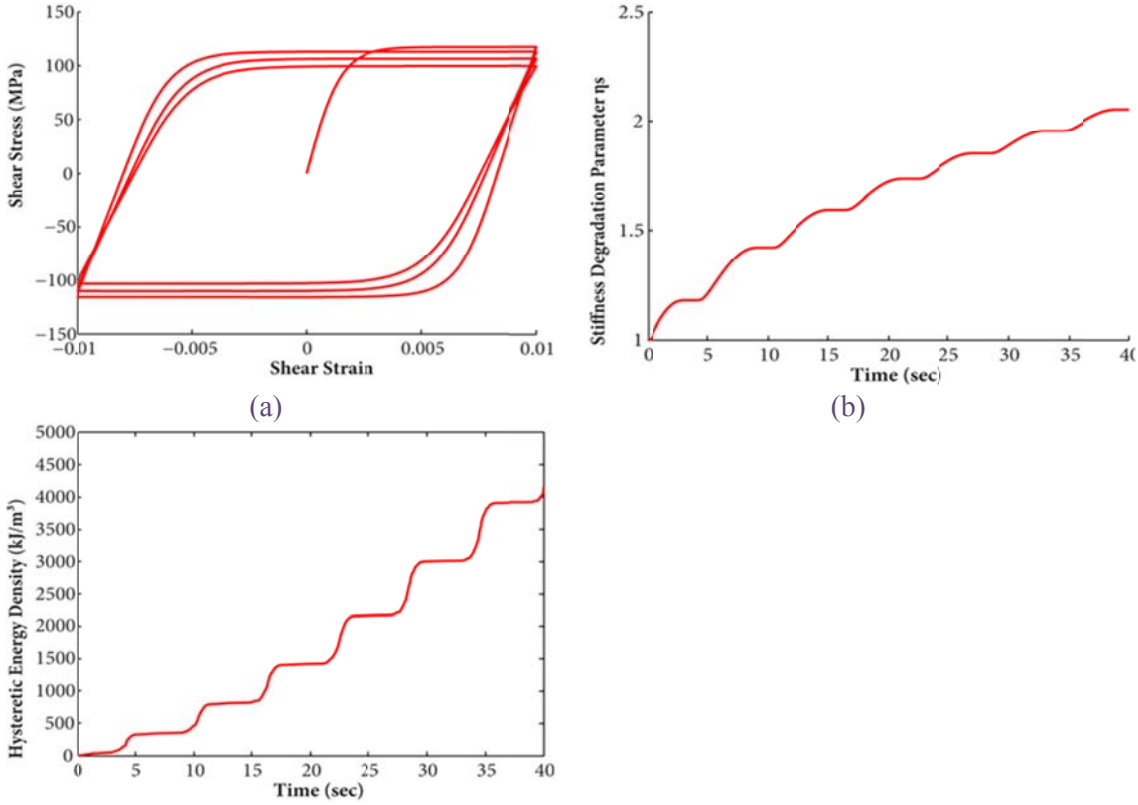

Fig.3.11(a) Shear Stress – Shear Strain hysteretic loop with stiffness degradation and strength deterioration (b) Evolution of the stiffness degradation parameter (c) Evolution of hysteretic energy

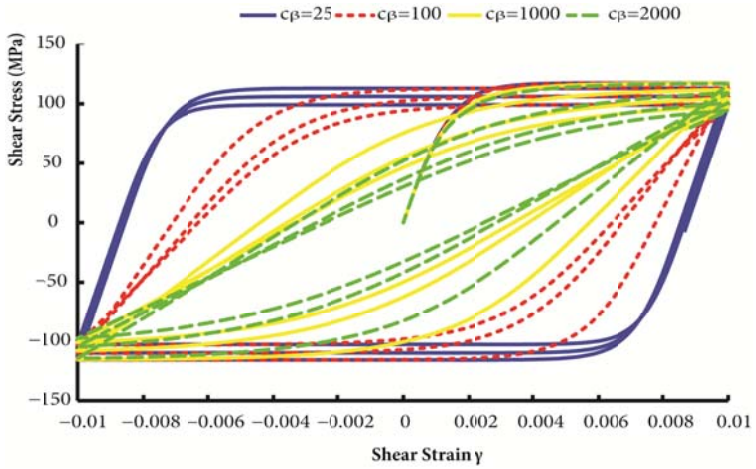

Fig. 3.12 Dependence of the hysteresis shape on the stiffness degradation parameter

The variation of the stiffness degradation parameter c_β greatly alters the shape of the hysteretic loop, as presented in Fig. 3.12. Parameter c_β controls the actual value of the

stiffness reduction between subsequent hysteretic loops. Large values of c_β lead to increasing values of stiffness degradation. In Fig. 3.12, four different values of c_β are considered while the strength deterioration parameter is set to $c_v = 0.0001$ and $m_u = 2$.

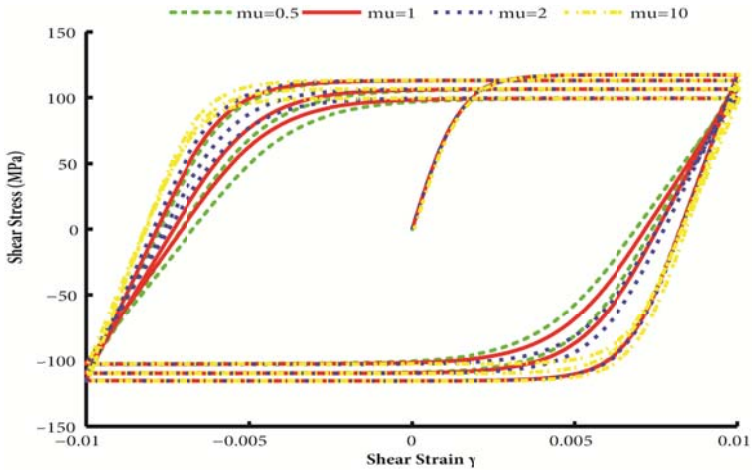

Fig. 3.13 The stiffness degradation parameter m_u

The effect of m_u on the stiffness degradation is presented in Fig. 3.13. Parameter m_u controls the rate of stiffness degradation, that is the speed by which the degradation phenomenon evolves. Smaller values of m_u give rise to quickly deteriorating hysteretic loops. In Fig. 3.13, four values of m_u are considered while $c_v = 0.0001$ and $c_\beta = 25$.

3.5.2 Generalization in the three dimensional stress space

In the work of Erlicher and Bursi (2009) stiffness degradation and strength deterioration relations are provided for a single degree and a two degree of freedom uncoupled hysteretic system in translational motion. Additionally, a stress-strain formulation of the Bouc-Wen model is presented for incompressible plasticity. This formulation is then extended to account for stiffness degradation and strength deterioration phenomena. Though precise, the relationships proposed cannot be directly introduced into the finite element scheme, as they involve the trace of the strain vector and the deviatoric stress and strain tensors. Moreover,

their derivation is explicitly based on the plastic incompressibility assumption and specifically on a von-Mises type of material.

In this work, equations (3.76) and (3.77) are extended to account for stiffness degradation and strength deterioration effects in a general elastoplastic solid, based on the derivation presented on section 3.4. The intrinsic time is extended herein for the 3d stress space as:

$$\dot{\xi} = \beta H_1 (1 + \frac{\gamma}{\beta} sign\left(\{\sigma\}^T \{\dot{\varepsilon}\} \right) \left| \{\sigma\}^T \{\dot{\varepsilon}\} \right| \tag{3.78}$$

where H_1 is defined in equation (3.79).

Introducing the same set of model parameters as in the uniaxial case, namely the stiffness degradation parameter c_b and the strength deterioration parameter v_s, the following equations are established:

$$\begin{aligned} \{\dot{\sigma}\} &= \frac{1}{\eta}[D]([I] - H_1 H_2 [R])\{\dot{\varepsilon}\} \\ \dot{\eta} &= c_b \left(\frac{1}{\eta} \right)^{m_u} \beta H_1 (1 + \frac{\gamma}{\beta} sign\left(\{\sigma\}^T \{\dot{\varepsilon}\} \right) \left| \{\sigma\}^T \{\dot{\varepsilon}\} \right| \\ \mathrm{v}_s &= 1 + c_b e_h \\ H_1 &= \mathrm{v}_s \left\| \Phi(\{\sigma\}) + 1 \right\|^n \end{aligned} \tag{3.79}$$

where, e_h is the energy density accumulated in the hysteretic component, and η, v_s are the stiffness degradation and strength deterioration parameters respectively. The hysteretic energy density is computed by means of numerical integration using the following relation:

$$e_h = \oint \{\sigma^h\} d\{\varepsilon\} \tag{3.80}$$

A computational advantage of this formulation is the fact that both the stiffness degradation and strength deterioration schemes are coupled through a single evolution

equation thus reducing the modeling to a single additional evolution equation rather than two as proposed in (Sivaselvan & Reinhorn, 2000).

3.5.3 The case of asymmetric hysteresis

In the general case of asymmetric hysteresis, one can use the extended Bouc-Wen model as defined by Dobson et al. (1997):

$$\dot{z}(t) = f(\dot{\varepsilon}(t), z(t)) = \dot{\varepsilon}(t)\left[1 - \beta_1 \,''_1 - \beta_2 \,''_2 - \beta_3 \,''_3 - \beta_4 \,''_4\right] \tag{3.81}$$

where B_1, B_2, B_3 and B_4 control the shape of the hysteretic loop for each direction of loading as illustrated in Fig.3.14, and their corresponding expressions are:

$$''_1 = \frac{1 + sign(\dot{\varepsilon}(t)z(t))}{2}\left(\frac{|\, z(t)\,| + z(t)}{2z_y^+}\right)^{n_B} \tag{3.82}$$

$$''_2 = \frac{1 + sign(\dot{\varepsilon}(t)z(t))}{2}\left(\frac{|\, z(t)\,| - z(t)}{2z_y^+}\right)^{n_C} \tag{3.83}$$

$$''_3 = \frac{1 - sign(\dot{\varepsilon}(t)z(t))}{2}\left(\frac{|\, z(t)\,| + z(t)}{2z_y^+}\right)^{n_D} \tag{3.84}$$

$$''_4 = \frac{1 - sign(\dot{\varepsilon}(t)z(t))}{2}\left(\frac{|\, z(t)\,| - z(t)}{2z_y^+}\right)^{n_E} \tag{3.85}$$

The exponents n_B, n_C, n_D and n_E in equations (3.82) to (3.85) control the smoothness of the transition from the elastic to the plastic regime. Parameters β_1, β_2, β_3, β_4 are switch type of parameters. If $\beta_i = 0, i = 1..4$ then the corresponding branch of the hysteretic loop is a straight line with an unloading stiffness equal to the elastic one. When $\beta_i > 0, i = 1..4$ then the corresponding branch is curved. Greater values of β_i

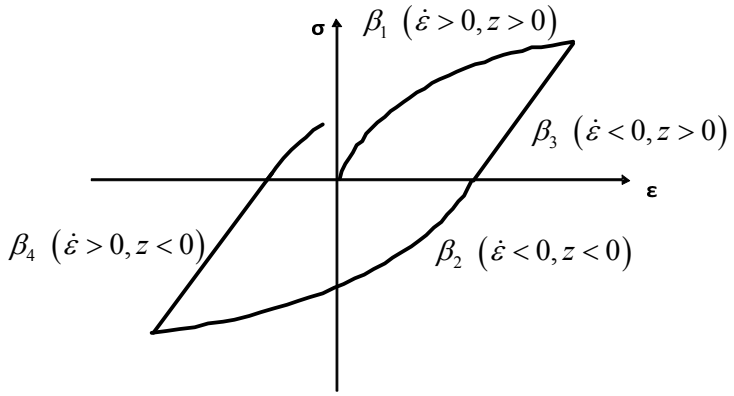

Fig.3.14Shape controlling coefficients of the extended Bouc-Wen model

The parameters β_3, β_4 control the stiffness of the hysteretic loop after unloading occurs. Assigning null values for both, results to unloading stiffness equal to that of the elastic branch. Also, the model is capable of simulating non symmetrical yielding, so if the positive yield strain z_y^+ is regarded as a reference point, the resulting values for β and γ result as follows:

$$\beta_1 = \frac{1}{d^{n_B}} \text{ where d=1}, \quad \beta_2 = \frac{1}{e^{n_C}} \text{ where, } e = \frac{-z_y^-}{z_y^+} \tag{3.86}$$

Replacing equations (3.86) into relation (3.81) and considering the expressions of the individual branches defined in equations (3.82) to (3.85), the following expression is derived for the reloading branch ($\left(\dot{\varepsilon}<0, z<0\right)$:

$$\dot{z}(t) = f(\dot{\varepsilon}(t), z(t)) = \dot{\varepsilon}(t)\left[\left(\frac{-z_y^+}{z_y^-}\right)^{nc} \frac{1+sign(\dot{\varepsilon}(t)z(t))}{2}\left(\frac{|z(t)|-z(t)}{2z_y^+}\right)^{n_C}\right] \tag{3.87}$$

The formulation introduced in relation (3.61) generalizes equation (3.81) in the sense that the hysteretic parameter is introduced in the three-dimensional space. Furthermore, the case of asymmetric hysteresis is treated in a consistent manner through the introduction of a proper yield function, as in the case of the Bresler-Pister yield surface in Section 3.4.2.

3.6 Conclusions

In this chapter, the properties of hysteretic systems are presented and the expression of the Bouc-Wen model is derived accordingly, based on concepts of the mathematical theory of hysteresis. As an example, the equation of the perfect slider is derived as the limit case of the initial model proposed by Bouc. Next, a general form of the Bouc-Wen model is derived in stress-strain form, based on the phenomenological concepts of the classical theory of plasticity. A rate form of the stress tensor is derived that accounts for the full cyclic behavior of the continuum. This rate form is general in the sense that it accounts for every combination of yield criteria and hardening laws whereas existing formulations only describe hysteretic behavior with linear kinematic hardening.

Based on concepts borrowed from the endochronic theory of plasticity, additional smooth operators are derived that account for the cyclic induced stiffness degradation and strength deterioration phenomena observed in brittle materials. The formulation derived depends on total stress components rather than their deviatoric parts, thus yielding a formulation that is easily incorporated in the Finite Element scheme, as will be presented in subsequent chapters.

3.7 APPENDIX I

The analytical relations of the interaction matrix [R] are presented below for the case of two widely used yield surfaces, namely the von-Mises yield surface and the Bresler – Pister yield surface. Similarly, other smooth surface models can be utilized, (Hinchberger S.D., 2009).

3.7.1 von-Mises yield surface

For the case of two-dimensional plasticity, the von-Mises yield surface is defined as the locus of points in the stress space defined by the following relation, (Lubliner 2008):

$$\left\{\Phi\right\}_{VM} = \frac{\left(\sigma_{11}-\sigma_{22}\right)^2+\left(\sigma_{11}\right)^2+\left(\sigma_{22}\right)^2+6\left(\sigma_{12}\right)^2}{2\left(\sigma_y\right)^2}-1=0 \tag{A1}$$

where $\sigma_y^h = \left(1-\alpha\right)\sigma_y$.

The yield gradient with respect to the von-Mises yield surface is:

$$\frac{\partial\Phi}{\partial\left\{\sigma\right\}} = \left\{\frac{2\sigma_{11}-\sigma_{22}}{\left(\sigma_y\right)^2} \quad \frac{2\sigma_{22}-\sigma_{11}}{\left(\sigma_y\right)^2} \quad 6\frac{\sigma_{12}}{\left(\sigma_y\right)^2}\right\}^T \tag{A2}$$

Utilizing relation (3.62), the interaction matrix $\left[R\right]$ is derived as:

$$\left[R\right]_{VM} = \lambda[IR] \tag{A3}$$

where $\left[IR\right]$ is a 3x3 matrix defined as:

$$
\begin{aligned}
[IR] &= \begin{bmatrix} -\Delta_1\Sigma_1 & \Delta_1\Sigma_2 & \dfrac{3\sigma_{12}\Delta_1}{1-\nu} \\ \Delta_2\Sigma_1 & -\Delta_2\Sigma_2 & -\dfrac{3\sigma_{12}\Delta_2}{1-\nu} \\ 6\sigma_{12}\Sigma_1 & 6\sigma_{12}\Sigma_2 & \dfrac{18\left(\sigma_{12}\right)^2}{1-\nu} \end{bmatrix} \\
\Delta_1 &= \left(2\sigma_{11}-\sigma_{22}\right),\ \ \Delta_2 = \left(\sigma_{11}-2\sigma_{22}\right) \\
\Sigma_1 &= \left(2\sigma_{11}-\sigma_{22}+\nu\sigma_{11}-2\nu\sigma_{22}\right),\ \ \Sigma_2 = \left(2\nu\sigma_{11}-\nu\sigma_{22}+\sigma_{11}-2\sigma_{22}\right)
\end{aligned}
\tag{A4}
$$

and λ is a constant:

$$
\begin{aligned}
\lambda &= -\frac{1}{5A+2\nu B-18\left(\sigma_{12}\right)^2-\Gamma} \\
A &= \left(\sigma_{11}\right)^2+\left(\sigma_{22}\right)^2-2\nu\sigma_{11}^h\sigma_{22}^h \\
B &= 2\left(\sigma_{11}\right)^2+2\left(\sigma_{22}\right)^2+9\left(\sigma_{12}\right)^2 \\
\Gamma &= 8\sigma_{11}\sigma_{22}
\end{aligned}
\tag{A5}
$$

The interaction matrix $\left[R\right]$ does not depend on the yield stress of the material σ_y, but is only a function of the current stress tensor.

3.7.2 Bresler - Pister yield surface

The Bresler - Pister yield criterion is a three parameter model that is used to simulate concrete plasticity. The yield surface is defined by equation:

$$
\begin{aligned}
\Phi_{BP} &= \frac{\frac{1}{\sqrt{6}}\sqrt{J_2}-c_1J_1-c_2{J_1}^2}{c_0}-1=0 \\
J_1 &= \sigma_{11}+\sigma_{22} \\
J_2 &= \left(\sigma_{11}-\sigma_{22}\right)^2+\left(\sigma_{11}\right)^2+\left(\sigma_{22}\right)^2+6\left(\sigma_{12}\right)^2
\end{aligned}
\tag{A6}
$$

where c_0, c_1, c_2 are material dependent coefficients (Deder & Ayvaz, 2010).

The yield gradient is defined by the following relations:

$$\frac{\partial \Phi}{\partial \left\{ \sigma \right\}} = \left\{ d\Phi_{11} \quad d\Phi_{12} \quad d\Phi_{13} \right\}^T \tag{A7}$$

where

$$d\Phi_{11} = \frac{1}{c_0}\left(\frac{\frac{\sqrt{6}}{6}\left(2\sigma_{11} - \sigma_{22}\right)}{\sqrt{\left[\left(\sigma_{11} - \sigma_{22}\right)^2 + \left(\sigma_{11}\right)^2 + \left(\sigma_{22}\right)^2 + 6\left(\sigma_{12}\right)^2\right]}} - c_1 - 2c_2\left(\sigma_{11} + \sigma_{22}\right) \right) \tag{A8}$$

$$d\Phi_{12} = \frac{1}{c_0}\left(-\frac{\frac{\sqrt{6}}{6}\left(2\sigma_{11} - \sigma_{22}\right)}{\sqrt{\left[\left(\sigma_{11} - \sigma_{22}\right)^2 + \left(\sigma_{11}\right)^2 + \left(\sigma_{22}\right)^2 + 6\left(\sigma_{12}\right)^2\right]}} - c_1 - 2c_2\left(\sigma_{11} + \sigma_{22}\right) \right) \tag{A9}$$

$$d\Phi_{13} = \frac{1}{c_0}\left(\frac{\sqrt{6}\sigma_{12}}{\sqrt{\left[\left(\sigma_{11} - \sigma_{22}\right)^2 + \left(\sigma_{11}\right)^2 + \left(\sigma_{22}\right)^2 + 6\left(\sigma_{12}\right)^2\right]}} \right) \tag{A10}$$

The interaction matrix $\left[R\right]$ is determined accordingly.

Chapter 4

HYSTERETIC MACRO-ELEMENTS

4.1 Introduction

In this chapter a set of linear hysteretic macro-elements is derived within the formal and consistent framework of phenomenological hysteresis. The classical elastic formulations of the rod element, the Euler/Bernoulli beam element formulation and the Timoshenko beam element formulation are extended by introducing additional, hysteretic, degrees of freedom. A constructive approach is implemented in the derivations presented in this chapter.

Firstly, a rod element formulation is presented where the additional degrees of freedom are considered to be hysteretic displacements, to highlight some important aspects of the procedure implemented in this work. Next, an advanced rod element formulation is constructed on the grounds of an updated Lagrangian formulation where plasticity is introduced through the concept of the hysteretic axial deformation that evolves according to a Bouc-Wen hysteretic law.

The hysteretic two-dimensional Euler/Bernoulli beam element is presented based on the hysteretic curvature and hysteretic centreline axial deformation measures. To demonstrate the implications that arise from the interaction of the stress resultants, a two-dimensional Timoshenko beam element formulation is next presented. Finally, the general case of a three-dimensional Timoshenko beam element formulation that takes into account torsional warping is presented.

4.2 The displacement based hysteretic truss element

Consider the two node truss element presented in Fig.4.1 with a cross section A, and material constants E for the Young modulus and $\alpha = E_p \big/ E$ for the inelastic to elastic stiffness ratio.

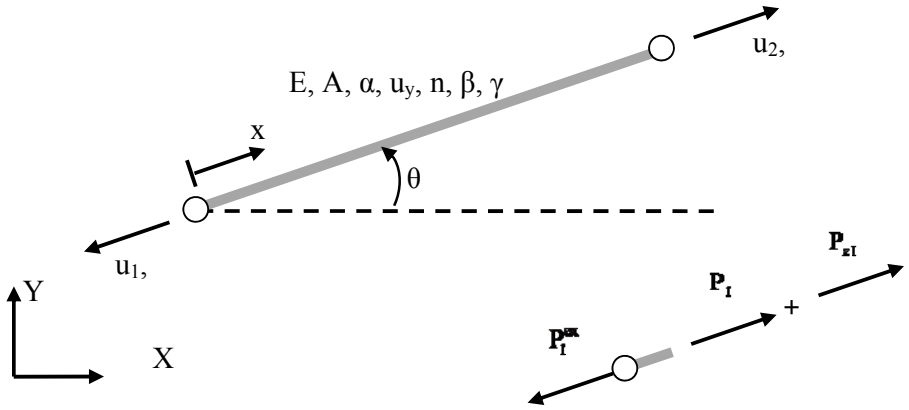

Fig.4.1 Rod Element degrees of freedom and internal forces

4.2.1 Material modeling

The element is formulated under the assumption that the axial force-axial displacement relation assumes the following form:

$$p = \alpha k u\left(x,t\right) + \left(1 - \alpha\right) k z\left(x,t\right) \tag{4.1}$$

where p is the axial force, $k = AE \big/ L$ is the axial stiffness of the truss element, u is the actual displacement and z is the hysteretic part of the actual displacement defined by the following evolution equation:

$$\dot{z} = \dot{u}_x \left[1 - \left| \frac{z}{z_Y} \right|^n \left(\beta + \gamma \operatorname{sgn}\left(\dot{u}_x z \right) \right) \right] \tag{4.2}$$

Thus, the total axial force imposed into the element is split into two components, a potentially elastic one and a hysteretic, defined below as:

$$\begin{aligned} p_{el} &= \alpha k u(x,t) \\ p_h &= \left(1-\alpha\right) k z\left(x,t\right) \end{aligned} \tag{4.3}$$

Within this framework, equation (4.1) denotes a potentially bilinear behavior, whereas the smoothness of the transition from the elastic to the inelastic regime is controlled by the model parameter n as implemented in equation (4.2). Concentrating on the deformed configuration of the element, relation (4.1) implies that the axial force is proportional to a generalized displacement measure:

$$p = k\tilde{u}(x,t) \tag{4.4}$$

that is defined as:

$$\tilde{u}(x,t) = \alpha u\left(x,t\right) + \left(1 - \alpha\right) z\left(x,t\right) \tag{4.5}$$

Thus, yielding merely defines a smooth transition from an elastic state of response to another one, non-elastic. The two displacement components, the actual and the hysteretic, are additively composed into a single quasi-elastic shape, $\tilde{\mathrm{u}}(\mathrm{x},\mathrm{t})$ which is a linear function of the applied load, and vice versa. This important property of the Bouc-Wen hysteretic model is also met in any other rate-independent smooth material model. This approach is in perfect agreement with the concepts of endochronic theory (Valanis, 1971) and the generalized plasticity theory (Panoskaltsis et al., 2008).

From relation (4.4) the following stress-strain relation is derived:

$$\sigma(x,t) = E\tilde{\varepsilon}(x,t) \tag{4.6}$$

where the deformation measure $\tilde{\varepsilon}$ is the axial deformation that is compatible to the generalized displacement measure $\tilde{\mathrm{u}}$. Using the definition of the small strain measure (equation (2.9)) the following relation holds:

$$\tilde{\varepsilon}(x,t) = \frac{\partial \tilde{u}(x,t)}{\partial x} = \alpha \frac{\partial u(x,t)}{\partial x} + \left(1 - \alpha\right) \frac{\partial z\left(x,t\right)}{\partial x} \tag{4.7}$$

or expressed in matrix form:

$$\tilde{\varepsilon}(x,t) = \left[\alpha \frac{\partial}{\partial x} \quad \left(1 - \alpha\right) \frac{\partial}{\partial x} \right] \begin{Bmatrix} u \\ z \end{Bmatrix} \tag{4.8}$$

The definition of the generalized displacement facilitates the derivation of the necessary energy forms as will be presented in the next paragraph.

Following the reasoning introduced in Chapter 2, in the elastic case, relation (4.1) is valid if and only if the generalized displacement is equal to the actual displacement. Thus, the hysteretic displacement should comply with the following relation:

$$z = u, \;\; u < u_Y \tag{4.9}$$

Furthermore, the maximum value attained by the hysteretic parameter must be equal to:

$$z_{\max} = u_Y \tag{4.10}$$

Combining equations (4.2) and (4.10) the following relation is derived:

$$\begin{aligned} \dot{z} = 0 \Rightarrow \dot{u} \left[1 - \left| \frac{z_{\max}}{z_Y} \right|^n \left(\beta + \gamma \operatorname{sgn}\left(\dot{u} z \right) \right) \right] = 0 \Rightarrow \\ 1 - \left| \frac{z_{\max}}{z_Y} \right|^n \left(\beta + \gamma \operatorname{sgn}\left(\dot{u} z \right) \right) = 0 \Rightarrow \\ \Rightarrow \left| \frac{z_{\max}}{z_Y} \right|^n = \frac{1}{\left(\beta + \gamma \operatorname{sgn}\left(\dot{u} z \right) \right)} \end{aligned} \tag{4.11}$$

Or equivalently:

$$z_{\max} = \sqrt[n]{\frac{z_Y^n}{\left(\beta + \gamma \right)}} = u_Y \Rightarrow z_Y = \sqrt[n]{\left(\beta + \gamma \right)} u_Y \tag{4.12}$$

4.2.2 Discrete modeling

For the case of the two-node truss element, the total displacement is considered to vary linearly along the element's length (Bathe, 2007). Due to the additive decomposition of the displacement as presented in relation (4.5) the same kinematic assumption is valid for the hysteretic part of the total displacement. In equation (4.13) the interpolation functions implemented for the displacement vector are presented:

$$\begin{Bmatrix} u \\ z \end{Bmatrix} = \begin{bmatrix} 1-\frac{x}{L} & 0 & \frac{x}{L} & 0 \\ 0 & 1-\frac{x}{L} & 0 & \frac{x}{L} \end{bmatrix} \{d\} \tag{4.13}$$

where $\{d\}$ is the vector of unknown nodal displacements:

$$\{d\} = \{u_1 \quad z_1 \quad u_2 \quad z_2\}^T \tag{4.14}$$

By substituting equation (4.13) into (4.8) the following relation is derived:

$$\varepsilon(x,t) = [B]\{d\} \tag{4.15}$$

where $[B]$ is the strain-displacement matrix of the element defined as:

$$[B] = \left[\alpha \frac{\partial}{\partial x} \quad (1\text{-}\alpha)\frac{\partial}{\partial x}\right] \begin{bmatrix} 1-\frac{x}{L} & 1-\frac{x}{L} & 0 & 0 \\ 0 & 0 & \frac{x}{L} & \frac{x}{L} \end{bmatrix} = \begin{bmatrix} -\frac{\alpha}{L} & -\frac{\alpha}{L} & \frac{(1-\alpha)}{L} & \frac{(1-\alpha)}{L} \end{bmatrix} \tag{4.16}$$

The principle of virtual work is formulated as:

$$\int_V \delta\varepsilon \cdot \sigma dV = P \cdot u \tag{4.17}$$

where $\delta\varepsilon$ is the potential centerline deformation of the element, σ is the normal stress, P is the axial force and u the corresponding axial displacement. Only concentrated loads are

considered in the external work for the sake of simplicity. Relation (4.17) is more conveniently written down in matrix form as:

$$\begin{aligned} &\int_V \{\delta\varepsilon\}^T \{\sigma\} dV = \{d\}^T \{p\} \Rightarrow \int_V \{d\}^T [B]^T E[B]\{d\} dV = \{d\}^T \{p\} \Rightarrow \\ &\Rightarrow \{d\}^T \left(\int_V [B]^T E[B] dV \{d\} - \{p\} \right) = 0 \Rightarrow \int_V [B]^T E[B] dV \{d\} = \{p\} \end{aligned} \tag{4.18}$$

where $\{d\}$ is the nodal displacement vector defined in relation (4.14) and $\{p\} = \{p_1 \quad p_{z1} \quad p_2 \quad p_{z2}\}^T$ is the nodal load vector. Loads p_{z1} and p_{z2} are fictitious load measures, work-conjugate to the hysteretic displacements z_1, z_2. Substituting equation (4.16) into equation (4.18) the stiffness matrix of the displacement based hysteretic truss element is derived:

$$[\tilde{K}] = \int_V [B]^T E[B] dV = \frac{AE}{L} \begin{bmatrix} \alpha^2 & \alpha(1-\alpha) & -\alpha^2 & -\alpha(1-\alpha) \\ \alpha(1-\alpha) & (1-\alpha)^2 & -\alpha(1-\alpha) & -(1-\alpha)^2 \\ -\alpha^2 & -\alpha(1-\alpha) & \alpha^2 & \alpha(1-\alpha) \\ -\alpha(1-\alpha) & -(1-\alpha)^2 & \alpha(1-\alpha) & (1-\alpha)^2 \end{bmatrix} \tag{4.19}$$

Setting $\alpha = 1$ the corresponding elastic stiffness matrix is evaluated:

$$[\tilde{k}] = \frac{AE}{L} \begin{bmatrix} 1 & 0 & -1 & 0 \\ 0 & 0 & 0 & 0 \\ -1 & 0 & 1 & 0 \\ 0 & 0 & 0 & 0 \end{bmatrix} \tag{4.20}$$

and since the hysteretic components z_1, z_2 in this case are by default equal to zero relation (4.20) can be condensed to the classic 2x2 elastic stiffness matrix of the two-node truss element.

To this point, the stiffness matrix of the hysteretic truss element is derived with respect to the actual deformation and load measures but also to the hysteretic quantities z_1, z_2, P_{z1}, P_{z2}. The latter are internally defined displacement and force measures respectively. As is, the stiffness matrix evaluated in equation (4.19) since it is derived from an energy principle where a fictitious quantity, namely the work produced from the hysteretic forces on the hysteretic displacements is added onto the energy of external forces.

Enforcing equilibrium, as presented in Fig.4.1(b), the following relation can be derived between the internally defined force components and the externally imposed nodal forces:

$$\left.\begin{aligned} p_1^{ex} &= p_1 + p_{z1} \\ p_2^{ex} &= p_2 + p_{z2} \end{aligned}\right\} \Rightarrow \begin{Bmatrix} p_1^{ex} \\ p_2^{ex} \end{Bmatrix} = \begin{bmatrix} 1 & 1 & 0 & 0 \\ 0 & 0 & 1 & 1 \end{bmatrix} \begin{Bmatrix} p_1 \\ p_{z1} \\ p_2 \\ p_{z2} \end{Bmatrix} = \left[R\right]\left\{p\right\} \tag{4.21}$$

Thus, the stiffness matrix of the hysteretic, displacement based, truss element is derived as:

$$\left[k\right] = \left[R\right]\left[\tilde{k}\right] = \frac{AE}{L}\begin{bmatrix} \alpha & 1-\alpha & -\alpha & -\left(1-\alpha\right) \\ -\alpha & -\left(1-\alpha\right) & \alpha & 1-\alpha \end{bmatrix} \tag{4.22}$$

The locally defined displacement and force components are transformed into the corresponding global components using the following transformation relations:

$$\begin{aligned} \left\{d\right\} &= \left[T\right]_1 \left\{D\right\} \\ \left\{p\right\} &= \left[T\right]_2 \left\{P\right\} \end{aligned} \tag{4.23}$$

where the transformation matrix $\left[T\right]_1$ is defined as:

$$\left[T\right]_1 = \begin{bmatrix} \cos\phi & 0 & \sin\phi & 0 & 0 & 0 & 0 & 0 \\ 0 & \cos\phi & 0 & \sin\phi & 0 & 0 & 0 & 0 \\ 0 & 0 & 0 & 0 & \cos\phi & 0 & \sin\phi & 0 \\ 0 & 0 & 0 & 0 & 0 & \cos\phi & 0 & \sin\phi \end{bmatrix} \tag{4.24}$$

and the transformation matrix $\left[T\right]_2$ respectively:

$$\left[T\right]_2 = \begin{bmatrix} \cos\phi & \sin\phi & 0 & 0 \\ 0 & 0 & \cos\phi & \sin\phi \end{bmatrix} \tag{4.25}$$

The global displacement and force vectors are of the following form:

$$\begin{aligned} \left\{D\right\} &= \left\{ u_x^1 \quad z_x^1 \quad u_y^1 \quad z_y^1 \quad u_x^2 \quad z_x^2 \quad u_y^2 \quad z_y^2 \right\}^T \\ \left\{P\right\} &= \left\{ P_x^1 \quad P_y^1 \quad P_x^2 \quad P_y^2 \right\}^T \end{aligned} \tag{4.26}$$

where z_{1x}, z_{1y}, z_{2x}, z_{2y} are the global hysteretic displacement components. Consequently, the global stiffness matrix is defined by the following relation:

$$\left[K\right] = \left[T\right]_2^T \left[k\right] \left[T\right]_1 \tag{4.27}$$

The global stiffness matrix of the hysteretic truss element is of size 4x8. The stiffness matrix defined in equation (4.27) is supplemented by four Bouc-Wen hysteretic equations, one for each global hysteretic displacement component. Thus, the following elemental set of constitutive equations is derived:

$$\left\{P\right\} = \left[K\right]\left\{D\right\} \tag{4.28}$$

and:

$$\dot{z}_k^{(x,y)} = \dot{u}_k \left[1 - \left| \frac{z_k^{(x,y)}}{z_Y} \right|^n \left(\beta + \gamma \operatorname{sgn}\left(\dot{u}_k z_k \right) \right) \right], \quad k = 1,2 \tag{4.29}$$

The evaluation of the hysteretic displacements in terms of global components is necessary so that the derived element can be fitted into the standard direct stiffness scheme.

4.2.3 A simple solution approach

Consider a truss structure comprising of n_{el} number of elements and n_{nod} number of nodes. The total number of unknown degrees of freedom is $n_{dof} = 4n_{nod}$. This corresponds to two global displacements and two global hysteretic displacements per node. However, the total number of external forces is $n_{ld} = 2n_{nod}$ as implied by the elemental constitutive relation (equation (4.28). Thus, only $2n_{nod}$ equations can be derived from equilibrium. The remaining equations are supplemented by the $2n_{nod}$ Bouc-Wen hysteretic equations, defined in equation (4.29).

The decomposition of the displacement field introduced in equation (4.5) together with the variational formulation introduced in equation (4.18) allow for the hysteretic components of the displacement to be treated as independent degrees of freedom. Enforcing compatibility, the stiffness matrix of the structure can be derived as usual, by means of the direct stiffness method. Thus, the equations of motion for the whole structure are derived:

$$\left[M\right]\left\{\ddot{D}\right\} + \left[K\right]\left\{D\right\} = \left\{P\right\} \tag{4.30}$$

where $\left[M\right]$ is the $n_{dof} x n_{dof}$ mass matrix of the structure, $\left[K\right]$ is the $2n_{nod} x 4n_{nod}$ stiffness matrix of the structure, $\left\{D\right\}$ is the $4n_{nod}$ vector of unknown internal forces, and $\left\{P\right\}$ is the $2n_{nod}$ vector of nodal forces. Boundary conditions are enforced numerically by adding a big number to the corresponding elements of the stiffness matrix. Since the hysteretic components are displacement measures they are submitted to the same inertia forces as the total displacement measures.

The evolution equations of the hysteretic displacements z expressed in the global coordinate system are given by the following relations:

$$\dot{z}_{ik}{}^{J} = \dot{u}_{ik}^{J}\left[1-\left|\frac{z_{ik}^{J}}{z_{Y}^{J}}\right|^{n}\left(\beta+\gamma\,\mathrm{sgn}\left(\dot{u}_{ik}^{J}z_{ik}^{J}\right)\right)\right] \tag{4.31}$$

where $i=1...n_{el}$, $k=1,2$ and J is either the x or y global axis. Equations (4.31) are derived from equations (4.2) utilizing the transformation (4.23). However, since the hysteretic displacements $\dot{z}_{ik}{}^{J}$ are defined in the global coordinate system, the definition if the associated yield parameters $z_{Y}^{(x,y)}$ is not straightforward. Letting z to be the nodal hysteretic displacement defined in the local coordinate system, the global components are evaluated as:

$$\begin{aligned} z_{x} &= z\cos\phi \\ z_{y} &= z\sin\phi \end{aligned} \tag{4.32}$$

Substituting relations (4.32) into equation (4.2) the following evolution equation is derived, concerning the hysteretic displacement component along the global x direction:

$$\dot{z}^{J} = \dot{u}^{J}\left[1-\left|\frac{z^{J}}{\cos\phi z_{Y}^{'}}\right|^{n}\left(\beta+\gamma\,\mathrm{sgn}\left(\dot{u}^{J}z^{J}\right)\right)\right] \tag{4.33}$$

where $z_{Y}^{'}$ is the «yield displacement» along the global direction. When at yield, the following relation holds:

$$z^{J} = \cos\phi z_{Y}^{'}{}^{J} = \frac{z_{y}}{\cos\phi} \Rightarrow z_{Y}^{'}{}^{J} = \frac{z_{y}}{\cos^{2}\phi} \tag{4.34}$$

and thus equation (4.34) is written as:

$$\dot{z}^{J} = \dot{u}^{J}\left[1-\left|\frac{z^{J}\cos\phi}{z_{y}}\right|^{n}\left(\beta+\gamma\,\mathrm{sgn}\left(\dot{u}^{J}z^{J}\right)\right)\right] \tag{4.35}$$

The set of equations (4.30) together with the evolution equations (4.31) fully define the nonlinear dynamical problem under consideration. The system of nonlinear equations can be solved either by standard implicit or explicit integration methods (Chopra, 2006) or by implementing the state-space approach (Sivaselvan and Reinhorn, 2003). In this work, the state-space approach is implemented. The system of second-order equations of motion is written as a system of first-order equations. This is accomplished by analytically evaluating the second derivative of z with respect to time:

$$\begin{aligned}\ddot{z}_1 = \ddot{u}_1 &\left[1-\left|\frac{z}{z_y}\right|^n \left(\beta+\gamma \mathrm{sgn}\left(\dot{u}_1 z\right)\right)\right] \\ -\dot{u}_1 &\left[\left|\frac{z}{z_y}\right|^{n-1} \mathrm{sgn}\left(z\left(t\right)\right)\dot{z}\left(t\right)\left(\beta+\gamma \mathrm{sgn}\left(\dot{u}_1 z\right)\right)\right] \\ -&\left|\frac{z}{z_y}\right|^n \gamma \mathrm{sgn}\left(1,\left(\dot{u}_1 z\right)\right)\end{aligned} \tag{4.36}$$

where $\gamma \mathrm{sgn}\left(1,\left(\dot{u}_1 z\right)\right)$ is the derivative of the sgn(.) function with respect to time.

Equation (4.36) is then inserted into equation (4.30) and the derived equations can be written in the following form:

$$\left\{\dot{x}\right\} = G\left(\left\{x\right\}\right) + \left\{P\left(t\right)\right\} \tag{37}$$

where the vector $\left\{x\right\}$ is defined as:

$$\left\{x\right\}^T = \left[\left\{D\right\}^T \quad \left\{\dot{D}\right\}^T\right] \tag{38}$$

and $G\left(\left\{x\right\}\right)$ is defined as follows:

$$G\left(\left\{x\right\}\right) = \begin{bmatrix} \mathbf{0} & \left\{I \quad Y\left(\left\{\dot{U}\right\},\left\{Z\right\}\right)\right\} \\ \left[M\right]^{-1}\left[K\right] & \left[M\right]^{-1}\left[K\right] \end{bmatrix} \tag{39}$$

The operator G is a state dependent operator since Y holds the evolution equations for each element i, that is:

$$Y_j^i\left(\{\dot{u}\}^i,\{z\}^i\right)=\left(1-\left|\frac{z_j(t)}{z_y}\right|^n\left(\beta+\gamma\,\mathrm{sgn}\left(z_j(t)[B]_j[\Lambda]\{\dot{u}\}\right)\right)\right)[B]_j[\Lambda]\{\dot{u}\}^i \quad (40)\backslash$$

This solution procedure is presented in the next section through an illustrative example

4.2.4 Example – 3-bar truss under monotonically increasing loading

In this example, a typical 3-bar truss is examined and the results are validated using the Nastran commercial code (Noran Engineering, 2007). The geometry of the truss is presented in Fig.4.2, while the parameters of the problem are defined in Table 4.1.

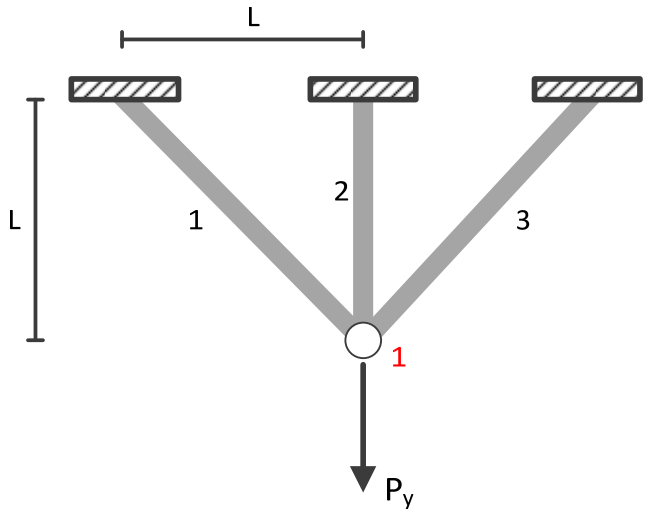

Fig.4.2 Three-bar truss

A monotonically increasing concentrated load is applied at node #1 (Fig.4.2) to a maximum value of 700 KN. This example serves for validation purposes only, thus no failure structural failure criteria are considered. The load is applied using a slow varying ramp function. The Runge-Kutta 45 solver is implemented for the proposed formulation, with an initial time-step equal to 0.01 sec and a relative tolerance error control equal to 0.001. Analysis in Nastran is performed utilizing a Modified Newton-Raphson scheme with 100

incremental steps. The 2-node truss element is implanted in Nastran with a bilinear elastic-plastic stress-strain relation with kinematic hardening.

Area	0.001 m^2
Length	1 m
φ	45^0
E_{young}	210 GPa
α	0.002
σ_y	235 MPa
n	25
β	0.5
γ	0.5

Table 4.1 Parameter definition

In Fig.4.3 the force-deflection curve from the two different formulations is presented. The two solutions coincide.

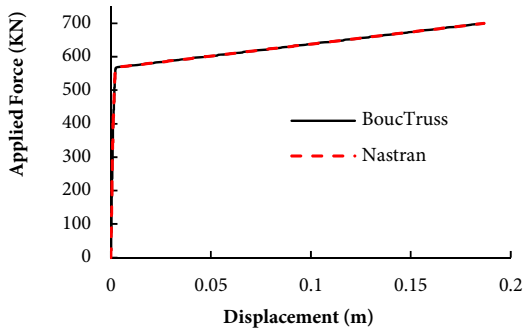

Fig.4.3 Validation of the proposed element with Nastran commercial code – Applied Load – Displacement curve at node #1

Even-though the proposed formulation utilizes twice the number of degrees of freedom as to Nastran both analyses conclude in 6.5 sec. This is because the proposed formulation allows for the simultaneous solution of the governing equations of the problem, that is, the equilibrium equations and the nonlinear plasticity equations.

In Fig.4.4(a) the member axial force is presented with respect to the vertical displacement at node #1. Due to symmetry, elements #1 and #3 coincide as expected. The evolution of the hysteretic parameter with respect to time is presented in Fig.4.4(b). Element #2 is the first one

to reach its yield displacement. The velocity of plastic deformation is then increased for elements #1 and #3, that reach their yield displacement at the same time, due to symmetry.

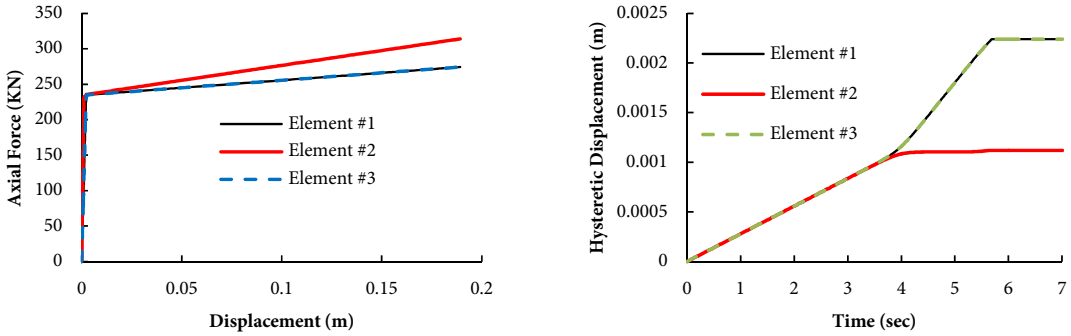

(a) (b)

Fig.4.4(a) Element Axial Force –Vertical Displacement at node #1 (b) Evolution of the hysteretic parameter

In Fig.4.5(a), the evolution of the hysteretic parameter is compared to the evolution of the total displacement in element #2.

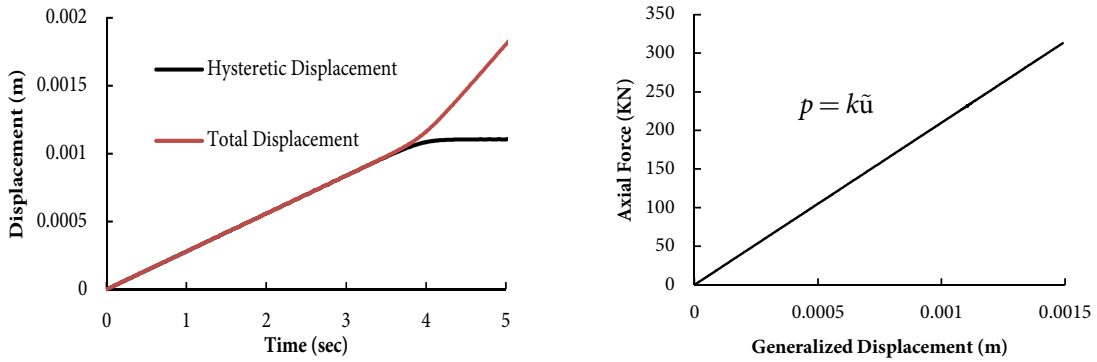

(a) (b)

Fig.4.5(a) Evolution of the hysteretic parameter and the total elongation at element #2 until yield (b) Evolution of the quasi-elastic generalized displacement measure at element #2

As predicted by equations (4.5), (4.9) and (4.10) the hysteretic displacement is equal to the total displacement until yield. At that point the hysteretic displacement assumes a constant value. The transition from the elastic to the plastic state is smooth, with the smoothness being controlled by parameter n as defined in equation (4.2). The evolution of the equivalent displacement measure as defined in equations (4.4) and (4.5) is presented in Fig.4.5(b).

4.3 Truss element formulation considering hysteretic axial deformations

4.3.1 Introduction

Though instructive, two main disadvantages can be argued for the hysteretic displacement formulation presented in the previous section. The dependence of the nonlinear law implemented on global displacement properties (equation (4.35)), yields an element with problem dependent material parameters, since the yield displacement cannot be unequivocally deducted in multidimensional displacement fields. Furthermore, a formulation is needed that can be easily extended to large displacement fields, thus being suitable for geometrically nonlinear problems. To circumvent this drawback the truss-element is re-examined based on the decomposition of the strain, rather than the displacement field, into quasi-elastic and hysteretic terms.

4.3.2 Material modeling

The Bouc-Wen hysteretic law is herein written in stress-strain terms as opposed to relation (4.1) where the constitutive relation was defined in terms of a force displacement relationship. Thus, the hysteretic stress-strain law is defined as:

$$\sigma_x(x,t) = \alpha E \varepsilon_x\left(x,t\right) + \left(1 - \alpha\right) E z\left(x,t\right) \tag{4.41}$$

where σ_{x} is the axial stress, ε_{x} the axial strain, E is the Young Modulus and α is the post-elastic to elastic moduli ratio. As implied by relation (4.41) z is now considered to be the hysteretic part of the total deformation, evolving through the following relation:

$$\dot{z} = \dot{\varepsilon}_x \left[1 - \left| \frac{z}{z_Y} \right|^n \left(\beta + \gamma \operatorname{sgn}\left(\dot{\varepsilon}_x z \right) \right) \right] \tag{4.42}$$

where z_Y is the yield axial deformation.

4.3.3 Small displacement formulation

Introducing the interpolation field defined in relation (4.13) for the axial displacement, the following relation holds:

$$u(x) = \left[1 - \frac{x}{L} \quad \frac{x}{L}\right]\{d\} \tag{4.43}$$

where $\{d\} = \left\{u_x^1 \quad u_x^2\right\}^T$ is the nodal displacement vector. Considering the compatibility equation:

$$\varepsilon_x = \frac{\partial u}{\partial x} \tag{4.44}$$

the strain displacement matrix $[B]$ is evaluated:

$$\varepsilon_x = [B]\{d\} = \frac{\partial}{\partial x}\left[1 - \frac{x}{L} \quad \frac{x}{L}\right]\{d\} = \left[-\frac{1}{L} \quad \frac{1}{L}\right]\{d\} \tag{4.45}$$

A similar interpolation field must be considered for the hysteretic displacement. The interpolation field has to comply with the actual constant deformation distribution, since the two-node truss is a constant axial force element. An equilibrium based interpolation field is defined as:

$$z = \left[-1 \quad 0\right]\begin{Bmatrix} z_1 \\ z_2 \end{Bmatrix} = [B_z]\{z\} \tag{4.46}$$

where $\{z\} = \left\{z_1 \quad z_2\right\}^T$ is the vector of the hysteretic nodal strains that evolve according to the Bouc-Wen relation defined in equation (4.42). Though such a definition reduces the number of additional degrees of freedom, since one nodal hysteretic strain suffices for the description of the problem, the following interpolation field is preferred:

$$z = \begin{bmatrix} 1/2 & 1/2 \end{bmatrix} \begin{Bmatrix} z_1 \\ z_2 \end{Bmatrix} = \begin{bmatrix} B_z \end{bmatrix} \begin{Bmatrix} z_1 \\ z_2 \end{Bmatrix} \tag{4.47}$$

Equation (4.47) allows for the simulation of elements with different hysteretic properties, e.g. different connection properties in each end. Having established the vectors of unknown quantities and the corresponding interpolation fields, the principle of virtual work is implemented to evaluate the stiffness matrix of the truss element:

$$\int_V \delta\varepsilon_x \sigma_x dV = \{d\}^T \{P\} \tag{4.48}$$

where $\delta\varepsilon_x$ is the potential strain and $\{p\} = \begin{Bmatrix} p_x^1 & p_x^2 \end{Bmatrix}^T$ is the work conjugate nodal load vector, both expressed in the local coordinate system. Substituting relation (4.41) into relation (4.48) the following expression is derived:

$$\int_V \delta\varepsilon \left(\alpha E\varepsilon + (1-\alpha) Ez \right) dV = \{d\}^T \{p\} \tag{4.49}$$

The lhs of equation (4.49) is written as:

$$\begin{aligned} &\int_V \delta\varepsilon \left(\alpha E\varepsilon + (1-\alpha) Ez \right) dV = \alpha \int_V \delta\varepsilon E\varepsilon dV + (1-\alpha) \int_V \delta\varepsilon Ez dV = \\ &= \alpha \{\delta u\}^T \int_V [B]^T E[B] dV \{\delta u\} + (1-\alpha) \{\delta u\}^T \int_V [B]^T E[B_z] dV \end{aligned} \tag{4.50}$$

where the interpolation scheme of equations (4.45) and (4.47) is implemented. Substituting the expressions of the strain-displacement matrices $[B]$, $[B_z]$ from equations (4.45) and (4.47) respectively, the integrals of the r.h.s. of equation (4.50) are reduced to the following expressions:

$$
\begin{aligned}
I_e &= \int_V \left[B\right]^T E \left[B\right] dV = \frac{EA}{L}\begin{bmatrix} 1 & -1 \\ -1 & 1 \end{bmatrix} \\
I_h &= \int_V \left[B\right]^T E \left[B_z\right] dV = EA\begin{bmatrix} -0.5 & -0.5 \\ 0.5 & 0.5 \end{bmatrix}
\end{aligned}
\tag{4.51}
$$

The integral I_e is equal to the elastic stiffness matrix of the two-node truss element.

Thus, the equilibrium equation of the truss element is written as:

$$
\left\{p\right\} = \alpha \frac{EA}{L}\begin{bmatrix} 1 & -1 \\ -1 & 1 \end{bmatrix}\left\{d\right\} + \left(1-\alpha\right) EA \begin{bmatrix} -0.5 & -0.5 \\ 0.5 & 0.5 \end{bmatrix}\left\{z\right\} \tag{4.52}
$$

The additive decomposition of the total stress into a quasi-elastic and a hysteretic part as described in equation (4.41) is retained in constitutive relation of the element. The stiffness relation presented in equation (4.52), together with the evolution equations of the nodal hysteretic deformations z_1, z_2 fully describe the nonlinear behavior of the two-node truss element.

The stiffness matrix, initially evaluated in local coordinates is transformed to the global coordinate system, using the following transformation relations:

$$
\begin{aligned}
\left\{p\right\} &= \left[\Lambda\right]\left\{P\right\} \\
\left\{d\right\} &= \left[\Lambda\right]\left\{D\right\}
\end{aligned}
\tag{4.53}
$$

where $\left\{P\right\} = \left\{P_x^1 \quad P_y^1 \quad P_z^1 \quad P_x^2 \quad P_y^2 \quad P_z^2\right\}^T$, $\{d\} = \{d_x^1 \quad d_y^1 \quad d_z^1 \quad d_x^2 \quad d_y^2 \quad d_z^2\}^T$ are the nodal force and nodal displacement vectors respectively, expressed in the global coordinate system.

Substituting equations (4.53) into relation (4.52) the following equation is derived:

$$
\left\{P\right\} = \alpha \frac{EA}{L}\left[\Lambda\right]^T\begin{bmatrix} 1 & -1 \\ -1 & 1 \end{bmatrix}\left[\Lambda\right]\left\{D\right\} + \left(1-\alpha\right) EA \left[\Lambda\right]^T\begin{bmatrix} -0.5 & -0.5 \\ 0.5 & 0.5 \end{bmatrix}\begin{Bmatrix} z_1 \\ z_2 \end{Bmatrix} \tag{4.54}
$$

where the elastic global stiffness matrix is defined as:

$$\left[K\right] = \alpha \frac{EA}{L} \left[\Lambda\right]^T \begin{bmatrix} 1 & -1 \\ -1 & 1 \end{bmatrix} \left[\Lambda\right] \tag{4.55}$$

As expected the elastic part of the stiffness matrix expressed in the global coordinate system is again identical to the classical small displacement elastic formulation of the truss element (Bathe, 2007).

4.3.4 Large displacement formulation

To account for large displacement fields, the compatibility equation presented in equation (4.44) is herein extended by introducing the contribution of the rotational field into the extension of the truss element. Thus, the axial strain of the rod element is expressed as:

$$\varepsilon_x = e_x + \eta_x \tag{4.56}$$

where e_x is the linear part of the strain:

$$e_x = \frac{\partial u_x}{\partial x} \tag{4.57}$$

and η_x is the nonlinear part of the axial strain containing the contribution of the rotational displacement field in the axial deformation:

$$\eta_x = \frac{1}{2}\left[\left(\frac{\partial u_x}{\partial x}\right)^2 + \left(\frac{\partial u_y}{\partial y}\right)^2 + \left(\frac{\partial u_z}{\partial z}\right)^2\right] \tag{4.58}$$

Material nonlinearity is introduced through relation (4.41). Since the hysteretic deformation measure z is a part of the total deformation measure ε_x, the geometrically nonlinear evolution of z is implicitly imposed by (4.56). Thus, the following nonlinear law applies for the stress-strain relation:

$$\begin{aligned}
&\sigma_x = \alpha E\left(e_x + \eta_x\right) + \left(1-\alpha\right) Ez \\
&\dot{z} = \left(\dot{\varepsilon}_x + \dot{\eta}_x\right)\left[1 - \left|\frac{z}{z_Y}\right|^n \left(\beta + \gamma\,\mathrm{sgn}\left(\left(\dot{\varepsilon}_x + \dot{\eta}_x\right) z\right)\right)\right]
\end{aligned} \tag{4.59}$$

Implementing the linear interpolation functions for the displacement field one gets:

$$\begin{aligned}
&\begin{Bmatrix} u_x \\ u_y \\ u_z \end{Bmatrix} = \begin{bmatrix} 1-\frac{s}{L} & 0 & 0 & \frac{s}{L} & 0 & 0 \\ 0 & 1-\frac{s}{L} & 0 & 0 & \frac{s}{L} & 0 \\ 0 & 0 & 1-\frac{s}{L} & 0 & 0 & \frac{s}{L} \end{bmatrix} \left\{d\right\} \\
&\left\{d\right\} = \left\{u_x^1 \quad u_y^1 \quad u_z^1 \quad u_x^2 \quad u_y^2 \quad u_z^2\right\}^T
\end{aligned} \tag{4.60}$$

The strain field is derived from the displacement field, by substituting (4.60) in (4.58) thus leading to the following matrix expression:

$$\varepsilon = \left(\left[B\right]_L + \left[B\right]_{NL}\right)\left\{d\right\} \tag{4.61}$$

where the nodal displacement matrix $\left\{d\right\}$ consists of 6 elements, namely:

$$\left\{d\right\} = \left\{u_x^1 \quad u_y^1 \quad u_z^1 \quad u_x^2 \quad u_x^2 \quad u_x^2\right\}^T \tag{4.62}$$

and the strain-displacement matrix consists of two parts, a linear $\left[B\right]_L$ and nonlinear $\left[B\right]_{NL}$ which are evaluated as follows:

$$\begin{aligned}
&\left[B\right]_L = \begin{bmatrix} -\frac{1}{L} & 0 & 0 & \frac{1}{L} & 0 & 0 \end{bmatrix} \\
&\left[B\right]_{NL} = \begin{bmatrix} -\frac{\Delta u_x}{2L^2} & -\frac{\Delta u_y}{2L^2} & -\frac{\Delta u_z}{2L^2} & \frac{\Delta u_x}{2L^2} & \frac{\Delta u_y}{2L^2} & \frac{\Delta u_z}{2L^2} \end{bmatrix} \\
&\Delta u_x = -u_x^1 + u_x^2, \Delta u_y = -u_y^1 + u_y^2, \Delta u_z = -u_z^1 + u_z^2
\end{aligned} \tag{4.63}$$

The interpolation scheme introduced in relation (4.47) for the hysteretic degrees of freedom is also utilized herein, letting:

$$\{z\} = [B]_z \begin{Bmatrix} z_1 \\ z_2 \end{Bmatrix} = \begin{bmatrix} -1 & 1 \end{bmatrix} \begin{Bmatrix} z_1 \\ z_2 \end{Bmatrix} \tag{4.64}$$

where z_1, z_2 are nodal hysteretic strains subject to the evolution law of relation(4.59). The principle of virtual work is therefore defined by the following relation:

$$\int_V \delta\varepsilon \cdot \sigma dV = \{d\}^T \{P\} \tag{4.65}$$

and by substituting (4.59) and (4.56) in (4.65) the following expression is derived:

$$\int_V \left(\delta e_x + \delta\eta_x\right)\left[\alpha E\left(e_x + \eta_x\right) + \left(1-\alpha\right)Ez\right]dV = \{d\}^T \{P\} \tag{4.66}$$

Taking into consideration equations (4.60) to (4.64) and after the necessary algebraic manipulations the following constitutive relation is derived:

$$\underbrace{\left[\begin{array}{ccccccc} \overbrace{k_e}^{(6x6)} & + & \overbrace{k_g}^{(6x6)} & + & \overbrace{s_1}^{(6x6)} & + & \overbrace{s_2}^{(6x6)} & + & \overbrace{s_3}^{(6x6)} \end{array} \middle| \overbrace{k_z}^{(6x2)}\right]}_{(6x8)} \underbrace{\{d|z\}}_{(8x1)} = \underbrace{\{P\}}_{(6x1)} \tag{4.67}$$

$$\{P\}^T = \begin{Bmatrix} P_x^1 & P_y^1 & P_z^1 & P_x^2 & P_y^2 & P_z^2 \end{Bmatrix}$$

Matrices k_g, k_s, s_1, s_2, s_3 are the same as in the updated Lagrangian formulation of the two node truss element (Bathe, 2007) multiplied by α and $[K_z]$ is defined as:

$$[K_z] = \left(1-\alpha\right)EA \begin{bmatrix} 1+\frac{\Delta u_x}{2L} & \frac{\Delta u_y}{2L} & \frac{\Delta u_z}{2L} & -1-\frac{\Delta u_x}{2L} & -\frac{\Delta u_y}{2L} & -\frac{\Delta u_z}{2L} \\ -1-\frac{\Delta u_x}{2L} & -\frac{\Delta u_y}{2L} & -\frac{\Delta u_z}{2L} & 1+\frac{\Delta u_x}{2L} & \frac{\Delta u_y}{2L} & \frac{\Delta u_z}{2L} \end{bmatrix}^T \tag{4.68}$$

The transformation matrix $[\Lambda]$ of the 3d truss element, is given by the following relation:

$$\left[\Lambda\right]=\begin{bmatrix} \kappa & \lambda & \mu & & & \\ -\lambda/D & \kappa/D & 0 & & \varnothing & \\ -\kappa\mu/D & -\lambda\mu/D & D & & & \\ & & & \kappa & \lambda & \mu \\ & \varnothing & & -\lambda/D & \kappa/D & 0 \\ & & & -\kappa\mu/D & -\lambda\mu/D & D \end{bmatrix} \tag{4.69}$$

where $\kappa=\cos\phi_x$, $\lambda=\cos\phi_y$, $\mu=\cos\phi_z$, $D=\sqrt{\kappa^2+\lambda^2}$, ϕ_x,ϕ_y,ϕ_z being the direction angles of the truss element.

4.4 The Euler – Bernoulli beam element

4.4.1 Introduction

In this section, the derivation of a plane beam element is presented, based on the concept of the hysteretic strain measure presented in the previous section. In section 4.4.2 the element matrices are derived under the assumption of small displacements. To demonstrate the generality of the proposed formulation, a large displacement formulation is also presented in section 4.4.7.

4.4.2 Small displacement formulation

The end forces of a prismatic beam element directed from node 1 to node 2, being a part of a plane frame structure that carries nodal static or dynamic loads, are presented in Fig. 4.6.

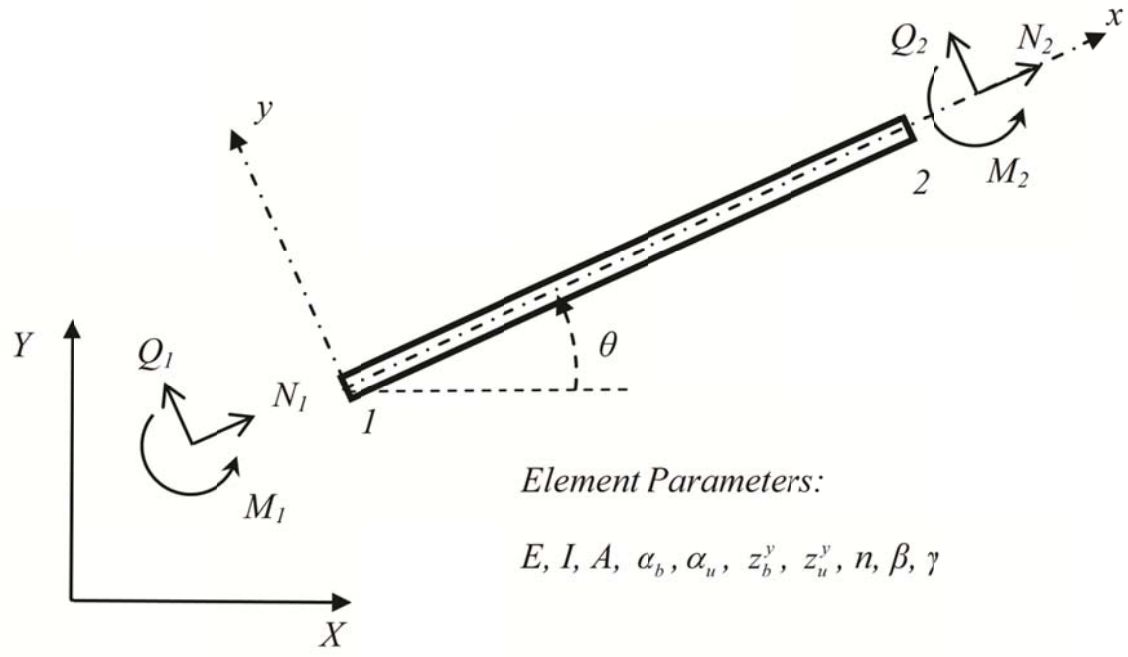

Fig. 4.6. Beam element

The inelastic moment-curvature relation at a particular cross section at distance x, is expressed in the following form:

$$M\left(x,t\right)=\alpha_b EI\phi\left(x,t\right)+\left(1-\alpha_b\right)\mathrm{E}Iz_b\left(x,t\right) \tag{4.70}$$

where M is the internal moment, ϕ the total curvature, while E and I are the Young's modulus and sectional moment of inertia respectively and a_b is the ratio of the post-yield to elastic bending stiffness ratio. In this formulation the hysteretic parameter z_b is defined as the hysteretic part of the curvature. Introducing the Bouc-Wen evolution equation defined in relations (3.36) and (3.37) the following relation is obtained:

$$\dot{z}_b\left(x,t\right)=\dot{\phi}\left[1-\left|\frac{z_b}{z_b^y}\right|^n\left(\beta+\gamma\,\mathrm{sgn}\left(z_b\cdot\dot{\phi}\right)\right)\right] \tag{4.71}$$

which expresses the rate of hysteretic curvature in terms of the rate of curvature times a nonlinear coefficient. In equation (4.71) z_b^y denotes the maximum value attained by the hysteretic curvature z_b .

By means of the Euler-Bernoulli assumptions the curvature is given by the following relation:

$$\phi = \frac{\partial^2 w}{\partial x^2} \tag{4.72}$$

where w is the transverse deflection of the beam. Substituting relation (4.72) into (4.70), the following expression is obtained:

$$\begin{aligned} M\left(x,t\right) &= EI\tilde{\phi}\left(x,t\right) \\ \tilde{\phi}\left(x,t\right) &= \alpha_b \frac{\partial^2 w\left(x,t\right)}{\partial x^2} + \left(1-\alpha_b\right) z_b\left(x,t\right) \end{aligned} \tag{4.73}$$

where $\tilde{\phi}\left(x,t\right)$ can be regarded as a measure of an "equivalent generalized curvature", though not directly related to the elastic line, which induces the elastoplastic moment. Additionally, plasticity with respect to axial deformations can be introduced in a similar way, as follows:

$$\begin{aligned} N\left(x,t\right) &= EA\tilde{\varepsilon}_0\left(x,t\right) \\ \tilde{\varepsilon}_0\left(x,t\right) &= \alpha_u\varepsilon_0 + \left(1-\alpha_u\right) z_u = \alpha_u \frac{\partial u\left(x,t\right)}{\partial x} + \left(1-\alpha_u\right) z_u\left(x,t\right) \end{aligned} \tag{4.74}$$

where N is the axial force, A is the cross-sectional area, $\tilde{\varepsilon}_0$ is the generalized axial centerline strain similar to the generalized curvature defined in equation (4.72), α_u is the post-yield to elastic axial stiffness ratio and z_u is the axial hysteretic deformation analogous to the hysteretic curvature concept introduced in relation (4.73). The evolution equation of the hysteretic axial centerline deformation is given by the following relation:

$$\dot{z}_u\left(x,t\right)=\dot{\varepsilon}_0\left[1-\left|\frac{z_u}{z_u^y}\right|^n\left(\beta+\gamma\,\mathrm{sgn}\left(z_u\cdot\dot{\varepsilon}_0\right)\right)\right] \tag{4.75}$$

where z_u^y is the maximum value attained by the hysteretic part of the axial centerline deformation z_u. In this work, the interaction between the axial force and the bending moment is only implicitly accounted for through the evaluation of a bending yield parameter z_b^y for an anticipated level of axial force. However, refined interaction schemes can be implemented through the proper manipulation of the evolution equations (4.71) and (4.75) as described in Symeonov et al., 2000. Parameters α_b and α_u are considered to be material dependent and can be determined after appropriate testing.

This constitutive modeling constitutes a phenomenological approach for the inelastic behavior of skeletal structures in the sense that the inelastic behavior is established on the basis of a stress-resultant – generalized displacement relation, resulting into certain advantages. The cyclic behavior is accurately and efficiently monitored without reverting into the evaluation of stresses at the cross-sectional level reducing significantly the computational cost of the proposed scheme. Moreover, cyclic induced phenomena such as stiffness degradation, strength deterioration and pinching can be easily simulated by properly modifying the evolution equation (Sivaselvan and Reinhorn, 2000). The combined nonlinear behavior of a structural assemblage (e.g. steel members and their connections) can be simulated using only one element, provided that the corresponding hysteretic parameters are calibrated.

However, this comes at the cost of lacking information on the exact stress distribution along the section's height. This though is readily available separately by imposing the curvature evaluated by the analysis procedure over the cross section when needed and computing the corresponding stress distribution based on a specific stress-strain law,

Charalampakis & Koumousis (2008b). Furthermore, the identification process of the model parameters that needs to be performed, implies the existence of experimental data, extracted either from numerical or real experiments (Khandelwal et. al, 2008, Chatzi et al., 2010).

4.4.3 FEM discretization

Using cubic polynomial interpolation functions for the displacement field, the following expression is derived:

$$\begin{bmatrix} u \\ w \end{bmatrix} = \begin{bmatrix} N_1 & 0 & 0 & N_2 & 0 & 0 \\ 0 & N_3 & N_4 & 0 & N_5 & N_6 \end{bmatrix} \{ d \} \tag{4.76}$$

where the nodal displacement vector $\{ d \}$ is defined as $\{ d \} = \{ u_1 \quad w_1 \quad \theta_1 \quad u_2 \quad w_2 \quad \theta_2 \}^T$ and N_i, i=1..8 are the shape functions as introduced in Bathe (2007). Equations (4.76) denote a polynomial interpolation scheme, accurate for an elastic beam. This is employed also in this work as a good approximation for an elastoplastic beam. According to equation (4.72) and using equation (4.76), the total curvature can be expressed as:

$$\phi = \begin{bmatrix} 0 & N_{3,xx} & N_{4,xx} & 0 & N_{5,xx} & N_{6,xx} \end{bmatrix} \{ d \} = \left[B_b(x) \right] \{ d \} \tag{4.77}$$

where subscript $,xx$ denotes double differentiation with respect to the space variable x. Since the total moments at the ends of the element are in equilibrium and there is no lateral intermediate loading, the following relationship is valid:

$$M(x,t) = \left(1 - \frac{x}{L} \right) M_1 + \frac{x}{L} M_2 \tag{4.78}$$

where M_1 and M_2 are the nodal moments and $M(x,t)$ is the internal bending moment. From equation (4.73) it follows that:

$$\tilde{\phi}\left(x,t\right)=\left(1-\frac{x}{L}\right)\tilde{\phi}_1+\frac{x}{L}\tilde{\phi}_2 \tag{4.79}$$

where $\tilde{\phi}_1$ and $\tilde{\phi}_2$ are the corresponding nodal quantities of the generalized curvature. Replacing the second of equations (4.73) into (4.79), it results:

$$\begin{aligned}&\alpha_b\frac{\partial^2 w\left(x,t\right)}{\partial x^2}+\left(1-\alpha_b\right)z_b\left(x,t\right)=\left(1-\frac{x}{L}\right)\left(\alpha_b\phi_1+\left(1-\alpha_b\right)z_{b1}\right)+\frac{x}{L}\left(\alpha_b\phi_2+\left(1-\alpha_b\right)z_{b2}\right)\Rightarrow\\&\alpha_b\frac{\partial^2 w\left(x,t\right)}{\partial x^2}+\left(1-\alpha_b\right)z_b\left(x,t\right)=\alpha_b\left(\left(1-\frac{x}{L}\right)\phi_1+\frac{x}{L}\phi_2\right)+\left(1-\alpha_b\right)\left(\left(1-\frac{x}{L}\right)z_{b1}+\frac{x}{L}z_{b2}\right)\end{aligned} \tag{4.80}$$

which means that in order for equation (4.80) to hold for every $\alpha_b\in\left(0\quad 1\right]$ the same interpolation field has to be adopted for both the total curvature φ and the hysteretic curvature z_b. In equation (4.80), z_{b1} and z_{b2} are the corresponding nodal quantities of the hysteretic curvature z_b. Consequently, the hysteretic curvature is defined via the following linear shape functions:

$$z_b\left(x,t\right)=\begin{bmatrix}N_7 & N_8\end{bmatrix}\begin{Bmatrix}z_{b1}\\z_{b2}\end{Bmatrix}=\begin{bmatrix}1-\frac{x}{L} & \frac{x}{L}\end{bmatrix}=\left[N\right]_z^b\left\{z_b\right\} \tag{4.81}$$

It turns out that equation (4.81) is an "exact" representation for the distribution of the hysteretic curvature with respect to equations (4.73) and (4.79), as long as the nonlinear behavior under examination is of a smooth type with kinematic hardening, as described in equation (4.70) and there is no lateral loading between the end nodes of the beam.

Substituting relations (4.77) and (4.81) into (4.73) results into the following expression:

$$\tilde{\phi}=\alpha_b\begin{bmatrix}0 & N_{2,xx} & N_{3,xx} & 0 & N_{5,xx} & N_{6,xx}\end{bmatrix}\left\{d\right\}+\left(1-\alpha_b\right)\begin{bmatrix}N_7 & N_8\end{bmatrix}\begin{Bmatrix}z_{b1}\\z_{b2}\end{Bmatrix} \tag{4.82}$$

Similarly, the centerline axial deformation is expressed as:

$$\varepsilon_0 = \begin{bmatrix} N_{1,x} & 0 & 0 & N_{2,x} & 0 & 0 \end{bmatrix} \{ d \} = \begin{bmatrix} B_u(x) \end{bmatrix} \{ d \} \tag{4.83}$$

and the corresponding hysteretic component is derived as:

$$z_u(x,t) = \begin{bmatrix} \frac{1}{2} & \frac{1}{2} \end{bmatrix} \begin{Bmatrix} z_{u1} \\ z_{u2} \end{Bmatrix} = \begin{bmatrix} N_z^u \end{bmatrix} \{ z_u \} \tag{4.84}$$

Substituting relations (4.83) and (4.84) in (4.74) the following interpolation scheme is derived in matrix form as:

$$\tilde{\varepsilon}_0 = \alpha_u \begin{bmatrix} N_{1,x} & 0 & 0 & N_{2,x} & 0 & 0 \end{bmatrix} \{ d \} + (1-\alpha_u) \begin{bmatrix} N_9 & N_{10} \end{bmatrix} \begin{Bmatrix} z_{u1} \\ z_{u2} \end{Bmatrix} \tag{4.85}$$

which as in relation (4.82) separates the elastic and hysteretic component.

4.4.4 Variational formulation

By means of the principle of virtual work and using equation (4.70), the following relation is obtained:

$$\int_0^L \left(\{ \delta\varepsilon_0 \}^T \{ N \} + \{ \delta\phi \}^T \{ M \} \right) dx = \{ \delta d \}^T \{ P \} \tag{4.86}$$

Taking into consideration equations (4.83) and (4.84), the first part of the left hand side integral that expresses the virtual work of the axial forces, can be written as:

$$I_1 = EA \left[\underbrace{\alpha_u \int_0^L \begin{bmatrix} B_u \end{bmatrix}^T \begin{bmatrix} B_u \end{bmatrix} dx}_{6x6} \;\vdots\; \underbrace{(1-\alpha_u) \int_0^L \begin{bmatrix} B_u \end{bmatrix}^T \begin{bmatrix} N \end{bmatrix}_z^u dx}_{6x2} \right] \begin{Bmatrix} \{ d \} \\ \hdashline z_{u1} \\ z_{u2} \end{Bmatrix} \tag{4.87}$$

Similarly, substituting relations (4.77) and (4.81) in relation (4.86) and performing the necessary algebraic operations, the second part of the integral in the left hand side that expresses the virtual work due to bending is derived:

$$I_2 = EI\left[\underbrace{\alpha_b\int_0^L \left[B_b\right]^T\left[B_b\right]dx}_{6x6} \;\vdots\; \underbrace{\left(1-\alpha_b\right)\int_0^L \left[B_b\right]^T\left[N\right]_z^b dx}_{6x2}\right]\left\{\begin{matrix}\{d\}\\ z_{b1}\\ z_{b2}\end{matrix}\right\} \tag{4.88}$$

Performing the indicated integrations and augmenting the displacement vector with the hysteretic parameters of the elements, the following relation is obtained:

$$\left[\left[K\right]_e \;\vdots\; \left[K\right]_h\right]\left\{\begin{matrix}\{d\}\\ \{z_u\}\\ \{z_b\}\end{matrix}\right\} = \left\{\begin{matrix}N_1\\ Q_1\\ M_1\\ N_2\\ Q_2\\ M_2\end{matrix}\right\} = \{f\} \tag{4.89}$$

where

$$\left[K\right]_e = \begin{bmatrix} \frac{\alpha_u EA}{L} & 0 & 0 & -\frac{\alpha_u EA}{L} & 0 & 0 \\ 0 & \frac{12\alpha_b EI}{L^3} & \frac{6\alpha_b EI}{L^2} & 0 & -\frac{12\alpha_b EI}{L^3} & \frac{6\alpha_b EI}{L^2} \\ 0 & \frac{6\alpha_b EI}{L^2} & \frac{4\alpha_{\ b} EI}{L} & 0 & -\frac{6\alpha_b EI}{L^2} & \frac{2\alpha_b EI}{L} \\ -\frac{\alpha_u EA}{L} & 0 & 0 & \frac{\alpha_u EA}{L} & 0 & 0 \\ 0 & -\frac{12\alpha_b EI}{L^3} & -\frac{6\alpha_b EI}{L^2} & 0 & \frac{12\alpha_b EI}{L^3} & -\frac{6\alpha_b EI}{L^2} \\ 0 & \frac{6\alpha_b EI}{L^2} & \frac{2\alpha_b EI}{L} & 0 & -\frac{6\alpha_b EI}{L^2} & \frac{4\alpha_b EI}{L} \end{bmatrix} \tag{4.90}$$

and

$$\left[K\right]_h = \begin{bmatrix} -\frac{\left(1-\alpha_u\right)}{2}EA & -\frac{\left(1-\alpha_u\right)}{2}EA & 0 & 0 \\ 0 & 0 & -\left(1-\alpha_b\right)\frac{EI}{L} & \left(1-\alpha_b\right)\frac{EI}{L} \\ 0 & 0 & -\left(1-\alpha_b\right)EI & 0 \\ \frac{\left(1-\alpha_u\right)}{2}EA & \frac{\left(1-\alpha_u\right)}{2}EA & 0 & 0 \\ 0 & 0 & \left(1-\alpha_b\right)\frac{EI}{L} & -\left(1-\alpha_b\right)\frac{EI}{L} \\ 0 & 0 & 0 & \left(1-\alpha_b\right)EI \end{bmatrix} \tag{4.91}$$

Equation (4.89) corresponds to the constitutive matrix relation of the element that includes the elastic (equation (4.90)) and the hysteretic (equation (4.91)) behavior, where the axial forces are uncoupled with bending moments and shear forces in both the elastic and hysteretic part.

4.4.5 Physical interpretation

The additive decomposition of the constitutive relations (4.73) and (4.74) into an elastic and a hysteretic part persists in the definition of the stiffness relation (4.89). To illuminate this fact, the case where $\alpha_u = \alpha_b = \alpha$ is examined. However, since axial forces and bending moments are uncoupled the same conclusions can be drawn for any value of the ratios α_u and α_b. When $\alpha_u = a_b = a$, the matrix equilibrium relation (4.89), can be cast in the following form:

$$\left\{f\right\} = \alpha\left[\tilde{K}\right]_e\left\{d\right\} + (1-\alpha)\left[\tilde{K}\right]_h\left\{z\right\} \tag{4.92}$$

where $\left[\tilde{K}\right]_e$ and $\left[\tilde{K}\right]_h$ are derived from relations (4.90) and (4.91) respectively by collecting terms. In equation (4.92), the first term represents an elastic behavior based on the reduced (plastic) stiffness and the second term adds the hysteretic part. This is interpreted as a supplement force vector to establish the elastic behavior before yielding and a constant force vector when yielding is exceeded.

It is evident that in the elastic case, where $\alpha = 1$, relation (4.92) reduces to the classical stiffness matrix of the elastic beam and the hysteretic degrees of freedom are wiped out as their coefficient matrix vanishes. Relation (4.92), together with the evolution equations of the hysteretic variables, suffice to define the constitutive behavior of the element. This constitutive matrix is fully determined at the elemental level and is computed once at the beginning of the analysis procedure thus, significantly reducing the computational cost of the proposed method.

Relation (4.89) can be expressed in terms of global end displacements $\{u\}$ of the element by using the following transformation relation $\{d\} = [\Lambda(\theta)]\{u\}$, where $[\Lambda(\theta)]$ is the 2D transformation matrix and θ is the right hand angle between the global X axis and the local x axis of the element, (Fig. 4.6). Taking into account that the global end forces $\{F\}$ relate to the end forces expressed in the local coordinate system through the transformation relation, equation (4.89) can be written as:

$$\{F\} = [\Lambda]^T [K]_e [\Lambda]\{u\} + [\Lambda]^T [K]_h \{z\} \tag{4.93}$$

for both axial and bending components.

4.4.6 Evolution equations

The nonlinear behavior of the element is governed by the Bouc-Wen evolution equations (4.71) and (4.75). These are nonlinear differential equations in time, depending on the hysteretic curvature $z_b(x,t)$ and the rate of curvature $\dot{\phi}$, as determined in relation (4.72) and in discretized form in relation (4.77) for the bending components. Similarly, the axial components are governed by hysteretic equations of the same form, depending on the hysteretic centerline axial deformation and the rate of total axial deformation. Therefore the evolution equation can be expressed in terms of nodal velocities as follows:

$$\dot{z}_b(x,t) = \left(1 - \left|\frac{z_b(x,t)}{z_b^y}\right|^n \left(\beta + \gamma\,\mathrm{sgn}\left(z_b(x,t)\left[B_b(x)\right]\left[\Lambda\right]\left\{\dot{u}\right\}\right)\right)\right)\left[B_b(x)\right]\left[\Lambda\right]\left\{\dot{u}\right\} \quad (4.94)$$

from which the discretized components at the nodal points are deduced as:

$$\dot{z}_{b1}(t) = \left(1 - \left|\frac{z_{b1}(t)}{z_b^y}\right|^n \left(\beta + \gamma\,\mathrm{sgn}\left(z_{b1}(t)\left[B_b(0)\right]\left[\Lambda\right]\left\{\dot{u}\right\}\right)\right)\right)\left[B_b(0)\right]\left[\Lambda\right]\left\{\dot{u}\right\} \quad (4.95)$$

and

$$\dot{z}_{b2}(t) = \left(1 - \left|\frac{z_{b2}(t)}{z_b^y}\right|^n \left(\beta + \gamma\,\mathrm{sgn}\left(z_{b2}(t)\left[B_b(L)\right]\left[\Lambda\right]\left\{\dot{u}\right\}\right)\right)\right)\left[B_b(L)\right]\left[\Lambda\right]\left\{\dot{u}\right\} \quad (4.96)$$

where $\left[B_b(0)\right]$ and $\left[B_b(L)\right]$ are derived from equation (4.77). Similar relations hold for the axial inelastic component, where in this case the strain displacement matrices are derived from equation (4.83). The corresponding discretized components at the nodal points are:

$$\dot{z}_{u1}(t) = \left(1 - \left|\frac{z_{u1}(t)}{z_u^y}\right|^n \left(\beta + \gamma\,\mathrm{sgn}\left(z_{u1}(t)\left[B_u(0)\right]\left[\Lambda\right]\left\{\dot{u}\right\}\right)\right)\right)\left[B_u(0)\right]\left[\Lambda\right]\left\{\dot{u}\right\} \quad (4.97)$$

and

$$\dot{z}_{u2}(t) = \left(1 - \left|\frac{z_{u2}(t)}{z_u^y}\right|^n \left(\beta + \gamma\,\mathrm{sgn}\left(z_{u2}(t)\left[B_u(L)\right]\left[\Lambda\right]\left\{\dot{u}\right\}\right)\right)\right)\left[B_u(L)\right]\left[\Lambda\right]\left\{\dot{u}\right\} \quad (4.98)$$

The evolution equations introduced in relations (4.95), (4.96), and (4.97), (4.98) adequately describe the nonlinear behavior of the beam element. One can notice that both evolution equations depend on the nodal velocities of the particular element and thus, can be treated separately at elemental level, processed in parallel for a given vector of nodal velocities. This constitutes the fundamental step in incorporating hysteretic modeling formulation into the finite element method and is of broader value.

It can be noticed also that the formulation of the governing equations of motion is independent of the type of the hysteretic model utilized in the analysis, since the evolution equations are introduced at the element level. However, the hysteretic model needs to be expressed in stress-resultant - generalized-displacement form and the hysteretic parameter in rate form in order to be implemented in the proposed scheme. Therefore if the appropriate hysteretic parameter is introduced in rate form any smooth hysteretic model can be treated by the proposed method (Thyagarajan, 1989), such as the Masing models of hysteresis (Chiang, 1999, Visintin, 2003), the Ramberg – Osgood model (Skelton et al.1997) or the bilinear Suzuki-Minai hysteretic model, (Guggenberger and Grundmann, 2005).

4.4.7 Large displacement formulation

The proposed element formulation can be extended into the field of large displacements, by introducing the appropriate non-linear strain measure, without modifying the governing constitutive equations.

Since the rotations, usually observed in structural members under seismic excitation, are small until failure, a large displacement but small rotation displacement field is implemented adhering to a Total Lagrangian Formulation approach. Such an approximation leads to an elegant, yet exact FEM formulation, Zienkiewicz and Taylor (2007). The following displacement field is introduced:

$$x = X + u\left(X\right) + Y\theta\left(X\right), \qquad y = w\left(X\right) + Y \tag{4.99}$$

where x denotes the position vector in the deformed configuration $\mathbf{C_0}$, X is the position vector with respect to the reference configuration $\mathbf{C_1}$, $u\left(X\right)$, $w\left(X\right)$ are the axial and transversal displacements of the cross section and $\theta\left(X\right)$ is the cross-sectional rotation as presented in Fig. 4.7.

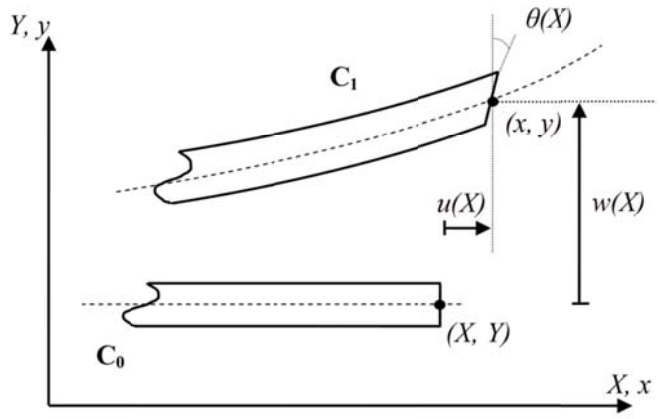

Fig. 4.7. Kinematics of large displacement beam element

The Green-Lagrange strain measure is defined as follows:

$$E_{xx} = \frac{\partial u}{\partial x} + \frac{1}{2}\left(\left(\frac{\partial u}{\partial x}\right)^2 + \left(\frac{\partial w}{\partial x}\right)^2\right) + Y\frac{\partial \theta}{\partial x} = E^0 + Y\phi \tag{4.100}$$

where E_{xx}, is the Green-Lagrange strain, θ is the rotation of the cross section and ϕ is the curvature defined in equation (4.72).

Using the second Piola stress tensor as the conjugate measure, the variational principle of virtual work is considered in terms of stresses and equivalently in terms of stress resultants as:

$$\delta\Pi = \int_{\Omega} \delta E_{xx} S_{xx} d\Omega - \delta\Pi_{ext} \Leftrightarrow \delta\Pi = \int_{L} \left(\delta E^0 N + \delta\phi M\right) dx - \delta\Pi_{ext} \tag{4.101}$$

where the axial force N and the bending moment M are defined respectively as:

$$N = \int_{A} S_{xx} dA, \qquad M = \int_{A} S_{xx} \mathrm{Y}\, dA \tag{4.102}$$

Substituting the Green-Lagrange strain measures into relations (4.73) and (4.74), the following constitutive relations are obtained:

$$N\left(x,t\right) = EA \cdot \tilde{E}_0\left(x,t\right)$$
$$\tilde{E}_0\left(x,t\right) = \alpha_u \left(\frac{\partial u}{\partial x} + \frac{1}{2}\left(\left(\frac{\partial u}{\partial x} \right)^2 + \left(\frac{\partial w}{\partial x} \right)^2 \right) \right) + \left(1-\alpha_u\right) z_u\left(x,t\right) \tag{4.103}$$

and

$$M\left(x,t\right) = EI\tilde{\phi}\left(x,t\right), \qquad \tilde{\phi}\left(x,t\right) = \alpha_b \frac{\partial^2 w}{\partial x^2} + \left(1-\alpha_b\right) z_b\left(x,t\right) \tag{4.104}$$

In addition, the axial deformation of the centerline E^0 is rewritten in the following form:

$$E^0 = \varepsilon_x + \eta_x \tag{4.105}$$

where ε_x is the geometrically linear part of the axial deformation and η_x is the geometrically nonlinear part of the deformation. Implementing the interpolation field introduced in equations (4.76) the following nonlinear strain displacement equation is derived:

$$E^0 = \varepsilon_x + \eta_x = \left[B_L\right]\left\{d\right\} + \left[B_{NL}\right]\left\{d\right\} \tag{4.106}$$

where:

$$\left[B_L\right] = \left[B_u\left(x\right)\right], \qquad \left[B\right]_{NL} = \frac{1}{2}\left(\left[B_1\right]\left\{d_u\right\}\left[B_u\left(x\right)\right] + \left[B_2\right]\left\{d_b\right\}\left[B_b\left(x\right)\right]\right) \tag{4.107}$$

and $\left\{d_u\right\} = \left\{u_1 \quad u_2\right\}^T$, $\left\{d_b\right\} = \left\{w_1 \quad \theta_1 \quad w_2 \quad \theta_2\right\}^T$ while $\left[B_b\left(x\right)\right]$ and $\left[B_u\left(x\right)\right]$ are defined in equations (4.77) and (4.83) respectively. The auxiliary matrices introduced in equation (4.107) assume the following form:

$$\left[B_1\right] = \left[N_{1,x} \quad N_{4,x}\right], \qquad \left[B_2\right] = \left[N_{3,xx} \quad N_{4,xx} \quad N_{5,xx} \quad N_{6,xx}\right] \tag{4.108}$$

Substituting equations (4.105) - (4.108) in the variational principle (4.101) and performing the necessary algebraic manipulations the expressions derived for the small displacement case (relations (4.87) and (4.88)) are reformulated as follows:

$$I_1 = EA\left[\underbrace{\alpha_u \int_0^L \left(\left[B_L\right]+\left[B_{NL}\right]\right)^T \left(\left[B_L\right]+\left[B_{NL}\right]\right) dx}_{6x6} \;\vdots\; \underbrace{\left(1-\alpha_u\right) \int_0^L \left(\left[B_L\right]+\left[B_{NL}\right]\right)^T \left[N\right]_z^u dx}_{6x2}\right] \begin{Bmatrix} \{d\} \\ z_{u1} \\ z_{u2} \end{Bmatrix} \tag{4.109}$$

and

$$I_2 = EI\left[\underbrace{\alpha_b \int_0^L \left[B_b\right]^T \left[B_b\right] dx}_{6x6} \;\vdots\; \underbrace{\left(1-\alpha_b\right) \int_0^L \left[B_b\right]^T \left[N\right]_z^b dx}_{6x2}\right] \begin{Bmatrix} \{d\} \\ z_{b1} \\ z_{b2} \end{Bmatrix} \tag{4.110}$$

where the $6x6$ sub matrices correspond to the standard large displacement stiffness matrix, Zienkiewicz and Taylor (2007) and the remaining parts can be deduced symbolically using one of the available symbolic languages such as Maple, MapleSoft (2007) or Mathematica, (Wolfram Mathematica, 2009). The matrix derived from equation (4.110) coincides with the bending contribution in the small displacement case presented in equation (4.89). The 6x2 submatrix of equation (4.109) is:

$$\left[H\right]_u = \begin{bmatrix} -\frac{1}{2}-\frac{\Delta u}{2L} & \frac{L\left(\theta_1+\theta_2\right)-12\Delta w}{20L} & \frac{L}{15}\left(\theta_1-\frac{1}{4}\theta_2\right)-\frac{1}{20}\Delta w & \frac{1}{2}+\frac{\Delta u}{2L} & -\frac{L\left(\theta_1+\theta_2\right)-12\Delta w}{20L} & \frac{L}{15}\left(\theta_2-\frac{1}{4}\theta_1\right)-\frac{1}{20}\Delta w \\ -\frac{1}{2}-\frac{\Delta u}{2L} & \frac{L\left(\theta_1+\theta_2\right)-12\Delta w}{20L} & \frac{L}{15}\left(\theta_1-\frac{1}{4}\theta_2\right)-\frac{1}{20}\Delta w & \frac{1}{2}+\frac{\Delta u}{2L} & -\frac{L\left(\theta_1+\theta_2\right)-12\Delta w}{20L} & \frac{L}{15}\left(\theta_2-\frac{1}{4}\theta_1\right)-\frac{1}{20}\Delta w \end{bmatrix}^T \tag{4.111}$$

where: $\Delta w = w_2 - w_1$ and $\Delta u = u_2 - u_1$.

The above relations are adequate for the geometrically nonlinear analysis where also separation of the elastic and hysteretic part is retained. As in the small displacement approach, this formulation is independent of the particular hysteretic model.

4.4.8 Standard second order representation

For a specific plane frame structure with n_f degrees of freedom and given connectivity of n_{el} elements, mass distribution and boundary conditions, dynamic equilibrium can be established in terms of nodal displacements, velocities and accelerations as follows:

$$\left[M\right]_S\left\{\ddot{U}\right\}+\left[C\right]_S\left\{\dot{U}\right\}+\left[K\right]_S\left\{U\right\}+\left[H\right]_S\left\{Z\right\}=\left\{P(t)\right\} \tag{4.112}$$

where $\left[M\right]_S, \left[C\right]_S, \left[K\right]_S$ are the mass, viscous damping and stiffness square symmetric $(n_f x\ n_f)$ matrices respectively and $\left[H\right]_S$ is the orthogonal $\left(n_f\ x\ 4n_{el}\right)$ hysteretic matrix of the structure, while $\left\{P(t)\right\}$ is the $\left(n_f x1\right)$ vector of external forces. These matrices are assembled following the direct stiffness method, Bathe (2007), where the stiffness matrix contains only the elastic part of the element stiffness of relation (4.89). The mass matrix may correspond to a lumped mass diagonal matrix, or a consistent mass matrix, Bathe (2007).

The viscous damping matrix in general may be of the form of a Rayleigh damping matrix, Chopra (2006). Furthermore, $\left\{U\right\}$ is the $\left(n_f x1\right)$ vector of unknown global nodal displacements and $\left\{Z\right\}$ is the $\left(4n_{el}x1\right)$ vector of unknown hysteretic degrees of freedom. These vectors dictate the dimensions of the hysteretic matrix $\left[H\right]_S$. The hysteretic behavior is defined at the element level in terms of hysteretic curvatures and centerline axial deformations from relation (4.91). The contribution of the hysteretic matrix of each element expressed in global terms is appended to form the corresponding hysteretic matrix $\left[H\right]_S$, which expresses the hysteretic contribution that corresponds to the total degrees of freedom of the structure. This assembly scheme is demonstrated in detail in Example 2. Equations (4.112), together with the evolution equations for the entire set of the introduced hysteretic parameters (4.95),

(4.96), and (4.97), (4.98), fully describe the response of the system to a given external force and initial conditions.

To comply with the formulation presented herein, modifications in the structure of a standard FEM code are required. These concern the evaluation of the hysteretic matrix $\left[H\right]_S$, the incorporation of the evolution equations and a first order ode algorithm to provide the solution in conjunction with a standard Newmark method for the integration of the equations of motion. Moreover, the element proposed herein can be easily incorporated in a joined analysis – identification software, as proposed in Piyawat K., Pei J. S 2009. In this work, the governing equations are written in state-space form and a predictor-corrector differential solver is implemented, Radhakrishnan and Hindmarsh (1993), as described in the next section.

4.4.9 State-space formulation

By introducing as auxiliary unknown the vector of global nodal velocities $\left\{\dot{U}\right\}$, the dynamic equilibrium equations (4.112) can stated in state-space the form of $2n_f$ linear differential equations of first order as follows:

$$\begin{Bmatrix}\left\{\dot{U}\right\}\\ \left\{\ddot{U}\right\}\end{Bmatrix}=\left[\begin{array}{ccc}0 & I & 0\\ \hline -\left[M\right]^{-1}\left[K\right] & -\left[M\right]^{-1}\left[C\right] & -\left[M\right]^{-1}\left[H\right]\end{array}\right]\begin{Bmatrix}\left\{U\right\}\\ \left\{\dot{U}\right\}\\ \left\{Z\right\}\end{Bmatrix}+\begin{Bmatrix}0\\ \left\{P(t)\right\}\end{Bmatrix} \quad (4.113)$$

These are coupled with the nonlinear set of $2n_{el}$ evolution equations of the form:

$$\left\{\dot{Z}\right\}=f(\left\{\dot{U}\right\},\left\{Z\right\}) \quad (4.114)$$

which are decomposed further in n_{el} sets of pairs of coupled equations as described in equations (4.95) and (4.96).

For small displacement analysis, equation (4.113) that expresses the dynamic equilibrium of the structure depends on global system matrices defined once at the beginning of the analysis, remaining constant in all subsequent steps. Moreover, the evolution of the elastoplastic behavior is treated at the element level in a decoupled and thus implicitly parallel form implementing relations (4.95), (4.96) and (4.97), (4.98) for the bending and the axial components respectively.

As the coupled system of equations (4.113) and (4.114) does not lend itself to an analytical solution, the system is cast in the form of a general nonlinear set of first order differential equations. Equations (4.113) can be written into a non-autonomous state–space formulation of the following form:

$$\{\dot{x}\} = G(\{x\}) + \{P(t)\} \tag{4.115}$$

where the vector $\{x\}$ is defined as:

$$\{x\}^T = \begin{bmatrix} \{U\}^T & \{\dot{U}\}^T & \{Z\}^T \end{bmatrix} \tag{4.116}$$

and $G(\{x\})$ is defined as follows:

$$G(\{x\}) = \begin{bmatrix} \mathbf{0} & I & \mathbf{0} \\ [M]^{-1}[K] & [M]^{-1}[K] & [M]^{-1}[H] \\ \mathbf{0} & V(\{\dot{U}\},\{Z\}) & \mathbf{0} \end{bmatrix} \tag{4.117}$$

The operator G is a state dependent operator since V holds the evolution equations for each element i, that is:

$$V_j^i\left(\{\dot{u}\}^i,\{z\}^i\right) = \left(1 - \left|\frac{z_j(t)}{z^y}\right|^n \left(\beta + \gamma\,\mathrm{sgn}\left(z_j(t)[B]_j[\Lambda]\{\dot{u}\}\right)\right)\right)[B]_j[\Lambda]\{\dot{u}\}^i \qquad j = 1,2 \tag{4.118}$$

where parameter z^y in (4.118) assumes the corresponding, axial (z_u^y) or bending (z_b^y), yield value. The above system, for specific dynamic loading and given initial conditions on $\{x\}$, is integrated using one of the robust numerical integrators such are those of Runge-Kutta type, or Livermore algorithms, Radhakrishnan and Hindmarsh (1993), which though are not usually included in standard FEM codes.

4.4.10 Cantilever beam under monotonically increasing load

A cantilever beam is analyzed based on the proposed formulation, and the results are compared with the ones obtained using Nastran FEM code, Noran Engineering (2007). The geometrical parameters and the mechanical properties of the problem are summarized in Fig. 4.8.

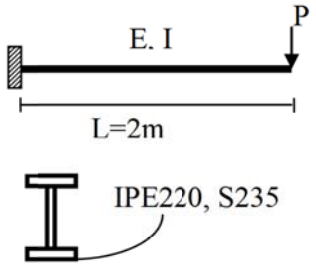

L	2 m
E_{young}	210 GPa
I	2770 cm^4
W_{el}	252 cm^3
W_{pl}	285 cm^3
$\bar{m}$	26.2 Kg/m

Problem parameters

Fig. 4.8 Beam Geometry

A bilinear moment-curvature relationship with kinematic hardening is considered, assigning appropriate Bouc-Wen parameters (n = 25, $\beta = \gamma$ = 0.5, $\alpha_u = \alpha_b$ = 0.002). The Belytschko – Schwer beam element formulation, Belytschko (1977), is used in Nastran code. The Belytschko – Schwer beam element recovers stress in fibers along the element's length, yielding a robust and accurate solution for elastoplastic problems exhibiting large displacements.

A monotonically increasing concentrated load is applied at the free end up to the failure load. The load is subdivided in 10 steps. The tip displacement against the imposed load is depicted in Fig. 4.9(a). The one element based on proposed development succeeds in determining the yield displacement and the ultimate load capacity of the cantilever beam, while at the same time reaches the ultimate displacement quite accurately as compared to a ten element model using Nastran code. In Fig. 4.9(b), a comparison of the load path for different discretization schemes of the proposed formulation is presented. It is noticeable that the proposed element has the same behavior as the Belytschko – Schwer element.

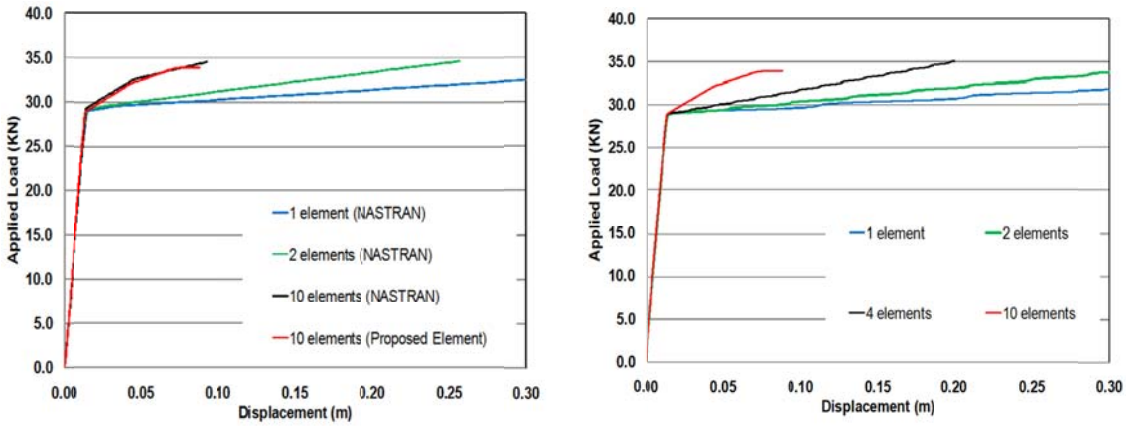

(a) (b)

Fig. 4.9 Tip Displacement – Imposed Load Diagram (a) Proposed Formulation vs. Nastran code (b) Results obtained for different discretization schemes (proposed formulation)

Next, a large displacement analysis is performed and the results are compared to the small displacement nonlinear formulation. The 10 element discretization is considered for this comparison since it yields accurate results. Plasticity is considered both in the flexural and the axial degrees of freedom. The nonlinear large displacement analysis lasted 10 seconds in a personal computer equipped with a Core Duo Processor and 4 GB of RAM.

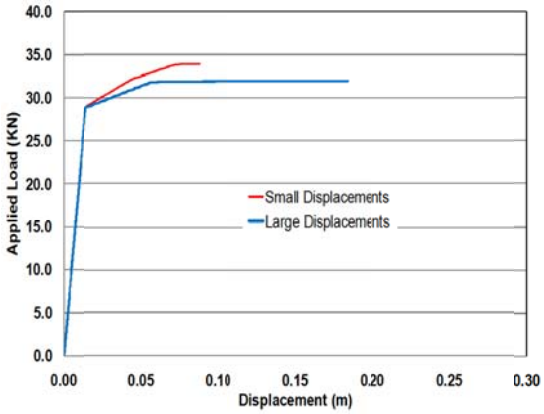

Fig. 4.10 Comparison of Large Displacement vs. Small Displacement approach

In Fig. 4.10 the results obtained from both analyses are presented. Since material nonlinearity dominates the response of the cantilever beam the two solutions almost coincide for the elastic branch. Differences are observed at the nonlinear branch. This is attributed to the fact that the beam undergoes nonlinear axial deformations. These axial deformations are the result of the large displacement theory and do not arize in a small displacement analysis as equilibrium is established at the initial configuration.

4.4.11 The staircase frame

This problem is analyzed by Barham et al. (2005). A staircase frame is considered as illustrated in Fig. 4.11. Each member is modeled using one element. The material is considered to be elastic perfectly plastic with a yield stress of 250 MPa and an elastic modulus of 200 GPa. The corresponding Bouc-Wen parameters are evaluated as presented in Fig. 4.11. Since this example is solely for the demonstration of the validity of the proposed formulation, the element is considered to be elastic with respect to axial centerline deformations. This is accomplished by setting α_u=1 in relations (4.90) and (4.91).

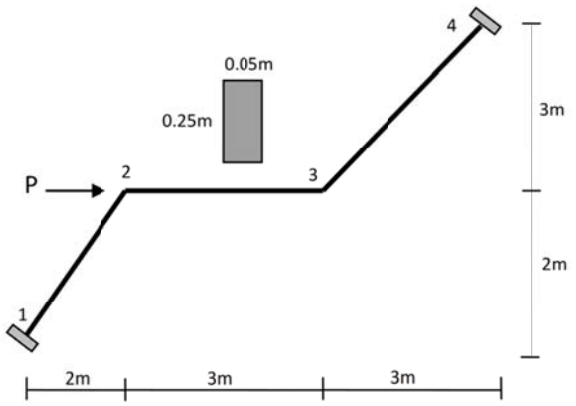

β	0.5
γ	0.5
n	25
z_b^y	0.0112 m^{-1}

Bouc-Wen Parameters

Fig. 4.11. Geometry of the staircase frame

The frame is considered fixed at its two ends, and the total number of nodal degrees of freedom is six, namely the horizontal and vertical displacement and the rotation of nodes 2 and 3. This vector of global nodal displacements $\{U\}$ and the hysteretic vector $\{Z\}$ that appears in the equation of motion (4.112) are presented in Fig. 4.12. As noted, the vector of the unknown displacements is augmented with the set of unknown hysteretic components that are defined at the end nodes of each element to depict the inelastic behavior, also at fixed ends.

The hysteretic matrices of the three elements in the local coordinate system are:

$$[H]^1=\begin{bmatrix} 0 & 0 & 0 & 0 \\ 0 & 0 & -4603.1 & 4603.1 \\ 0 & 0 & -13019.53 & 0 \\ 0 & 0 & 0 & 0 \\ 0 & 0 & 4603.1 & -4603.1 \\ 0 & 0 & 0 & -13019.53 \end{bmatrix}$$

$$[H]^2=\begin{bmatrix} 0 & 0 & 0 & 0 \\ 0 & 0 & -4339.84 & 4339.84 \\ 0 & 0 & -13019.53 & 0 \\ 0 & 0 & 0 & 0 \\ 0 & 0 & 4339.84 & -4339.84 \\ 0 & 0 & 0 & -13019.53 \end{bmatrix}, [H]^3=\begin{bmatrix} 0 & 0 & 0 & 0 \\ 0 & 0 & -3068.73 & 3068.73 \\ 0 & 0 & -13019.53 & 0 \\ 0 & 0 & 0 & 0 \\ 0 & 0 & 3068.73 & -3068.73 \\ 0 & 0 & 0 & -13019.53 \end{bmatrix} \quad (4.119)$$

The matrices corresponding to the global coordinate system evaluated as indicated in relation (4.93) as:

$$\left[\bar{H}\right]^1 = \begin{bmatrix} 0 & 0 & 3254.88 & -3254.88 \\ 0 & 0 & -3254.88 & 3254.88 \\ 0 & 0 & -13019.53 & 0 \\ 0 & 0 & -3254.88 & 3254.88 \\ 0 & 0 & 3254.88 & -3254.88 \\ 0 & 0 & 0 & 13019.53 \end{bmatrix}$$

$$\left[\bar{H}\right]^2 = \begin{bmatrix} 0 & 0 & 0 & 0 \\ 0 & 0 & -4339.84 & 4339.84 \\ 0 & 0 & -13019.53 & 0 \\ 0 & 0 & 0 & 0 \\ 0 & 0 & 4339.84 & -4339.84 \\ 0 & 0 & 0 & -13019.53 \end{bmatrix}, \quad \left[\bar{H}\right]^3 = \begin{bmatrix} 0 & 0 & 2169.92 & -2169.92 \\ 0 & 0 & -2169.92 & 2169.92 \\ 0 & 0 & -13019.53 & 0 \\ 0 & 0 & -2169.92 & 2169.92 \\ 0 & 0 & 2169.92 & -2169.92 \\ 0 & 0 & 0 & 13019.53 \end{bmatrix} \tag{4.120}$$

Consequently, the hysteretic matrix of the structure is derived by appending the global hysteretic element matrices, yielding:

$$\left[H\right]_S = \begin{bmatrix} 0 & 0 & -3254.88 & 3254.88 & 0 & 0 & 0 & 0 & 0 & 0 & 0 & 0 \\ 0 & 0 & 3254.88 & -3254.88 & 0 & 0 & -4339.84 & 4339.84 & 0 & 0 & 0 & 0 \\ 0 & 0 & 0 & 13019.53 & 0 & 0 & -13019.53 & 0 & 0 & 0 & 0 & 0 \\ 0 & 0 & 0 & 0 & 0 & 0 & 0 & 0 & 0 & 0 & 2169.92 & -2169.92 \\ 0 & 0 & 0 & 0 & 0 & 0 & 4339.84 & -4339.84 & 0 & 0 & -2169.92 & 2169.92 \\ 0 & 0 & 0 & 0 & 0 & 0 & 0 & -13019.53 & 0 & 0 & -13019.53 & 0 \end{bmatrix} \tag{4.121}$$

This matrix, when inserted into the equation of motion (4.112), yields the nonlinear correction nodal loads to the elastic ones, $F_i, i = 1...6$, which are illustrated in Fig. 4.12.

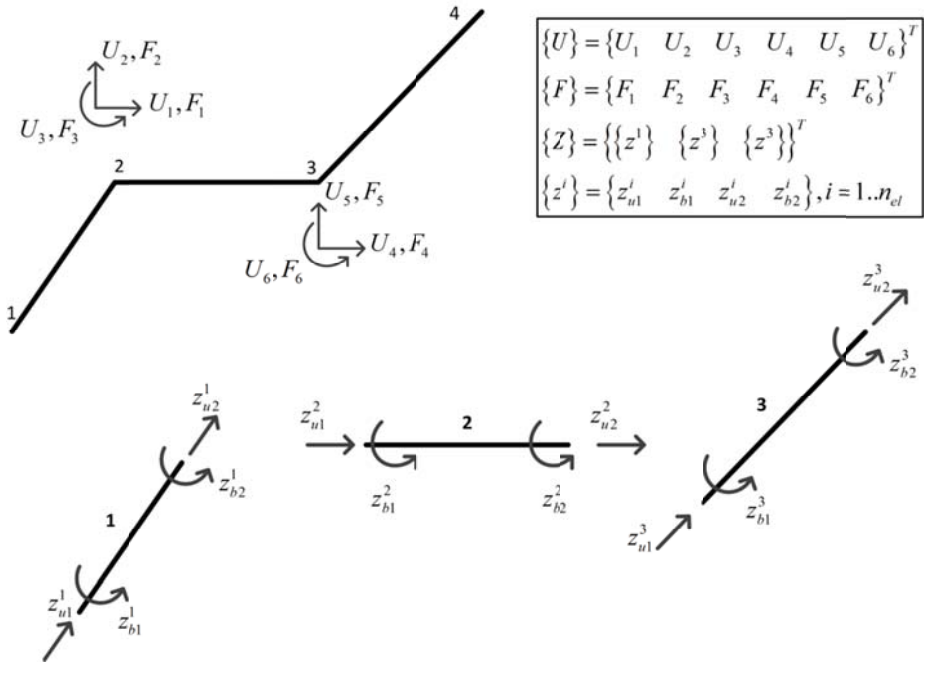

Fig. 4.12 Global and hysteretic degrees of freedom

To compare the results, a conventional finite element analysis is performed using the Abaqus code (Karlsson & Sorensenn, 2000). In total, 202 elements were needed to achieve a satisfactory agreement. Exact integration along the element's height was implemented in Abaqus to determine the collapse load. A force control pushover analysis is also conducted, implementing the fiber force based element of the OPENSEES code (McKenna et al., 2000). The full Newton-Raphson solution scheme is implemented with a force increment of 0.05 kN. To facilitate numerical convergence, a slight kinematical hardening was allowed in the OPENSEES analysis, letting the kinematic hardening modulus equal to $H_{kin} = 0.34MPa$. Three force based elements are used to discretize the structure while 4 integration points along each element's length are considered. Ten fibers are considered along the section's height. The load displacement path of the problem is presented in Fig. 4.13, where the results of the OPENSEES analysis model considering an elastic perfect plastic material are also plotted.

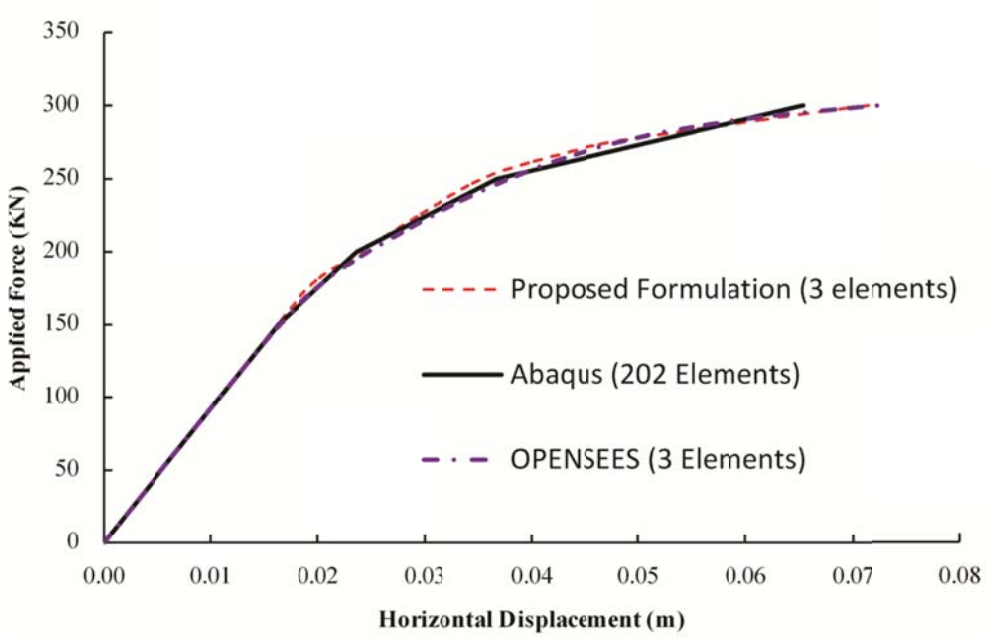

Fig. 4.13. Load Displacement Curves

It is evident from Fig. 4.13 that the three solution procedures yield practically the same nonlinear path. The proposed method converges much faster than the Abacus code, since only 3 elements are needed. This is attributed to the solution method which avoids linearization as discussed in the preceding paragraphs, but also to the element formulation that assumes an exact interpolation field for the hysteretic curvatures of the two node beam element. The results obtained from the OPENSEES code also agree with the results obtained from the proposed formulation. All the analyses were conducted on a personal computer equipped with a Core Duo processor and 4 GB of RAM. The computational time required was 55 sec for the Abaqus model, 5 sec for the OPENSEES model and 3 sec for the proposed formulation.

4.5 The Timoshenko beam element

4.5.1 The multi-axial formulation of Bouc-Wen hysteresis

The Bouc-Wen model was introduced by Bouc (1967) and modified subsequently by Wen (1976), Baber &Noori (1985) and Sivaselvan & Reinhorn (2000). To account for yield criteria involving more than one components of the stress tensor, a general formulation is needed to address the inherent interaction. Following Sivaselvan and Reinhorn (2003), the stress tensor can be decomposed into an elastic and hysteretic part as follows:

$$\{\sigma\} = \{\sigma^e\} + \{\sigma^h\} = [\alpha][E]\{\varepsilon\} + ([I] - [\alpha])[E]\{z\} \tag{4.122}$$

where $\{\sigma\}$ is the 6x1 stress vector, $\{\sigma^e\}$ is considered the elastic part of the stress tensor, $\{\sigma^h\}$ the hysteretic part of the stress tensor, $[\alpha]$ denotes a square diagonal matrix with post yield to elastic stiffness ratios, which for an isotropic material is considered constant, $[E]$, is the elastic constitutive matrix (Den Hartog, 1999), $[I]$ is the identity matrix, $\{\varepsilon\}$ is the 6x1

strain vector and $\{z\}$ is a 6x1 hysteretic strain vector. A hysteretic 6x1 stress vector is thus defined as:

$$\{\sigma^h\} = [E]\{z\} \tag{4.123}$$

Casciati (2006) proved that if the hysteretic vector evolves according to the following Bouc-Wen hysteretic rule:

$$\{\dot{\sigma}^h\} = [E]\{\dot{z}\} = [E]([I] - H_1 H_2 [R])\{\dot{\varepsilon}\} \tag{4.124}$$

then equation (4.122) accurately describes the nonlinear hysteretic behaviour of a material in the 3D stress space. In relation (4.124) H_1 and H_2 are smoothed Heaviside functions expressed in the following form:

$$\begin{aligned} H_1 &= \left\| \Phi\left(\{\sigma^h\}\right) + 1 \right\|^n, \; n \geq 2 \\ H_2 &= \gamma \, \mathrm{sgn}\left(\{\sigma^h\}^T \{\dot{\varepsilon}\} \right) + \beta \end{aligned} \tag{4.125}$$

where $\Phi\left(\{\sigma^h\}\right)$ is a yield criterion such that:

$$\Phi\left(\{\sigma^h\}\right) - 1 \leq 0 \tag{4.126}$$

with the equality holding when yield has occurred. In equation (4.125) n is the smoothing parameter and β, γ are shape factors that define the shape of the loading and unloading branches of the hysteretic loop. The first of equations (4.125) smooths the transition from the elastic to the inelastic region. The second controls the unloading phases under cyclic excitation. Equations (4.122) to (4.126) can be alternatively formulated in the stress-resultant space considering the proper, elastic, constitutive matrix and the proper vector of strains, conjugate to the stress-resultants (Symeonov et al., 2000).

Since rates of the corresponding parameter appear in both sides of equation (4.124) the hysteretic vector z is rate independent. The typical elastic-perfectly plastic hysteretic behaviour can be derived for $\beta = \gamma = 0.5$, $n > 6$ and $a = 0$ while a variety of other responses can be also obtained (Sivaselvan and Reinhorn, 2000).

Matrix [R] in relation (4.124) is an interaction matrix that depends on the yield function, given as:

$$\left[R\right] = \left[\left(\frac{\partial \Phi}{\partial \left\{\sigma^h\right\}}\right)^T \left[E\right]\left(\frac{\partial \Phi}{\partial \left\{\sigma^h\right\}}\right)\right]^{-1}\left[\left(\frac{\partial \Phi}{\partial \left\{\sigma^h\right\}}\right)\left(\frac{\partial \Phi}{\partial \left\{\sigma^h\right\}}\right)^T \left[E\right]\right] \tag{4.127}$$

The interaction matrix $\left[R\right]$ is formally derived by taking into account the consistency condition of associative plasticity (Casciati, 2006). Equations (4.122)and (4.124), yield a versatile formulation within the classical plasticity framework, where most of the associative flow rules are expressed in the stress space, (Lubliner, 2008).

4.5.2 Kinematic relations

A typical element of length L is considered (Fig.4.14 (a)) in which the nodal degrees of freedom in the local coordinate system are:

$$\left\{d\right\} = \left\{u_1 \quad w_1 \quad \theta_1 \quad u_2 \quad w_2 \quad \theta_2\right\}^T \tag{4.128}$$

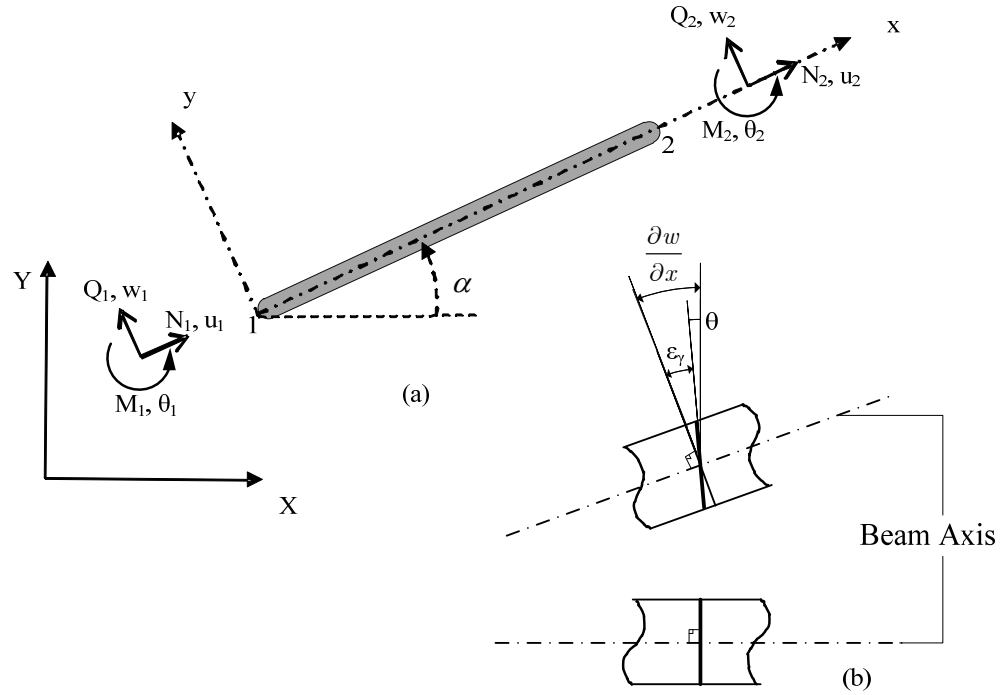

Fig.4.14 (a) Nodal displacements and loads (b) Timoshenko kinematic assumption

The following kinematic assumptions are considered according to the Timoshenko theory of bending (Fig.4.14 (b)):

$$\varepsilon_u = \frac{\partial u}{\partial x}, \quad \varepsilon_\phi = \frac{\partial \theta}{\partial x}, \quad \varepsilon_\gamma = \frac{\partial w}{\partial x} - \theta \tag{4.129}$$

4.5.3 Exact shape functions

In the work presented herein, the shape functions implemented are explicitly derived from the exact solution of the homogeneous Timoshenko beam differential equations:

$$\begin{cases} EI\dfrac{\partial^2 \theta}{\partial x^2} + kGA\left(\dfrac{\partial w}{\partial x} - \theta\right) = 0 \\ kGA\left(\dfrac{\partial^2 w}{\partial x^2} - \dfrac{\partial \theta}{\partial x}\right) = 0 \end{cases} \tag{4.130}$$

where k is the shear correction coefficient of the cross section (Dong et al., 2010). An exact solution can be evaluated for a variable cross-section along the element's length. For the sake

of presentation the case of a constant cross-section is considered in this work. The solution of the system of differential equations (4.130) is:

$$\begin{aligned} \theta_z\left(x\right) &= \left(\frac{EI}{kGA}+\frac{1}{2}\right)C_1x^2+C_2x+C_3 \\ w\left(x\right) &= \frac{1}{6}C_1x^3+\frac{1}{2}C_2x^2+C_3x+C_4 \end{aligned} \tag{4.131}$$

where $C_i,\ i=1..4$ are integration constants. Imposing the set of boundary conditions $w_1=w\left(0\right),\ \theta_1=\theta\left(0\right),\ w_2=w\left(L\right),\ \theta_2=\theta\left(L\right)$ and solving for the integration constants the following interpolation field is derived, including also the axial displacements:

$$\begin{aligned} u\left(x\right) &= N_1u_1+N_4u_2 \\ w\left(x\right) &= N_2w_1+N_3\theta_1+N_5w_2+N_6\theta_2 \\ \theta\left(x\right) &= N_7w_1+N_8\theta_1+N_9w_2+N_{10}\theta_2 \end{aligned} \tag{4.132}$$

where the interpolation functions N_i introduced in equation (4.132) assume the following form:

$$\begin{aligned} N_1 &= 1-\frac{x}{L} & N_4 &= \frac{x}{L} \\ N_2 &= \frac{2\mu}{L^3}x^3-\frac{3\mu}{L^2}x^2-\frac{12\lambda\mu}{L}x+1 & N_3 &= \frac{\mu}{L^2}x^3-\frac{2\left(1+3\lambda\right)\mu}{L}x^2+\left(6\lambda+1\right)\mu x \\ N_5 &= -\frac{2\mu}{L^3}x^3+\frac{3\mu}{L^2}x^2+\frac{12\lambda\mu}{L}x & N_6 &= \frac{\mu}{L^2}x^3-\frac{\left(-6\lambda+1\right)\mu}{L}x^2-6\lambda\mu x \\ N_7 &= \frac{6\mu}{L^3}x^2-\frac{6\mu}{L^2}x & N_8 &= \frac{3\mu}{L^2}x^2-\frac{4\left(1+3\lambda\right)\mu}{L}x+\mu\left(12\lambda+1\right) \\ N_9 &= -\frac{6\mu}{L^3}x^2+\frac{6\mu}{L^2}x & N_{10} &= \frac{3\mu}{L^2}x^2-\frac{2\mu\left(1-6\lambda\right)}{L}x \end{aligned} \tag{4.133}$$

with:

$$\mu=\frac{1}{1+12\lambda},\quad \lambda=\frac{EI}{kGAL^2} \tag{4.134}$$

The stiffness matrix of the element is then derived following the standard procedure of the Finite Element Method (Bathe, 2007) as:

$$K = \frac{EI}{L^3}\begin{bmatrix} 12\mu & 6\mu L & -12\mu & 6\mu L \\ 6\mu L & 4\mu\left(1+3\lambda\right)L^2 & -6\mu L & 2\mu\left(1-6\lambda\right)L^2 \\ -12\mu & -6\mu L & 12\mu & -6\mu L \\ 6\mu L & 2\mu\left(1-6\lambda\right)L^2 & -6\mu L & 4\mu\left(1+3\lambda\right)L^2 \end{bmatrix} \tag{4.135}$$

Contrary to the isoparametric finite element method, the element material properties are naturally considered in the interpolation functions through the constants λ and μ. As λ tends to zero, μ approaches unity, and the stiffness matrix of equation (4.135) degenerates into the Euler-Bernoulli stiffness matrix. The stiffness matrix is identical to the stiffness matrix of the Timoshenko beam element proposed by Macneal (1978) through the residual bending flexibility method or RBF. The proposed approach offers an interesting alternative with a better insight on the mechanics of the locking phenomenon. Moreover, the derived stiffness matrix is identical to the one derived by the exact, force based Timoshenko beam element formulation as described in Taylor et al. (2003).

Taking into account the axial degrees of freedom the following, augmented, strain-displacement matrix is derived:

$$\left[B\right] = \begin{bmatrix} -\frac{1}{L} & 0 & 0 & \frac{1}{L} & 0 & 0 \\ 0 & -\frac{12\lambda\mu}{L} & -6\lambda\mu & 0 & \frac{12\lambda\mu}{L} & -6\lambda\mu \\ 0 & -\frac{6\mu\left(-2x+L\right)}{L^3} & -\frac{2\mu}{L}\left(-3\frac{x}{L}+2\left(1+3\lambda\right)\right) & 0 & \frac{6\mu\left(-2x+L\right)}{L^3} & \frac{2\mu}{L}\left(3\frac{x}{L}-1+6\lambda\right) \end{bmatrix} \tag{4.136}$$

that corresponds to the 6x1 nodal displacement vector of relation (4.128).

Throughout the work presented herein, axial and bending deformations are considered to be uncoupled as implied by the kinematic assumptions assumed in equation (4.129).

4.5.4 The hysteretic degrees of freedom

Based on the previous results, the elastic deformation field is extended herein by introducing an additional vector of corresponding hysteretic degrees of freedom:

$$\varepsilon = \left\{ \varepsilon_u \quad \varepsilon_\gamma \quad \varepsilon_\phi \right\}^T \rightarrow \tilde{\varepsilon} = \left\{ \left\{ \varepsilon \right\} \,\middle|\, \left\{ \varepsilon^h \right\} \right\}^T = \left\{ \varepsilon_u \quad \varepsilon_\gamma \quad \varepsilon_\phi \,\middle|\, z_u \quad z_\gamma \quad z_\phi \right\}^T \quad (4.137)$$

In equation (4.137), the elastic strain vector ε, which consist of the centreline axial deformation ε_u, the shear deformation ε_γ and the curvature ε_ϕ, is extended to its generalized counterpart $\tilde{\varepsilon}$ comprising of the total strain vector $\left\{ \varepsilon \right\}$ and the hysteretic strain vector $\left\{ \varepsilon^h \right\}$. In the latter, z_u stands for the hysteretic part of the total centreline axial deformation, z_γ is the hysteretic part of the total shear strain and z_ϕ is the hysteretic part of the total curvature.

The following nonlinear hysteretic laws are considered for the stress resultants:

$$\begin{aligned} N\left(x\right) &= \alpha_u EA\varepsilon_u\left(x\right) + \left(1-\alpha_u\right)EAz_u\left(x\right) \\ Q\left(x\right) &= \alpha_\gamma GA_s\varepsilon_\gamma\left(x\right) + \left(1-\alpha_\gamma\right)GA_sz_\gamma\left(x\right),\ A_s = kA \\ M\left(x\right) &= \alpha_\phi EI\varepsilon_\phi\left(x\right) + \left(1-\alpha_\phi\right)EIz_\phi\left(x\right) \end{aligned} \quad (4.138)$$

where $\alpha_u, \alpha_\gamma, \alpha_\phi$ are the axial, shear and bending inelastic to elastic stiffness ratios respectively. If $\alpha_i = 0, i = u,\gamma,\phi$ then the corresponding nonlinear relation assumes an elastic perfectly plastic behaviour. If $\alpha_i = 1$ then the corresponding behaviour is elastic. According to the generalized hysteretic formulation presented in section 2.1, relation (4.138) can be cast in matrix form as:

$$\begin{aligned}\begin{Bmatrix} N \\ Q \\ M \end{Bmatrix}_{(x)} &= \begin{Bmatrix} N^e \\ Q^e \\ M^e \end{Bmatrix}_{(x)} + \begin{Bmatrix} N^h \\ Q^h \\ M^h \end{Bmatrix}_{(x)} \\ &= \begin{bmatrix} \alpha_u EA & & \\ & \alpha_\gamma GA_s & \\ & & \alpha_\phi EI \end{bmatrix} \begin{Bmatrix} \varepsilon_u \\ \varepsilon_\gamma \\ \varepsilon_\phi \end{Bmatrix}_{(x)} + \begin{bmatrix} (1-\alpha_u)EA & & \\ & (1-\alpha_\gamma)GA_s & \\ & & (1-\alpha_\phi)EI \end{bmatrix} \begin{Bmatrix} z_u \\ z_\gamma \\ z_\phi \end{Bmatrix}_{(x)}\end{aligned} \tag{4.139}$$

where (x) denotes dependence on the space variable. The evolution equations of the hysteretic components are equivalently defined as:

$$\begin{aligned}\begin{Bmatrix} \dot{N}^h \\ \dot{Q}^h \\ \dot{M}^h \end{Bmatrix}_{(x)} &= \begin{bmatrix} (1-\alpha_u)EA & & \\ & (1-\alpha_\gamma)GA_s & \\ & & (1-\alpha_\phi)EI \end{bmatrix} \begin{Bmatrix} \dot{z}_u \\ \dot{z}_\gamma \\ \dot{z}_\phi \end{Bmatrix}_{(x)} \\ &= \begin{bmatrix} (1-\alpha_u)EA & & \\ & (1-\alpha_\gamma)GA_s & \\ & & (1-\alpha_\phi)EI \end{bmatrix} ([I] - H_1 H_2 [R]) \begin{Bmatrix} \dot{\varepsilon}_u \\ \dot{\varepsilon}_\gamma \\ \dot{\varepsilon}_\phi \end{Bmatrix}_{(x)}\end{aligned} \tag{4.140}$$

where according to equation (4.125) H_1, H_2 may assume the following form:

$$\begin{aligned} H_1 &= \left\| \Phi\left(\begin{Bmatrix} N^h & Q^h & M^h \end{Bmatrix}^T \right) + 1 \right\|^n, \; n \geq 2 \\ H_2 &= \gamma \operatorname{sgn}\left(\begin{Bmatrix} N^h & Q^h & M^h \end{Bmatrix}^T \begin{Bmatrix} \dot{\varepsilon}_u \\ \dot{\varepsilon}_\gamma \\ \dot{\varepsilon}_\phi \end{Bmatrix} \right) + \beta \end{aligned} \tag{4.141}$$

where the yield surface Φ is expressed as a function of the hysteretic parts of the stress resultants that, referring to equation (4.139), are defined as:

$$\begin{Bmatrix} P^h \end{Bmatrix}_{(x)} = \begin{Bmatrix} N^h \\ Q^h \\ M^h \end{Bmatrix}_{(x)} = \begin{bmatrix} (1-\alpha_u)EA & & \\ & (1-\alpha_\gamma)GA_s & \\ & & (1-\alpha_\phi)EI \end{bmatrix} \begin{Bmatrix} z_u \\ z_\gamma \\ z_\phi \end{Bmatrix}_{(x)} \tag{4.142}$$

Furthermore, the interaction matrix $[R]$ is now expressed with respect to a stress-resultant based interaction surface Φ as:

$$\left[R\right]=\left[\left(\frac{\partial\Phi}{\partial\left\{P^{h}\right\}}\right)^{T}\left[D\right]\left(\frac{\partial\Phi}{\partial\left\{P^{h}\right\}}\right)\right]^{-1}\left[\left(\frac{\partial\Phi}{\partial\left\{P^{h}\right\}}\right)\left(\frac{\partial\Phi}{\partial\left\{P^{h}\right\}}\right)^{T}\left[D\right]\right] \tag{4.143}$$

The definition of the yield surface Φ depends on the geometric properties of the cross-section under consideration. Different formulations exist for rectangular, hollow and I-shaped, concrete or steel sections such as the Hodge's scheme (Lubliner, 2008) and the general yield function proposed by Neal, (1961). The yield surface can also be derived numerically on the grounds of a fibre analysis (Charalampakis and Koumousis, 2008). In this case, relation (4.143) is also evaluated numerically. In the example section of this work several yield surface formulations are exhibited.

Usually the nonlinear interaction between moment and shear is considered to be negligible, contrary to the axial-moment interaction. In this case, relation (4.140) is reformulated, to account for coupled axial-moment and uncoupled shear plasticity patterns as follows:

$$\begin{aligned}&\begin{Bmatrix}\dot{N}^{h}\\ \dot{M}^{h}\end{Bmatrix}_{(x)}=\begin{bmatrix}EA & \\ & EI\end{bmatrix}\begin{Bmatrix}\dot{z}_{u}\\ \dot{z}_{\phi}\end{Bmatrix}_{(x)}=\begin{bmatrix}EA & \\ & EI\end{bmatrix}\left(\left[I\right]-H_{1}H_{2}\left[R\right]\right)\begin{Bmatrix}\dot{\varepsilon}_{u}\\ \dot{\varepsilon}_{\phi}\end{Bmatrix}_{(x)}\\ &\dot{Q}^{h}=GA_{s}\dot{z}_{\gamma}=GA_{s}\left(1-H_{1}^{s}H_{2}^{s}\right)\dot{\varepsilon}_{\gamma}\end{aligned} \tag{4.144}$$

or

$$\begin{Bmatrix}\dot{z}_{u}\\ \dot{z}_{\phi}\\ \dot{z}_{\gamma}\end{Bmatrix}_{(x)}=\begin{bmatrix}\left[I\right]-H_{1}H_{2}\left[R\right] & 0\\ 0\quad 0 & \left(1-H_{1}^{s}H_{2}^{s}\right)\end{bmatrix}\begin{Bmatrix}\dot{\varepsilon}_{u}\\ \dot{\varepsilon}_{\phi}\\ \dot{\varepsilon}_{\gamma}\end{Bmatrix}_{(x)} \tag{4.145}$$

where in the first of equations (4.144) H_1, H_2 and $\left[R\right]$, are functions of the hysteretic axial force and the hysteretic moment. In the second of equations (4.144):

$$H_1^s = \left| \frac{Q^h}{Q_y^h} \right|^n$$
$$H_2^s = \beta_s + \gamma_s \operatorname{sgn}\left(Q^h \dot{\varepsilon}_\gamma \right) \tag{4.146}$$

and $Q_y^h = \left(1 - \alpha_s\right) Q_y$ is the hysteretic yield shear force.

4.5.5 Additional shape functions

Based on the deformation vector defined in equation (4.137), the vector of nodal degrees of freedom introduced in section 4.5.2is herein extended to the 12x1 vector $\left\{\tilde{d}\right\}$:

$$\left\{\tilde{d}\right\} = \left\{ \left\{d\right\} \,\vdots\, \left\{z\right\} \right\} = \left\{ u_1 \quad w_1 \quad \theta_1 \quad u_2 \quad w_2 \quad \theta_2 \,\vdots\, z_u^1 \quad z_u^2 \quad z_\gamma^1 \quad z_\gamma^2 \quad z_\phi^1 \quad z_\phi^2 \right\}^T \tag{4.147}$$

which consists of the total displacement vector $\left\{d\right\}$ and the hysteretic part of the total deformation $\left\{z\right\}$.

Equations (4.138) are rewritten in the following equivalent form:

$$\begin{aligned} N\left(x\right) &= EA\left(\alpha_u \varepsilon_u\left(x\right) + \left(1 - \alpha_u\right) z_u\left(x\right) \right) \\ Q\left(x\right) &= GA_s\left(\alpha_\gamma \varepsilon_\gamma\left(x\right) + \left(1 - \alpha_\gamma\right) z_\gamma\left(x\right) \right) \\ M\left(x\right) &= EI\left(\alpha_\phi \varepsilon_\phi\left(x\right) + \left(1 - \alpha_\phi\right) z_\phi\left(x\right) \right) \end{aligned} \tag{4.148}$$

The total part of the deformation component $\left\{\varepsilon\right\}$ depends solely on the total part of the displacement field through the compatibility relations introduced in equation (4.129). Thus, the shape functions introduced in equations (4.133) are also used in the nonlinear case for the interpolation of the total displacement component $\left\{d\right\}$.

The hysteretic deformation components are considered a perturbation of the total deformation components and as such, they are inserted into the problem with their

correspondent interpolation functions. Since equation (4.148) must hold for every possible value of α_i it must hold for $\alpha_i = 0$. Thus the following relations are derived:

$$\begin{aligned} N(x) &= EAz_u(x) \\ Q(x) &= GA_s z_\gamma(x) \\ M(x) &= EIz_\phi(x) \end{aligned} \tag{4.149}$$

Considering nodal equilibrium of the stress-resultants and relations (4.149), the following, exact, interpolation functions are derived for the corresponding hysteretic degrees of freedom:

$$\begin{aligned} z_u(x) &= \begin{bmatrix} 1/2 & 1/2 \end{bmatrix} \begin{Bmatrix} z_u^1 & z_u^2 \end{Bmatrix}^T \\ z_\gamma(x) &= \begin{bmatrix} 1/2 & 1/2 \end{bmatrix} \begin{Bmatrix} z_\gamma^1 & z_\gamma^2 \end{Bmatrix}^T \\ z_\phi(x) &= \begin{bmatrix} 1-\dfrac{x}{L} & \dfrac{x}{L} \end{bmatrix} \begin{Bmatrix} z_\phi^1 & z_\phi^2 \end{Bmatrix}^T \end{aligned} \tag{4.150}$$

where $z_i^j, j = 1,2, i = u,\gamma,\phi$ are the nodal hysteretic deformations. Thus, a hysteretic interpolation field is established denoted herein as $\left[N_z\right]$.

$$\left[N_z\right] = \begin{bmatrix} 1/2 & 1/2 & 0 & 0 & 0 & 0 \\ 0 & 0 & 1/2 & 1/2 & 0 & 0 \\ 0 & 0 & 0 & 0 & 1-\dfrac{x}{L} & \dfrac{x}{L} \end{bmatrix} \tag{4.151}$$

The interpolation field $\left[N_z\right]$ maps the continuous hysteretic deformation components into their corresponding nodal quantities.

Since no distributed axial and transverse loads are considered, a constant axial force and shear force is generated along the element's length. Consequently, the hysteretic components of the deformation are a function of the corresponding nodal components at the first end of the beam element. Thus, a total of 4 hysteretic degrees of freedom are necessary for the

derivation of the finite element. For the sake of completeness however, the presentation adopts the generalized nodal displacement vector of relation (4.147).

4.5.6 Derivation of stiffness matrix

Taking into account bending, shear and axial deformations, the principle of virtual work is formulated as:

$$\Pi_e = \{d\}^T \{P\} = \delta V = \int_0^L \left(M\delta\varepsilon_\phi + Q\delta\varepsilon_\gamma + N\delta\varepsilon_u \right) dx \tag{4.152}$$

where only nodal external loads are considered for the sake of simplicity. Substituting equations (4.138) into (4.152) the following relation is derived:

$$\begin{aligned} \{d\}^T \{P\} = & \int_0^L \left(\left(\alpha_\phi EI\varepsilon_\phi + \left(1-\alpha_\phi\right) EIz_\phi \right) \delta\varepsilon_\phi + \left(\alpha_\gamma GA_s\varepsilon_\gamma + \left(1-\alpha_\gamma\right) GA_s z_\gamma \right) \delta\varepsilon_\gamma \right) dx + \\ & \int_0^L \left(\alpha_u EA\varepsilon_u + \left(1-\alpha_u\right) EA \right) \delta\varepsilon_u dx \end{aligned} \tag{4.153}$$

Collecting the hysteretic parts of the above integrals, equation (4.153) is reformulated as:

$$\begin{aligned} \{d\}^T \{P\} = & \left(\int_0^L \left(\alpha_\phi EI\varepsilon_\phi \right) \delta\varepsilon_\phi dx + \int_0^L \alpha_\gamma GA_s\varepsilon_\gamma \delta\varepsilon_\gamma dx + \int_0^L \alpha_u EA\varepsilon_u \delta\varepsilon_u dx \right) + \\ & + \left(\int_0^L \left(\left(1-\alpha_\phi\right) EIz_\phi \right) \delta\varepsilon_\phi dx + \int_0^L \left(1-\alpha_\gamma\right) GA_s z_\gamma \delta\varepsilon_\gamma dx + \int_0^L \left(1-\alpha_u\right) EAz_u \delta\varepsilon_u dx \right) \end{aligned} \tag{4.154}$$

Writing the above integrals in matrix notation and substituting for the expressions of the interpolated fields introduced in equations (4.133) and (4.151) the following relations are derived:

$$\{\delta d\}^T \{P\} = \{\delta d\}^T I_e \{\delta d\} + \{\delta d\}^T I_h \{\varepsilon_h\} \tag{4.155}$$

where

$$I_e = \int_0^L \left[B\right]^T \left[D\right]\left[B\right] dx \tag{4.156}$$

and

$$I_h = \int_0^L \left[B\right]^T \left[D\right]\left[N_z\right] dx \tag{4.157}$$

where I_e is the internal energy corresponding to the total deformation components, I_h is the internal energy corresponding to the hysteretic deformation components , $\left[B\right]$ is defined in equation (4.136), $\left[N_z\right]$ in equation (4.151), $\left\{\varepsilon_h\right\}$ is the vector of hysteretic nodal degrees of freedom and $\left[D\right]$ is the constitutive matrix:

$$\left[D\right] = \begin{bmatrix} \alpha_u EA & & \\ & a_\gamma GA_s & \\ & & \alpha_\phi EI \end{bmatrix} \tag{4.158}$$

Equation (4.156) yields the elastic stiffness matrix of the beam element:

$$\left[k_e\right] = \frac{\alpha_\phi EI}{L} \begin{bmatrix} \frac{\alpha_u EA}{\alpha_\phi EI} & 0 & 0 & -\frac{\alpha_u EA}{\alpha_\phi EI} & 0 & 0 \\ 0 & 12\Phi_3 & 6\Phi_3 & 0 & -12\Phi_3 & 6\Phi_3 \\ 0 & 6\Phi_3 & 4\Phi_1 & 0 & -6\Phi_3 & 2\Phi_2 \\ -\frac{\alpha_u EA}{\alpha_\phi EI} & 0 & 0 & \frac{\alpha_u EA}{\alpha_\phi EI} & 0 & 0 \\ 0 & -12\Phi_3 & -6\Phi_3 & 0 & 12\Phi_3 & -6\Phi_3 \\ 0 & 6\Phi_3 & 2\Phi_2 & 0 & -6\Phi_3 & 4\Phi_1 \end{bmatrix} \tag{4.159}$$

where:

$$\Phi_1 = \left(1 + 6\lambda + 9\frac{\alpha_\gamma}{\alpha_\phi}\lambda + 36\lambda^2\right)\mu^2$$
$$\Phi_2 = \left(1 - 12\lambda + 18\frac{\alpha_\gamma}{\alpha_\phi}\lambda - 72\lambda^2\right)\mu^2$$
$$\Phi_3 = \beta GAL\left(1 + 12\frac{\alpha_\gamma}{\alpha_\phi}\lambda\right)\mu^2$$

while λ, μ are defined in relation (4.134). When $\alpha_v = \alpha_\phi = \alpha_\gamma = 1$ the stiffness matrix reduces to the Timoshenko formulation presented in relation (4.135).

Similarly, the integral of equation (4.157) yields the nonlinear hysteretic stiffness matrix of the element:

$$\left[k_h\right] = \begin{bmatrix} -\left(1-\alpha_u\right)EA & -\left(1-\alpha_u\right)EA & 0 & 0 & 0 & 0 \\ 0 & 0 & -6\mu_\gamma & 6\mu_\gamma & -\mu_\phi EI/L & \mu_\phi EI/L \\ 0 & 0 & -3\mu_\gamma & 3\mu_\gamma & -\mu_\phi EI\left(1+6\lambda\right) & -6\mu_\phi\lambda EI \\ \left(1-\alpha_u\right)EA & \left(1-\alpha_u\right)EA & 0 & 0 & 0 & 0 \\ 0 & 0 & 6\mu_\gamma & -6\mu_\gamma & \mu_\phi EI/L & -\mu_\phi EI/L \\ 0 & 0 & -3\mu_\gamma & 3\mu_\gamma & 6\mu_\phi\lambda EI & \mu_\phi EI\left(1+6\lambda\right) \end{bmatrix} \tag{4.160}$$

where:

$$\begin{aligned} \mu_\gamma &= \left(1-\alpha_\gamma\right)\mu \\ \mu_\phi &= \left(1-\alpha_\phi\right)\mu \end{aligned} \tag{4.161}$$

Similar to the elastic case, as λ tends to zero, μ tends to unity and the hysteretic matrix coincides with the one derived for the Euler-Bernoulli case (Triantafyllou & Koumousis, 2008). Substituting the derived expressions back to the principle of virtual work (equation (4.155)), the following constitutive equation is obtained at the element level:

$$\left\{P\right\} = \left[k_e\right]\left\{d\right\} + \left[k_h\right]\left\{z\right\} = \left[\left[k_e\right] \vdots \left[k_h\right]\right]\left\{\begin{matrix}\left\{d\right\} \\ \hline \left\{z\right\}\end{matrix}\right\} = \left[\tilde{k}\right]\left\{\tilde{d}\right\} \tag{4.162}$$

Equation (4.162) together with the set of Bouc-Wen evolution equations defined in relation (4.140) or relation (4.145) at $x = 0$ and $x = L$ smoothly describe the nonlinear cyclic response of a Timoshenko beam element. Considering for example relation(4.145), the corresponding nodal hysteretic quantities are expressed as:

$$\begin{Bmatrix} \dot{z}_u \\ \dot{z}_\phi \\ \dot{z}_\gamma \end{Bmatrix}_{x=0,L} = \begin{Bmatrix} \dot{z}_u^{1,2} \\ \dot{z}_\phi^{1,2} \\ \dot{z}_\gamma^{1,2} \end{Bmatrix} = \begin{bmatrix} [I] - H_1 H_2 [R] & 0 \\ 0 \quad 0 & 0 \\ & \left(1 - H_1^s H_2^s\right) \end{bmatrix}_{x=0,L} \left[\bar{B}\right]_{x=0,L} \{d\} \quad (4.163)$$

where $\left[\bar{B}\right]$ is the strain displacement matrix introduced in equation (4.136), properly reordered to account for the strain vector in relation (4.145).

4.5.7 State-space formulation

As in the Euler/Bernoulli formulation, the equations of motion are written into a non-autonomous state – space formulation of the following form:

$$\{\dot{x}\} = G(\{x\})\{x\} + \{P(t)\} \quad (4.164)$$

where the vector $\{x\}$ is defined as:

$$\{x\}^T = \begin{bmatrix} \{U\}^T & \{\dot{U}\}^T & \{Z\}^T \end{bmatrix} \quad (4.165)$$

and $G(\{x\})$ is defined as follows:

$$G(\{x\}) = \begin{bmatrix} \mathbf{0} & I & \mathbf{0} \\ [M]^{-1}[K] & [M]^{-1}[K] & [M]^{-1}[H] \\ \mathbf{0} & Y(\{\dot{U}\},\{Z\}) & \mathbf{0} \end{bmatrix} \quad (4.166)$$

The operator G is a state dependent operator since Y holds the evolution equations for each element i. Moreover, the evolution of the elastoplastic behaviour is treated at the element

level in a decoupled and thus implicitly parallel form considering an interaction scheme for the bending shear and axial components through relation (4.140) or the interaction of bending and axial components through relation (4.145). Considering the interaction scheme of relation (4.145), vector Y is defined as:

$$Y_j^i\left(\left\{\dot{u}\right\}^i,\left\{z\right\}^i\right)=\begin{bmatrix}[I]-H_1H_2\left[R\right] & 0\\ 0\quad 0 & \left(1-H_1^sH_2^s\right)\end{bmatrix}_j\left[\bar{B}\right]_j\left[\Lambda\right]\left\{\dot{u}\right\}^i,\ j=1,2 \quad (4.167)$$

where $\left[\Lambda\right]$ in equation (4.167) is the transformation matrix of the 2D beam element from the global to the local coordinate system defined in equation .

$$\left[\Lambda\right]=\begin{bmatrix}\cos\alpha & \sin\alpha & 0\\ -\sin\alpha & \cos\alpha & 0\\ 0 & 0 & 1\end{bmatrix} \quad (4.168)$$

where α is the angle between the local x axis and the global X axis, as presented in Fig.4.14(a).

4.5.8 Example 1 – Cantilever Beam

In this example, an aluminum cantilever beam presented in Fig.4.15 is examined. At first, a horizontal load is applied at the tip and the elastic response of the cantilever is compared to the analytical solution to validate the behaviour of the element in terms of shear-locking. Next, a nonlinear static analysis is conducted and the load – tip deflection curve is plotted for different values of the vertical load $\mathbf{P_y}$.

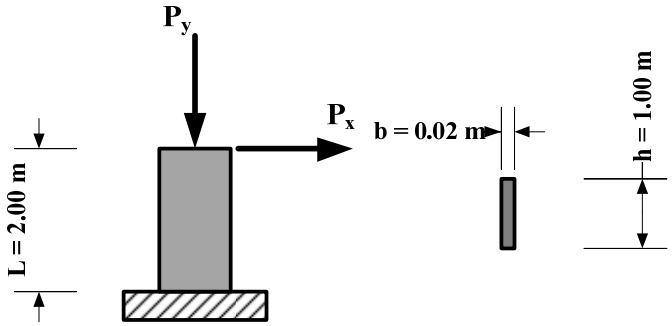

Fig.4.15 Cantilever beam

For the nonlinear analysis, full interaction between axial, shear and bending is considered through relations (4.140) to (4.143). The yield criterion proposed by Simo et al. (1983) is implemented:

$$\Phi = \left|\frac{M^h}{M_u^h}\right| + \left(\frac{N^h}{N_u^h}\right)^2 \left(1 + \left(\frac{V^h}{V_u^h}\right)^2\right) + \left(\frac{V^h}{V_u^h}\right)^4 \tag{4.169}$$

where for the rectangular cross-section $N_u^h = \left(1-\alpha_u\right)\sigma_y bh$, $V_u^h = \left(1-\alpha_\gamma\right)\sigma_y \Big/ \sqrt{3}\, bh$ $M_u^h = \left(1-\alpha_\phi\right)\sigma_y bh^2 \Big/ 4$, σ_y being the yield stress under uniaxial tension. The material properties considered are E=69 GPa, G=26 GPa, $\alpha_u = \alpha_\gamma = \alpha_\phi = 0.0$, $n = 25$, $\beta = \gamma = 0.5$, $\sigma_y = 275$ MPa. The shear coefficient for the rectangular cross-section is $k = 5 \Big/ 6$. The tip horizontal displacement and the tip rotation are evaluated analytically as:

$$\begin{aligned} u_{x,exact} &= \frac{P_x L^3}{3EI} + \frac{P_x L}{\beta GA} \\ \theta_{exact} &= -\frac{P_x L^2}{2EI} \end{aligned} \tag{4.170}$$

Considering the stiffness matrix of the proposed beam element presented in relations (4.159) to (4.161) and under the assumption of elasticity, the tip displacement of the cantilever beam discretized into 1 element is evaluated as:

$$\left.\begin{aligned} k_{55}^{el}u_x + k_{56}^{el}\theta = P_x \\ k_{65}^{el}u_x + k_{66}^{el}\theta = 0 \end{aligned}\right\} \Rightarrow \begin{aligned} u_x &= \frac{P_x L^3}{3EI} + \frac{P_x L}{\beta GA} = u_{x,exact} \\ \theta &= -\frac{P_x L^2}{2EI} = \theta_{exact} \end{aligned} \tag{4.171}$$

The proposed formulation yields an exact solution and no shear locking is developed, contrary to the Reduced Integration Timoshenko beam element and the Consistent Interpolation Beam Element that both yield the following results (Reddy, 1997):

$$\begin{aligned} u_x^{RIE,CIE} &= \frac{P_x L^3}{4EI} + \frac{P_x L}{\beta GA} \neq u_{x,exact} \\ \theta^{RIE,CIE} &= -\frac{P_x L^2}{2EI} = \theta_{exact} \end{aligned} \tag{4.172}$$

in which, the rotation evaluated is exact but the translation is smaller.

Next, a monotonically increasing load is imposed at the tip of the cantilever, and the force-displacement diagram is plotted, considering the yield criterion presented in relation(4.169). In Fig.4.16(a), the effect of the normalized axial load $n_p = N^h \big/ N_u^h$ on the nonlinear response of the cantilever is presented. The results obtained with the proposed formulation are compared with results obtained from Abaqus code (Karlsson & Sorensenn, 2000).

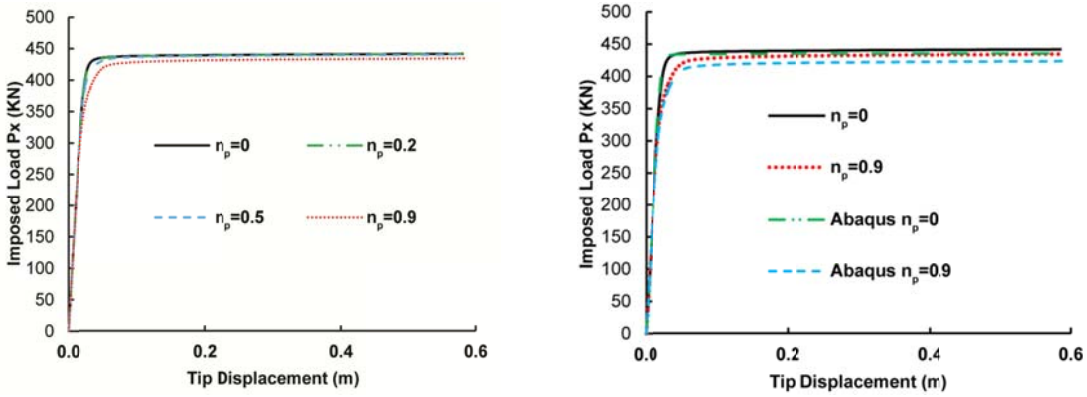

(a) (b)

Fig.4.16 (a) Effect of the axial force on the bearing capacity of the element (b) Comparison of proposed formulation with plane stress solution

In the latter, the cantilever is discretized with 160 quadrilateral plane stress elements considering a J_2 plasticity model, namely an elastic-perfectly plastic von-Mises material. Two cases are presented in Fig.4.16(b) for $n_p = 0$ and $n_p = 0.9$.

The ultimate load predicted from plasticity theory for zero axial load is (Lubliner, 2008) $P_U = \sigma_y bh^2 \big/ 4L = 440KN$. The value predicted by the proposed formulation is P_U=440.8 KN, while Abaqus predicts a value of P_U=439.2 KN. In both cases the error is less than 1.0%. The differences observed are due to the approximate nature of relation (4.169) as compared to the exact FEM solution. Nevertheless, the deviation of the proposed formulation from the exact solution for n_p=0.9 is 2.6%.

4.6 The 3d Hysteretic Timoshenko beam element formulation

In this section, the general case of a 3d Timoshenko hysteretic beam element formulation is presented. Shear-locking is also treated by extending the methodology proposed in section 4.5.3 at the three dimensional space. Furthermore, torsional warping is incorporated in the proposed formulation by introducing an additional degree of freedom, corresponding to the variation of the twisting angle along the element's length. The prismatic beam element and its corresponding degrees of freedom and nodal forces are presented in Fig. 4.17.

Inelasticity is introduced in all degrees of freedom through the interaction Bouc-Wen scheme presented in section 4.5.1. The most general case of yield criterion is considered where all the stress-resultants, namely the axial force, the shear forces, the bending and torsional moments, and the warping bi-moment interact.

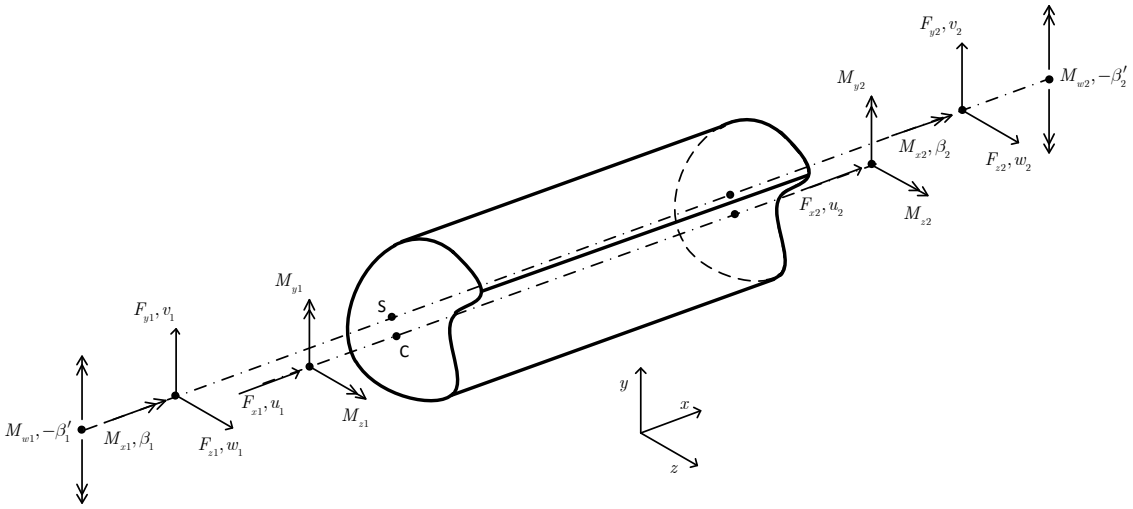

Fig. 4.17 Nodal displacement and forces

4.6.1 Bending in two directions

In the three dimensional case, the nodal displacement vector introduced in relation (4.128) is extended to a 12x1 vector defined as:

$$\{d\} = \{u_1 \quad v_1 \quad w_1 \quad \theta_{x1} \quad \theta_{y1} \quad \theta_{z1} \quad u_2 \quad v_2 \quad w_2 \quad \theta_{x2} \quad \theta_{y2} \quad \theta_{z2}\}^T \qquad (4.173)$$

where u, v, w are translations with respect to x, y, z axes and θ_x, θ_y, θ_z are the corresponding rotations as presented in Fig. 4.17. Having evaluated the expressions for the two dimensional case, the 3-dimensional case can be readily derived since bending in the two directions is considered to be uncoupled. Thus, the stiffness and hysteretic coefficients corresponding to displacements v_1, θ_{y1}, v_2, θ_{y2} and hysteretic deformations z_{sz1}, z_{by1}, z_{sz2}, z_{by2} are derived from their plane counterparts, minding the sign convention as presented in Fig. 4.18. Within this framework, the differential equation of bending in the xz plane is defined as:

$$\begin{cases} EI\dfrac{\partial^2\theta_z}{\partial x^2} - kGA\left(\dfrac{\partial v}{\partial x} + \theta_z\right) = 0 \\ kGA\left(\dfrac{\partial^2 v}{\partial x^2} + \dfrac{\partial\theta_z}{\partial x}\right) = 0 \end{cases} \tag{4.174}$$

whereas in the xy plane has been defined in relation (4.130). The derivation of equation (4.174) is presented in the Appendix. By applying the procedure introduced in section 4.5.3, the following set of exact shape functions is derived:

$$\begin{Bmatrix} v(x) \\ w(x) \\ \theta_y(x) \\ \theta_z(x) \end{Bmatrix} = \left[N\right]_b \left\{d\right\}_b \tag{4.175}$$

In relation (4.175), $\left\{d\right\}_b = \left\{v_1 \quad w_1 \quad \theta_{y1} \quad \theta_{z1} \quad v_2 \quad w_2 \quad \theta_{y2} \quad \theta_{z2}\right\}^T$ while the matrix $\left[N\right]_b$ is defined as:

$$\left[N\right]_b = \begin{bmatrix} N_2 & 0 & 0 & N_3 & N_5 & 0 & 0 & N_6 \\ 0 & N_9 & N_{10} & 0 & 0 & N_{12} & N_{13} & 0 \\ 0 & N_{15} & N_{16} & 0 & 0 & N_{17} & N_{18} & 0 \\ N_{19} & 0 & 0 & N_{20} & N_{21} & 0 & 0 & N_{22} \end{bmatrix} \tag{4.176}$$

where:

$$\begin{aligned} N_2 &= \frac{2\mu_{xz}}{L^3}x^3 - \frac{3\mu_{xz}}{L^2}x^2 - \frac{12\lambda_{xy}\mu_{xz}}{L}x + 1 & N_3 &= \frac{\mu_{xz}}{L^2}x^3 - \frac{2\left(1+3\,\lambda_{xz}\right)\mu_{xz}}{L}x^2 + \left(6\,\lambda_{xz}+1\right)\mu_{xz}x \\ N_5 &= -\frac{2\mu_{xz}}{L^3}x^3 + \frac{3\mu_{xz}}{L^2}x^2 + \frac{12\,\lambda_{xz}\mu_{xz}}{L}x & N_6 &= \frac{\mu_{xz}}{L^2}x^3 - \frac{\left(1-6\,\lambda_{xz}\right)\mu_{xz}}{L}x^2 - 6\lambda_{xz}\mu_{xz}x \\ N_{19} &= \frac{6\mu_{xz}}{L^3}x^2 - \frac{6\mu_{xz}}{L^2}x & N_{20} &= \frac{3\mu_{xz}}{L^2}x^2 - \frac{4\left(1+3\,\lambda_{xz}\right)\mu_{xz}}{L}x + \mu_{xz}\left(12\,\lambda_{xz}+1\right) \\ N_{21} &= -\frac{6\mu_{xz}}{L^3}x^2 + \frac{6\mu_{xz}}{L^2}x & N_{22} &= \frac{3\mu_{xz}}{L^2}x^2 - \frac{2\mu\left(1-6\,\lambda_{xz}\right)}{L}x \end{aligned} \tag{4.177}$$

with the constants μ_{xz} and λ_{xz} defined as:

$$\mu_{xz} = \frac{1}{1+12\lambda_{xz}},\ \lambda_{xz} = \frac{EI_z}{\kappa_y GAL^2} \tag{4.178}$$

Accordingly, the shape functions corresponding to bending in the xy plane are defined as:

$$\begin{aligned}
N_9 &= \frac{2\mu_{xy}}{L^3}x^3 - \frac{3\mu_{xy}}{L^2}x^2 - \frac{12\lambda_{xy}\mu_{xy}}{L}x + 1 & N_{10} &= -\frac{\mu_{xy}}{L^2}x^3 + \frac{2\left(1+3\lambda_{xy}\right)\mu_{xy}}{L}x^2 - \left(6\lambda_{xy}+1\right)\mu_{xy}x \\
N_{12} &= -\frac{2\mu_{xy}}{L^3}x^3 + \frac{3\mu_{xy}}{L^2}x^2 + \frac{12\lambda_{xy}\mu_{xy}}{L}x & N_{13} &= -\frac{\mu_{xy}}{L^2}x^3 + \frac{\left(1-6\lambda_{xy}\right)\mu_{xy}}{L}x^2 + 6\lambda_{xy}\mu_{xy}x \\
N_{15} &= -\frac{6\mu_{xy}}{L^3}x^2 + \frac{6\mu_{xy}}{L^2}x & N_{16} &= \frac{3\mu_{xy}}{L^2}x^2 - \frac{4\left(1+3\lambda_{xy}\right)\mu_{xy}}{L}x + \mu_{xy}\left(12\lambda_{xy}+1\right) \\
N_{17} &= \frac{6\mu_{xy}}{L^3}x^2 - \frac{6\mu_{xy}}{L^2}x & N_{18} &= \frac{3\mu_{xy}}{L^2}x^2 - \frac{2\mu_{xy}\left(1-6\lambda_{xy}\right)}{L}x
\end{aligned} \tag{4.179}$$

with the constants μ_{xy} and λ_{xy} defined as:

$$\mu_{xy} = \frac{1}{1+12\lambda_{xy}},\ \lambda_{xy} = \frac{EI_y}{\kappa_z GAL^2} \tag{4.180}$$

Considering the kinematic relations of the Timoshenko theory of bending as presented in the Appendix, the exact strain-displacement matrix of the 3d Timoshenko beam element is defined as:

$$\left\{\varepsilon_b\right\} = \left[\tilde{B}\right]_b \left\{d\right\}_b \tag{4.181}$$

where $\left\{\varepsilon_b\right\} = \left\{\phi_y \quad \gamma_{xz} \quad \phi_z \quad \gamma_{xy}\right\}^T$ and:

$$\left[\tilde{B}\right]_b = \begin{bmatrix}
0 & N_{15,x,x} & N_{16,x,x} & 0 & 0 & N_{17,x,x} & N_{18,x,x} & 0 \\
0 & N_{9,x} - N_{15} & N_{10,x} - N_{16} & 0 & 0 & N_{12,x} - N_{17} & N_{13,x} - N_{18} & 0 \\
N_{19,x,x} & 0 & 0 & N_{20,x,x} & N_{21,x,x} & 0 & 0 & N_{22,x,x} \\
N_{2,x} - N_{19} & 0 & 0 & N_{3,x} - N_{20} & N_{5,x} - N_{21} & 0 & 0 & N_{6,x} - N_{22}
\end{bmatrix} \tag{4.182}$$

In relation (4.182) $(,x)$ denotes differentiation with respect to x.

4.6.2 Torsion and torsional warping

In the standard 3D beam element formulations, (Cook et al., 2002), torsion is introduced through the linear interpolation of the twisting angle θ_x. Although adequate for warping free sections, this approach does not account for the additional normal and shear stresses induced when warping is considered (Schulz and Filippou, 1998, Sapountzakis and Mokos, 2003 &

2004). These additional stresses are a result of the non-uniform variation of the twisting angle along the element's length. Thus, enhanced beam element formulations have been proposed that include warping effects by introducing additional degrees of freedom corresponding to this variation (Park et al., 2005).

According to the theory of non-uniform torsion, the torsional moment is additively decomposed into two components:

$$T = T_{SV} + T_W \tag{4.183}$$

where:

$$T_{SV} = GK_t\theta'_x\left(x\right) \tag{4.184}$$

is the pure torsional or St Venant while K_t is the pure torsional constant of the cross-section. Accordingly the warping torsional component is expressed as:

$$T_W = M'_W = -EI_W\theta'''_x\left(x\right) \tag{4.185}$$

where M_W is the warping bi-moment and I_W is the warping torsional component. In equations (4.184) and (4.185), prime denotes differentiation with respect to the space variable x.

Considering that the distribution of the torsional moment across the element's length is constant, and differentiating (4.183) with respect to x, the following homogeneous differential equation is derived:

$$EI_W\frac{\partial^4\theta_x}{\partial x^4} - GK_t\frac{\partial^2\theta_x}{\partial x^2} = 0 \tag{4.186}$$

Equation (4.186) can be solved analytically with respect to the twisting angle, bearing the following solution, expressed in exponential form:

$$\theta_x\left(x\right) = C_1 + C_2 x + C_3 e^{\rho_W x} + C_4 e^{-\rho_W x} \tag{4.187}$$

where $\rho_W = \sqrt{GK_t / EI_W}$ and $C_1,\ C_2,\ C_3,\ C_4$ are arbitrary integration constants. As ρ_W increases, the influence of warping torsional effects reduce and vice-versa. The expression of the warping angle $\beta\left(x\right)$ is then readily derived as:

$$\beta\left(x\right) = \frac{d\theta\left(x\right)}{dx} = C_2 + \rho_W C_3 e^{\rho_W x} - \alpha C_4 e^{-\rho_W x} \tag{4.188}$$

Considering an arbitrary set of boundary conditions, namely $\theta_x\left(0\right) = \theta_{x1},\ \beta\left(0\right) = \beta_1,$ $\theta_x\left(L\right) = \theta_{x2},\ \beta\left(L\right) = \beta_2$ and substituting in equations (4.187) and (4.188), the following system of linear equations, in terms of the integration constants, is derived:

$$\begin{bmatrix} 1 & 0 & 1 & 1 \\ 0 & 1 & \rho_W & -\rho_W \\ 1 & L & e^{\rho_W L} & e^{-\rho_W L} \\ 0 & 1 & \alpha_W e^{\rho_W L} & -\rho_W e^{-\rho_W L} \end{bmatrix} \begin{Bmatrix} C_1 \\ C_2 \\ C_3 \\ C_4 \end{Bmatrix} = \left\{ d_{\theta x} \right\} \tag{4.189}$$

Where $\left\{ d_{\theta x} \right\} = \left\{ \theta_{x1} \quad \beta_1 \quad \theta_{x2} \quad \beta_2 \right\}^T$.

Solving equation (4.189) for the unknown constants of integration $C_i, i = 1..4$, substituting into equations (4.187) and (4.188), and collecting terms, the following interpolation scheme is derived:

$$\theta_x\left(x\right) = \left[N_{\theta x} \right] \left\{ d_{\theta x} \right\} \tag{4.190}$$

where $\left[N \right]_{\theta x} = \left[N_4 \quad N_7 \quad N_{11} \quad N_{14} \right]$ is the interpolation matrix. The corresponding interpolation functions are defined as:

$$N_4 = \frac{\left(\rho_W L - \rho_W x + \Gamma\right) A + \left(1 + \Delta\right)\left(1 - B\right)}{2 - 2B + \rho_W L A} \tag{4.191}$$

$$N_7 = \frac{\Gamma + \rho_W x + \mathrm{A}\left(\Delta + \rho_W L\Delta - 1\right) + \mathrm{B}\left(\rho_W L - \Gamma - \rho_W x - \Delta\rho_W L\right)}{\rho_W\left(2 - 2B + \rho_W L\mathrm{A}\right)} \quad (4.192)$$

$$N_{11} = \frac{A\left(\Gamma - \rho_W x\right) - \left(1 - B\right)\left(1 - \Delta\right)}{2 - 2B + \rho_W LA} \quad (4.193)$$

$$N_{14} = \frac{\left(A - \rho_W L\right)\left(1 - \Delta\right) - \left(\Gamma - \rho_W x\right)\left(1 - \mathrm{B}\right)}{\rho_W\left(2 - 2B + \rho_W L\mathrm{A}\right)} \quad (4.194)$$

where $A = \sinh\left(\rho_W L\right)$, $B = \cosh\left(\rho_W L\right)$, $\Gamma = \sinh\left(\rho_W x\right)$, $\Delta = \cosh\left(\rho_W x\right)$.

Equations (4.184) and (4.185) can be expressed in matrix form as:

$$\begin{Bmatrix} T_{SV} \\ M_W \end{Bmatrix} = \begin{bmatrix} GK_t & 0 \\ 0 & EI_W \end{bmatrix} \begin{Bmatrix} \theta'\left(x\right) \\ -\theta''\left(x\right) \end{Bmatrix} \quad (4.195)$$

Substituting the interpolation field presented in equation (4.190), the following relation is derived:

$$\begin{Bmatrix} T_{SV} \\ T_W \end{Bmatrix} = \begin{bmatrix} GK_t & 0 \\ 0 & EI_W \end{bmatrix} \left[\tilde{B}_{tw}\right] \left\{d_{\theta_x}\right\} \quad (4.196)$$

where the torsional strain-displacement matrix $\left[\tilde{B}_{tw}\right]$ is defined as:

$$\left[\tilde{B}_{tw}\right] = \begin{bmatrix} N_4' & N_7' & N_{11}' & N_{14}' \\ N_4'' & N_7'' & N_{11}'' & N_{14}'' \end{bmatrix} \quad (4.197)$$

Taking into account the additional degrees of freedom corresponding to warping, the nodal displacement vector introduced in relation (4.173) is further augmented into the following $14x1$ vector:

$$\left\{d\right\} = \left\{u_1 \quad v_1 \quad w_1 \quad \theta_{x1} \quad \theta_{y1} \quad \theta_{z1} \quad \beta_1' \quad u_2 \quad v_2 \quad w_2 \quad \theta_{x2} \quad \theta_{y2} \quad \theta_{z2} \quad \beta_2'\right\}^T \quad (4.198)$$

The accompanying, augmented, torsional strain-displacement matrix is defined as:

$$\left[B_{tw}\right]=\begin{bmatrix} 0 & 0 & 0 & N_4' & 0 & 0 & N_7' & 0 & 0 & 0 & N_{11}' & 0 & 0 & N_{14}' \\ 0 & 0 & 0 & N_4'' & 0 & 0 & N_7'' & 0 & 0 & 0 & N_{11}'' & 0 & 0 & N_{14}'' \end{bmatrix} \tag{4.199}$$

Similarly, relation (4.182) is augmented to account for the new displacement vector as:

$$\left[B\right]_b=\begin{bmatrix} 0 & 0 & N_{15,x,x} & 0 & N_{16,x,x} & 0 & 0 & 0 & 0 & N_{17,x,x} & 0 & N_{18,x,x} & 0 & 0 \\ 0 & 0 & N_{9,x}-N_{15} & 0 & N_{10,x}-N_{16} & 0 & 0 & 0 & 0 & N_{12,x}-N_{17} & 0 & N_{13,x}-N_{18} & 0 & 0 \\ 0 & N_{19,x,x} & 0 & 0 & 0 & N_{20,x,x} & 0 & 0 & N_{21,x,x} & 0 & 0 & 0 & N_{22,x,x} & 0 \\ 0 & N_{2,x}-N_{19} & 0 & 0 & 0 & N_{3,x}-N_{20} & 0 & 0 & N_{5,x}-N_{21} & 0 & 0 & 0 & N_{6,x}-N_{22} & 0 \end{bmatrix} \tag{4.200}$$

The centerline axial deformation displacement matrix is derived accordingly as:

$$\left[B_u\right]=\begin{bmatrix} N_1 & 0 & 0 & 0 & 0 & 0 & 0 & N_8 & 0 & 0 & 0 & 0 & 0 & 0 \\ N_1 & 0 & 0 & 0 & 0 & 0 & 0 & N_8 & 0 & 0 & 0 & 0 & 0 & 0 \end{bmatrix} \tag{4.201}$$

where $N_1=1-x/L$ and $N_8=x/L$.

Relations (4.199) to (4.201) and (4.197) establish the "generalized strain"-"generalized displacement" matrices that are necessary for subsequent analysis.

4.6.3 Hysteretic field

A 7-dimensional hysteretic field is defined, corresponding to the following set of "generalized stress"-"generalized displacement" relations. The axial components are defined as:

$$N\left(x\right)=\alpha_u EA\varepsilon_x+\left(1-\alpha_u\right)EAz_u \tag{4.202}$$

where z_u is the hysteretic part of the axial centerline deformation and α_u is the post-elastic to elastic axial stiffness ratio. The shear and bending components are defined through the following relations:

$$\begin{aligned} Q_y\left(x\right) &= \alpha_s GA_{sy}\gamma_{xy} + \left(1-\alpha_s\right)GA_{sy}z_{sy} \\ Q_z\left(x\right) &= \alpha_s GA_{sz}\gamma_{xz} + \left(1-\alpha_s\right)GA_{sz}z_{sz} \\ M_y\left(x\right) &= \alpha_b EI_y\phi_y + \left(1-\alpha_b\right)EI_y z_{by} \\ M_z\left(x\right) &= \alpha_b EI_z\phi_z + \left(1-\alpha_b\right)EI_z z_{bz} \end{aligned} \tag{4.203}$$

where z_{sy} and z_{sz} are the hysteretic parts of the shear deformation components γ_{xy} and γ_{xz} respectively, while z_{by}, z_{bz} are the hysteretic parts of the curvatures.

Similarly, the torsional and warping components are defined as:

$$\begin{aligned} M_x &= T_{SV} + T_W \\ T_W &= dM_W/dx \\ T_{SV}\left(x\right) &= \alpha_t GK_t\theta_x + \left(1-\alpha_t\right)GK_t z_t \\ M_W\left(x\right) &= \alpha_W EI_W\beta' + \left(1-\alpha_W\right)EI_W z_W \end{aligned} \tag{4.204}$$

where z_t is the hysteretic part of the twist and z_W is the hysteretic part of the variation of the warping angle while α_t and α_W are the nonlinear to elastic torsional rigidity and warping rigidity ratios respectively.

The decomposition introduced in relations (4.202) to (4.204) is established in matrix form as:

$$\left\{P\right\} = \left\{P^e\right\} + \left\{P^h\right\} \tag{4.205}$$

where $\left\{P\right\} = \left\{N\left(x\right) \quad Q_y\left(x\right) \quad Q_z\left(x\right) \quad M_x\left(x\right) \quad M_y\left(x\right) \quad M_z\left(x\right) \quad M_W\left(x\right)\right\}^T$ while the elastic part of the force vector is defined as:

$$\left\{P^e\right\} = \left[D\right]_e\left\{\varepsilon\right\} \tag{4.206}$$

where $\left\{\varepsilon\right\} = \left\{\varepsilon_x \quad \gamma_{xy} \quad \gamma_{xz} \quad \theta_x \quad \phi_y \quad \phi_z \quad \beta'\right\}^T$ and $\left[D\right]_e$ is defined as:

$$\left[D\right]_e = \begin{bmatrix} \alpha_u EA & & & & & & & \\ & \alpha_\gamma EA_y & & & & & & \\ & & \alpha_\gamma EA_z & & & & & \\ & & & \alpha_t GK_t & & & & \\ & & & & \alpha_b EI_y & & & \\ & & & & & \alpha_b EI_z & & \\ & & & & & & \alpha_W EI_W & \end{bmatrix} \tag{4.207}$$

Accordingly, the hysteretic force vector is defined as:

$$\left\{P^h\right\} = \left[D\right]_h \left\{z\right\} \tag{4.208}$$

where $\left\{z\right\} = \left\{z_u \quad z_{sy} \quad z_{sz} \quad z_t \quad z_{by} \quad z_{bz} \quad z_W\right\}^T$ and

$$\left[D\right]_h = \begin{bmatrix} (1-\alpha_u)EA & & & & & & & \\ & (1-\alpha_s)EA_y & & & & & & \\ & & (1-\alpha_s)EA_z & & & & & \\ & & & (1-\alpha_t)GK_t & & & & \\ & & & & (1-\alpha_b)EI_y & & & \\ & & & & & (1-\alpha_b)EI_z & & \\ & & & & & & (1-\alpha_W)EI_W & \end{bmatrix} \tag{4.209}$$

The evolution of the hysteretic field is defined through the Bouc-Wen interaction scheme in a form similar to equation (4.140) defined in the two dimensional case, thus:

$$\begin{aligned} \left\{\dot{P}^h\right\} = \left[D\right]_h \left\{\dot{z}\right\} = \left[D\right]_h \left(\left[I\right] - H_1 H_2 \left[R\right]\right)\left\{\dot{\varepsilon}\right\} \Rightarrow \\ \left\{\dot{z}\right\} = \left[D\right]_h \left(\left[I\right] - H_1 H_2 \left[R\right]\right)\left\{\dot{\varepsilon}\right\} \end{aligned} \tag{4.210}$$

where $\left[I\right]$ is the 6x6 identity matrix and H_1, H_2 are smoothed Heaviside functions defined as:

$$\begin{aligned} H_1 &= \left\|\Phi\left(\left\{P^h\right\}\right) + 1\right\|^n, \; n \geq 2 \\ H_2 &= \gamma \,\mathrm{sgn}\left(\left\{P^h\right\}^T \left\{\dot{\varepsilon}\right\}\right) + \beta \end{aligned} \tag{4.211}$$

where $\Phi\left(\left\{P^h\right\}\right)$ is a general yield function that depends on the stress-resultants.

4.6.4 Hysteretic interpolation functions

The derivation of the 2-node beam element is based on the interpolation of the continuous hysteretic field defined in section 4.6.3. Similar to section 4.5.5, these shape functions are evaluated through the equilibrium consideration of the corresponding stress resultants. Thus, the following interpolation scheme is established:

$$\left\{z\right\} = \left[N\right]_z \left\{\tilde{z}\right\} \tag{4.212}$$

where $\left\{\tilde{z}\right\}$ is the 14x1 vector of hysteretic nodal quantities and $\left[N\right]_z$ is the 14x14 matrix of the corresponding shape functions. The individual nonzero components of $\left[N\right]_z$ are presented in Table 4.2.

Hysteretic Variable	Shape Functions	Nodal Hysteretic Component
z_u	$N_{z11} = 1/2, N_{z18} = 1/2$	$\tilde{z}_1, \tilde{z}_8$
z_{sy}	$N_{z22} = 1/2, N_{z29} = 1/2$	$\tilde{z}_2, \tilde{z}_9$
z_{sz}	$N_{z33} = 1/2, N_{z310} = 1/2$	$\tilde{z}_3, \tilde{z}_{10}$
z_t	$N_{z44} = 1/2, N_{z411} = 1/2$	$\tilde{z}_4, \tilde{z}_{11}$
z_W	$N_{z44} = 1/2, N_{z412} = 1/2$	$\tilde{z}_5, \tilde{z}_{12}$
z_{by}	$N_{z55} = x/L, N_{z513} = 1 - x/L$	$\tilde{z}_6, \tilde{z}_{13}$
z_{bz}	$N_{z66} = x/L, N_{z614} = 1 - x/L$	$\tilde{z}_7, \tilde{z}_{14}$

Table 4.2 Hysteretic Shape Functions of 3d beam element

4.6.5 Derivation of stiffness matrix

The first variation of the potential energy is formulated in terms of stress-strains as:

$$\delta V = \int_V \sigma_x \delta\varepsilon_x dV + \int_V \left(\tau_{xz}\delta\varepsilon_{xz} + \tau_{xy}\delta\varepsilon_{xy}\right) dV \tag{4.213}$$

Consequently, relation (4.213) can be established in terms of stress resultants and their conjugate generalized strain measures as:

$$\delta V = \int_0^L \left(N\delta\varepsilon_u + M_y\delta\phi_y + M_z\delta\phi_z \right)dx + \int_0^L \left(T_{sv}\delta\beta + M_W\delta\beta' + Q_y\delta\gamma_{xy} + Q_z\delta\gamma_{xz} \right)dx \tag{4.214}$$

where the total torsional moment M_x has been decomposed into its pure torsion and warping torsion components. Substituting the constitutive equations (4.202) to (4.204) into equation (4.214), the following relation is derived:

$$\begin{aligned}
\delta V = & \int_0^L \left(\left(\alpha_b EI\varepsilon_{\phi y} + \left(1-\alpha_\phi\right) EIz_{by} \right)\delta\varepsilon_{\phi y} + \left(\alpha_\gamma GA_{sz}\varepsilon_{\gamma z} + \left(1-\alpha_s\right) GA_{sz}z_{sz} \right)\delta\varepsilon_{\gamma z} \right)dx \\
& + \int_0^L \left(\left(\alpha_\phi EI\varepsilon_{\phi z} + \left(1-\alpha_b\right) EIz_{bz} \right)\delta\varepsilon_{\phi z} + \left(\alpha_\gamma GA_{sy}\varepsilon_{\gamma z} + \left(1-\alpha_s\right) GA_{sy}z_{sy} \right)\delta\varepsilon_{\gamma y} \right)dx \\
& + \int_0^L \left(\left(\alpha_t GK_t\theta' + \left(1-\alpha_t\right) GK_t z_t \right)\delta\theta' + \left(\alpha_W EI_W\beta' + \left(1-\alpha_W\right) EI_W z_W \right)\delta\beta' \right)dx \\
& + \int_0^L \left(\alpha_u EA\varepsilon_u + \left(1-\alpha_u\right) EA \right)\delta\varepsilon_u dx
\end{aligned} \tag{4.215}$$

Relation (4.215) can be reformulated in matrix notation as:

$$\delta V = \int_0^L \left\{\delta\varepsilon\right\}^T \left(\left[D\right]_e \left\{\varepsilon\right\} + \left[D\right]_h \left\{z\right\} \right)dx \tag{4.216}$$

where $\left[D\right]_e$ and $\left[D\right]_h$ are defined in equations (4.207) and (4.209) respectively while $\left\{\varepsilon\right\}$ and $\left\{z\right\}$ are defined in relations (4.206) and (4.208) respectively.

Using the strain-displacement matrices established in equation (4.201) for the axial components, (4.200) for the bending components and (4.199) for the torsional components and following the procedure introduced in section 4.5.6 the 14x14 stiffness matrix of the 3d Timoshenko element with warping torsion is derived. The equilibrium equation at the element level is defined as:

$$\left\{P\right\} = \left[k\right]_e \left\{d\right\} + \left[k_h\right]\left\{z\right\} \tag{4.217}$$

The procedure of deriving equation (4.217) is presented in detail in Appendix II. The elastic stiffness matrix $\left[k_h\right]$ assumes the following form

$$\left[k\right]_e = \begin{bmatrix} k_{1,1} & & & & & & & k_{1,8} & & & & & & \\ & k_{2,2} & & & k_{2,6} & & & k_{2,9} & & & & k_{2,13} & & \\ & & k_{3,3} & & k_{3,5} & & & & k_{3,10} & & k_{3,12} & & & \\ & & & k_{4,4} & & & k_{4,7} & & & k_{4,11} & & & & k_{4,14} \\ & & k_{5,3} & & k_{5,5} & & & & k_{5,10} & & k_{5,12} & & & \\ & k_{6,2} & & & k_{6,6} & & & k_{6,9} & & & & k_{6,13} & & \\ & & & k_{7,4} & & & k_{7,7} & & & k_{7,11} & & & & k_{7,14} \\ k_{8,1} & & & & & & & k_{8,8} & & & & & & \\ & k_{9,2} & & & k_{9,6} & & & k_{9,9} & & & & k_{9,13} & & \\ & & k_{10,3} & & k_{10,5} & & & & k_{10,10} & & k_{10,12} & & & \\ & & & k_{11,4} & & & k_{11,7} & & & k_{11,11} & & & & k_{11,14} \\ & & k_{12,3} & & k_{12,5} & & & & k_{12,10} & & k_{12,12} & & & \\ & k_{13,2} & & & k_{13,6} & & & k_{13,9} & & & & k_{13,13} & & \\ & & & k_{14,4} & & & k_{14,7} & & & k_{14,11} & & & & k_{14,14} \end{bmatrix} \tag{4.218}$$

where the bending stiffness coefficients coincide with those derived for the plane element, considering the proper sign convention for bending with respect to the y axis:

The torsional degrees of freedom are evaluated as:

$$k_{4,4} = EI_w \int_0^L N_4'' N_4'' dz + GK_t \int_0^L N_4' N_4' dz, \quad k_{4,7} = EI_w \int_0^L N_4'' N_7'' dz + GK_t \int_0^L N_4' N_7' dz \tag{4.219}$$

$$k_{4,11} = EI_w \int_0^L N_4'' N_{13}'' dz + GK_t \int_0^L N_4' N_{13}' dz, \quad k_{4,14} = EI_w \int_0^L N_4'' N_{16}'' dz + GK_t \int_0^L N_4' N_{16}' dz \tag{4.220}$$

$$k_{7,7} = EI_w \int_0^L N_7'' N_7'' dz + GK_t \int_0^L N_7' N_7' dz, \quad k_{7,11} = EI_w \int_0^L N_7'' N_{13}'' dz + GK_t \int_0^L N_7' N_{13}' dz \tag{4.221}$$

$$k_{7,14} = EI_w \int_0^L N_7'' N_{16}'' dz + GK_t \int_0^L N_7' N_{16}' dz, \quad k_{11,11} = EI_w \int_0^L N_{13}'' N_{13}'' dz + GK_t \int_0^L N_{13}' N_{13}' dz \tag{4.222}$$

$$k_{11,14} = EI_w \int_0^L N_{11}'' N_{14}'' dz + GK_t \int_0^L N_{11}' N_{14}' dz, \quad k_{14,14} = EI_w \int_0^L N_{14}'' N_{14}'' dz + GK_t \int_0^L N_{14}' N_{14}' dz \tag{4.223}$$

$$k_{74} = k_{47}, \quad k_{11,4} = k_{4,11}, \quad k_{11,7} = k_{7,11} \tag{4.224}$$

$$k_{14,4} = k_{4,14}, \quad k_{14,7} = k_{7,14}, \quad k_{14,11} = k_{11,14} \tag{4.225}$$

Analytical expressions for the torsional stiffness coefficients are presented in Appendix II. The hysteretic matrix $\left[k_h\right]$ of equation (4.217) is defined accordingly as:

$$\left[k_h\right]=\begin{bmatrix}
h_{1,1} & & & & & & & h_{1,8} & & & & & & \\
& h_{2,2} & & & h_{2,6} & & & & h_{2,9} & & & & h_{2,13} & \\
& & h_{3,3} & & h_{3,5} & & & & & h_{3,10} & & h_{3,12} & & \\
& & & h_{4,4} & & & & & & & h_{4,11} & & & \\
& & h_{5,3} & & h_{5,5} & & & & & h_{5,10} & & h_{5,12} & & \\
& h_{6,2} & & & & h_{6,6} & & & h_{6,9} & & & & h_{6,13} & \\
& & & & & & h_{7,7} & & & & & & & h_{7,14} \\
h_{8,1} & & & & & & & h_{8,8} & & & & & & \\
& h_{9,2} & & & h_{9,6} & & & & h_{9,9} & & & & h_{9,13} & \\
& & h_{10,3} & & h_{10,5} & & & & & h_{10,10} & & h_{10,12} & & \\
& & & h_{11,4} & & & & & & & h_{11,11} & & & \\
& & h_{12,3} & & h_{12,5} & & & & & h_{12,10} & & h_{12,12} & & \\
& h_{13,2} & & & & h_{13,6} & & & h_{13,9} & & & & h_{13,13} & \\
& & & & & & h_{14,7} & & & & & & & h_{14,14}
\end{bmatrix} \tag{4.226}$$

where the axial and bending coefficients are readily derived from the two-dimensional case of equation (4.160) while the torsional coefficients are defined by the following relations:

$$\begin{aligned}
h_{44} &= h_{411} = -0.5\left(1-\alpha_T\right)GK_T \\
h_{114} &= -h_{44} \\
h_{1111} &= -h_{44}
\end{aligned} \tag{4.227}$$

and the warping hysteretic coefficients are defined as:

$$\begin{aligned}
h_{77} &= h_{714} = -0.5\left(1-\alpha_W\right)\mathrm{EI}_w \\
h_{1414} &= -h_{77} \\
h_{147} &= -h_{714}
\end{aligned} \tag{4.228}$$

4.7 Conclusions

A new three-dimensional hysteretic rod element formulation is presented based on the concept of hysteretic axial deformation. Geometrical nonlinearities are considered through a Total Lagrangian formulation.

A new nonlinear beam element is presented, together with efficient methods for the solution of the equations of motion, avoiding linearization and treating nonlinearities at the element level. The beam element is formulated within the framework of the Timoshenko beam theory by adding six new degrees of freedom accounting for the hysteretic part of the curvature, axial centerline deformation and shear strain. The field consistence method is used to avoid shear locking.

The Bouc-Wen hysteretic model is implemented to simulate the nonlinear constitutive behavior of the material. A wide range of hysteretic behavior can be modeled by properly controlling the parameters of the hysteresis law, namely the "yield" parameter, the smoothness parameter, and the shape factors. As a whole, the proposed method constitutes a successful confluence of the hysteretic modeling into the realm of the Finite Element Method.

By writing down the governing equations in state space form and implementing a predictor-corrector integration scheme the linearization of the constitutive equations is avoided. The Bouc-Wen hysteretic model is implemented in order to simulate the nonlinear constitutive behavior of the material, in terms of stress - strain relation. Various loops can be modeled by properly controlling the parameters of the hysteresis law. The problem is partitioned into two sets of equations, which are solved simultaneously. The numerical examples presented demonstrate the validity of the proposed approach as well as its versatility as compared to displacement formulation.

Appendix I- Derivation of the Timoshenko beam differential equations

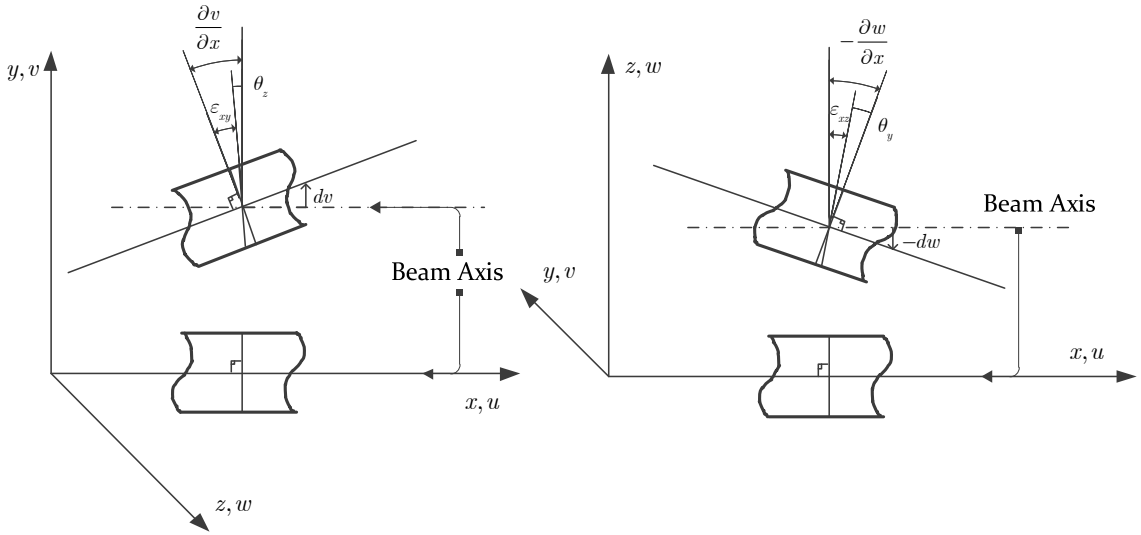

Fig. 4.18 Timoshenko beam kinematic assumptions in space

If bending in the xy plane is considered, the Timoshenko kinematic assumptions are given by the following relations, where the centerline axial deformation component is omitted for the sake of simplicity:

$$u\left(x,y,z\right)=-y\theta_z\left(x\right),\ v\left(x,y,z\right)=v\left(x\right),\ w\left(x,y,z\right)=0 \tag{4.229}$$

Thus, the non-zero components of the strain tensor are derived as:

$$\varepsilon_{xx}=\frac{\partial u}{\partial x}=-y\frac{\partial\theta_z}{\partial x},\ \varepsilon_{xy}=\frac{1}{2}\left(\frac{\partial u}{\partial y}+\frac{\partial v}{\partial x}\right)=\frac{1}{2}\left(-\theta_z+\frac{\partial v}{\partial x}\right) \tag{4.230}$$

Since the actual shear strain varies along the section's height, the shear correction factor is introduced, such that:

$$\varepsilon_{xy}=\kappa\varepsilon_{xy,real}=\frac{\kappa}{2}\left(-\theta_z+\frac{\partial v}{\partial x}\right) \tag{4.231}$$

The equilibrium conditions for an infitensimal beam with length dx are defined as:

$$\frac{\partial M_z}{\partial x} - Q_y = 0,\ \frac{\partial Q_y}{\partial x} + q_y = 0 \tag{4.232}$$

Taking advantage of the linear elastic stress-strain relations, the following equations hold:

$$M_z = \int_A y\sigma_{xx} dA = \int_A yE\varepsilon_{xx} dA = -\int_A y^2 E \frac{\partial \theta_z}{\partial x} dA = -EI \frac{\partial \theta_z}{\partial x} \tag{4.233}$$

and

$$Q_y = \int_A \sigma_{xy} dA = \int_A 2G\varepsilon_{xy} dA = \kappa \int_A G\left(-\theta_z + \frac{\partial v}{\partial x}\right) dA = \kappa GA\left(-\theta_z + \frac{\partial v}{\partial x}\right) \tag{4.234}$$

Thus, replacing equations (4.233) and (4.234) to the equilibrium equations (4.232) the following system of differential equations is derived:

$$\left.\begin{aligned} \frac{\partial}{\partial x}\left(-EI\frac{\partial \theta_z}{\partial x}\right) - \kappa GA\left(-\theta_z + \frac{\partial v}{\partial x}\right) = 0 \\ \kappa GA\frac{\partial}{\partial x}\left(-\theta_z + \frac{\partial v}{\partial x}\right) + q_y = 0 \end{aligned}\right\} \Rightarrow \begin{aligned} EI\left(\frac{\partial^2 \theta_z}{\partial x^2}\right) + \kappa GA\left(-\theta_z + \frac{\partial v}{\partial x}\right) = 0 \\ \kappa GA\left(-\frac{\partial \theta_z}{\partial x} + \frac{\partial^2 v}{\partial x^2}\right) + q_y = 0 \end{aligned} \tag{4.235}$$

If bending in the xy plane is considered then the kinematic relations are expressed as:

$$u(x,y,z) = z\theta_y(x),\ v(x,y,z) = 0,\ w(x,y,z) = w(x) \tag{4.236}$$

and the non-zero strain components are:

$$\varepsilon_{xx} = \frac{\partial u}{\partial x} = z\frac{\partial \theta_y}{\partial x},\ \varepsilon_{xz} = \frac{1}{2}\left(\frac{\partial u}{\partial z} + \frac{\partial w}{\partial x}\right) = \frac{1}{2}\left(\theta_y + \frac{\partial w}{\partial x}\right) \tag{4.237}$$

Thus, the differential equations of bending in the xy plane assume the following form:

$$\begin{aligned} EI\left(\frac{\partial^2 \theta_y}{\partial x^2}\right) - \kappa GA\left(\theta_y + \frac{\partial w}{\partial x}\right) = 0 \\ \kappa GA\left(\frac{\partial \theta_y}{\partial x} + \frac{\partial^2 w}{\partial x^2}\right) + q_z = 0 \end{aligned} \tag{4.238}$$

which are bound to the general solution:

$$\theta_y(x) = -\frac{1}{2}C_1x^2 - C_2x - \left(C_3 + \frac{EI}{kGA}C_1\right)$$
$$w(x) = \frac{1}{6}C_1x^3 + \frac{1}{2}C_2x^2 + C_3x + C_4 \tag{4.239}$$

As expected, the rotation for a beam element bearing the same properties, namely kA and I in both directions of bending is exactly the opposite, due to the orientation of the coordinate system, as presented in Fig. 4.18.The expression for the displacement $w(x)$ coincides with the expression derived for the xy plane (equation (4.131)).

Appendix II – Torsional and warping stiffness coefficients

The torsional and warping stiffness coefficients of the 3-dimensional hysteretic beam element, defined in relations (4.218) to (4.225) are evaluated using a symbolic mathematical programming toolbox such as Maple (MapleSoft, 2007) or Mathematica (Wolfram Mathematica, 2009). Though cumbersome, the derived expressions are analytical and thus exact, for the case of the 2-node three-dimensional beam element that is developed in this work.

The torsional and torsional warping stiffness coefficients can be implemented in the following Fortran code:

```
C TORSIONAL AND DISTORTIONAL STIFFNESS COEFFICIENTS
C L          ----→ MEMBER LENGTH
C aw         ----→ ρw
C awar       ----→ αw
C GKt ----→ Tortional Rigidity
C EIw ----→ Warping Rigidity

C     k44 Stiffness Element

      t2 = aw**2
      t4 = log(e)
      t5 = t4**2
```

```
      t8 = aw*L
      t10 = e**(2*t8)
      t12 = L**2
      t13 = t12*t5
      t16 = L*t4
      t19 = e**t8
      t25 = t4*t8
      t30 = 1/(t13*t2*t10-4*t16*aw*t10+2*t13*t2*t19+4*t10-
     #8*t19+4+4*t25+t5*t12*t2)
      t31 = t10*t30
      t33 = t25*t19*t30
      t49 = -(-t31+t30+2*t33)*t5*t4*t2*aw*awar*EIw+(-
     #3*t31+3*t30+t25*t31
     #+t16*aw*t30+4*t33)*t4*aw*at*GKt

C     k47 Stiffness Element

      t2 = aw**2
      t5 = log(e)
      t6 = t5**2
      t9 = aw*L
      t11 = e**(2*t9)
      t13 = L**2
      t14 = t13*t6
      t17 = L*t5
      t20 = e**t9
      t26 = t5*t9
      t29 = t6*t13*t2
      t31 = 1/(t14*t2*t11-4*t17*aw*t11+2*t14*t2*t20+4*t11-
     #8*t20+4+4*t26+t29)
      t32 = t11*t31
      t33 = t20*t31
      Vk47 = (-t32+t31+2*t26*t33)*L*t6*t5*t2*aw*EIw*awar/2+(-
     #t26*t32/2+2*t32-t29*t33-4*t33+2*t31+t17*aw*t31/2)*GKt*at


C     k411 Stiffness Element

      t2 = aw**2
      t4 = log(e)
      t5 = t4**2
      t8 = aw*L
      t10 = e**(2*t8)
      t12 = L**2
      t13 = t12*t5
      t16 = L*t4
      t19 = e**t8
      t25 = t4*t8
      t30 = 1/(t13*t2*t10-4*t16*aw*t10+2*t13*t2*t19+4*t10-
     #8*t19+4+4*t25+t5*t12*t2)
      t31 = t10*t30
      t33 = t25*t19*t30
      Vk411 = (-t31+t30+2*t33)*t5*t4*t2*aw*awar*EIw-(-
     #3*t31+3*t30+t25*t31+t16*aw*t30+4*t33)*t4*aw*at*GKt


C     k414 Stiffness Element

      t2 = aw**2
      t5 = log(e)
      t6 = t5**2
      t9 = aw*L
      t11 = e**(2*t9)
      t13 = L**2
      t14 = t13*t6
      t17 = L*t5
      t20 = e**t9
      t26 = t5*t9
```

```
      t29 = t6*t13*t2
      t31 = 1/(t14*t2*t11-4*t17*aw*t11+2*t14*t2*t20+4*t11-
     #8*t20+4+4*t26+t29)
      t32 = t11*t31
      t33 = t20*t31
      Vk414 = (-t32+t31+2*t26*t33)*L*t6*t5*t2*aw*EIw*awar/2+(-
     #t26*t32/2+2*t32-t29*t33-4*t33+2*t31+t17*aw*t31/2)*GKt*at

C     k77 Stiffness Element

      t2 = log(e)
      t3 = t2*aw
      t4 = aw*L
      t5 = e**t4
      t8 = e**(3*t4)
      t11 = e**(2*t4)
      t12 = aw**2
      t14 = t2**2
      t15 = L**2
      t16 = t15*t14
      t20 = e**(4*t4)
      t23 = L*t2
      t36 = t14*t15*t12
      t37 = t2*t4
      t40 = -4+16*t5+16*t8+2*t16*t12*t11-
     #4*t20+8*t23*aw*t5+4*L*t20*t3-t1
     #5*t20*t14*t12-8*L*t8*t3-t36-4*t37-24*t11
      t41 = 1/t40
      t49 = 4*t15*L*t11*t14*t2*t12*aw*t41
      t50 = t12*t41
      t53 = t15*t20*t14*t50
      t54 = t8*t41
      t56 = 4*t36*t54
      t57 = t5*t41
      t59 = 4*t36*t57
      t60 = t16*t50
      t61 = aw*t41
      t64 = L*t20*t2*t61
      t69 = 4*L*t8*t2*t61
      t74 = 4*t37*t57
      t75 = t23*t61
      t78 = 2*t20*t41
      t79 = 4*t54
      t80 = 4*t57
      t81 = 2*t41
      t82 = t49+t53-t56+t59-t60-2*t64+t69-4*t37*t11*t41+t74-
     #2*t75+t78-t79+t80-t81
      t91 = t49-t53-t56+t59+t60+4*t64-t69-t74+4*t75-t78+t79-
     #t80+t81
      Vk77 = -t82*t3*awar*EIw/2+t91/t2/aw*at*GKt/2


C     k7111 Stiffness Element

      t2 = aw**2
      t5 = log(e)
      t6 = t5**2
      t9 = aw*L
      t11 = e**(2*t9)
      t13 = L**2
      t14 = t13*t6
      t17 = L*t5
      t20 = e**t9
      t26 = t5*t9
      t29 = t6*t13*t2
      t31 = 1/(t14*t2*t11-4*t17*aw*t11+2*t14*t2*t20+4*t11-
     #8*t20+4+4*t26+t29)
      t32 = t11*t31
```

```
      t33 = t20*t31
      Vk711 = -(-t32+t31+2*t26*t33)*L*t6*t5*t2*aw*EIw*awar/2
     #+(t26*t32/2-2*
     #t32+t29*t33+4*t33-2*t31-t17*aw*t31/2)*GKt*at


C     k714 Stiffness Element

      t2 = log(e)
      t3 = t2*aw
      t4 = aw*L
      t5 = e**t4
      t8 = e**(3*t4)
      t11 = e**(2*t4)
      t12 = aw**2
      t14 = t2**2
      t15 = L**2
      t20 = e**(4*t4)
      t23 = L*t2
      t36 = t14*t15*t12
      t37 = t2*t4
      t40 = -4+16*t5+16*t8+2*t15*t14*t12*t11-
     #4*t20+8*t23*aw*t5+4*L*t20*t
     #3-t15*t20*t14*t12-8*L*t8*t3-t36-4*t37-24*t11
      t41 = 1/t40
      t43 = t12*aw*t41
      t44 = t14*t2
      t46 = t15*L
      t48 = t46*t8*t44*t43
      t51 = t46*t5*t44*t43
      t52 = t5*t41
      t53 = t36*t52
      t54 = t8*t41
      t55 = t36*t54
      t56 = aw*t41
      t62 = t37*t11*t41
      t66 = L*t8*t2*t56
      t68 = t37*t52
      t70 = t20*t41
      t71 = 2*t54
      t72 = 2*t52
      t73 = t48+t51+t53-t55-t23*t56-L*t20*t2*t56-
     #2*t62+2*t66+2*t68+t70-t41-t71+t72
      t85 = t48+t51-3*t55+3*t53+6*t66-12*t62+6*t68+t41-t70-
     #t72+t71
      Vk714 = t73*t3*awar*EIw-t85/t2/aw*at*GKt


C     k1111 Stiffness Element

      t2 = aw**2
      t4 = log(e)
      t5 = t4**2
      t8 = aw*L
      t10 = e**(2*t8)
      t12 = L**2
      t13 = t12*t5
      t16 = L*t4
      t19 = e**t8
      t25 = t4*t8
      t30 = 1/(t13*t2*t10-4*t16*aw*t10+2*t13*t2*t19+4*t10-
     #8*t19+4+4*t25+
     #t5*t12*t2)
      t31 = t10*t30
      t33 = t25*t19*t30
      Vk1111 = -(-t31+t30+2*t33)*t5*t4*t2*aw*awar*EIw+(-
     #3*t31+3*t30+t25*t31+t16*aw*t30+4*t33)*t4*aw*at*GKt
```

```
C     k1114 Stiffness Element

      t2 = aw**2
      t5 = log(e)
      t6 = t5**2
      t9 = aw*L
      t11 = e**(2*t9)
      t13 = L**2
      t14 = t13*t6
      t17 = L*t5
      t20 = e**t9
      t26 = t5*t9
      t29 = t6*t13*t2
      t31 = 1/(t14*t2*t11-4*t17*aw*t11+2*t14*t2*t20+4*t11-
     #8*t20+4+4*t26+t29)
      t32 = t11*t31
      t33 = t20*t31
      Vk1114 = -(-t32+t31+2*t26*t33)*L*t6*t5*t2*aw*EIw*awar/2
     #+(t26*t32/2-2*
     #t32+t29*t33+4*t33-2*t31-t17*aw*t31/2)*GKt*at

C     k1414 Stiffness Element

      t2 = log(e)
      t3 = t2*aw
      t4 = aw*L
      t5 = e**t4
      t8 = e**(3*t4)
      t11 = e**(2*t4)
      t12 = aw**2
      t14 = t2**2
      t15 = L**2
      t16 = t15*t14
      t20 = e**(4*t4)
      t23 = L*t2
      t36 = t14*t15*t12
      t37 = t2*t4
      t40 = -4+16*t5+16*t8+2*t16*t12*t11-
     #4*t20+8*t23*aw*t5+4*L*t20*t3-t1
     #5*t20*t14*t12-8*L*t8*t3-t36-4*t37-24*t11
      t41 = 1/t40
      t49 = 4*t15*L*t11*t14*t2*t12*aw*t41
      t50 = t12*t41
      t53 = t15*t20*t14*t50
      t54 = t8*t41
      t56 = 4*t36*t54
      t57 = t5*t41
      t59 = 4*t36*t57
      t60 = t16*t50
      t61 = aw*t41
      t64 = L*t20*t2*t61
      t69 = 4*L*t8*t2*t61
      t74 = 4*t37*t57
      t75 = t23*t61
      t78 = 2*t20*t41
      t79 = 4*t54
      t80 = 4*t57
      t81 = 2*t41
      t82 = t49+t53-t56+t59-t60-2*t64+t69-4*t37*t11*t41+t74-
     #2*t75+t78-t7
     #9+t80-t81
      t91 = t49-t53-t56+t59+t60+4*t64-t69-t74+4*t75-t78+t79-
     #t80+t81
      Vk1414 = -t82*t3*awar*EIw/2+t91/t2/aw*at*GKt/2
```

Chapter 5

HYSTERETIC FINITE ELEMENTS

5.1 Introduction

The inelastic behavior of shear walls in buildings and in general plane members in structures is of major importance in earthquake engineering, as due to their stiffness, they carry a significant part of the external lateral load. Their mode of failure is mainly in shear and modeling of their response, especially under cyclic loading exhibiting hysteretic behavior, is decisive for a realistic prediction of the structural response under earthquake excitations.

Plane stress plasticity problems have been addressed for decades, (Hill, 1998, Kachanov, 2004). Analytical solutions have been derived following slip line theory offering robust solutions especially for metal forming problems, (Lubliner, 2008). Slip line theory, though precise, was dominated by the finite element method, due to the applicability of the latter in the majority of structural analysis problems, leading to a remarkable ongoing development, creating efficient and accurate algorithms (Souza et al, 2008). Recently, Valoroso and Rosati (2009) developed a consistent solution scheme for plane stress problems under the framework of the return mapping algorithm of Simo and Taylor (1985). Nevertheless, phenomenological models are also implemented in several cases of metal forming simulation as described in Taherizadeh et al. (2010).

In this work, Bouc-Wen hysteretic modeling is implemented into the framework of finite elements yielding a consistent methodology for the analysis of static, quasi-static and dynamic 2-D problems. The constant stress/constant strain element, though simple in its formulation, constitutes the basis for escalating the development to higher order elements, such as the shell element Bathe (2007), or advanced membrane elements, Zhang H .& Kuang, J. S (2009). Nevertheless, its advantages are well established in the analysis of 2-D structures, like masonry shear walls (Brasile, 2009) and concrete shear walls (Kwan et al., 2001). Moreover, their reduced order of complexity, as opposed to shell elements and solid elements,

significantly enhances the computational performance retaining the desired accuracy of the analysis. Furthermore, recent advances in mesh refinement, (Munoz, 2009) can be utilized to yield a robust and cost effective computational scheme.

In the present work, the Bouc-Wen model is incorporated in the finite element formulation to determine the inelastic-hysteretic behavior of triangular elements. A plane stress element is developed that accounts for different yielding criteria under the framework of Bouc-Wen hysteresis modeling.

Contrary to the incremental approach of classical plasticity, where the tangent stiffness matrix is evaluated considering small increments on the point-wise monotonic, or cyclic material envelope, the stiffness matrix presented herein constitutes a continuous function of the stress state. From a computational perspective, following the proposed approach, the problem is treated in modular form, thus yielding a potentially parallel scheme. Numerical examples are presented that demonstrate the applicability of the proposed formulation in terms of computational efficiency and accuracy. To extend the versatility of the univariate Bouc-Wen model to 2D problems, the triangular constant strain element is used in this work due to its simplicity. The method can be applied to other elements, considering the proper displacement field and the corresponding strain matrices, addressing in addition numerical integration issues in developing the element stiffness matrices.

5.2 The finite element formulation

In this section, a brief presentation of the finite element method is conducted so as to facilitate subsequent analysis. Attention is drawn towards the kinematics of the deformable continuum and the necessary definitions of the deformation gradient, the strain measure and the stress measure are presented.

5.2.1 Incorporating the generalized hysteretic constitutive law

In Chapter 2 a general nonlinear hysteretic stress-strain relation has been introduced, that is rewritten herein for the sake of reference:

$$\left\{\dot{S}\right\} = \left[D\right]\left(\left[I\right] - \left|\frac{\Phi}{\Phi_0}\right|^N \left(\beta + \gamma \operatorname{sgn}\left(\left\{E\right\}^T \left\{\dot{S}\right\}\right)\right)\left[R\right]\right)\left\{\dot{E}\right\} \tag{5.1}$$

where $\left[D\right]$ is the elastic constitutive matrix, $\left[I\right]$ is the identity matrix, Φ is a yield function, Φ_0 is the critical value of the yield function, N, β, γ are model parameters and $\left[R\right]$ is an interaction matrix defined by the following relation:

$$\left[R\right] = \left(-\left(\frac{\partial \Phi}{\partial \left\{\eta\right\}}\right)^T G\left(\left\{\eta\right\},\Phi\right) + \left(\frac{\partial \Phi}{\partial \left\{S\right\}}\right)^T \left[D\right] \frac{\partial \Phi}{\partial \left\{S\right\}}\right)^{-1} \left(\frac{\partial \Phi}{\partial \left\{S\right\}}\right)\left(\frac{\partial \Phi}{\partial \left\{S\right\}}\right)^T \left[D\right] \tag{5.2}$$

where $G\left(\left\{\eta\right\},\Phi\right)$ is a function of the back-stress and the yield function defining the evolution of the kinematic hardening law that is derived from the following relation:

$$\left\{\dot{\eta}\right\} = \left(-\left(\frac{\partial \Phi}{\partial \left\{\eta\right\}}\right)^T G\left(\left\{\eta\right\},\Phi\right) + \left(\frac{\partial \Phi}{\partial \left\{S\right\}}\right)^T \left[D\right] \frac{\partial \Phi}{\partial \left\{S\right\}}\right)^{-1} \left(\frac{\partial \Phi}{\partial \left\{S\right\}}\right)^T G\left(\left\{\eta\right\},\Phi\right)\left[D\right]\left\{\dot{\varepsilon}\right\} \tag{5.3}$$

Since no consideration has been made on the kinematics of the problem during the derivation of equation (5.1), the stress and strain tensors can be substituted accordingly. Relation (5.1) is more conveniently written in the following form:

$$\left\{\dot{S}\right\} = \left\{\dot{S}\right\}^e + \left\{\dot{S}\right\}^h \tag{5.4}$$

where:

$$\left\{\dot{S}^e\right\} = \left[D\right]\left\{\dot{\varepsilon}\right\} \tag{5.5}$$

is the elastic part of the stress tensor and:

$$\left\{\dot{S}^h\right\} = \left[D_H\left(\Phi, G, \varepsilon\right)\right]\left\{\dot{\varepsilon}\right\} \tag{5.6}$$

is the hysteretic part of the stress tensor, where the hysteretic constitutive matrix $\left[H\right]$ is defined as:

$$\left[D_H\left(\Phi, G, \varepsilon\right)\right] = -\left[D\right]\left|\frac{\Phi}{\Phi_0}\right|^N \left(\beta + \gamma \operatorname{sgn}\left(\left\{\varepsilon\right\}^T \left\{\dot{S}\right\}\right)\right)\left[R\right] \tag{5.7}$$

Thus, the elastic constitutive matrix $\left[D\right]$ is substituted by its hysteretic counterpart:

$$\left[D\left(\Phi, G, \varepsilon\right)\right]_H = \left[D\right] + \left[D_H\left(\Phi, G, \varepsilon\right)\right] \tag{5.8}$$

and the nonlinear stress-strain hysteretic law is written as:

$$\left\{\dot{S}\right\} = \left[D\left(\Phi, G, \varepsilon\right)\right]_H \left\{\dot{\varepsilon}\right\} \tag{5.9}$$

Equations (5.7) to (5.9) define a smooth and rate-independent model of classical plasticity.

5.2.2 The rate form of the principle of virtual work

The principle of virtual work can be stated in the following form (Cook et al., 2002)

$$\int \left\{\delta E\right\}^T \left\{S\right\} dV = \int \left\{\delta u\right\}^T \left\{F\right\} dV + \int \left\{\delta u\right\}^T \left\{\Phi\right\} dS_A \tag{5.10}$$

where $\left\{\delta E\right\}$ is the vector of potential strains, $\left\{S\right\}$ is the vector of stresses, $\left\{\delta u\right\}$ is the vector of potential displacements , $\left\{F\right\}$ are the body forces acting over the volume V and $\left\{\Phi\right\}$ is the vector of surface tractions acting on the surface S_A. Differentiating relation (5.10) with respect to time and choosing the potential displacements such that $\left\{\delta \dot{u}\right\} = 0$, the following variational form is derived (Washizu, 1980)

$$\int \{\delta E\}^T \{\dot{S}\} dV = \int \{\delta u\}^T \{\dot{F}\} dV + \int \{\delta u\}^T \{\dot{\Phi}\} dS_A \tag{5.11}$$

Substituting the rate form of the stress-strain relation (5.9) into relation (5.11) the following equation is derived:

$$\int \{\delta E\}^T [D(\Phi, G, E)]_H \{\dot{E}\} dV = \int \{\delta u\}^T \{\dot{F}\} dV + \int \{\delta u\}^T \{\dot{\Phi}\} dS_A \tag{5.12}$$

According to the standard procedure of nonlinear finite elements (Bathe, 2008), an interpolation scheme for the displacement field is introduced, bearing the following form:

$$\{u\} = [N]\{d\} \tag{5.13}$$

where $[N]$ is a matrix baring the shape functions and $\{d\}$ is the vector of nodal displacements. By considering the kinematics of the problem a relation of the following form is finally derived:

$$\{E\} = \left([B]_l + [B(\{d\})]_{NL}\right)\{d\} = [B]\{d\} \tag{5.14}$$

where $[B]_l$ is the linear strain-displacement matrix and $[B(\{d\})]_{NL}$ is the nonlinear strain-displacement matrix which is a function of the current displacements. In case of the small displacement formulation relation (5.14) becomes:

$$\{\varepsilon\} = [B]_l \{d\} \tag{5.15}$$

Substituting relations (5.13) and (5.14) into (5.12), the following equation is derived:

$$\int \{\delta d\}^T [B]^T [D(\Phi, G, \varepsilon)]_H [B]\{d\} dV = \int \{\delta d\}^T [B]^T \{\dot{F}\} dV + \int \{\delta d\}^T [B]^T \{\dot{\Phi}\} dS_A \tag{5.16}$$

Finally, the classical finite element equilibrium equation is derived:

$$[K]_H \{\dot{d}\} = \{\dot{r}\} \tag{5.17}$$

where $\left[K\right]_H = \left[K\left(\Phi, G, E\right)\right]_H$ is a smooth, history dependent but rate independent stiffness matrix evaluated as:

$$\left[K\right]_H = \int \left[B\right]^T \left[D\left(\Phi, G, \varepsilon\right)\right]_H \left[B\right] dV \tag{5.18}$$

while

$$\left\{\dot{r}\right\} = \int \left\{\delta d\right\}^T \left[B\right]^T \left\{\dot{F}\right\} dV + \int \left\{\delta d\right\}^T \left[B\right]^T \left\{\dot{\Phi}\right\} dS_A \tag{5.19}$$

is the equivalent nodal load vector. Since rates of the corresponding force and displacement measures appear on both sides of equation (5.17) the hysteretic stiffness matrix is rate-independent and assumes the following form:

$$\left[K\right]_H = \frac{\mathrm{d}\left\{r\right\}}{\mathrm{d}\left\{d\right\}} \tag{5.20}$$

Thus, the uniaxial formulation of the Bouc-Wen model introduced in Chapter 2 is herein extended into the stiffness formulation of a finite element, while its hysteretic properties, namely rate-independency causality and are retained.

5.3 The constant strain triangle

5.3.1 Kinematics of the constant stress triangle

The following triangular plane stress/ strain element with two translational degrees of freedom per node in the global coordinate system is considered (Fig. 5.1). The global axes X_1 and X_2 are identical to the Cartesian axes X and Y respectively. The first notation is adopted throughout this work, to be consistent with tensorial mechanics, while the latter is only used when spatial quantities are addressed.

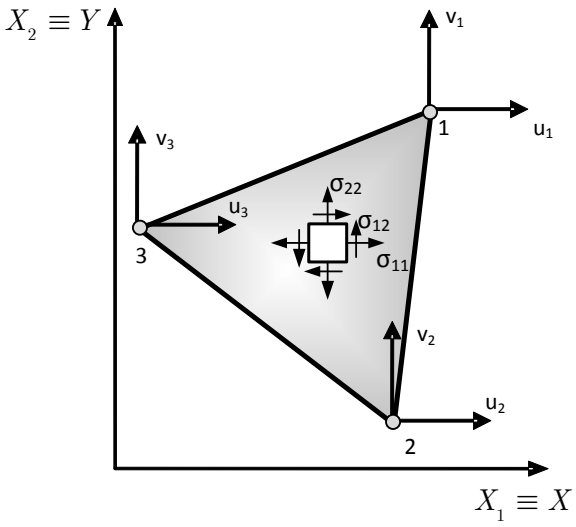

Fig. 5.1. Triangular plane stress/ strain FEM

By means of the classical formulation procedure of the plane stress/strain finite element the following interpolation functions are introduced:

$$\begin{aligned} u\left(x,y\right) &= \alpha_1 + \alpha_2 x + \alpha_3 y \\ v\left(x,y\right) &= \alpha_4 + \alpha_5 x + \alpha_6 y \end{aligned} \tag{5.21}$$

or in matrix form:

$$\begin{bmatrix} u \\ v \end{bmatrix} = \begin{bmatrix} 1 & x & y & 0 & 0 & 0 \\ 0 & 0 & 0 & 1 & x & y \end{bmatrix} \begin{Bmatrix} \alpha_1 \\ \alpha_2 \\ \alpha_3 \\ \alpha_4 \\ \alpha_5 \\ \alpha_6 \end{Bmatrix} \tag{5.22}$$

Substituting the nodal displacements $u_i, v_i,\ i = 1..3$ (Fig. 5.1) in equation (5.22), the following matrix relation is derived:

$$\left\{d\right\}=\begin{bmatrix}u_1\\v_1\\u_2\\v_2\\u_3\\v_3\end{bmatrix}=\begin{bmatrix}1&x_1&y_1&0&0&0\\0&0&0&1&x_1&y_1\\1&x_2&y_2&0&0&0\\0&0&0&1&x_2&y_2\\1&x_3&y_3&0&0&0\\0&0&0&1&x_3&y_3\end{bmatrix}\begin{Bmatrix}\alpha_1\\\alpha_2\\\alpha_3\\\alpha_4\\\alpha_5\\\alpha_6\end{Bmatrix} \tag{5.23}$$

Once equation (5.23) is inverted and the derived expression is substituted in equation (5.22) the shape functions of the triangular FEM are expressed as:

$$\begin{bmatrix}u\\v\end{bmatrix}=\begin{bmatrix}1&x&y&0&0&0\\0&0&0&1&x&y\end{bmatrix}\begin{bmatrix}1&x_1&y_1&0&0&0\\0&0&0&1&x_1&y_1\\1&x_2&y_2&0&0&0\\0&0&0&1&x_2&y_2\\1&x_3&y_3&0&0&0\\0&0&0&1&x_3&y_3\end{bmatrix}^{-1}\begin{bmatrix}u_1\\v_1\\u_2\\v_2\\u_3\\v_3\end{bmatrix} \tag{5.24}$$

After the necessary algebraic manipulation, the following linear shape functions are evaluated:

$$\left[N\right]=\begin{bmatrix}N_1&0&N_2&0&N_3&0\\0&N_1&0&N_2&0&N_3\end{bmatrix} \tag{5.25}$$

where:

$$N_i=\frac{1}{2A_e}\left(\beta_i+\gamma_i x+\delta_i y\right),\ i=1,2,3 \tag{5.26}$$

and:

$$\beta_1=\begin{vmatrix}x_2&y_2\\x_3&y_3\end{vmatrix},\ \gamma_1=-\begin{vmatrix}1&y_2\\1&y_3\end{vmatrix},\ \delta_1=\begin{vmatrix}1&x_2\\1&x_3\end{vmatrix}$$
$$2A_e=\begin{vmatrix}1&x_1&y_1\\1&x_2&y_2\\1&x_3&y_3\end{vmatrix}=\beta_1+\beta_2+\beta_3 \tag{5.27}$$

The remaining coefficients δ_i, γ_i are defined by cyclic permutation of the indices. Compatibility equations for the case of a plane deformable body undergoing small displacements are expressed as:

$$\varepsilon_x = \frac{\partial u}{\partial x}, \qquad \varepsilon_y = \frac{\partial v}{\partial y}, \qquad \gamma_{xy} = \frac{\partial u}{\partial y} + \frac{\partial v}{\partial x} \tag{5.28}$$

and in matrix form:

$$\begin{Bmatrix} \varepsilon_x \\ \varepsilon_y \\ \gamma_{xy} \end{Bmatrix} = \begin{bmatrix} \frac{\partial}{\partial x} & 0 \\ 0 & \frac{\partial}{\partial y} \\ \frac{\partial}{\partial y} & \frac{\partial}{\partial x} \end{bmatrix} \begin{Bmatrix} u \\ v \end{Bmatrix} \tag{5.29}$$

Substituting equation (5.24) in (5.29) the strain displacement equation is derived:

$$\{\varepsilon\} = [B]\{d\} \tag{5.30}$$

Thus, based on the shape functions defined in equation (5.25), the strain displacement equation is derived:

$$\{\varepsilon\} = [B]\{d\} \tag{5.31}$$

where the strain matrix B is given by the following relation:

$$[B] = \begin{bmatrix} N_{1,x} & 0 & N_{2,x} & 0 & N_{3,x} & 0 \\ 0 & N_{1,y} & 0 & N_{2,y} & 0 & N_{3,y} \\ N_{1,y} & N_{1,x} & N_{2,y} & N_{2,x} & N_{3,y} & N_{3,x} \end{bmatrix} \tag{5.32}$$

while $,x$ or $,y$ denotes differentiation with respect to X or Y respectively (Fig. 5.1). Thus, according to equation (5.27) the strain matrix $[B]$ is determined as:

$$\left[B\right]=\frac{1}{2A_e}\begin{bmatrix}\gamma_1 & 0 & \gamma_2 & 0 & \gamma_3 & 0\\ 0 & \delta_1 & 0 & \delta_2 & 0 & \delta_3\\ \delta_1 & \gamma_1 & \delta_2 & \gamma_2 & \delta_3 & \gamma_3\end{bmatrix} \tag{5.33}$$

which for the plane stress element is constant, thus facilitating integration in the subsequent analysis.

5.3.2 Derivation of stiffness matrices – variational formulation

To derive the appropriate stiffness relations, the principle of virtual work is implemented:

$$\int_V \left\{\delta\varepsilon\right\}^T\left\{\sigma\right\}dV=\left\{\delta u\right\}^T\left\{P\right\} \tag{5.34}$$

Since the vector of virtual nodal displacements is constant, the following rate form of equation (5.34) is derived:

$$\int_V \left\{\delta\varepsilon\right\}^T\left\{\dot{\sigma}\right\}dV=\left\{\delta u\right\}^T\left\{\dot{P}\right\} \tag{5.35}$$

In addition, equation (5.9) can be written in a condensed form as:

$$\left\{\dot{\sigma}^h\right\}=G\left(\alpha,\Phi,\varepsilon\right)\left\{\dot{\varepsilon}\right\},\ \text{where}\ \ G\left(\alpha,\Phi,\varepsilon\right)=\left[D\right]\left(\left[I\right]-H_1H_2\left[R\right]\right) \tag{5.36}$$

Substituting equation (5.4) into the rate form of the principle of virtual work, the following relation is derived:

$$\begin{aligned}&\int_V \left\{\delta\varepsilon\right\}^T\left(\left[\alpha\right]\left\{\dot{\sigma}^e\right\}+\left(\left[I\right]-\left[\alpha\right]\right)\left\{\dot{\sigma}^h\right\}\right)dV=\left\{\delta u\right\}^T\left\{\dot{P}\right\}\Rightarrow\\ &\Rightarrow\int_V \left\{\delta\varepsilon\right\}^T\left[\alpha\right]\left\{\dot{\sigma}^e\right\}dV+\int_V \left\{\delta\varepsilon\right\}^T\left(\left[I\right]-\left[\alpha\right]\right)\left\{\dot{\sigma}^h\right\}dV=\left\{\delta u\right\}^T\left\{\dot{P}\right\}\end{aligned} \tag{5.37}$$

Further, introducing the kinematic relations (5.15) and the constitutive relations of equations (5.36), the first and second integral of the l.h.s. of equation (5.37) are expressed as:

$$\begin{aligned}\int_V \{\delta\varepsilon\}^T [\alpha]\{\dot{\sigma}^e\} dV &= \{\delta u\}^T \int_V [B]^T [\alpha][D][B] dV \{\dot{u}\} \\ &= \{\delta u\}^T [\alpha][k_e]\{\dot{u}\} \\ \int_V \{\delta\varepsilon\}^T ([I]-[\alpha])\{\dot{\sigma}^h\} dV &= \{\delta u\}^T \int_V [B]^T ([I]-[\alpha])[G][B] dV \{\dot{u}\} \\ &= \{\delta u\}^T ([I]-[\alpha])\left[k_h\left(\{\sigma^h\}\right)\right]\{\dot{u}\}\end{aligned} \tag{5.38}$$

The first integral of equations (5.38) constitutes the elastic stiffness matrix of the plane stress/ element that corresponds to matrix [D], while the second is the introduced herein hysteretic stiffness matrix.

$$\left[k_h\left(\{\sigma^h\}\right)\right] = \int_V [B]^T [G][B] dV \tag{5.39}$$

The hysteretic stiffness matrix can be defined as the nonlinear supplement of the elastic component introduced by the hysteretic model implemented. The actual form of the hysteretic matrix is dependent on the yield criteria used since the hysteretic matrix is a function of the interaction matrix $[R]$.

After the necessary algebraic manipulation, the following relation is obtained:

$$\{\dot{P}\} = \left[k_t\left(\{\sigma^h\}\right)\right]\{\dot{u}\} \tag{5.40}$$

where the matrix:

$$\left[k_t\left(\{\sigma^h\}\right)\right] = [\alpha][k_e] + ([I]-[\alpha])\left[k_h\left(\{\sigma^h\}\right)\right] \tag{5.41}$$

is the nonlinear tangent stiffness matrix of the plane stress element. In relation (5.41) $[k_e]$ is the stiffness matrix of the elastic constant strain triangular element (Bathe 2007), that is only computed once throughout the solution procedure and $[k_h]$ is the hysteretic stiffness matrix.

In general, the matrix $\left[G\right]$ is a function of the stress vector, but in our case is constant along the element, allowing for the analytical integration of relation (5.39).

It is also evident that the hysteretic stiffness matrix is directly derived from the elastic one by mere substitution of the constitutive matrix, as the strain matrix $\left[B\right]$ remains the same. Since the hysteretic matrix implicitly depends on the yield criterion considered, it remains symmetric as long as the yield criterion is symmetric on the stress space. Since the shape functions used are the same as in the elastic case, the equivalent nodal loads of surface tractions remain also the same.

The notation implemented underlines the dependence of the hysteretic part of the stiffness to the current stress state of the element. This stiffness matrix depends only on material properties, namely the Poisson ratio, the Young modulus of elasticity, the post yield to elastic stiffness ratio and the yield criterion incorporated in the evolution equation of Bouc-Wen. The formulation described in the preceding paragraphs does not depend on the particular hysteretic model used in the analysis. As long as a model is smooth and rate independent, it can be incorporated into the standard displacement based FEM scheme.

At this point one can notice that a direct relation is established between the element stiffness matrix and the current state of stress. This relation is well defined in the stress-strain space and smoothly follows the loading-unloading response of the element under cyclic excitation. It is also important to notice that the element proposed herein can be easily used in conjunction with classical elastic elements, within the framework of the direct stiffness method. The proposed element can be implemented in damage identification and nonlinear structural identification methods for plane structures where strain localization is observed, see for example in Carpinteri et al. (2009). Such aspects though, are beyond the scope of this work.

From the computational perspective in standard dynamic analysis procedure a predictor-corrector scheme is used in conjunction with a Newton-Raphson procedure for the solution of nonlinear problems. The algorithm iterates through an elastic prediction and inelastic correction scheme, into a specific computational step, in order to determine the elemental tangent stiffness matrix (Neto et al., 2008). During these iterations the current stress state is continuously evaluated through various integration schemes, and the stress state computed at the end of a computational step is considered to be the same with the stress state at the beginning of the next computational step. Consequently, the entire procedure is accurate for sufficient small incremental steps (Barham et al., 2005).

5.4 Numerical examples

A computer software was developed to implement and test the efficiency of the proposed formulation. The code performs incremental static and dynamic analysis of plane structures. The triangulation of the surface structure is performed using Matlab code, while the analysis is performed using Fortran Code. A Delaunay unstructured mesh scheme is implemented for this purpose, (Hjelle & Daehlen, 2006).

5.4.1 Low yield shear panel

The hysteretic response of low yield strength, steel shear panel is examined. Shear panels of this type are effectively implemented as energy dissipation mechanisms in steel braced buildings (Chen et al., 2006). Shear panels are also used in retrofitting concrete buildings (Formisano et al., 2010).

The computational model of the shear panel is presented in Fig. 5.2. The panel thickness is set at 6mm. The panel is considered simply supported at the base, while at the two side perpendicular edges the vertical displacement is considered fixed. The proposed formulation is used for the analysis of the problem and the results are compared to those obtained using

the NASTRAN Code and the CTRIA3 plane stress element. A crude mesh is implemented consisting of 18 triangular elements with a maximum edge size of 0.30 cm.

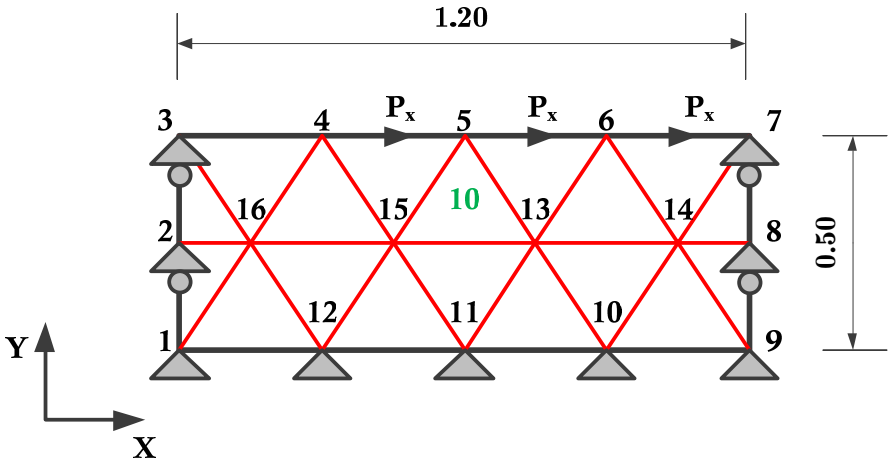

Fig. 5.2 Computational Model - Node Numbering and Boundary Conditions

At first, a nonlinear static analysis is performed with the proposed formulation, by assigning monotonically increasing horizontal loads to nodes #4, #5 and #6. The maximum value of each load is $\mathbf{P_x}$=300 KN. Three values of the smoothing parameter n are considered, namely $n = 2$, $n = 4$ and $n = 25$.

The resulting applied force lateral displacement diagrams are presented in Fig. 5.3. The lateral displacement is measured at node #5. As predicted by the hysteretic model introduced in equation (5.1), larger values of the smoothing parameter lead to a sharper transition from the elastic to the inelastic regime.

A sinusoidal excitation is next imposed on nodes #4, 5, 6 with an amplitude of 400 KN and a cyclic frequency of π rad/sec. The analysis is performed over a time period of 10 sec. The results obtained with the proposed formulation are compared with results obtained from Nastran Code. A modified Newton-Raphson scheme is implemented in Nastran. The time integration is performed with the average acceleration Newmark method. A time increment of 0.01 sec is selected. The parameters of the Newton Raphson scheme are presented in Table

5.1. A bilinear stress-strain relation is considered, setting $n = 25$ in the proposed formulation.

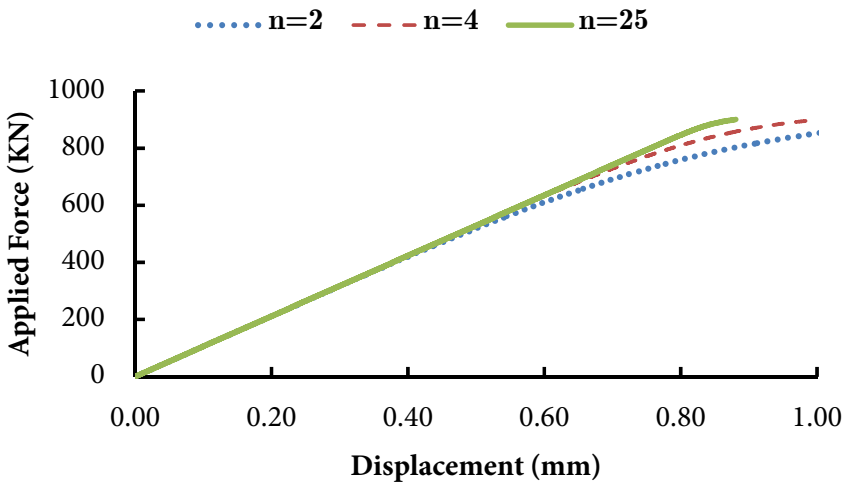

Fig. 5.3 Force-Displacement curve of the shear panel

Newton Raphson Analysis Parameters	
Material Nonlinearity	Bilinear Model
Kinematic Hardening	α=0.002
Total Number of Steps	1000
Time Increment	0.01 sec
Work error tolerance	10^{-6}
Displacement error tolerance	10^{-4}

Table 5.1 Nonlinear Analysis Parameters (Nastran Code)

The time history of the horizontal displacement at node #5 is presented in Fig. 5.4 where results from both the proposed formulation and the Nastran code are plotted. The discrepancies between the two formulations are negligible.

The analysis performed with the proposed formulation was performed in half the time of the Nastran analysis, i.e. 1.9 sec instead of 3.8 sec. This is attributed to the decoupling of the local nonlinear equations from the global linear equations of equilibrium as described in the next Chapter. Both analyses were in a PC fitted with a Core Duo Quad CPU and 2 GBs of RAM.

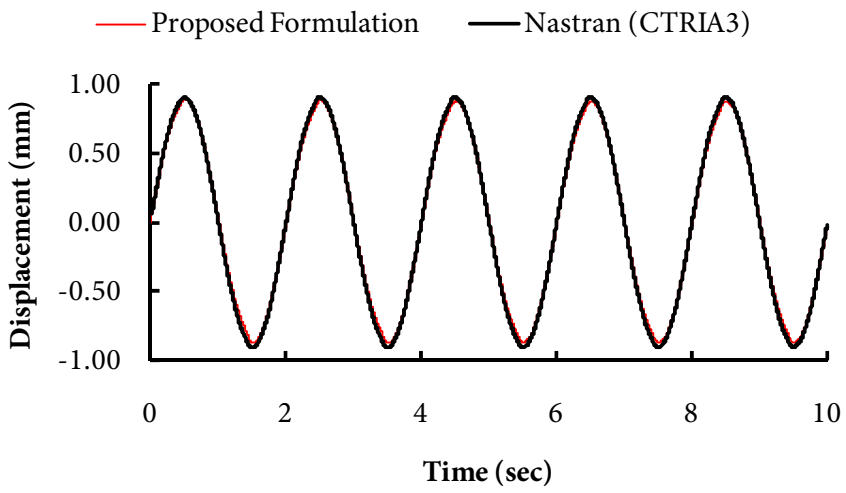

Fig. 5.4 Comparison of the proposed formulation to Nastran code

Next, an analysis is performed with the proposed formulation, considering the following values of the Bouc-Wen model parameters, namely $n = 2$, $\beta = 0.8$ and $\gamma = 0.2$. The time history of the tip displacement, measured at node 5 is presented in and the two solutions result in good agreement. The two elements exhibit almost the same elastic stiffness with some differences in the maximum negative displacements.

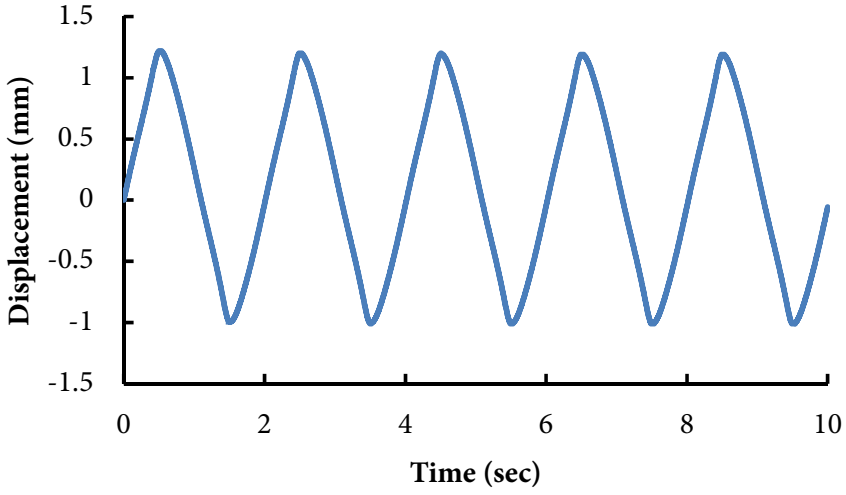

Fig. 5.5 Displacement Time History

In Fig. 5.6(a)-(c) the stress-strain hysteretic loops, evaluated at element #16 are presented. As expected, the shear stresses dominate the panel response, yet plastic deformations accumulate on all directions, due to the interaction scheme introduced through relation (5.2). In Fig. 5.6(d) the shear stress- shear strain hysteretic loop is presented, evaluated on element #10. Due to the antisymmetrical loading, this is the only non-zero stress component at that element. Yielding occurs exactly at 117.5 MPa, as predicted by the Von-Mises flow rule considered. Yet, the transition from the elastic to the inelastic regime commences at a lower stress level, due to the value of the smoothing parameter n. Moreover, the umloading branches are slightly curved due to the the values of the shape paremeters β and γ.

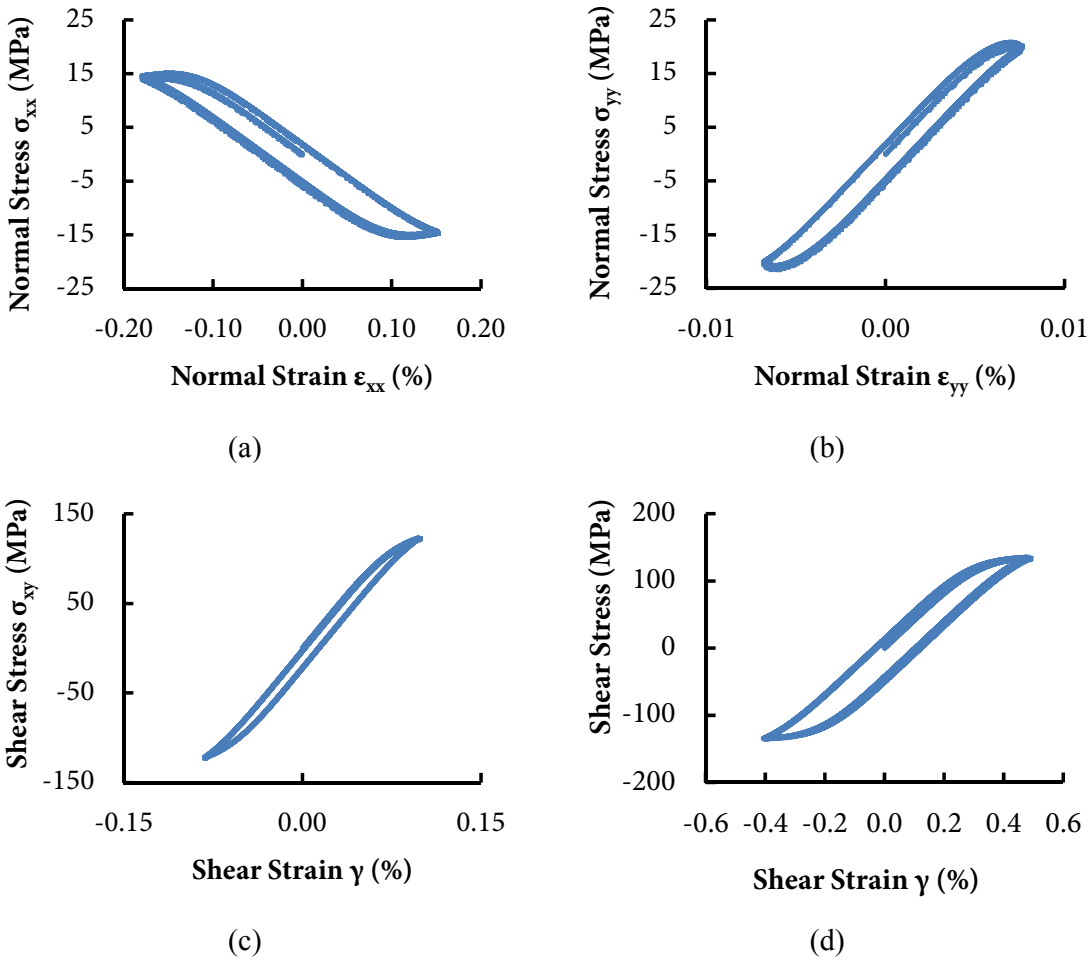

Fig. 5.6 Stress-Strain hysteretic loops (a) σ_{xx}-ε_{xx} (Element 16) (b) σ_{yy}-ε_{yy} (Elemement 16) (c) τ_{xy}-γ (Elemement 16) (d) τ_{xy}-γ (Elemement 10)

5.4.2 Cantilever Beam with Tip Load

In this example, a cantilever beam, consisting of plane-stress elements, carrying a concentrated tip load is examined. An elastic perfectly plastic material is considered with E = 210 GPa, v = 0.3, σ_y = 240 MPa, $\beta = \gamma = 0.5$. The geometric properties of the beam are presented in Fig. 5.7.

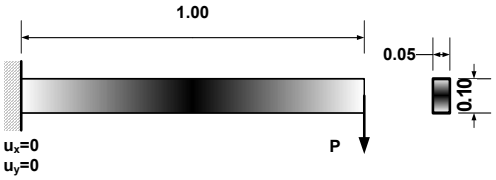

Fig. 5.7 Example 1-Cantilever beam

Two different analyses cases are performed. At first, the cantilever is subjected to a monotonically increasing concentrated tip load and the theoretical limit load is compared to the calculated one. The initial yield load and the ultimate load can be analytically evaluated as:

$$P_y = \frac{\sigma_y b h^2}{6L} = 20KN, \qquad P_u = \frac{\sigma_y b h^2}{4L} = 30KN$$

In Fig. 5.8 the applied load is plotted against the vertical deflection at the tip of the cantilever beam. Two different discretization schemes are considered and the results are compared to those obtained using the CPS3 element of the Abaqus v6.5 code (Abaqus, 2005). A Full Newton Raphson solution scheme is implemented in Abaqus, with 1000 incremental steps and a fixed increment step equal to 0.001 KN.

The proposed formulation predicts accurately both the initial yield load and the ultimate load with a fine mesh of 328 elements, with the difference between the predicted and the computed value being less than 1%. The smoothed plasticity concept adopted in the present work captures accurately the elastic-perfectly plastic behavior of the material. In Fig. 5.8, the results from Abaqus and the present formulation are compared for different discretization

schemes. Compared to the CPS3 element, the proposed formulation yields results that converge to the analytical solution faster in terms of the discretization needed to reach an acceptable solution. The CPS3 element fails to predict accurately both the initial yield and the ultimate load. Since the element formulation is similar in both cases, the difference in the convergence rate is attributed to the different solution scheme implemented.

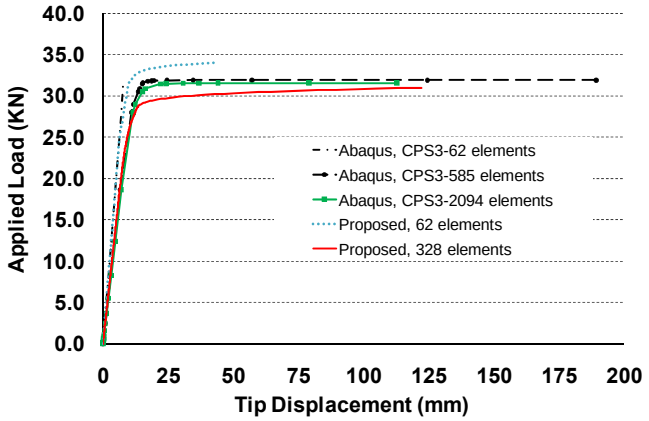

Fig. 5.8 Load Deflection Curve for the cantilever beam

In Fig. 5.9, the distribution of the normalized von-Mises Yield Criterion is plotted, when the imposed load reaches the value of the theoretically derived collapse load. At this time, the plastic hinge mechanism predicted by theory is fully formed. Notice that although the mesh implemented in the Matlab simulations is unstructured the solution reached the critical load predicted by theory.

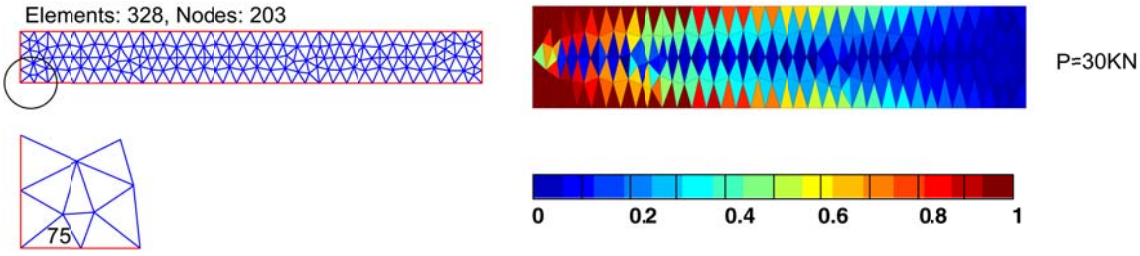

Fig. 5.9 Normalized von-Mises Yield Criterion

The evolution of the stress tensor at element 75 is presented in Fig. 5.10 with respect to the corresponding normal strain ε_{xx}. As long as the element remains elastic, the stresses evolve linearly following closely the assumptions of beam theory. Since the element is adjacent to

the end fiber of the beam, normal stresses σ_{xx} dominate, while the other components fluctuate near zero. When the element undergoes inelastic deformation, the stress components increase to a maximum value and then remain constant. According to Lubliner (2008), all the stress components are expected to remain constant inside the plastic boundary of an elastic perfectly plastic beam following von-Mises, or Tresca yield criteria.

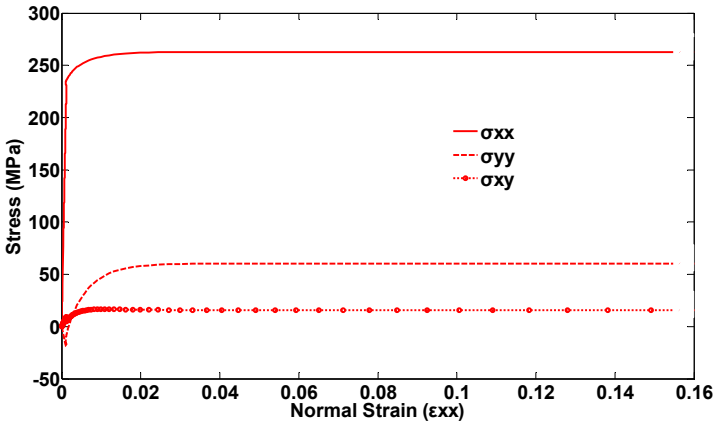

Fig. 5.10 (a) Evolution of stress–strain at element 75

The evolution of the von-Mises Yield Stress is presented in Fig. 5.11(a). Since the von Mises yield function is used in the example, the maximum value of the equivalent von-Mises Stress is:

$$\sigma_{\max} = \sigma_y \sqrt{2} = 339.5\, MPa$$

Finally, in Fig. 5.11(b), the evolution of the principal stresses is plotted. At the end fiber of the beam, the principal axes are almost parallel to the global axes X and Y due to pure bending conditions. As such, the principal stress σ_I, which is closer to the X axis, increases much faster than stress σ_{II}. When yielding occurs, the principal stress σ_{II} remains practically constant, whereas stress σ_I increases so as to maintain equilibrium.

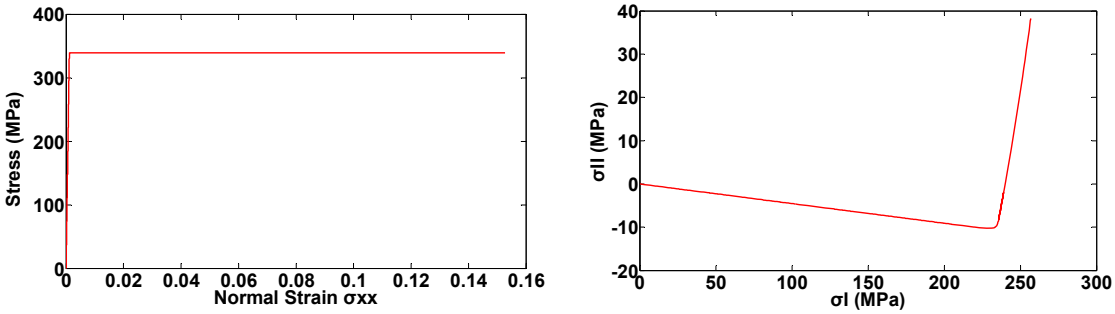

(a) (b)

Fig. 5.11 (a) Evolution of principal stresses (b) Evolution of the equivalent von-Mises Stress

Next, the beam is subjected to a sinusoidal excitation of increasing amplitude using the 328 element mesh presented in Fig. 5.9. For this case, a hardening ratio of α=0.002 is used, while no stiffness degradation and strength deterioration is considered (c_β=0.0, c_v=0.0). The analytical expression of the applied time history (Fig. 5.12(a)) is:

$$P(t) = 40\frac{t}{T_{tot}}\sin\left(\frac{3\pi}{4}t\right)$$

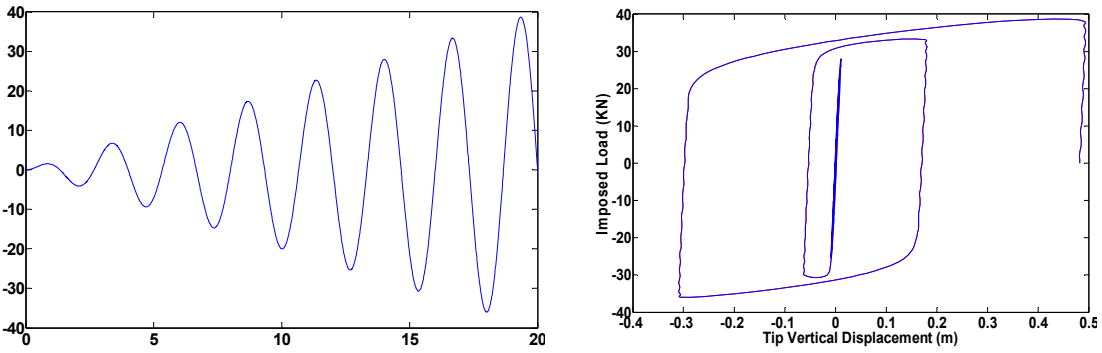

(a) (b)

Fig. 5.12(a) Applied Load Time History (b) Load Deflection Response of Cantilever beam

In Fig. 5.12(b) the response of the cantilever is plotted in terms of applied load versus vertical displacement at the tip of the cantilever. There is a smooth transition from the elastic to the inelastic regime of the response, while at the unloading phases the stiffness of the cantilever remains constant.

Next, the same problem is analyzed considering stiffness degradation and strength deterioration, with the following set of model parameters (c_v = 0.00001, c_b=0.002, m=0). The evolution of the normal stress at element 75 (Fig. 5.9) is presented in Fig. 5.13 as a function of the correspondent normal strain. For the sake of demonstration and clarity, the plots are presented for the first five successive loading-unloading phases of the imposed load. The unloading stiffness is decreasing between cycles as predicted by the hysteretic model. At the same time the yield strength is also decreasing from Point A, to Point B as presented in Fig. 5.13(b). The decrease in the yield strength in the opposite direction is larger than the one dictated by the linear kinematic hardening model with no deterioration. The element stress initially increases to approximately 270 MPa, thus the aniticipated yield stress in the opposite direction should be equal to 240-30=210 MPa. However, yielding in the opposite direction occurs at 188 MPa.

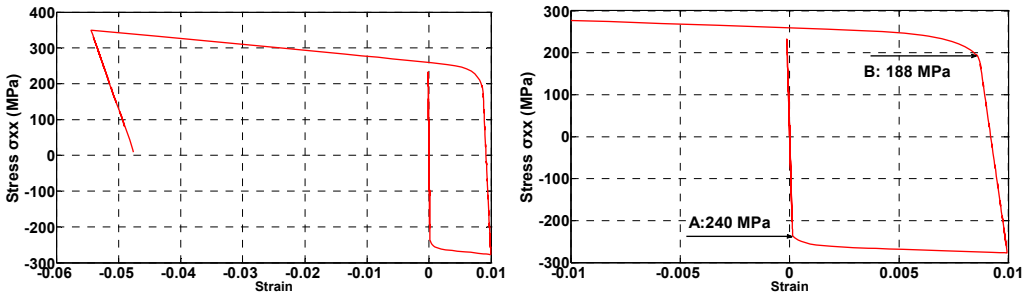

(a) (b)

Fig. 5.13 Stiffness degradation and Strength deterioration analysis

The change in the dynamic response of the cantilever is better depicted in the load-deflection diagram presented in Fig. 5.14, where it is evident that the period of oscillation is increasing, not only due to the plastic deformations accumulating, but also due to the decrease in the unloading stiffness of the cantilever.

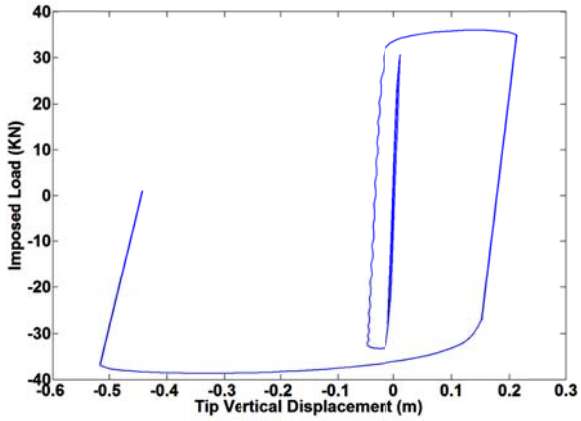

Fig. 5.14 Load Deflection Response of Cantilever beam with stiffness degradation and strength deterioration

5.4.3 Perforated Metal Sheet

An aluminum sheet with a circular notch (Fig. 5.15(a)) is examined next. The sheet is subjected to a monotonically increasing uniform tensile pressure along the y-axis. The elastic parameters of the material are; E=72 GPa, G=29.5 GPa, ν=0.22, $\sigma_y = 262$ MPa, while a hardening modulus of 0.002E is considered. Due to symmetry, only one fourth of the sheet is examined. The solutions are compared with those obtained from the HYPLAS code (Neto et. al, 2008). Analysis in HYPLAS is performed implementing a Newton scheme with 100 incremental steps. In Fig. 5.15(b), the computational model is presented for the case of a Delaunay triangulation scheme with a maximum element size of 0.05m (284 elements), together with the imposed boundary conditions.

The load-deflection response of the specimen is presented in 5.16(a). Deflection is measured at node 4, as depicted in Fig. 5.15(b). Three discretization schemes are considered. The exact solution is considered to be the one derived from the fine discretization of 414 elements. The ultimate load capacity of the specimen is approximately p_u = 110 KN. Further increment in the load, results in large displacement increments since the boundaries of the computational model are fully yielded.

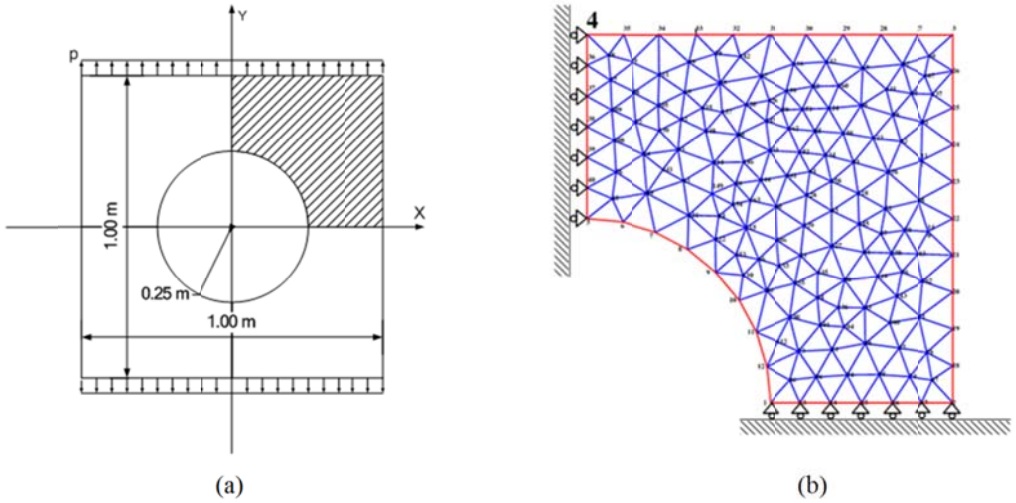

Fig. 5.15. (a) Perforated Aluminum Sheet Specimen (b) Computational Model (284 elements)

In 5.16(b) the advance of the plastic boundary is presented for specific values of the applied load as a proportion of the ultimate load. Each element that reaches the von-Mises yield criterion is colored, while different colors correspond to different load levels as specified in the legend.

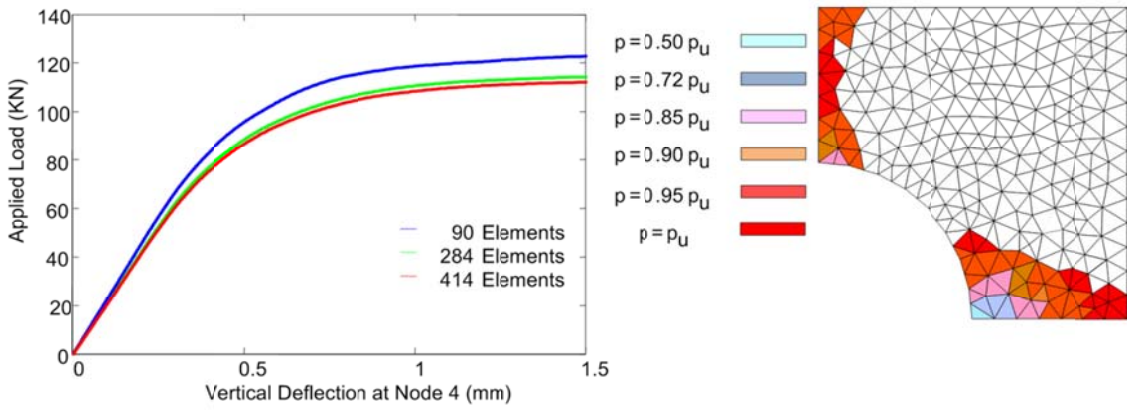

5.16 (a) Load Deflection curves for different discretization schemes (b) Plastic boundary evolution

The plastic boundary is propagating from the tips of the perforation towards the adjacent free surfaces of the specimen as predicted by theory, (Lubliner, 2008). In Fig. 5.17, the derived load deflection curve is compared against the one derived using HYPLAS.

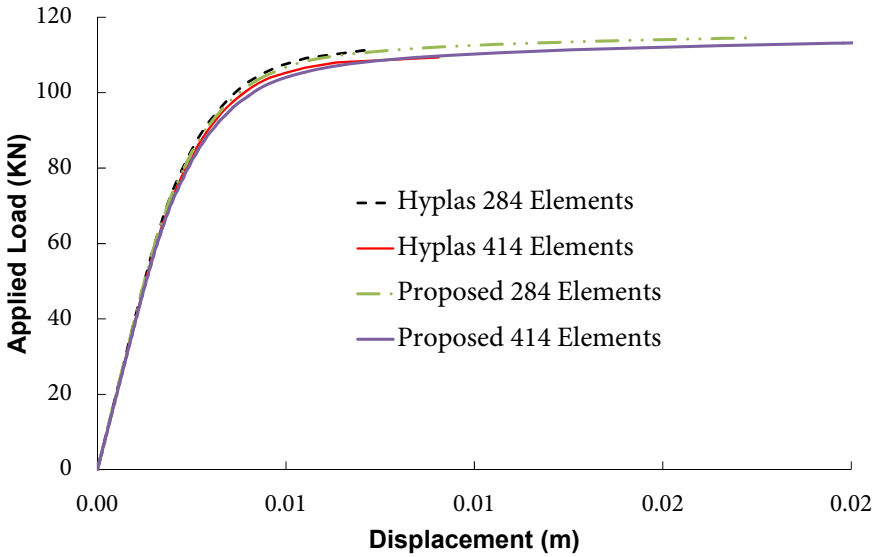

Fig. 5.17. Comparison of the proposed method to HYPLAS Code

The solution obtained based on the proposed formulation agrees well with the solution obtained using the HYPLAS code, though the latter does not converge at displacements close to 1.5mm. This is attributed to the different solution schemes, as the Livermore solver allows for a more robust error control when the stiffness matrix rapidly degrades.

5.5 Conclusions

Although, the univariate Bouc-Wen formulation that expresses yielding and the associative flow rule in rate form has found extensive application in skeletal structures, implementation into the finite element computational scheme for 2-D and 3-D problems has not yet been investigated. To implement such concepts, a new plane stress / strain element is formulated, based on the elastic constant strain triangle element and the Bouc-Wen hysteretic model. The governing equations are determined within the framework of the direct stiffness method, in state-space form, thus allowing for the use of advanced ode solvers.

This approach, together with the implementation of the smooth Bouc-Wen model in constitutive relations, is proved computationally efficient, as it avoids the errors accumulated due to the linearization of the governing equations in the usual Newton-based solution schemes. The main features and advantages of the proposed formulation were demonstrated with numerical examples. It is shown that the Bouc-Wen model introduced in the analysis can accurately simulate both the well-established bilinear von-Mises model with kinematic hardening as well as complex dynamical behavior with stiffness degradation and strength deterioration. Moreover, the accuracy of the proposed formulation is demonstrated through comparison with the Abaqus commercial code and the HYPLAS code.

The entire scheme can be easily extended to different elastic finite elements introducing appropriate constitutive relations and the corresponding interaction matrices that depend on specific yield criteria. Since the derivation of the element matrices is consistent with the direct stiffness method, the formulation allows for the implementation of inelastic finite elements, either in standalone structural meshes, as in the examples presented herein, or in conjunction with other types of finite elements. The implementation of the hysteretic Bouc-Wen model proposed herein, with stiffness degradation and strength deterioration offers a versatile tool for the nonlinear identification of plane structures, as it can simulate a variety of cyclic responses. From the engineering and design perspective, relying on the direct identification of model parameters resulting from component testing of members and connections, the method offers the ability for realistic simulations of the inelastic behavior of degrading structures under cyclic loading.

Chapter 6

STRUCTURAL ANALYSIS IMPLEMENTING BOUC-WEN HYSTERESIS

6.1 Introduction

The numerical solution of structural analysis problems relies on the proper definition of a mathematical model that is bound to be both conceptually simple and computationally accurate. The mathematical model is a discrete representation of the continuous and real structure. In Chapters 3 and 4, the necessary elements for the space discretization of a nonlinear hysteretic structure have been presented. The elements presented are based on either macroscopically or microscopically defined hysteretic properties.

In this chapter time discretization schemes are presented that allow for the solution of the dynamic problem. The sets of global governing equations are presented that are assembled according to the direct stiffness method. The hysteretic properties of the macro-elements are incorporated into the equations of motion through the global hysteretic matrix of the structure.

In Hughes, 1994 the following list is defined as the necessary list of properties, methods in linear structural dynamics should possess:

1. Unconditional stability
2. No more than one set of implicit equations to be solved at each step
3. Second order accuracy
4. Controllable algorithmic dissipation in the higher modes
5. Self-starting

The property of unconditional stability is related to the behaviour of the method when applied to the scalar test equation $\ddot{u} = -\omega^2 u$. The connection between conditions 1 and 3 is commented in Hughes, 1994. Apart from (2) the rest of the properties ensure the stability and accuracy of the time integration scheme. Property (2) sets un upper bound on the computational time needed to solve the numerical problem. In nonlinear problems this cannot be the case, since an iterative procedure is necessary within its integration step (Chopra,

2008). Property (5) comments on the necessary initial conditions for the algorithmic process to commence, since multistep methods need initial values in time instances prior to t_0.

Nevertheless, a solver that is well-suited for linear problems does not automatically qualify for non-linear problems. The Newmark method, one of the most popular implicit schemes that is unconditionally stable for linear problems but this stability condition is lost when applied to nonlinear problems. The Houbolt and Wilson-θ methods (Bathe, 2008) introduce strong numerical damping, which casts them unsuitable for any practical application to nonlinear dynamic systems if the duration over which the integration is required is long.

6.2 Expanding the capabilities of the Direct-Stiffness Method

In this section, the governing equations of the problem are formulated, following the direct stiffness approach. The elemental stiffness matrices derived using the methods presented in Chapters 3 and 4 are assembled to form the structural stiffness matrix $\left[K_S\right]$which, in the general case, consists of a constant elastic part due to the macro-elements and a smoothly varying part (equation 3.18) due to the hysteretic finite elements of the model. The equation of motion is then expressed as:

$$\left[M\right]_S\left\{\ddot{U}\right\}+\left[C\right]_S\left\{\dot{U}\right\}+\left[K\right]_S\left\{U\right\}+\left[H\right]_S\left\{z\right\}=\left\{P(t)\right\} \tag{6.1}$$

where $\left[M_S\right],\left[C_S\right],\left[K_S\right]$ are the mass, viscous damping, stiffness square symmetric $(n_f x\ n_f)$ matrices of the structure respectively while $\left[H\right]_S$ is the $(n_f x\ n_{hys})$ orthogonal global hysteretic matrix of the structure and $\left(n_{hys}x1\right)\ \left\{z\right\}$ is the vector of hysteretic degrees of freedom, n_{hys} being the number of hysteretic degrees of freedom. Additionally, $\left\{P(t)\right\}$ is the (n_f x 1) vector of external forces, n_f being the number of degrees of freedom of the

structure. The mass matrix may correspond to a lumped mass diagonal matrix, or a consistent mass matrix, Bathe (2007). The viscous damping matrix in general, may be of the form of a Rayleigh damping matrix.

As described in previous chapters, the hysteretic matrix $\left[H\right]_S$ needs to be evaluated only once in the beginning of the analysis procedure. However, the stiffness matrix varies as a function of the vector $\left\{\sigma\right\}$ consisting of the (n_{el}) stress vectors. The variation of the stress tensor is defined in equation 3.9 at the element level and is assembled at the structural level as:

$$\underbrace{\left\{\dot{\sigma}\right\}_S}_{3n_{el}} = \underbrace{\left[D_H\right]_S}_{3n_{el}\times 3n_{el}} \underbrace{\left\{\dot{\varepsilon}\right\}}_{3n_{el}} \tag{6.2}$$

where $\left[D_H\right]_S$ is a diagonal matrix containing the individual elemental contributions of matrices $\left[D_H\right]$ of equation 3.7. Considering the stress –strain matrix and assembling for the whole structure, equation (6.2) can be written as:

$$\underbrace{\left\{\dot{\sigma}\right\}_S}_{3n_{el}} = \underbrace{\left[D_H\right]_S}_{3n_{el}\times 3n_{el}} \underbrace{\left[B\right]_S}_{3n_{el}\times n_f} \underbrace{\left\{\dot{d}\right\}}_{n_f} \tag{6.3}$$

where $\left[B\right]_S$ is a block diagonal matrix consisting of the elemental strain-displacement matrices. Furthermore, equations (4.112) are supplemented by the set of evolution equations of the hysteretic quantities $\left\{z\right\}$ that assume the following form:

$$\left\{\dot{z}\right\} = f(\left\{\dot{U}\right\},\left\{z\right\}) \tag{6.4}$$

Expressions of this form are given in Chapter 2 for the case of Bouc-Wen modeling. If stiffness degradation and strength deterioration phenomena are accounted for, equations (6.4)

are accompanied with a corresponding set of evolution equations as presented in Chapter 2. For the case of the simple Bouc-Wen model equations (6.4) assume the following form:

$$z_j^i = \left(1 - \left|\frac{z_j(t)}{z_y}\right|^n \left(\beta + \gamma \operatorname{sgn}\left(z_j(t)\left[B\right]_j\left[\Lambda\right]\left\{\dot{u}\right\}\right)\right)\right)\left[B\right]_j\left[\Lambda\right]\left\{\dot{D}\right\}^i \tag{6.5}$$

where z_j^i is the i_{th} hysteretic parameter of the j_{th} macro-element $\left[B\right]_j$ is the corresponding strain-displacement matrix, $\left[\Lambda\right]$ is the transformation matrix and $\left\{\dot{D}\right\}^i$ is the vector of global nodal displacements of the element.

The necessary modifications in a standard FEM code, so as to comply with the formulation presented herein mainly concern the evaluation of the hysteretic matrix $\left[H\right]_S$ and the establishment of the evolution equations. Moreover, the element proposed herein can be easily incorporated in a joined analysis – identification software, as proposed in Piyawat K., Pei J. S 2009

The system of equations of motion (4.112) can be transformed into state space form introducing the nodal velocities as additional unknowns:

$$\begin{aligned}
\left\{\dot{X}\right\}_1 &= \left\{X\right\}_2 \\
\left\{\dot{X}\right\}_2 &= -\left[M\right]_S^{-1}\left(\left[C\right]_S\left\{X\right\}_2 + K\left(\left\{X\right\}_3\right)_S\left\{X\right\}_1 + \left[H\right]_S\left\{X\right\}_4 + \left\{P(t)\right\}\right) \\
\left\{\dot{X}\right\}_3 &= \left[G\right]_S\left[B\right]_S\left\{X\right\}_2 \\
\left\{\dot{X}\right\}_4 &= f(\left\{X\right\}_2, \left\{X\right\}_4)
\end{aligned} \tag{6.6}$$

where $\left\{X\right\}_1$ is the $\left(n_f x1\right)$ vector of unknown displacements, $\left\{X\right\}_2$ the corresponding vector of unknown velocities, $\left\{X\right\}_3$ the vector of the hysteretic stress components as defined

in equation (6.2) and $\{X\}_4$ the vector of hysteretic deformation components as defined in equation (6.4). The set of equations (6.6) together with the evolution equations of relation (6.2) and (6.4) suffice to determine the nonlinear dynamic behavior of the structure.

The nonlinear system of equations (4.112) can be solved using any particular numerical integrator such as the classical Newmark scheme. In this case, a Newton-like numerical scheme is needed in order to solve the nonlinear constitutive equations, in each time integration step (Bathe 2007). However, in the formulation introduced herein, the hysteretic stress tensor is considered as an additional unknown evolving through the rate form of the constitutive equation. This allows for the simultaneous solution of the governing equations of the system. In this way the computational error accumulated in the analysis procedure is reduced. The system of first order nonlinear differential equations (6.6) can be solved using optimal Runge – Kutta operators (Sivaselvan & Reinhorn 2003). In this work, the Livermore family of solvers (Radhakrishnan and Hindmarsh 1993) is implemented, allowing for a robust and unconditionally stable approach.

6.3 Second order representation solution methods

The case of the nonlinear system of equations of motion (4.112) is considered, where the applied force is defined as a set of discrete values $\{P\}_n = \{P(t_n)\}, n = 1..N$ subject to the following set of initial conditions:

$$\{u(0)\} = \{u\}_0, \{\dot{u}(0)\} = \{\dot{u}\}_0, \{z(0)\} = \{z\}_0, \{\sigma_h(0)\} = \{\sigma_h\}_0 \tag{6.7}$$

The solution is evaluated as a sequence of discrete values of displacement $\{u\}_i$, velocity $\{\dot{u}\}_i$ and acceleration $\{\ddot{u}\}_i$ at time instances t_i. The time increment of the marching process

$\Delta t = t_{i+1} - t_i$ may or may not be considered constant. Thus, the continuous problem defined in (4.112) is transformed to its discrete counterpart at t_i

$$\begin{aligned} &\left[M\right]_S \left\{\ddot{U}\right\}_i + \left[C\right]_S \left\{\dot{U}\right\}_i + \left[K\left(\left\{\sigma_h\right\}_i\right)\right]_S \left\{U\right\}_i + \left[H\right]_s \left\{Z\right\}_i = \left\{P\right\}_i \\ &\left\{\dot{\sigma}^h\right\}_i = \left[G\right]_{S,i} \left[B\right]_s \left\{\dot{U}\right\}_i \\ &\left\{\dot{Z}\right\}_i = f(\left\{\dot{U}\right\}_i, \left\{Z\right\}_i) \end{aligned} \tag{6.8}$$

Similar to any established time-marching process, the solution at the time increment $i+1$ is sought, where

$$\begin{aligned} &\left[M\right]_S \left\{\ddot{U}\right\}_{i+1} + \left[C\right]_S \left\{\dot{U}\right\}_{i+1} + \left[K\left(\left\{\sigma_h\right\}_{i+1}\right)\right]_S \left\{U\right\}_{i+1} + \left[H\right]_s \left\{Z\right\}_{i+1} = \left\{P\right\}_{i+1} \\ &\left\{\dot{\sigma}^h\right\}_{i+1} = \left[G\right]_{S,i+1} \left[B\right]_s \left\{\dot{U}\right\}_{i+1} \\ &\left\{\dot{Z}\right\}_{i+1} = f(\left\{\dot{U}\right\}_{i+1}, \left\{Z\right\}_{i+1}) \end{aligned} \tag{6.9}$$

where attention should be drawn to the fact that the hysteretic constitutive matrix $\left[G\right]_{S,i+1}$ also depends on the current stress distribution.

6.3.1 The method of central differences

According to the method of central differences, the displacement rates are approximated through the following finite difference scheme (Chopra, 2006)

$$\left\{\dot{U}\right\}_i = \frac{\left\{U\right\}_{i+1} - \left\{U\right\}_{i-1}}{2\Delta t}, \quad \left\{\ddot{U}\right\}_i = \frac{\left\{U\right\}_{i+1} - 2\left\{U\right\}_i + \left\{U\right\}_{i-1}}{\Delta t^2} \tag{6.10}$$

The same scheme is also implemented for the rate of the hysteretic stress vector, thus

$$\left\{\dot{\sigma}\right\}_{h,i} = \frac{\left\{\sigma\right\}_{h,i+1} - \left\{\sigma\right\}_{h,i-1}}{2\Delta t} \tag{6.11}$$

and the hysteretic deformation vector:

$$\left\{\dot{Z}\right\}_i = \frac{\left\{Z\right\}_{i+1} - \left\{Z\right\}_{i-1}}{2\Delta t} \tag{6.12}$$

Replacing equations (6.10) and (6.11) into (6.8), the following set of discretized algebraic equations is derived

$$\begin{aligned}
&\left[M\right]_S \frac{\left\{U\right\}_{i+1} - 2\left\{U\right\}_i + \left\{U\right\}_{i-1}}{\Delta t^2} + \left[C\right]_S \frac{\left\{U\right\}_{i+1} - \left\{U\right\}_{i-1}}{2\Delta t} + \left[K\left(\left\{\sigma_h\right\}_i\right)\right]_S \left\{U\right\}_i + \left[H\right]_s \left\{Z\right\}_i = \left\{P\right\}_i \\
&\frac{\left\{\sigma\right\}_{h,i+1} - \left\{\sigma\right\}_{h,i-1}}{2\Delta t} = \left[G\right]_{S,i} \left[B\right]_s \frac{\left\{U\right\}_{i+1} - \left\{U\right\}_{i-1}}{2\Delta t} \\
&\frac{\left\{Z\right\}_{i+1} - \left\{Z\right\}_{i-1}}{2\Delta t} = f\left(\frac{\left\{U\right\}_{i+1} - \left\{U\right\}_{i-1}}{2\Delta t}, \left\{Z\right\}_{i+1}\right)
\end{aligned} \tag{6.13}$$

Rearranging and solving for the unknown quantities the following relations are derived

$$\begin{aligned}
&\left[\hat{K}\right]\left\{U\right\}_{i+1} = \left[\hat{p}\right] \\
&\left\{\sigma\right\}_{h,i+1} - \left[G\right]_{S,i} \left[B\right]_s \left\{U\right\}_{i+1} = \left\{\sigma\right\}_{h,i-1} - \left[G\right]_{S,i} \left[B\right]_s \left\{U\right\}_{i-1} \\
&\frac{\left\{Z\right\}_{i+1} - \left\{Z\right\}_{i-1}}{2\Delta t} = f\left(\frac{\left\{U\right\}_{i+1} - \left\{U\right\}_{i-1}}{2\Delta t}, \left\{Z\right\}_{i+1}\right)
\end{aligned} \tag{6.14}$$

where the equivalent stiffness matrix $\left[\hat{K}\right]$ is defined as:

$$\left[\hat{K}\right] = \frac{1}{\Delta t^2}\left[M\right]_S + \frac{1}{2\Delta t}\left[C\right]_S \tag{6.15}$$

and the equivalent load vector $\left[\hat{p}\right]$ is defined accordingly as:

$$\left[\hat{p}\right] = \left\{P\right\}_i - \left[K\left(\left\{\sigma_h\right\}_i\right)\right]_S \left\{U\right\}_i - \left[H\right]_s \left\{Z\right\}_i + \frac{1}{\Delta t^2}\left[M\right]_S \left(-2\left\{U\right\}_i + \left\{U\right\}_{i-1}\right) + \frac{1}{2\Delta t}\left[C\right]_S \left\{U\right\}_{i-1} \tag{6.16}$$

In general, the system of equations (6.14) is highly nonlinear, due to the hysteretic function $f\left(.\right)$. Still, it is an algebraic system that can be solved with standard solution algorithms. In

case where the macro-hysteretic matrix $\left[H\right]_s$ vanishes, the displacements at time step $i+1$ can be derived from the first of equations (6.14) as:

$$\left\{U\right\}_{i+1} = \left[\hat{K}\right]^{-1}\left[\hat{p}\right] \tag{6.17}$$

Substituting to the second, the corresponding hysteretic stress vector is derived as:

$$\left\{\sigma\right\}_{h,i+1} = \left\{\sigma\right\}_{h,i-1} - \left[G\right]_{S,i}\left[B\right]_s\left\{U\right\}_{i-1} + \left[G\right]_{S,i}\left[B\right]_s\left[\hat{K}\right]^{-1}\left[\hat{p}\right] \tag{6.18}$$

This is an explicit integration scheme, since the values of the unknown quantities at the current integration step are derived using values of the quantities at the previous integration step. However, these quantities do not necessarily satisfy the governing equations (6.9) at time step $i+1$, since the structural stiffness may have changed due to nonlinearities. Thus, an iterative procedure needs to be implemented in order to satisfy equilibrium. Upon this point, the analysis performed demonstrates that usual analysis procedures can be implemented in order to solve the governing equations of the nonlinear hysteretic problem. The iterative formulation proposed will be discussed on the next chapter.

6.3.2 The Newmark family of solvers

Newmark (1959) developed a set of time integration schemes based on the following equations:

$$\left\{\dot{U}\right\}_{i+1} = \left\{\dot{U}\right\}_i + \left[\left(1-\gamma\right)\Delta t\right]\left\{\ddot{U}\right\}_i + \left(\gamma\Delta t\right)\left\{\ddot{U}\right\}_{i+1} \tag{6.19}$$

and

$$\left\{U\right\}_{i+1} = \left\{U\right\}_i + \Delta t\left\{\dot{U}\right\}_i + \left[\left(0.5-\beta\right)\Delta t^2\right]\left\{\ddot{U}\right\}_i + \left[\beta\Delta t^2\right]\left\{\ddot{U}\right\}_{i+1} \tag{6.20}$$

Parameters β and γ determine the acceleration increment within the time step and are essential in the evaluation of the stability and accuracy measures of the method. Usually the

values $\gamma = 1/2$ and $1/6 \le \beta \le 1/4$ are considered. Solving equation (6.20) for the velocity vector and substituting into equation (6.19) respectively, the following relations are derived:

$$\begin{aligned} \{\ddot{U}\}_{i+1} &= \frac{1}{\beta\Delta t^2}\Big(\{U\}_{i+1} - \{U\}_i - \Delta t\{\dot{U}\}_i - (0.5-\beta)\Delta t^2\{\ddot{U}\}_i\Big) \\ \{\dot{U}\}_{i+1} &= \Delta t\left(1-\frac{\gamma}{2\beta}\right)\{\ddot{U}\}_i + \left(1-\frac{\gamma}{\beta}\right)\{\dot{U}\}_i + \frac{\gamma}{\beta\Delta t}\Big(\{U\}_{i+1} - \{U\}_i\Big) \end{aligned} \tag{6.21}$$

Replacing equations (6.21) in the first of equations (6.9) the following algebraic relations are derived:

$$[K]_{eff,i+1}\{U\}_{i+1} = \{p\}_{eff,i+1} \tag{6.22}$$

where:

$$\begin{aligned} [K]_{eff,i+1} &= [\alpha_1] + \Big[K\Big(\{\sigma_h\}_{i+1}\Big)\Big] \\ \{p\}_{eff,i+1} &= \{P\}_{i+1} + \Big([\alpha_1]\{U\}_i + [\alpha_2]\{\dot{U}\}_i + [\alpha_3]\{\ddot{U}\}_i\Big) \end{aligned} \tag{6.23}$$

and:

$$\begin{aligned} [\alpha_1] &= \left(\frac{1}{\beta\Delta t^2}[M]_S + \frac{\gamma}{\beta\Delta t}[C]_s\right) \\ [\alpha_2] &= \left(\frac{1}{\beta\Delta t}[M]_S - \left(1-\frac{\gamma}{\beta}\right)\right) \\ [\alpha_3] &= \left(\frac{1}{\beta}[M]_S - \Delta t\left(1-\frac{\gamma}{2\beta}\right)[C]_S\right) \end{aligned} \tag{6.24}$$

Similarly, replacing the displacement rate relation from equation (6.21) and implementing a central difference approximation for the stress rate, the second of equations (6.9) is written in discrete form as:

$$\{\sigma\}_{h,i+1} = 2\Delta t\{\sigma\}_{h,i} + [G]_{S,i+1}[B]_s\{L\} \tag{6.25}$$

where $\{L\} = \Delta t^2\left(2-\frac{\gamma}{\beta}\right)\{\ddot{U}\}_i + 2\Delta t\left(1-\frac{\gamma}{\beta}\right)\{\dot{U}\}_i + \frac{2\gamma}{\beta}\left(\{U\}_{i+1} - \{U\}_i\right)$.

The effective stiffness matrix of equation (6.23) is a function of the current hysteretic stress tensor, which in turn is a function of the current displacement vector (equation (6.25)). Thus, an iterative procedure has to be implemented.

This is achieved by casting equations (6.21) to (6.25) into incremental form, letting $d\{U\}_{i+1} = \{U\}_{i+1} - \{U\}_i$. Consequently, equations (6.21) and (6.25) can be iterated within a specific time step i following the standard procedure for the solution of nonlinear dynamic equations (Bathe, 2008, Chopra, 2008).

The advantage over the existing solutions lies in the fact that the system of equations (6.21) and (6.25) embodies all the information concerning classical plasticity theory. The elastic, or plastic state of the material is not derived through a radial-return mapping scheme (Simo and Hughes, 1998) at the end of the iteration step but is rather evaluated as a smooth function of the current displacement.

The relations for the Newmark methods of average acceleration and linear acceleration are presented in Table 6.1 for the sake of reference.

Average Acceleration	Linear Acceleration
$\{\ddot{U}(\tau)\} = \frac{1}{2}\left(\{\ddot{U}\}_{i+1} + \{\ddot{U}\}_i\right)$	$\{\ddot{U}(\tau)\} = \{\ddot{U}\}_i + \frac{\tau}{\Delta t}\left(\{\ddot{U}\}_{i+1} - \{\ddot{U}\}_i\right)$
$\{\dot{U}(\tau)\} = \{\dot{U}\}_i + \frac{\tau}{2}\left(\{\ddot{U}\}_{i+1} + \{\ddot{U}\}_i\right)$	$\{\dot{U}(\tau)\} = \{\dot{U}\}_i + \{\ddot{U}\}_i\,\tau + \frac{\tau^2}{2\Delta t}\left(\{\ddot{U}\}_{i+1} -$
$\{\dot{U}\}_{i+1} = \{\dot{U}\}_i + \frac{\Delta t}{2}\left(\{\ddot{U}\}_{i+1} + \{\ddot{U}\}_i\right)$	$\{\dot{U}\}_{i+1} = \{\dot{U}\}_i + \frac{\Delta t}{2}\left(\{\ddot{U}\}_{i+1} + \{\ddot{U}\}_i\right)$
$\{U(\tau)\} = \{U\}_i + \{\dot{U}\}_i\,\tau + \frac{\tau^2}{4}\left(\{\ddot{U}\}_{i+1} + \{\ddot{U}\}_i\right)$	$\{U(\tau)\} = \{U\}_i + \{\dot{U}\}_i\,\tau + \{\ddot{U}\}_i\frac{\tau^2}{2} + \frac{\tau^3}{6\Delta t}\left(\{\ddot{U}\}_{i+1} + \{\ddot{U}\}_i\right)$
$\{U\}_{i+1} = \{U\}_i + \{\dot{U}\}_i\,\Delta t + \frac{(\Delta t)^2}{4}\left(\{\ddot{U}\}_{i+1} + \{\ddot{U}\}_i\right)$	$\{U\}_{i+1} = \{U\}_i + \{\dot{U}\}_i\,\Delta t + (\Delta t)^2\left[\frac{1}{6}\{\ddot{U}\}_{i+1} + \frac{1}{3}\{\ddot{U}\}_i\right]$

Table 6.1: Methods of average and linear acceleration

6.4 First order representation

6.4.1 General remarks

In this section, the general properties of the mathematical structure at hand are described. As shown in the previous paragraph we are interested in the solution of an m.d.o.f. system of nonlinear first order ordinary differential equations. Such a problem can be written as

$$\begin{aligned} \{\dot{y}\} &= \frac{d\{t\}}{dx} = f\left(\{y(t)\},t\right) \\ \{y(t_0)\} &= \{y\}_0 \end{aligned} \tag{6.26}$$

where $\{y\}$, $\{y\}_0$, $\{\dot{y}\}$ and f are column vectors.

The computational time needed for an accurate solution of the system of equations (6.26) is directly related to a property called the "stiffness" of the system. In general, a stiff ode is one that includes both rapidly and slowly varying terms. Shampine and Gordon (1975) discuss some fundamental issues related to the property of stiffness. The most important of those is the fact that the Jacobian of (6.26)

$$[J] = \frac{\partial f\left(\{y(t)\},t\right)}{\partial \{y(t)\}} \tag{6.27}$$

has eigenvalues with both negative and positive real parts that also vary widely in magnitude. Thus, some of the solution components will be decaying whereas others will be non-decaying over time. Since the eigenvalues are, in general, not constant over time, as in the case of material and geometric nonlinearities, some equations might be stiff in some time interval but not in another. Thus, the property of stiffness is local.

A quantitative measure of stiffness is usually given by the stiffness ratio $\max\left[-\mathrm{Re}(\lambda_i)\right]/\min\left[-\mathrm{Re}(\lambda_i)\right]$ which is a local quantity also. Another standard measure

for stiffness is the quantity $\max\left[-\mathrm{Re}\left(\lambda_i\right)\right]\left|dt\right|$. Since $\left|dt\right|$ is a direct indicator of the time-marching process while in many cases $\min\left[-\mathrm{Re}\left(\lambda_i\right)\right] \to 0$, the second measure is preferred during the qualitative description of a system of odes.

The difficulty with stiff problems is the prohibitive amounts of computer time required for their solution by classical ODE solution methods, such as the popular explicit Runge-Kutta and Adams methods. The reason is the excessively small step sizes that these methods must use to satisfy stability requirements. Because of the approximate nature of the solutions generated by numerical integration methods, errors are inevitably introduced at every step. For a numerical method to be stable, errors introduced at any one step should not grow unbounded as the calculation proceeds.

To maintain numerical stability, classical ODE solution methods must use small step sizes of order $1/\max\left[-\mathrm{Re}\left(\lambda_i\right)\right]$ even after the rapidly decaying components have decreased to negligible levels. Examples of the step size pattern used by an explicit Runge-Kutta method in solving stiff ODE problems arising in combustion chemistry are given in Radhakrishnan and, Hindmarsh (1993)**.** Now, the size of the integration interval for the evolution of the slowly varying components is of order $1/\min\left[-\mathrm{Re}\left(\lambda_i\right)\right]$. Consequently, the number of steps required by classical methods to solve the problem is of order $\max\left[-\mathrm{Re}\left(\lambda_i\right)\right]/\min\left[-\mathrm{Re}\left(\lambda_i\right)\right]$ which is very large for stiff ODE'S.

6.4.2 Description of linear multistep predictor corrector methods

In general, linear multistep methods evaluate the solution of (6.26) at the n_{th} step, implementing the following formula:

$$\left\{Y\right\}_n = \sum_{j=1}^{K_1} \alpha_j \left\{Y\right\}_{n-j} + h_n \sum_{j=0}^{K_2} \beta_j \left\{f\right\}_{n-j} \tag{6.28}$$

where the coefficient vectors α_j, β_j depend on the specific method while $h_n = t_n - t_{n-1}$ is the time increment which can vary as the time-marching process evolves. Parameters K_1 and K_2 also depend on the method implemented and are equal to the number of previous solution points used to evaluate the current solution. The coefficient vectors are determined assuming that the solution of equation (6.26) is polynomial of order $K_1 + K_2$ and demanding that the anzaz (6.28) is exact in this case. The second term in the r.h.s of equation (6.28) may or may not involve the value of the derivative at the current time step (setting $\beta_0 = 0$) which is unknown giving rise to either implicit or explicit differentiation formulas.

In case $K_1 = K_2 = 1$ and $\alpha_1 = \beta_1 = 1$ equation (6.28) degenerates into the Euler forward differentiation scheme (Bathe, 2007). Accordingly the values $K_1 = 1$, $K_2 = q - 1$ produce the Adams-Moulton method of order q:

$$\left\{Y\right\}_n = \left\{Y\right\}_{n-1} + h_n \sum_{j=0}^{q-1} \beta_j \left\{f\right\}_{n-j} \tag{6.29}$$

while the choice $K_1 = q$, $K_2 = 0$ gives rise to the Backward Differentiation Formula of BDF for brevity. Equation (6.28) can be rewritten in the following equivalent form:

$$\left\{Y\right\}_n = \left\{\Psi\right\}_n + h_n \beta_0 \left\{f\right\}_n \tag{6.30}$$

where the quantity

$$\left\{\Psi\right\}_n = \sum_{j=1}^{K_1} \alpha_j \left\{Y\right\}_{n-j} + h_n \sum_{j=1}^{K_2} \beta_j \left\{f\right\}_{n-j} \tag{6.31}$$

involves the function evaluations at previous time steps.

Implicit methods are in general expensive to solve in terms of functions evaluations. Nevertheless they have been proven to be more stable and more accurate for the same order

and step size compared to the explicit ones (Lambert, 1973). Thus, implicit methods can be implemented with larger time steps.

In a predictor-corrector scheme, an explicit method is used as a predictor, generating an initial guess for $\{Y\}_n$. Next, an implicit scheme is implemented in order to correct the initial guess. Thus, a predictor-corrector scheme first evaluates in a single function evaluation the predicted value, denoted $\{Y\}_n^{(0)}$ and then corrects this value by iterating equation (6.30) until convergence. Referring to equation (6.30), at each iteration m the quantity $h_n\{\dot{Y}\}_n$ is evaluated through the following relation:

$$\{f\}_n^{(m)} = \frac{1}{h_n\beta_0}\left(\{Y\}_n^{(m)} - \{\Psi\}_n\right) \tag{6.32}$$

Different iterative techniques can be implemented at this point . In this work, the classical Newton-Raphson scheme is implemented that converges quadratically, thus allowing for fewer iterations and larger time steps. For this reason the following residual quantity is defined:

$$\mathrm{Re}\,s\left(\{Y\}_n^{(m+1)}\right) = \{Y\}_n^{(m)} - \{\Psi\}_n - h_n\beta_0\{f\}_n^{(m)} \tag{6.33}$$

and the iteration process evolves until the corresponding Taylor expansion assumes a small value (Radhakrishnan and Hindmarsh, 1993).

6.5 The continuum and consistent formulations of the constitutive tensor

The Newton-Raphson method that is implemented within the corrector step reduces the nonlinear problem to a sequence of linearized problems (through Taylor expansion) referred to as iterations in the previous section. The linearized incremental problem requires the evaluation of the tangent stiffness matrix of the structure. In general, this tangent stiffness

matrix can be computed from the material tangent moduli (operators) at the material (or integration point) level. In rate-independent plasticity, the material constitutive behavior is described by rate constitutive equations as presented in Chapter 2 and implemented in Chapter 3. According to the incremental-iterative process discussed in the previous section, these rate constitutive equations are numerically integrated over a sequence of discrete time or load steps.

The hysteretic nonlinear rate equations defined in relations (6.3) and (6.5) can be written in the following generic form, for brevity:

$$\{\dot{Q}\} = [G]\{\dot{q}\} \tag{6.34}$$

where $\{Q\}$ is a generalized action measure and $\{q\}$ is a generalized deformation measure. In relation (6.34) $[G]$ is the smooth constitutive matrix of the material under consideration directly defined from the ratio of the rates of the generalized measures. The global stiffness matrix that is derived from $[G]$ is called the continuum tangent moduli of the structure. Nevertheless, Nagtegaal and de Jong, 1981where amongst the first to notice that when using an iterative procedure like the Newton-Raphson algorithm, the use of the continuum stiffness matrix leads to problems as it is not consistent to the incremental strains being evaluated at each step. Additionally, the use of this stiffness matrix would not guaranty the quadratic convergence rate of the algorithm unless it is evaluated with respect to the incremental deformation component Δq.

Thus, referring to equation (3.49) the incremental stress-strain relation at the i_{th} iteration is evaluated as:

$$\Delta\left\{\sigma^{(i)}\right\} = \left[D\right]\left(\Delta\left\{\varepsilon^{(i)}\right\} - \Delta\lambda^{(i)}\frac{\partial\Phi\left(\left\{\sigma^{(i)}\right\}\right)}{\partial\left\{\sigma^{(i)}\right\}}\right) \tag{6.35}$$

where the increment of the hysteretic plastic multiplier is

$$\Delta\lambda = H_1 H_2\left(-\left[A_p\right]^T G\left(\left\{\eta^{(i)}\right\},\Phi\right) + \left[B_p\right]^T\left[D\right]\left[B_p\right]\right)^{-1}\left[B_p\right]^T\left[D\right]\Delta\left\{\varepsilon^{(i)}\right\} \tag{6.36}$$

where $\left[A_p\right] = \partial\Phi\big/\partial\left\{\eta^{(i)}\right\}$ and $\left[B_p\right] = \partial\Phi\big/\partial\left\{\sigma^{(i)}\right\}$ The differential of the stress increment is defined as:

$$d\Delta\left\{\sigma^{(i)}\right\} = \left[D\right]\left(d\Delta\left\{\varepsilon^{(i)}\right\} - \Delta\lambda^{(i)}\frac{\partial\left(\left[B_p\right]\right)^2}{\partial\Delta\left\{\sigma^{(i)}\right\}}d\Delta\left\{\sigma^{(i)}\right\} - d\Delta\lambda^{(i)}\left[B_p\right]\right) \tag{6.37}$$

and solving for $d\Delta\left\{\sigma^{(i)}\right\}$ the following incremental relation is derived:

$$d\Delta\left\{\sigma^{(i)}\right\} = \left[G^*\right]\left(d\Delta\left\{\varepsilon^{(i)}\right\} - d\Delta\lambda^{(i)}\left[B_p\right]\right) \tag{6.38}$$

from which it is concluded that the quantity relating the increment of stress to the increment of strain is:

$$\left[G^*\right] = \left(I + \Delta\lambda^{(i)}\left[D\right]\frac{\partial\left[B_p\right]}{\partial\Delta\left\{\sigma^{(i)}\right\}}\right)^{-1}\left[D\right] \tag{6.39}$$

Simo and Taylor, 1985 prove that this derivation ensures the quadratic convergence of the Newton scheme, since it accounts for the change on the gradient $\left[B_p\right]$ as the iterations evolve. Substituting equations (3.59) and (3.60) into (6.36) and finally into (6.38) and (6.39), the following expression for the hysteretic consistent constitutive matrix is derived:

$$\left[\hat{G}\right] = \left[G^*\right]\left(\left[I\right] - \left|\frac{\Phi}{\Phi_0}\right|^N\left(\beta + \gamma\,\mathrm{sgn}\left(\left\{\Delta\varepsilon^{(i)}\right\}^T\left\{\Delta\sigma^{(i)}\right\}\right)\right)\left[R^*\right]\right) \tag{6.40}$$

where the incremental interaction matrix is defined as:

$$\left[-\left(\frac{\partial \Phi}{\partial \left\{ \eta^{(i)} \right\}} \right)^{T} G\left(\left\{ \eta^{(i)} \right\}, \Phi \right) + \left(\frac{\partial \Phi}{\partial \left\{ \sigma^{(i)} \right\}} \right)^{T} [D] \frac{\partial \Phi\left(\left\{ \sigma^{(i)} \right\} \right)}{\partial \left\{ \sigma^{(i)} \right\}} \right]^{-1} \left(\frac{\partial \Phi}{\partial \left\{ \sigma^{(i)} \right\}} \right) \left(\frac{\partial \Phi}{\partial \left\{ \sigma^{(i)} \right\}} \right)^{T} [D] \tag{6.41}$$

The derivation of the consistent constitutive matrix is crucial for the implementation of the return-mapping algorithm scheme that is mainly used in plasticity (Simo and Hughes, 1998).

6.6 An equilibrium based approach of the first order representation method

In the general case of a structure consisting of both hysteretic finite elements and macro-elements, the nonlinear part of the stiffness matrix $[K]_S$ (equation (6.1), varies with respect to the vector of hysteretic stress components. Moreover, the hysteretic stress components are introduced as additional unknowns into the solution scheme, through the rate equations (6.3).

On the other hand, the structural hysteretic matrix $[K]_S$, comprising of the individual hysteretic components of the macro-elements, remains constant throughout the analysis procedure. The inelastic behavior at the ends of the macro-elements is controlled by the additional hysteretic degrees of freedom and the corresponding evolution equations.

In a time marching algorithm, such as the nonlinear dynamic analysis of structures, the evaluation, at each time step, of the structural stiffness matrix is a time and memory consuming process. In this Section, a method is examined that is based on the evaluation of constant system matrices for the hysteretic finite elements.

6.6.1 The Incidence Matrix of a Constant Stress / Strain finite element

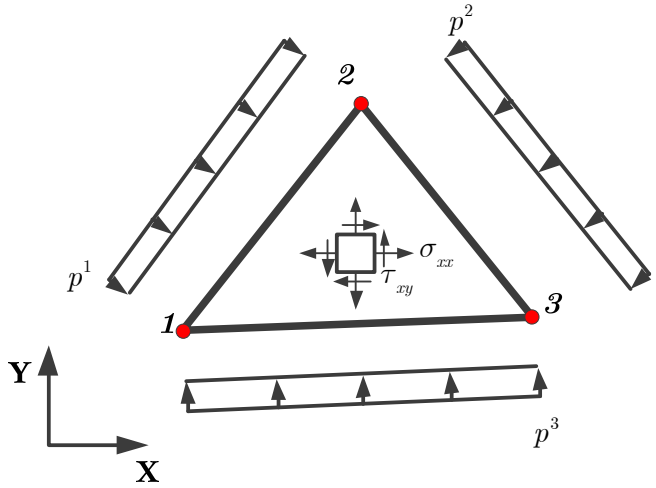

Fig. 6.1 Plane Stress Element and corresponding edge loads

Since the triangular element is a constant stress / constant strain element, equilibrium requirements are fulfilled within the element. Assuming that on each side $i, i = 1,2,3$ of the triangle a distributed load p^i is applied with components p_x^i, p_y^i that gives rise to the corresponding edge tractions, namely q_x^i and q_y^i, the equilibrium condition on the edge i is:

$$\begin{aligned} q_x^i &= \sigma_x n_x^i + \tau_{xy} n_y^i \\ q_y^i &= \tau_{xy} n_x^i + \sigma_y n_y^i \end{aligned} \tag{6.42}$$

where n_x^i, n_y^i are the direction cosines of the i^{th} boundary of the element while σ_x, σ_y, are the normal stresses and τ_{xy} is the shear stress of the element (Fig. 6.1). The direction cosines of the first side are defined as:

$$\begin{aligned} n_x^1 &= \frac{y_3 - y_2}{L_1} \\ n_y^1 &= -\frac{x_3 - x_2}{L_1} \end{aligned} \tag{6.43}$$

while the rest are derived by cyclic permutation of subscripts where $L_i, i = 1,2,3$ is the length of the i^{th} boundary of the element. Equation (6.42) is conveniently written in matrix form as:

$$\left\{\mathbf{q}^{\mathbf{i}}\right\} = \left[T^i\right]\left\{\sigma\right\} \tag{6.44}$$

where $\left\{\mathbf{q}^{\mathbf{i}}\right\} = \left\{q_x^i \quad q_y^i\right\}^T$, $\left\{\sigma\right\} = \left\{\sigma_x \quad \sigma_y \quad \tau_{xy}\right\}^T$ and $\left[T^i\right]$ is a transformation matrix defined as:

$$T^i = \begin{bmatrix} n_x^i & 0 & n_y^i \\ 0 & n_y^i & n_x^i \end{bmatrix} \tag{6.45}$$

Appending for the three sides of the elements, equation (6.44) is re-written as:

$$\underbrace{\begin{Bmatrix} q_1 \\ q_2 \\ q_3 \end{Bmatrix}}_{(6x1)} = \underbrace{\begin{bmatrix} T^1 \\ T^2 \\ T^3 \end{bmatrix}}_{(6x3)} \underbrace{\begin{Bmatrix} \sigma_x \\ \sigma_y \\ \tau_{xy} \end{Bmatrix}}_{(3x1)} \tag{6.46}$$

or in a more compact form:

$$\left\{Q\right\} = \left[J\right]\left\{\sigma\right\} \tag{6.47}$$

By means of the principle of complementary virtual work (Washizu, 1980) and using the shape functions of the plane stress element presented in equation (5.25), the equivalent nodal forces of the tractions can be computed and assigned on each node as:

$$\begin{Bmatrix} P_{x1}^{(j)} \\ P_{y1}^{(j)} \\ P_{x2}^{(j)} \\ P_{y2}^{(j)} \\ P_{x3}^{(j)} \\ P_{y3}^{(j)} \end{Bmatrix} = \frac{t}{2} \begin{bmatrix} 0 & 0 & L_2 & 0 & L_3 & 0 \\ 0 & 0 & 0 & L_2 & 0 & L_3 \\ L_1 & 0 & 0 & 0 & L_3 & 0 \\ 0 & L_1 & 0 & 0 & 0 & L_3 \\ L_1 & 0 & L_2 & 0 & 0 & 0 \\ 0 & L_1 & 0 & L_2 & 0 & 0 \end{bmatrix} \begin{Bmatrix} q_{x1} \\ q_{y1} \\ q_{x2} \\ q_{y2} \\ q_{x3} \\ q_{y3} \end{Bmatrix} \tag{6.48}$$

or:

$$\{P\} = [L]\{Q\} \tag{6.49}$$

where t is the thickness of the element and $L_i, i = 1,2,3$ is the length of the corresponding boundary while the superscript (j) denotes the index of the element. Combining equations (6.46) and (6.49), the equilibrium expression between the internal stress field of the element and the external applied nodal forces is obtained:

$$\{P\} = \frac{t}{2} \underbrace{[L]}_{(6x6)} \underbrace{[J]}_{(6x3)} \underbrace{\{\sigma\}}_{(3x1)} \tag{6.50}$$

After some matrix manipulation the following compact form of equation (6.50) is derived:

$$\{P\} = V \underbrace{[A]}_{(6x3)} \underbrace{\{\sigma\}}_{(3x1)} = [C^e]\{\sigma\} \tag{6.51}$$

where V is the elemental volume, and A is the equilibrium matrix of the triangular plane stress element defined as:

$$[A] = \begin{bmatrix} b_1 & 0 & c_1 \\ 0 & c_1 & b_1 \\ b_2 & 0 & c_2 \\ 0 & c_2 & b_2 \\ b_3 & 0 & c_3 \\ 0 & c_3 & b_3 \end{bmatrix} \tag{6.52}$$

and $b_1 = y_2 - y_3$, $c_1 = x_3 - x_2$, $b_2 = y_3 - y_1$, $c_1 = x_1 - x_3$, $b_2 = y_1 - y_2$ and $c_3 = x_2 - x_1$.

It can be easily noticed that the equilibrium matrix is the transpose of the strain matrix introduced in equation (5.33) multiplied by twice the area of the triangular element.

6.6.2 The node method for the case of plane problems

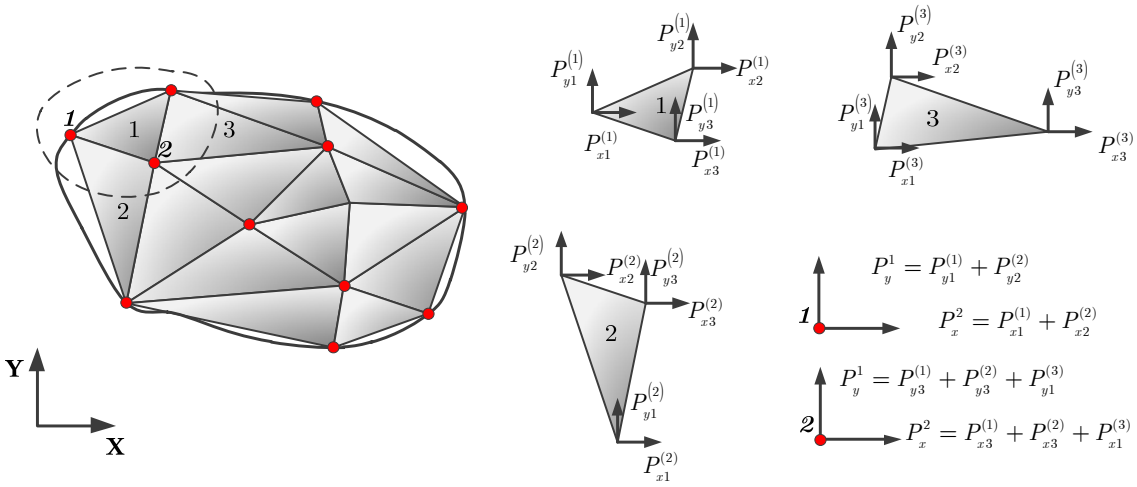

Fig. 6.2 Equilibrium matrix derivation of a plane mesh

In Fig. 6.2 an arbitrary mesh of constant stress triangular elements is presented that consists of a plane stress element mesh with n_{nod} nodes and n_{el} elements. The equilibrium conditions of the mesh are established by additively appending the elemental contributions on the nodal equilibrium through equations (6.51). Thus, global equation of equilibrium can be cast onto the following form:

$$\underbrace{\left[A^e\right]_S}_{\left(2n_{nod}\right)\left(3_{nel}\right)}\underbrace{\left\{\sigma\right\}_S}_{\left(3_{nel}\right)} = \underbrace{\left\{P\right\}}_{\left(2n_{nod}\right)} \tag{6.53}$$

where $\left[A^e\right]_S$ is defined as the equilibrium matrix of the structure, $\left\{\sigma\right\}_S$ is the stress vector of the whole structure and $\left\{P\right\}$ is the nodal force vector. Equation (6.53) is a static equilibrium equation which can be extended for the dynamic case by taking into account inertia forces. Thus, the dynamic equilibrium equations assume the following hybrid form:

$$\left[M\right]\left\{\ddot{U}\right\} + \left[A^e\right]_S\left\{\sigma\right\}_S = \left\{P\left(t\right)\right\} \tag{6.54}$$

Considering the principle of complementary virtual work, the following relation can be established in terms of compatibility:

$$\underbrace{\left[A\right]^{T}}_{(3n_{el})(2n_{nod})}\underbrace{\left\{d\right\}}_{(2n_{nod})}=\underbrace{\left\{\varepsilon\right\}}_{(3n_{el})} \tag{6.55}$$

The main advantage of the proposed method is that it separates the problem into two sets of equations. The first consists of the global linear equilibrium and compatibility equations, while the second one of local nonlinear constitutive equations, together with the hysteretic evolutionary equations.

In the general case where a structure consists of both plane stress elements and macro-elements, equation (6.54) can be cast in the following form:

$$\left[M\right]_S\left\{\ddot{U}\right\}+\left[C\right]_S\left\{\dot{U}\right\}+\left[A^e\right]_S^{Aug}\left\{\sigma\right\}+\left[K\right]_S^{Aug}\left\{U\right\}+\left[H\right]_S^{Aug}\left\{z\right\}=\left\{P(t)\right\} \tag{6.56}$$

where the equilibrium matrix $\left[A^e\right]_S^{Aug}$ and the stiffness and hysteretic matrices $\left[K\right]_S^{Aug}$ and $\left[H\right]_S^{Aug}$ are augmented for the whole structure. Equation (6.56) is linear with respect to the vector of stresses $\left\{\sigma\right\}$, the global displacement vector $\left\{U\right\}$ and the hysteretic deformation vector $\left\{z\right\}$. These set of equations is accompanied with a set of hysteretic equations for the stress field and the hysteretic deformation field, namely:

$$\left\{\dot{\sigma}\right\}_S=\left[D_H\right]_S\left[B\right]_S\left\{\dot{d}\right\} \tag{6.57}$$

and:

$$\left\{\dot{z}\right\}=f(\left\{\dot{U}\right\},\left\{z\right\}) \tag{6.58}$$

6.7 Conclusions

In this Chapter, the computational aspects of the proposed hysteretic finite elements and macro-elements are presented. The standard second order solution schemes, namely the central difference method and the Newmark method are modified, to account for the

additional equations introduced by the rate form of the hysteretic parameters. Moreover, the numerical aspect of stiffness is introduced and the family of linear multistep predictor-corrector methods is presented that successfully deals with stiff numerical problems.

Finally, a method is proposed for the dynamic nonlinear analysis of structures based on the node method (Spillers, 1962), initially developed for the case of skeletal structures. By considering the stress field of the hysteretic finite elements as additional unknown the nonlinear equations of motion are formulated in terms of the constant equilibrium matrix of the finite elements and the constant elastic stiffness and hysteretic matrices of the macro-elements. In this way, inelasticity is introduced only at the element level, through the evolution equations of the additional unknowns, namely the hysteretic stress field and the hysteretic deformation field. This method bares the advantage of not requiring the evaluation of global system matrices at each time step of a nonlinear marching process, at the cost of introducing additional unknowns. Yet, if properly programmed, the resulting problem of solving a linear system is more efficiently handled computationally than the iterative evaluation of stiffness components.

In the present thesis, the method is developed and presented only for the case of plane stress triangular elements. Further development is required to derive the necessary incidence matrices for other types of surface and three-dimensional elements.

Chapter 7

EXAMPLES

7.1 Introduction

In this chapter, examples are presented that demonstrate both the validity of the proposed formulation and its applicability on different types of structures. Validity is established through comparison with well documented computer codes such as Idarc (Valles et al., 1996) Abaqus (Abaqus, 2005) and OpenSees (McKenna et al., 2000).

In the first example, a shallow arch is subjected to a sinusoidal excitation and its response its examined considering material and geometric nonlinearities. In the second example, the response of a shear link is examined under cyclic loading. Shear links are frequently implemented as an effective mechanism of energy dissipation. Roeder and Popov (1978) conducted a series of experiments using shear links in eccentrically braced frames (EBFs). These and subsequent studies by Hjelmstad and Popov (1983), and Kasai and Popov (1986) proved that localized ductile yielding in shear, bares significant advantages over bending failure. Recently, EBFs bearing shear links have been proposed as rehabilitation mechanisms of reinforced concrete frames (Ghobarah and Elfath, 2001, Mazzolani, 2008).

Next, the proposed beam formulation is used to verify the dynamic response of a typical steel moment frame of a hospital building located at Woodland Hills, California. The solution is compared to results obtained from the Force analogy Method, described in Wong & Yang (1999), the Idarc computer code and OpenSees.

Finally, a three-dimensional steel building is examined, imposed to seismic excitation in two horizontal excitations. Two cases of lateral load resisting mechanics are used. In the first, typical (inverted V) concentric braced frames are implemented while in the second suspended zipper braced frame are implemented. The zipper braced frame configuration (Fig.7.1b) was first proposed by Khatib (Khatib et al.1988). The frame has geometry similar to that of the conventional inverted-V braced frame (Fig.7.1a), except that a vertical structural element, the

zipper column, is added at the beam mid-span points from the second to the top story of the frame.

The advantages of the zipper frame as an energy dissipation mechanism have been well documented in Khatib et al. (1988). The mechanism relies on the successive buckling of the compression braces, from the first story and moving upwards. Referring to the three story brace in Fig.7.1(b), after the brace of the first story buckles, the vertical force of the corresponding beam is transmitted to the second story through the zipper column. Further increased lateral deformations, will inevitably lead to a mechanism in which all compression braces have buckled and also beam plastic hinges have been activated. However, as this mechanism evolves, the structural stiffness is significantly reduced leading to a softening behavior that is difficult to assess, thus limiting the applicability of the zipper frame, especially in high rise buildings where lateral stability and second order effects are of the utmost importance.

Leon and Yang (2009) introduced the suspended zipper frame Fig.7.1c, by modifying the conventional zipper braced frame. In their proposal, overdesigned members are used as braces at selected stories along the frame height such that they remain elastic, thus preventing the formation of the complete zipper mechanism. The primary function of the zipper column is to transfer the unbalanced vertical force to the upper story braces and to support the beams at mid-span. Leon and Yang (2003) have shown that by providing the support at mid-span of the beams, a reduction of the beam sizes can be achieved, which may save material and makes the suspended zipper braced frame more economical. This configuration also provides a clear force path and makes the capacity design for the frame structural members relatively straightforward.

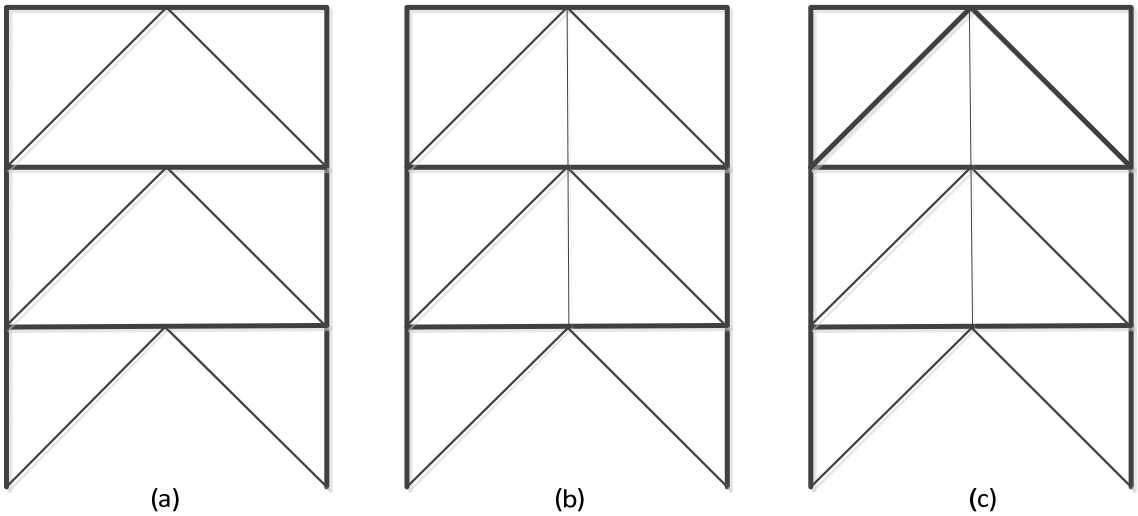

Fig.7.1Typical concentric braced frames (a) inverted V (b) zipper type (c) suspended zipper type

The building presented in this example is also examined by Yang et al. (2009) and conclusions have been drawn on the advantages of the second type of framing.

7.2 Shallow arch

A shallow arch is examined with a rise to span ratio of about 2%. The arch is considered restrained against out of plane motions while care has been taken to prevent member buckling. Pinned boundary conditions are imposed at both ends of the structure. Apart from self-weight, an additional mass of 3.5 KN is considered to be lumped at each node of the lower chord. The geometry of the arch is presented in Fig. 7.2 while the material and cross-sectional properties are presented in Table 7.1. A minor value of kinematic hardening is considered for the S235 steel. The rupture strain is considered at 6%.

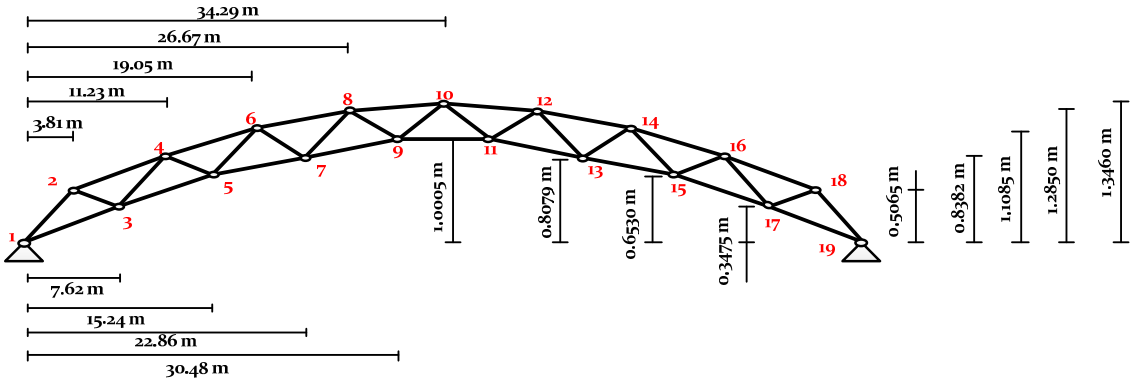

Fig. 7.2 Shallow Arch Geometry (shape out of scale)

Area	0.0006 m^2
E_{young}	210 GPa
α	0.00015
σ_y	235 MPa
n	25
β	0.5
γ	0.5

Table 7.1 Cross-Sectional and material properties

The truss structure is modeled using one truss element per member, implementing the hysteretic strain truss element formulation presented in Chapter 4. Two loading scenarios are considered in this example. In the first, the truss is imposed into monotonically increasing vertical loads until collapse. In the second scenario, a combined horizontal and vertical sinusoidal excitation is imposed, distributed at the upper chord of the truss.

7.2.1 Nonlinear static analysis

The proportional loading applied in the truss is presented in Fig. 7.3. The load is monotonically increased until collapse. In Fig. 7.4, the capacity curve of the truss is presented, in terms of applied load with respect to the vertical displacement at node #10.

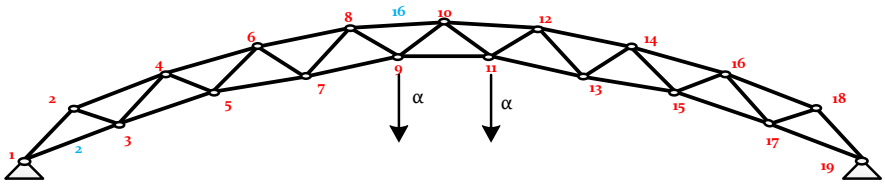

Fig. 7.3 Proportional static loading

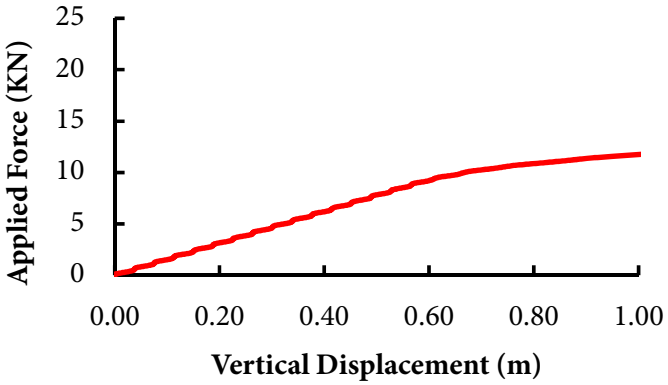

Fig. 7.4 Applied Force – Vertical Displacement Capacity Curve

The solution provided by the proposed formulation is compared to results obtained also from SAP2000 commercial code. The displacement based beam element is used in SAP2000, with moment releases at both ends, while plasticity is simulated through properly calibrated axial force-axial displacement springs at both ends of each element. Both the bending stiffness and shear area of the beam element in SAP2000 are reduced by a factor of 10^{-4} to fully avoid any bending deformations.

A force control pushover analysis is performed in SAP2000, using the modified Newton-Raphson solution procedure. The load is subdivided in 100 incremental steps. The results obtained are compared in Fig. 7.5 in terms of applied force with respect to the vertical displacement at node #10.

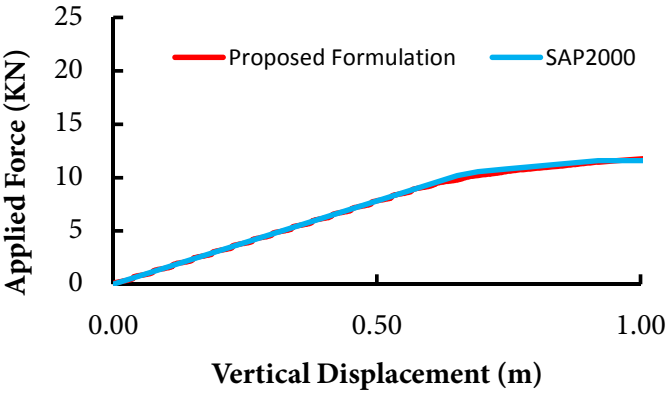

Fig. 7.5 Comparison of the proposed formulation to SAP2000

The solutions are practically the same both in the elastic and in the inelastic regime. In Fig. 7.6, axial force – axial deformation diagrams are presented for elements #2 at the lower chord and #16 at the upper chord of the truss (Fig. 7.3). The behavior of the truss elements is bilinear with a sharp transition from the elastic to the inelastic regime.

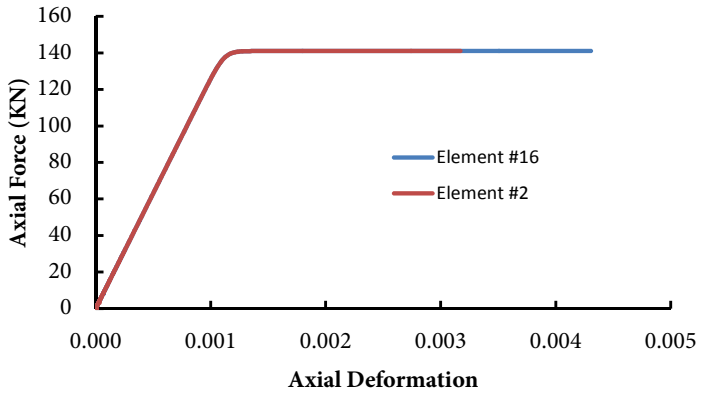

Fig. 7.6 Axial Force – Axial Deformation plots of elements #2 and #16

7.2.2 Nonlinear dynamic analysis

In this analysis scenario a time varying horizontal and vertical loading, distributed at the left side of the upper chord, is imposed. The distribution is presented in Fig. 7.7 while the amplitude of the loading varies according to the following sinusoidal relation:

$$\mathrm{P} = 2.5\sin\left(\pi t\right)$$

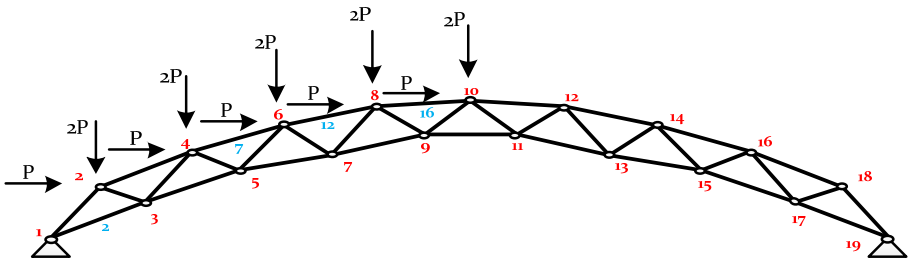

Fig. 7.7 Dynamic load distribution

Ten seconds of analysis are considered while the time integration step is $dt = 0.2$ sec. In Fig.7.8(a) time history of the horizontal displacement of node #6 is presented. The time history of the vertical displacement at mid-span is presented in Fig.7.8(b). The time-histories

presented demonstrate a time varying period of oscillation, thus, the truss undergoes inelastic deformation.

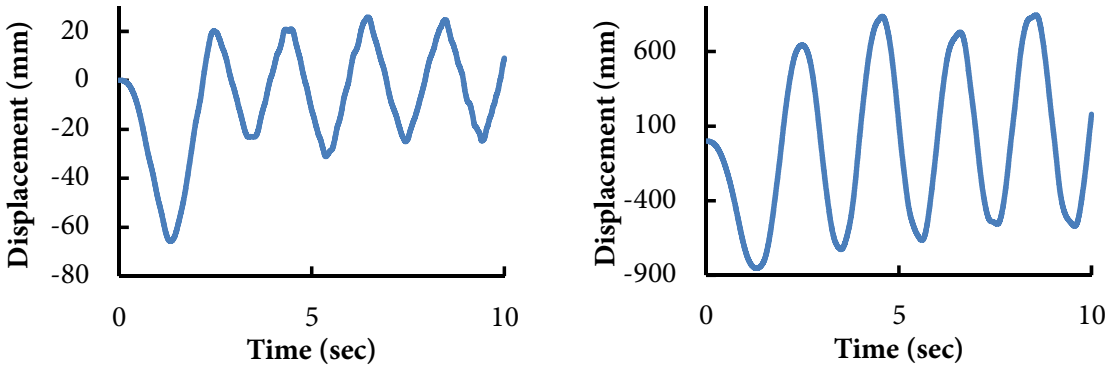

(a) (b)

Fig.7.8 (a) Horizontal Displacement at node #6 (b) Vertical Displacement at node #10

In Fig. 7.9(a) and (b), axial force – axial deformation hysteretic loops are presented for elements #7 and #12 respectively. Due to kinematic hardening, only two inelastic branches are observed, upon the first loading-unloading-reloading cycle of the structure. After that, the members respond elastically due to the linear increase in the back-stress.

In Fig. 7.10 the effect of the smoothness parameter n of the Bouc-Wen model is examined both on the global response of the structure and on an element basis. Two extreme values of parameter n are considered namely $n = 25$, that results in a sharp transition from the elastic to the inelastic regime and $n = 2$, that results on a smooth transition from the elastic to the inelastic regime. In Fig. 7.10(a), the time history of the vertical displacement at node #10 is presented for the two cases. Though the extreme values of the displacement are not affected, the overall behavior of the truss changes, since extreme values occur at the opposite direction of loading. This distinction is clearly depicted in Fig. 7.10(b), where the axial force - axial deformation hysteretic loop of element #7 is presented.

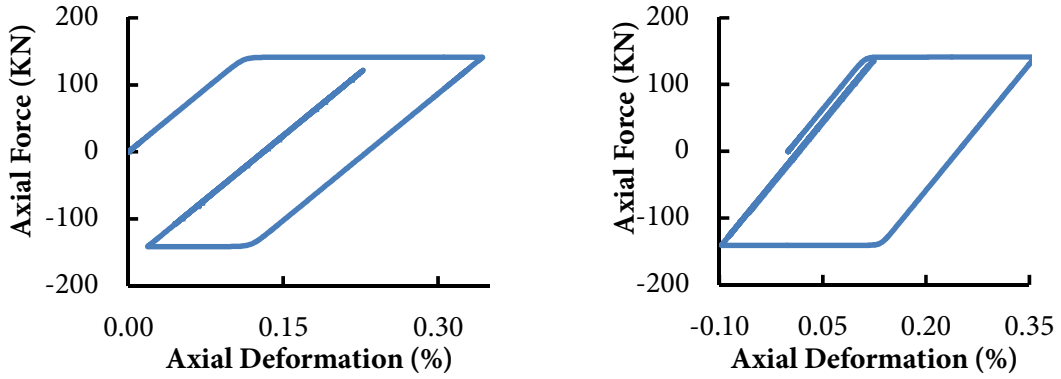

(a) (b)

Fig. 7.9 Axial force – axial deformation hysteretic loops (a) element #7 (b) element #12

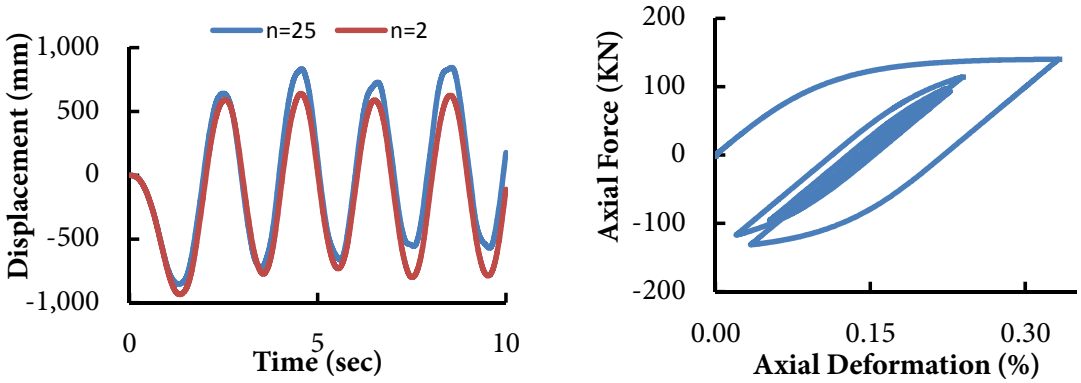

(a) (b)

Fig. 7.10 Response comparison for extreme smoothing parameters (a) Vertical Displacement at node #10 (b) Axial force – axial deformation hysteretic loop at element #7 for the case where (n =2)

7.2.3 Large displacement analysis

The shallow arch undergoes large displacements, as presented in the corresponding capacity curve (Fig. 7.4). Thus, a geometrically nonlinear analysis needs to be performed to accurately predict the actual response of the structure.

A dynamic analysis is performed, imposing the load distribution presented in Fig. 7.7 where $\mathrm{P} = 2.5\sin\left(\pi t\right)$. The following set of Bouc-Wen parameters is considered, namely $n = 2$, $\beta = 0.8$, $\gamma = 0.6$. The corresponding time-history of the vertical displacement at node #10 is presented in

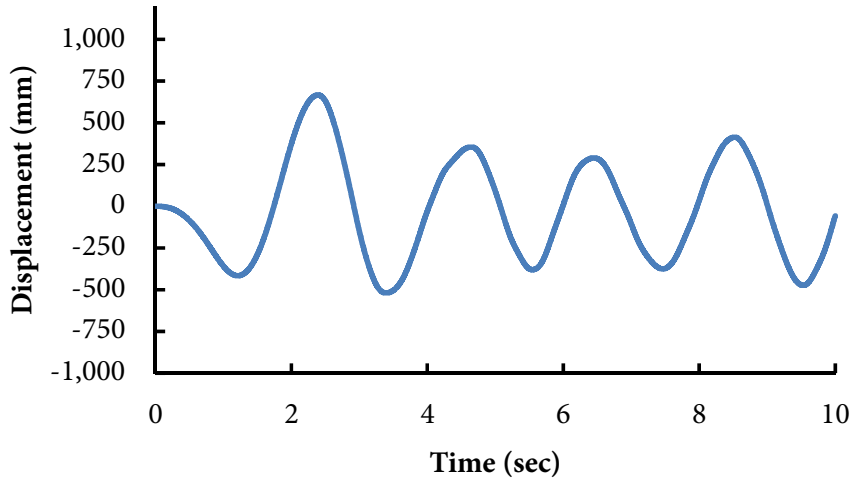

Fig. 7.11 Vertical Displacement at node #10 (Large Displacement Analysis)

7.3 Cyclically loaded shear beam

A 70 cm shear link of an IPE400 cross-section is examined in this paragraph. Material properties are S275 with an Elastic modulus of 210 GPa and a yield stress equal to 275 MPa. The solution obtained with the proposed formulation is compared against a solution obtained using Abaqus. The structural model implemented in Abaqus consists of 3712 quadrilateral shell elements and is presented in Fig.7.12(b). An elastic perfectly plastic material behaviour is considered in the Abaqus model. The computational model implemented in the proposed formulation is presented in Fig.7.12(c). The parameters chosen for the Bouc-Wen model are $n = 6,\ \beta = \gamma = 0.5,\ \alpha_i = 0.025$. The Orbison criterion is considered (Orbison et al., 1982), defined by the following relation:

$$\Phi = 1.15n^2 + m_y^2 + m_z^4 + 3.67n^2m_y^2 + 3.0n^6m_z^2 + 4.65m_y^4m_z^2$$

where $n = P/P_u$, $m_y = M_y/M_{yu}$, $m_z = M_z/M_{zu}$ while y refers to the strong axis and z refers to the weak axis of the cross-section. Yielding in shear is defined by the following relation:

$$Q_y = \frac{A_s \sigma_y}{\sqrt{3}} \tag{7.1}$$

where A_s is the shear area of the cross-section and σ_y is the yield stress of the material under uniaxial tension. The plastic moment implemented into the Orbison criterion is considered a function of the shear force as defined by the following relation (Heyman and Dutton, 1954):

$$M_{pq} = M_p \left[1 - \frac{M_w}{M_p} \left(1 - \sqrt{1 - \left(\frac{Q}{Q_p} \right)^2} \right) \right]$$

where M_w is the portion of bending retrieved from the web. A quasi-static analysis is performed under a periodic excitation, presented in Fig.7.12(a).

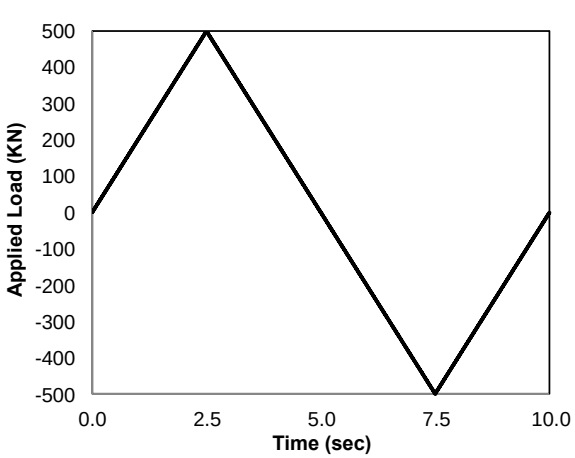

(a)

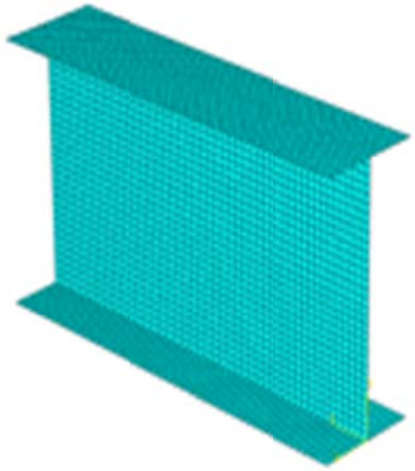

(b)

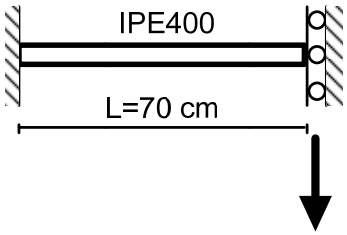

(c)

Fig.7.12 (a) Applied Load, (b) Abaqus FEM mesh, (c) Idealised beam model

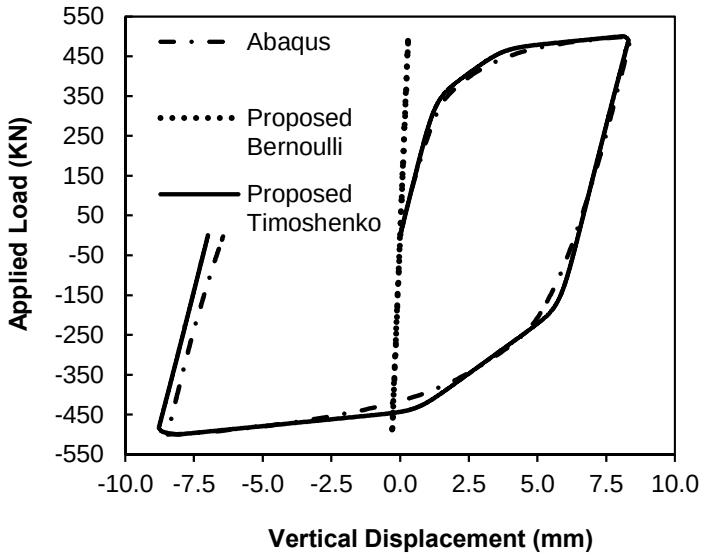

Fig.7.13 Force Displacement curve - IPE 400 shear link

The force-displacement plot is presented in Fig.7.13. Since the link yields in shear, the Bernoulli formulation fails to predict the nonlinear behaviour of the specimen. On the opposite, the Timoshenko formulation agrees well with the Abaqus results. The minor deviation both in the reloading phase and in the residual displacements is due to the inability of the proposed formulation to accurately predict the exact distribution of residual stresses on the cross-section that would give rise to a smoother transition from the elastic to the inelastic regime. However, allowing for a different set of parameters in the Bouc-Wen model, namely $n = 3,\ \beta = \gamma = 0.5,\ \alpha_i = 0.025$, the following plot of Fig.7.14 is produced.

The versatility of the implemented Bouc-Wen hysteretic rule on macro-modelling overcomes the inherent inability of the concentrated plasticity formulation to predict the smooth transition from the elastic to the inelastic regime due to the gradual yielding of the web.

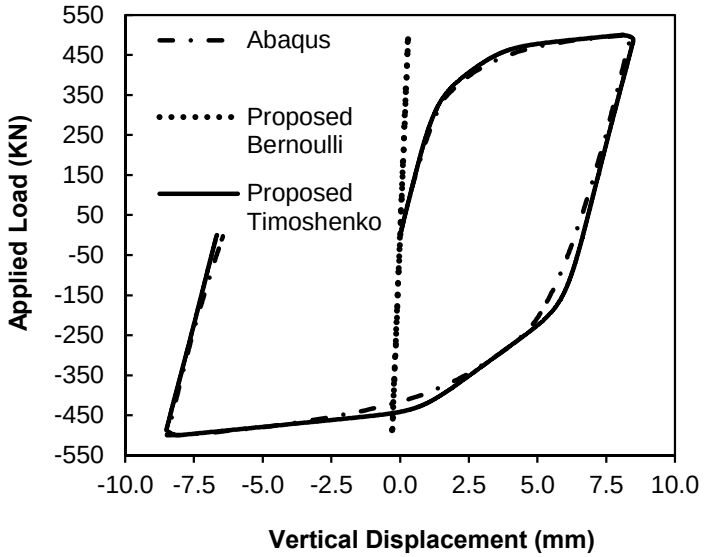

Fig.7.14 Force Displacement curve – n=3

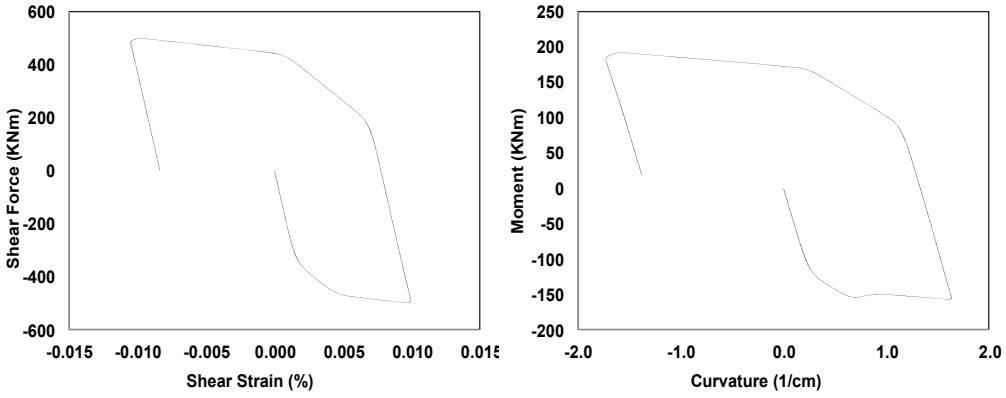

(a) (b)

Fig.7.15(a) Shear force – Shear strain diagram (b) Moment-Curvature diagram

In Fig.7.15(a) and (b) the shear force – shear strain and moment – curvature hysteresis loops are presented respectively. This verifies the result from the comparison of the Bernoulli and Timoshenko solutions that the shear link yields in shear since the ultimate moment developed in the element is less than the plastic moment of the IPE400 section (359 KNm).

7.4 Woodland Hills Hospital– moment frame

In this example a typical 6 story frame of a hospital building located at Woodland Hills, California is subjected to the El Centro accelerogram, scaled up with a factor of 1.8. The

geometry of the frame is presented inFig.7.16. The mechanical properties of the members are also presented in Fig.7.16, while the scaled accelerogram is presented in Fig.7.17. The yield curvature, the yield axial strain and the yield shear strain are computed based on the cross sectional data. Two subcases are considered.

In the first one, the Euler Bernoulli theory of bending is considered (setting $\lambda = 0$) and the obtained solution is compared to results obtained from the Force analogy Method, described in Wong & Yang (1999). For the purpose of this analysis no interaction between axial, shear and bending moment is considered. An analysis is also performed considering interaction between axial and bending through the Orbison criterion and the validity of the proposed scheme is proved through comparison to the OpenSees code (McKenna et al., 2000).

In the second subcase, the Timoshenko formulation is used where yielding in shear is again defined by relation (7.1)

The force-based element is implemented in OpenSees while plasticity is introduced into the element through a fibre approach, at integration points defined along the element's length. In this way, the interaction between axial and bending plastic deformations is accurately attributed, while plasticity in shear is considered uncoupled. The modified Newton scheme is utilized with an average acceleration Newmark integrator. A uniaxial elastic-plastic material model with kinematic hardening is used in the OpenSees code with the hardening constant being equal to $H\_kin = 45\ \mathrm{GPa}$. This corresponds to a post-elastic to elastic stiffness ratio $a = 0.0015$.Viscous damping is not considered in both cases. The value of the shear correction factor is equal to 0.255 for all sections.

The parameters of the Bouc-Wen model and the floor masses are presented in Fig.7.16. The derived moment – curvature diagrams are bilinear with a sharp transition from the elastic to the inelastic regime. The mass of the structure is considered lumped at the floor levels. The

dynamic analysis is carried out for a time period of 20 seconds with a time integration step of 0.02 sec.

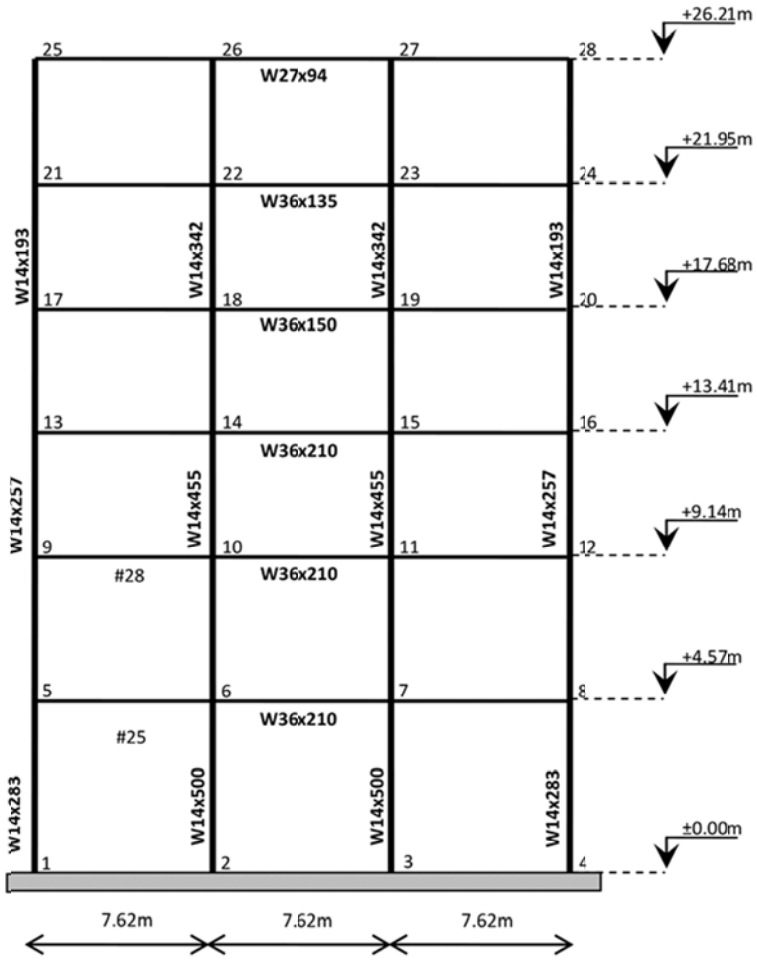

Parameter	Value
n	25
αcol	1
αbeam	0.0015
β	0.5
γ	0.5
σ_y (KPa)	248200

Material Parameters

Cross Section	z_h^y	z_u^y
	Beams	
W36x210	0.00388	0.00118
W36x150	0.00293	0.00118
W36x135	0.00290	0.00118
W27x94	0.00284	0.00118
	Columns	
W14x283	0.00578	0.00118
W14x257	0.00594	0.00118
W14x193	0.00530	0.00118
W14x500	0.00673	0.00118
W14x455	0.00636	0.00118
W14x342	0.00623	0.00118

Section Yield Parameters

Floor	Mass (tn)
1	402.8
2	231.2
3	180.4
4	180.4
5	180.4
6	182.1

Floor Masses

Fig.7.16Typical Frame of Woodland Hills Hospital, California

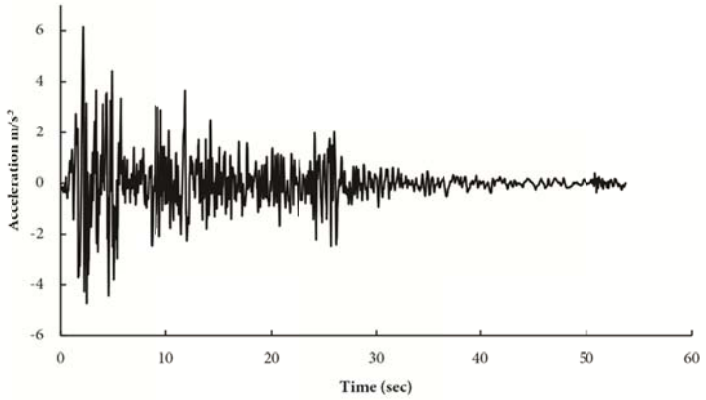

Fig.7.17. Scaled accelerogram of El Centro Earthquake

7.4.1 Comparison to the Force Analogy method

In this example, the proposed element formulation and solution procedure is tested against the Force analogy Method Wong & Yang (1999). As in the reference solution of Wong & Yang (1999), columns are modeled by elastic members and only beams are allowed to undergo inelastic deformations. The columns are kept elastic throughout the analysis by letting the post elastic to elastic bending stiffness ratio α_b equal to unity. The yield curvature and the axial strain at yield are computed based on the cross sectional data. Since, no axial plastic deformation is accounted for in the Force Analogy approach, axial deformations are also kept elastic by letting a_u equal to unity in this analysis.

The time history of the tip displacement is plotted in Fig.7.18(a) and compared to the plot presented in Wong & Yang (1999) for the case of strain hardening. There is a good agreement between the results taken from the two methods especially in the first 10 seconds of the excitation where inelastic deformation occurs. The different analysis schemes show the same maximum displacement. Differences are observed towards the end of the response where Force Analogy results appear more damped. These differences can also be attributed to the different inelastic models utilized, and thus, to the different amount of hysteretic energy dissipated during the inelastic response.

The same model is solved with the IDARC code, Valles et al. (1996), utilizing a Bouc-Wen hysteretic model, with the same parameter set used in this analysis. The corresponding plots are compared in Fig.7.18(b).

The results obtained using the Idarc code are in even better agreement to the results obtained from the proposed formulation. Differences are still observed during the last response cycles. These differences can be attributed to different truncation errors introduced by the different solution schemes. Idarc code utilizes a Newton scheme with an average

acceleration Newmark integrator. Such an approach, though unconditionally stable, yields integration errors not introduced in the proposed analysis procedure, Bonnet et al. 2008. In Fig.7.19(a) and (b) moment-curvature hysteresis loops are presented for the left node of beams 25 and 28 respectively. It is evident that the selected set of parameters gives rise to bilinear hysteretic loops with kinematic hardening.

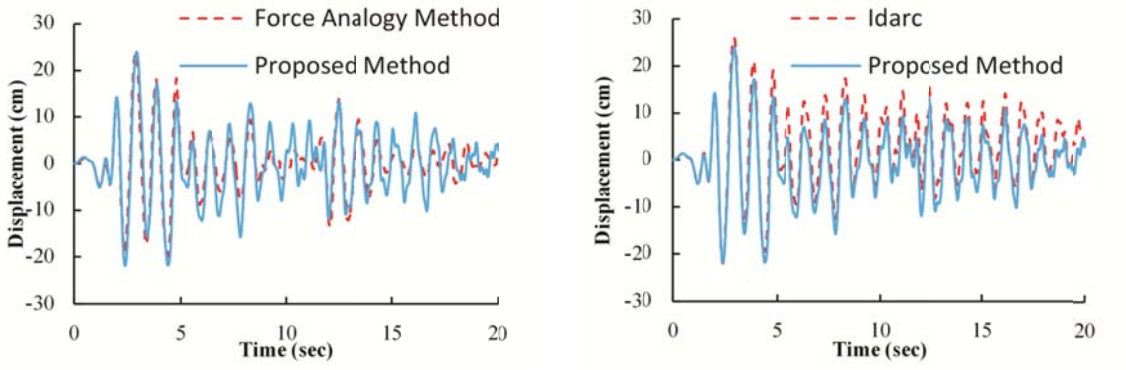

(a) (b)

Fig.7.18. Top story horizontal displacement time history (a) Force Analogy Method vs. Proposed Formulation (b) Idarc vs. Proposed Formulation

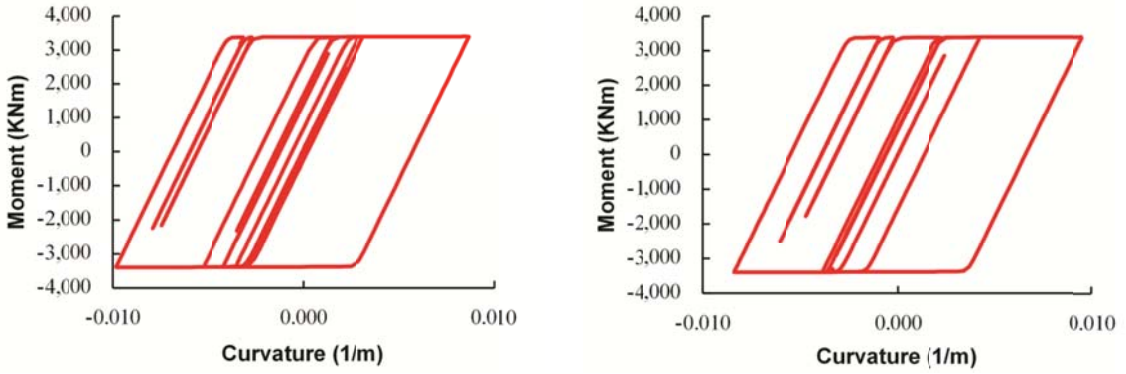

(a) (b)

Fig.7.19. Moment-Curvature plots at (a) the left node of beam 25 (b) at the left node of beam 28

In Fig.7.20, the results obtained from the proposed formulation are compared to the results obtained using OpenSees. A fiber force based element is utilized in OpenSees with 4 integration points along each element's length and considering 18 fibers along the section's

height; 2 for the flanges and 16 for the web. Only bending inelastic deformations are considered, while both columns and beams are allowed to undergo plastic deformation.

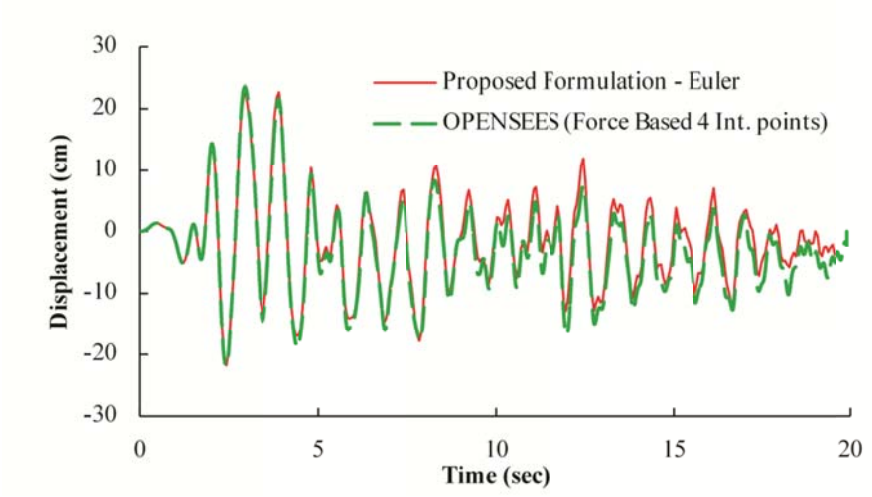

Fig.7.20. Top floor lateral displacement- Comparison of proposed formulation with respect to OpenSees

The results obtained by the two analysis procedures are in very good agreement. The computational time was 67 sec for the proposed formulation as opposed to 118 sec for the OpenSees.

In Fig.7.21(a), the results obtained with the large displacement approach are compared to those of the small displacement approach. As expected, the lateral displacements of the structure are increased, mainly due to P-D effects at the vertical elements.

Finally, an analysis is performed by modeling the nonlinear behavior of columns and beams following the proposed formulation, allowing for both flexural and axial deformations. The time history of the top story lateral displacement is presented in Fig.7.21(b). The actual response of the moment frame is slightly different than the one considering plastic deformations in beams only. Comparing Fig.7.21(a) and Fig.7.21(b), it is evident that the behavior of the frame in terms of maximum displacements and residual deformations is similar. This is attributed to the high strength columns implemented in the design. It is

important to mention though, that the same amount of computational time is needed to perform the two analyses cases, since the method proposed herein handles hysteresis in a unified way both in the elastic and in the inelastic regime. The time needed for the large displacement analysis to conclude was two minutes in a personal computer equipped with a Core Duo processor and 4 GB of RAM.

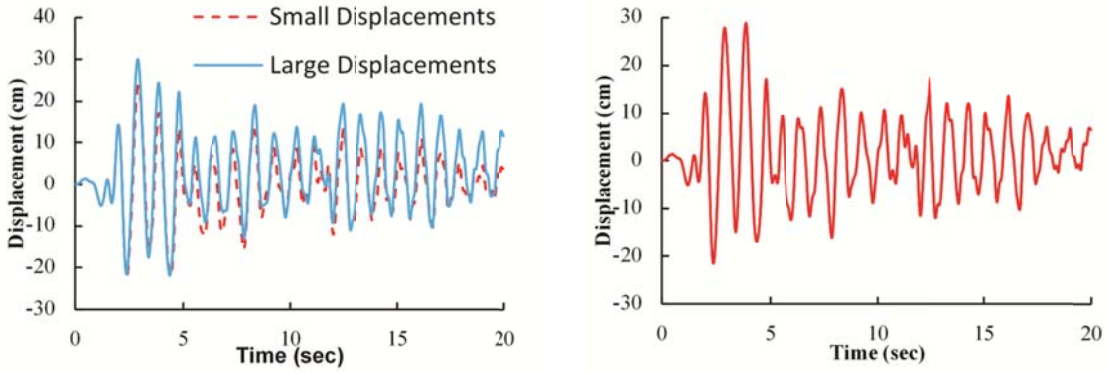

(a) (b)

Fig.7.21. Top floor lateral displacement: (a) small-large displacements, (b) large displacements allowing for plastic deformations at beams and columns

7.4.2 Timoshenko beam modeling

For the first analysis case, the time history of the top story horizontal displacement (node 28) is plotted in Fig.7.22. The results obtained from the the proposed method and OpenSees are in perfect agreement. Differences are observed towards the end of the response, due to the different solution procedures implemented.

In the second analysis case, where the Timoshenko beam theory is considered, the dynamic response of the structure is considerably different. In Fig.7.23, the time-history of the top-story horizontal displacement is again compared to the results obtained from OpenSees. The Timoshenko formulation yields a more flexible structure than the Euler one. The flexibility of the structure is further increased due to shear apart from bending plastic deformations. Thus, larger displacements are observed, especially towards the last 10 seconds of the response

when plastic deformations accumulate, while the max and min response differ by 20% to 25%.

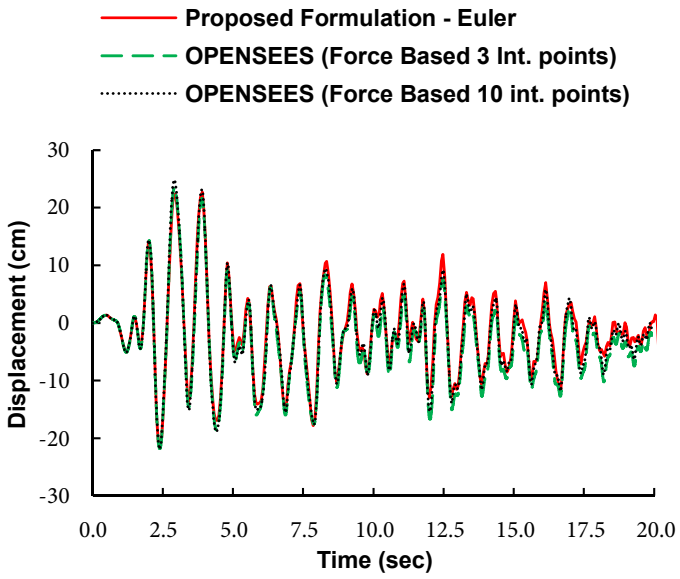

Fig.7.22Top story horizontal displacement time history (Euler Theory)

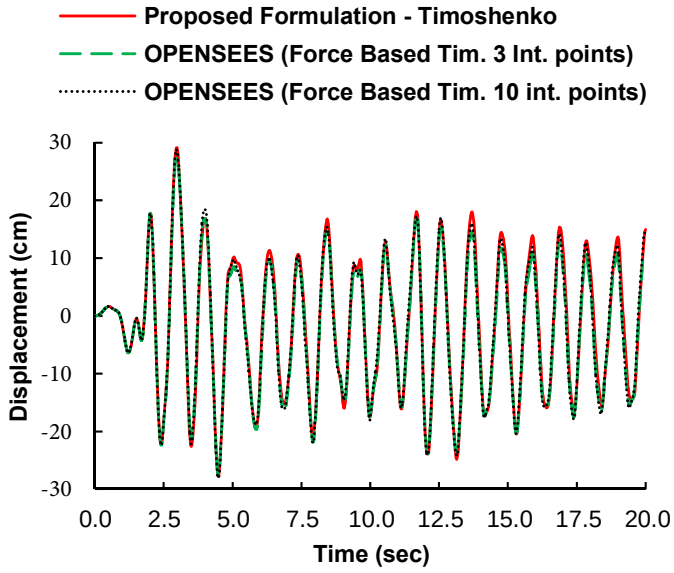

Fig.7.23Top story horizontal displacement time history (Timoshenko Theory)

In 7.24 the maximum interstorey drift ratios are presented for the two analysis cases. It is concluded that the dynamics of the structure are not significantly altered considering either the Euler or Timoshenko formulation, since the distribution of the maximum shear drifts

remains the same. Plastic deformations in both cases are concentrated in the first storey columns. Thus, the differences observed between Fig.7.22 and Fig.7.23 are due to the shear plastic deformations being developed in the first storey columns leading to a more flexible structure in the Timoshenko formulation.

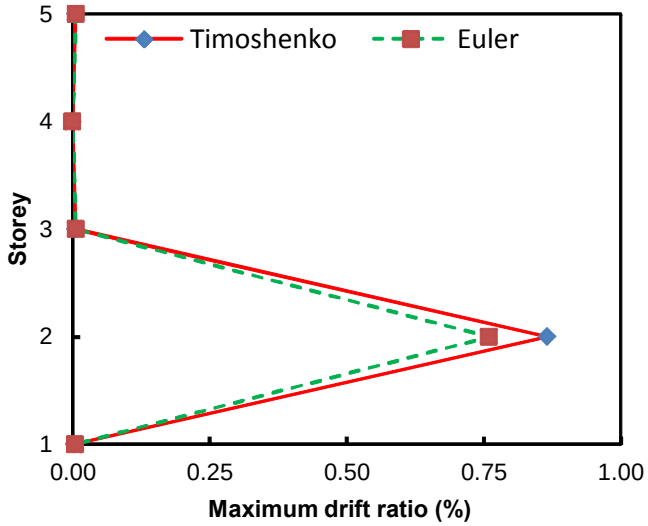

7.24 Maximum interstorey drift ratio

In Fig. 7.25 the time history of the upper storey horizontal displacement is presented as evaluated from the Timoshenko and Euler formulation. The Timoshenko formulation yields larger displacements, especially in the last 10 seconds of the excitation where the differences are larger than 50%.

This is attributed to the accumulations of plastic shear deformations that are not accounted for in the Euler formulation. Increasing shear deformations in the columns lead to increasing lateral displacements.

In the next figures, the efficiency of the proposed hysteretic interaction scheme is presented. The axial force – axial deformation and moment - curvature diagrams of element #1 (Fig.7.16) are presented in Fig.7.26(a) and (c) respectively. In Fig.7.26(b), the normalized axial force and the normalized bending moment are plotted when yielding has occurred. These points foliate the corresponding space and do not lay on a single curve due to kinematic

hardening. For the same reason normalized values exceed unity in the figure. As expected, yielding in bending is predominant in the nonlinear behaviour of the frame member. However, the interaction scheme significantly alters its plastic deformation potential.

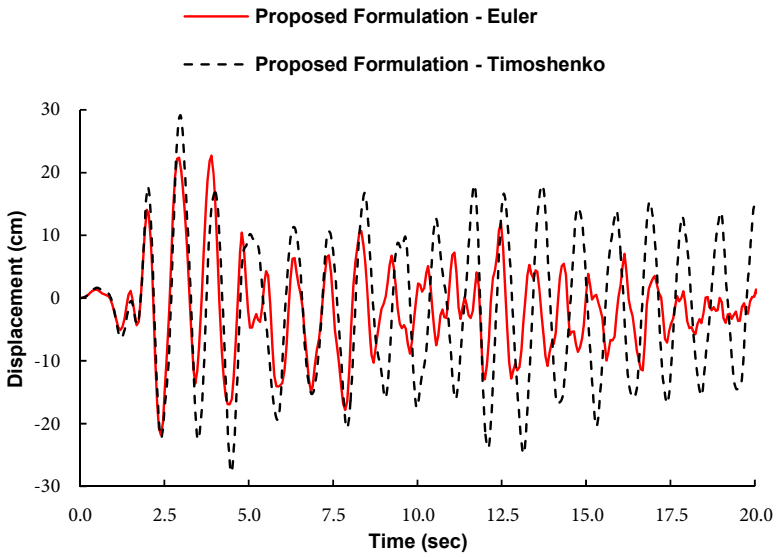

Fig. 7.25 Comparison of Euler and Timoshenko formulations - Top story horizontal displacement time history

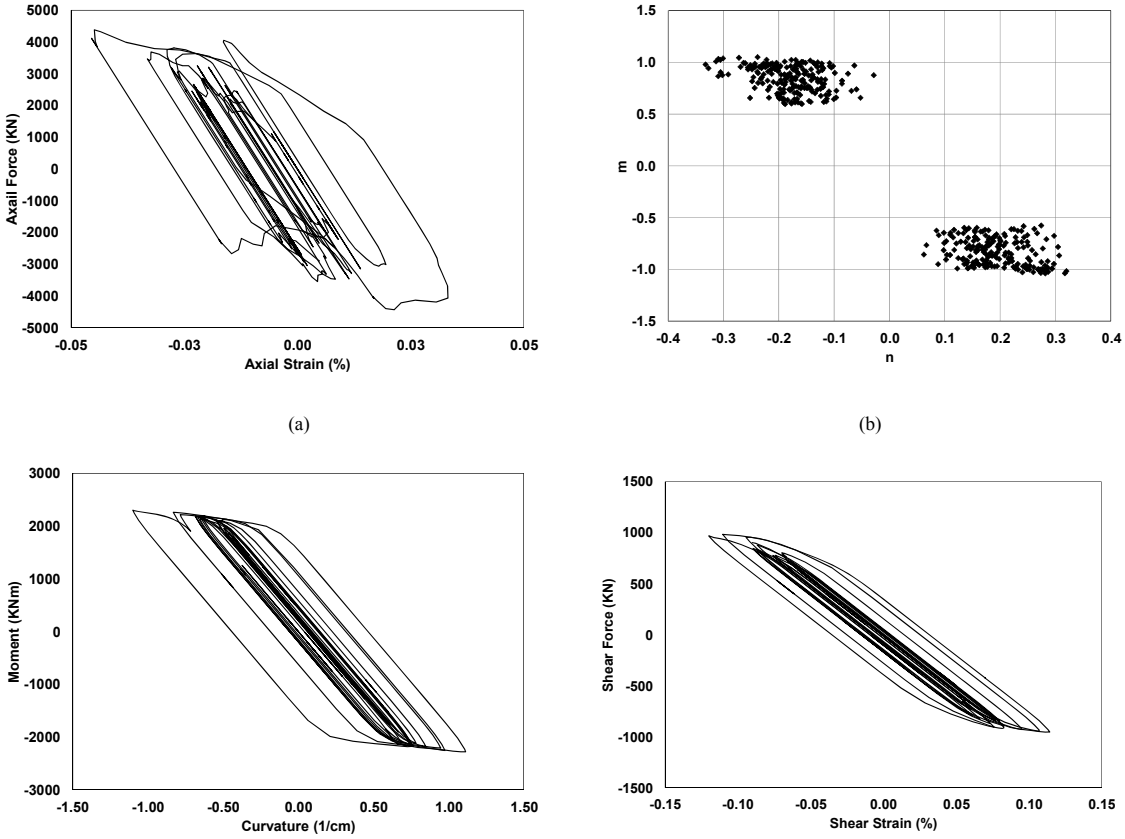

(a) (b)

(c) (d)

Fig.7.26 (a) Axial force – axial deformation (b) Axial – Moment Dynamic Interaction (c) Moment – Curvature (d) Shear force – shear deformation

In Fig.7.26(d) the shear force-shear deformation hysteretic loop is plotted. Contrary to the Euler-Bernoulli case where energy is dissipated only through the hysteretic moment-curvature mechanism, in this case the shear hysteretic energy is also considered.

A Fortran code has been developed for the analysis of skeletal structures with the proposed formulation. All the analyses were performed in a PC fitted with a Core Duo Quad CPU and 4 GBs of RAM. The analysis time with the proposed formulation was 67 sec. The analysis time of OpenSees was 118 sec for three integration points.

7.5 Steel building with concentric braced frames

7.5.1 Structure geometry

In this example, the dynamic response of an idealized steel structure is examined. The lateral load resisting mechanism of the building consists of concentric braced frames. Two cases are considered. In the first, the braced frames are of the inverted V type, while in the second zipper suspended frames are implemented. In Fig.7.27, a general view of the steel structure is presented. The building is doubly symmetrical, while braces exist in both its transversal and longitudinal direction.

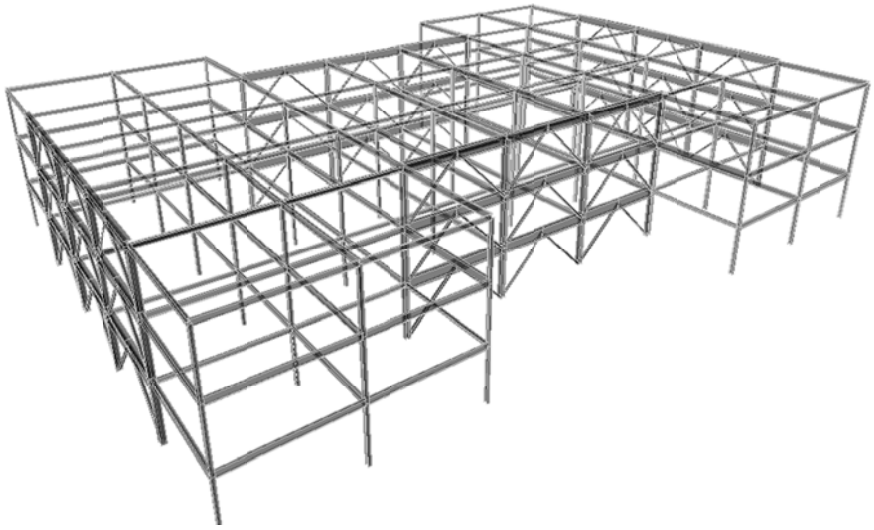

Fig.7.27 Three-dimensional model with inverted V braced frames

The beam member sizes are presented in Fig.7.28 to Fig. 7.30. Column sections are W10x49 for all members, except from the corner columns which are W10x39. The sizing of the bracing systems is presented in Section 7.5.2. The structural design of the building has been conducted following the IBC 2000 standard. A detailed analysis of the sizing is conducted in Leon and Yang (2009).

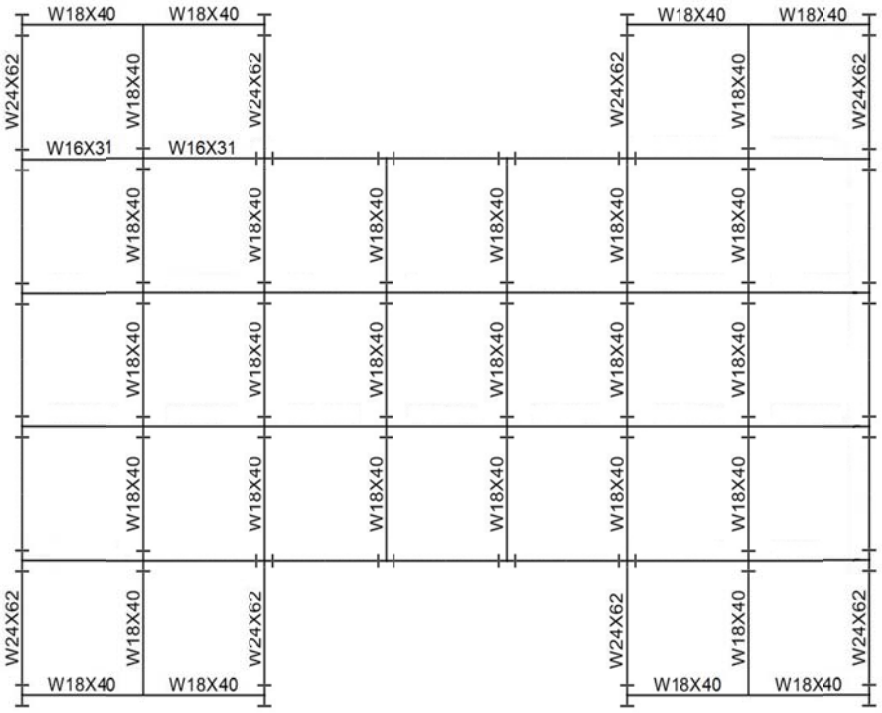

Fig.7.28 Plan View – 1st floor

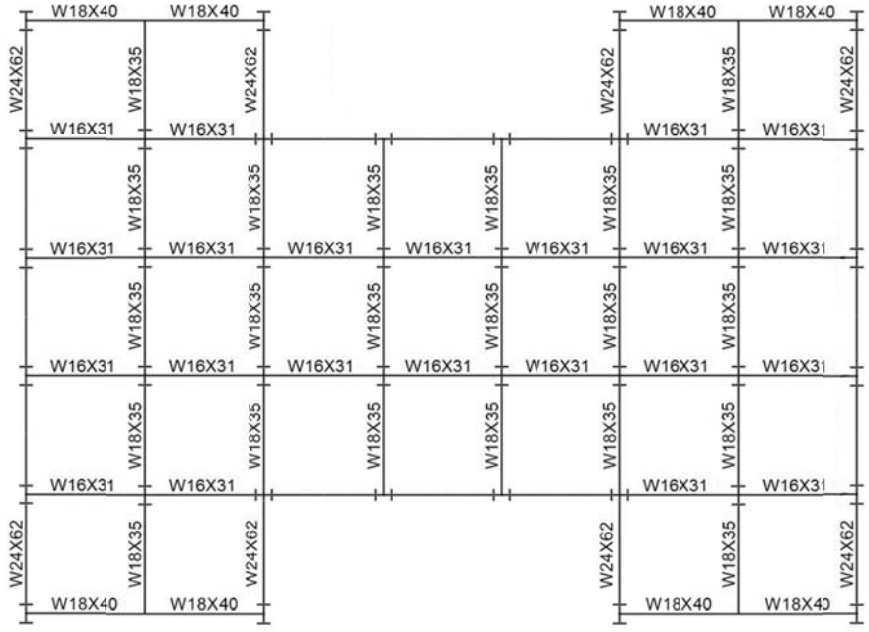

Fig.7.29 Plan View – 2nd floor

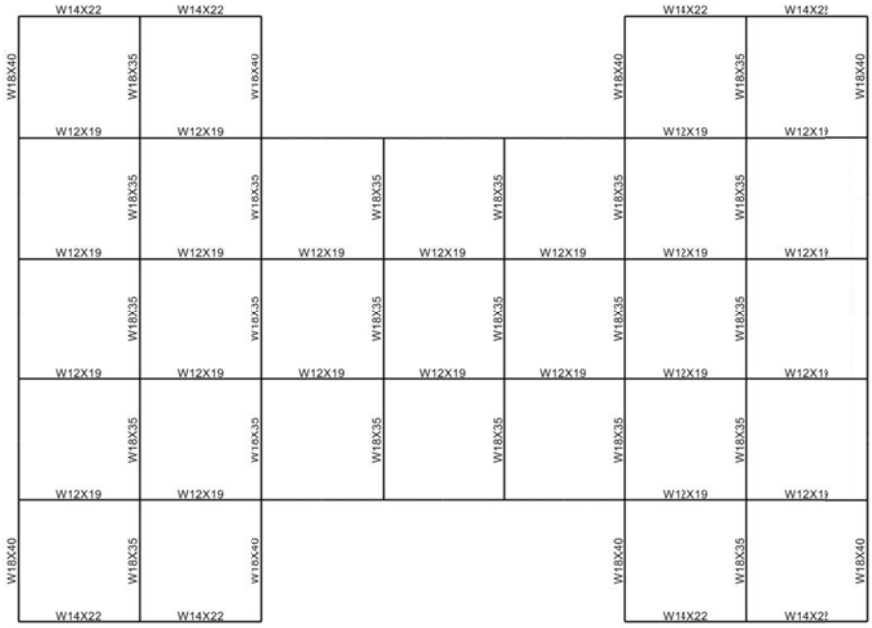

Fig. 7.30 Plan View – 3rd floor

7.5.2 Bracing geometry

Two types of bracing mechanisms are considered and the corresponding structural responses are compared. The member sizes of the bracing systems are presented in Fig. 7.31(a) and (b) for the inverted V brace and the suspended zipper brace respectively.

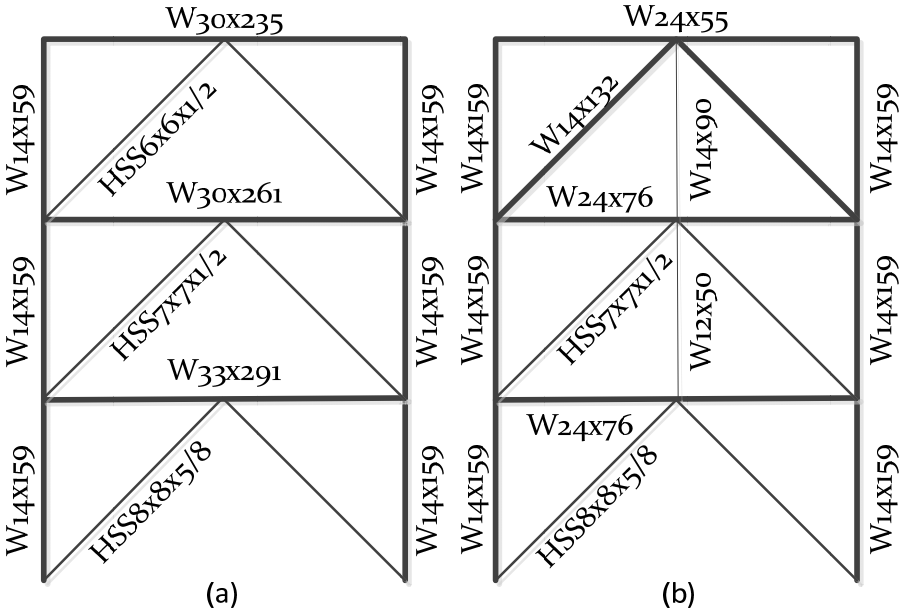

Fig. 7.31 Sizing of bracing systems (a) Inverted V (b) Suspended zipper brace

Apart from the suspension column the suspended zipper brace has stronger brace members on the upper floor. However, weaker girders are used that yield a lighter design than that of the inverted brace.

7.5.3 Analysis procedure and modeling

The analysis procedure consists of the following steps. A series of unidirectional nonlinear dynamic analyses is performed, and the results obtained from Leon and Yang (2009) are qualitatively verified. Masses are considered lumped at structural nodes. The total floor masses considered for the nonlinear dynamic analyses conducted are presented in Table 7.2.

Floor	Total Mass (tn)
1	1140.9
2	1388.7
3	1289.5

Table 7.2 Floor Masses

The beams and columns of the structure are modeled using the three-dimensional hysteretic beam element presented in Chapter 4. The beams are considered rigid with respect to in-plane bending. Pinned support conditions are considered for the base nodes of the columns. A smooth elastic plastic relation with kinematic hardening is considered in the axial, shear, bending and torsional degrees of freedom, setting $n = 8$ and $\alpha_u = \alpha_s = \alpha_b = \alpha_T = \alpha_W = 0.001$.

The diagonal members of the braced frames are modeled using the hysteretic truss element presented in Chapter 4. Since the compressive strength of the struts is limited by buckling, the modified Baber-Noori Bouc-Wen model presented in Section 2.5.3 is implemented that simulates asymmetric hysteretic loops. The elements are allowed to undergo inelastic deformations only in tension while in compression the member fails when the buckling strength is reached.

7.5.4 Ground motion records

A set of 7 ground acceleration records is used. The records are scaled to match the ASCE-05 response spectrum according to the building's design requirements (Leon and Yang, 2009). The records are presented in Fig. 7.32 while the corresponding seismological data is summarized in Table 7.3.

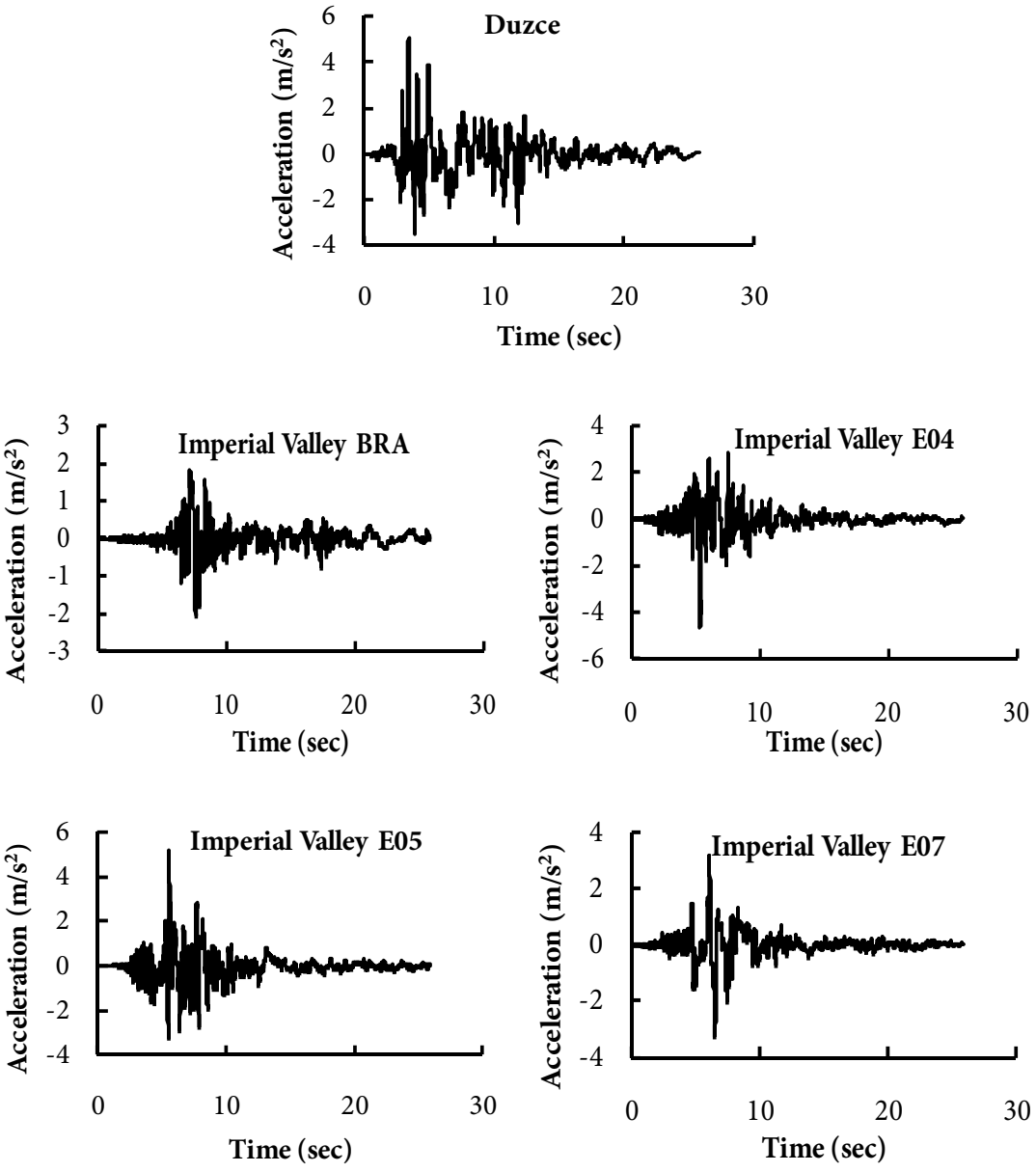

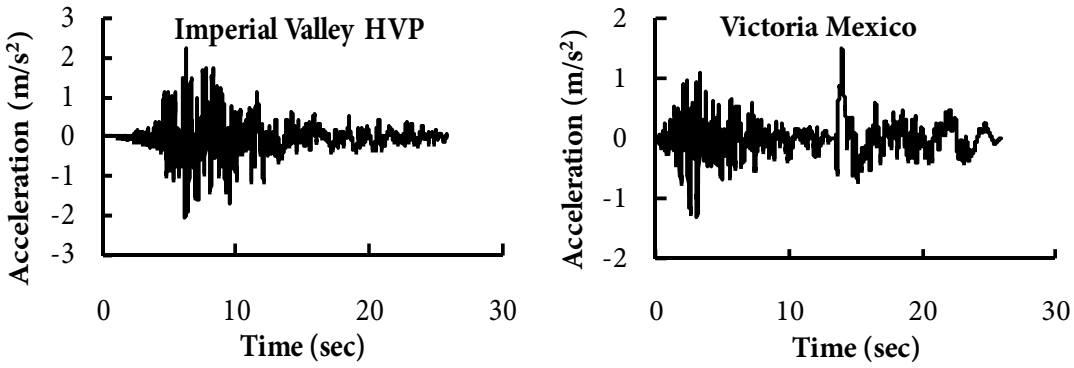

Fig. 7.32 Ground motion records parallel to the fault

Event	Year	Station	Mag	Mechanism
Duzce	1999	Duzce	7.40	Strike-Slip
Imperial Valley	1979	Brawley Airport	6.53	Strike-Slip
Imperial Valley	1979	El Centro Array #4	6.53	Strike-Slip
Imperial Valley	1979	El Centro Array #5	6.53	Strike-Slip
Imperial Valley	1979	El Centro Array #7	6.53	Strike-Slip
Imperial Valley	1979	Holtville Post Office	6.53	Strike-Slip
Victoria Mexico	1980	Chihuahua	6.33	Strike-Slip

Table 7.3 Ground motion records – Seismological Data

All records were retrieved from the PEER Ground Motion Database Center. The scaling of the records was also performed through the Database Center. The scale factors of the individual records are presented in Table 7.4.

Event	Station	Scale Factor
Duzce	Duzce	1.0615
Imperial Valley	Brawley Airport	2.7432
Imperial Valley	El Centro Array #4	1.4607
Imperial Valley	El Centro Array #5	1.1635
Imperial Valley	El Centro Array #7	1.3279
Imperial Valley	Holtville Post Office	1.8931
Victoria Mexico	Chihuahua	3.6495

Table 7.4 Scale factors of ground motion records

In Fig. 7.33, the average spectrum of the scaled records is compared to the ASCE-05 demand spectrum.

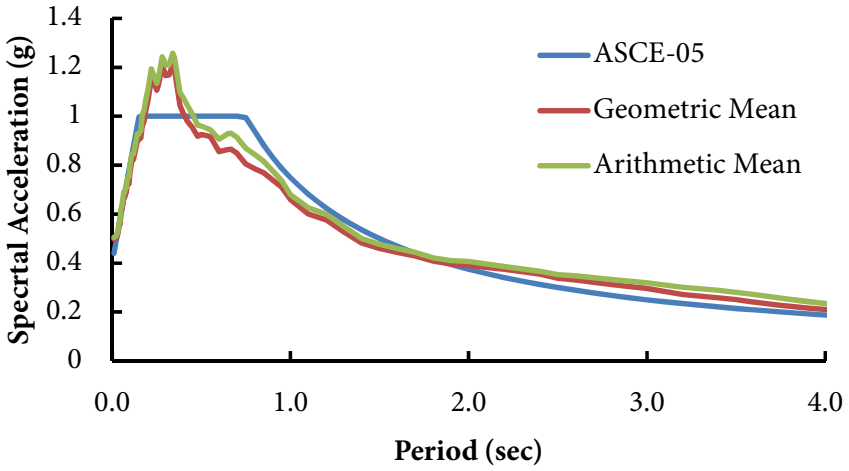

Fig. 7.33 Scaled average spectral acceleration of ground motion records

Both the geometric mean and the arithmetic mean of the scaled spectra converge to the demand, especially in the range of periods from 0.6 sec to 1 sec where the primary eigen-periods of the structure reside. The individual scaled spectra are presented in Fig. 7.34.

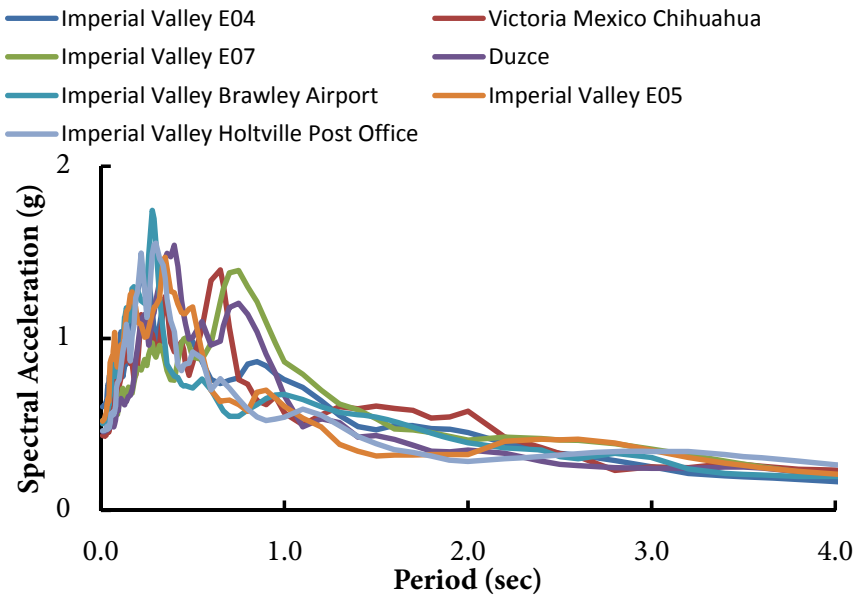

Fig. 7.34 Response spectra of scaled ground motion records

7.5.5 Analysis results

In Fig. 7.35 to Fig. 7.37 the time-histories of the longitudinal displacement of the simple zipper frame are presented for the case of the Duzce motion record. The peak story displacements coincide with the peak accelerations of the record.

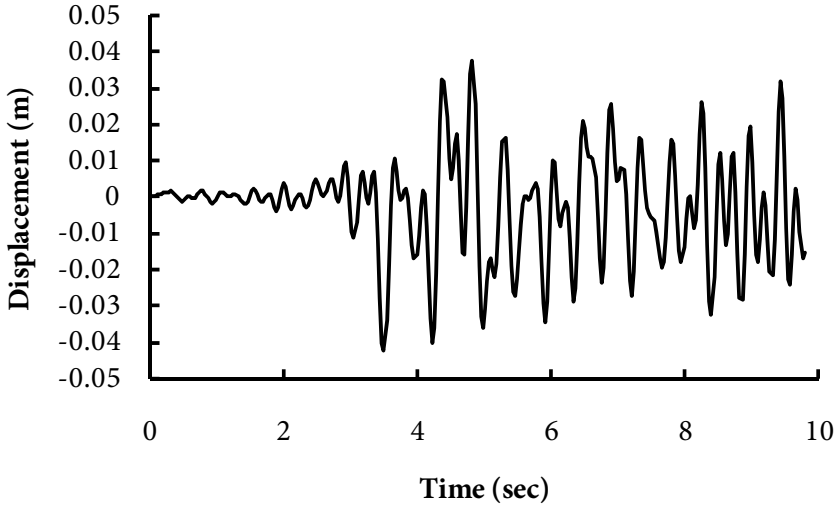

Fig. 7.35 Duzce record - Longitudinal Displacement – 1st floor

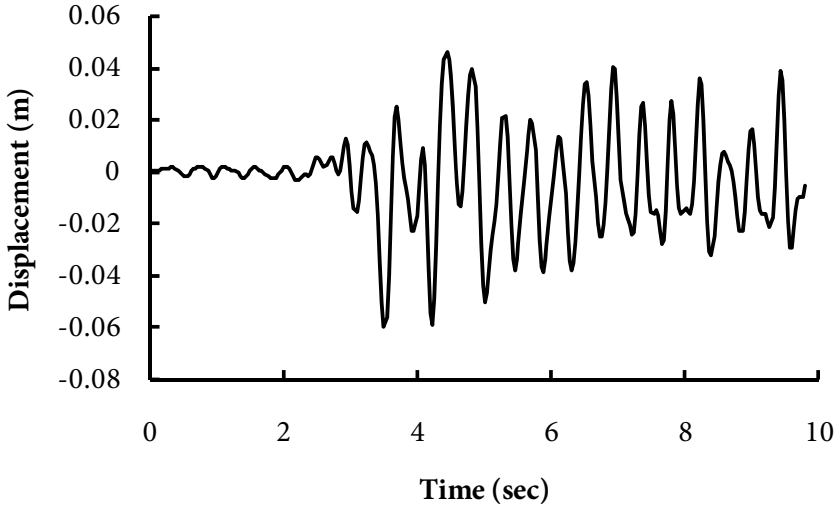

Fig. 7.36 Duzce record - Longitudinal Displacement – 2nd floor

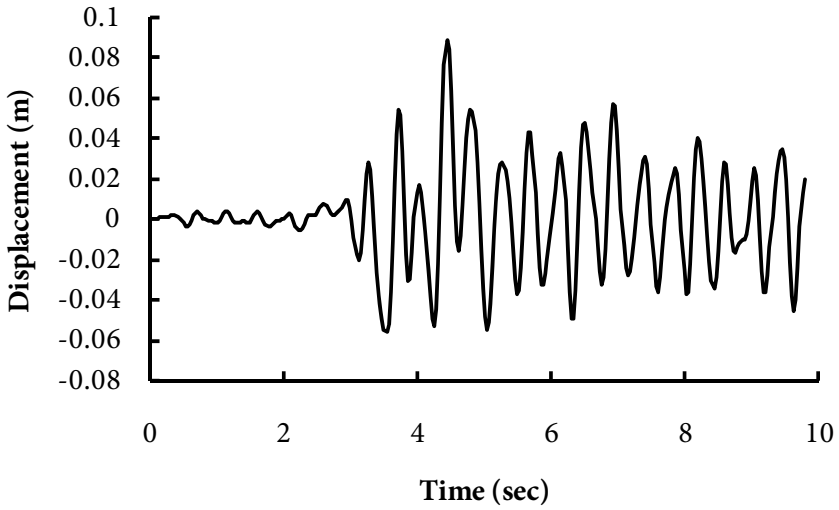

Fig. 7.37 Duzce record - Longitudinal Displacement – 3rd floor

The time histories of the interstorey drift ratios (IDR) are presented in Fig. 7.38. The larger relative displacements are observed in 0-1 and 2-3 storey columns.

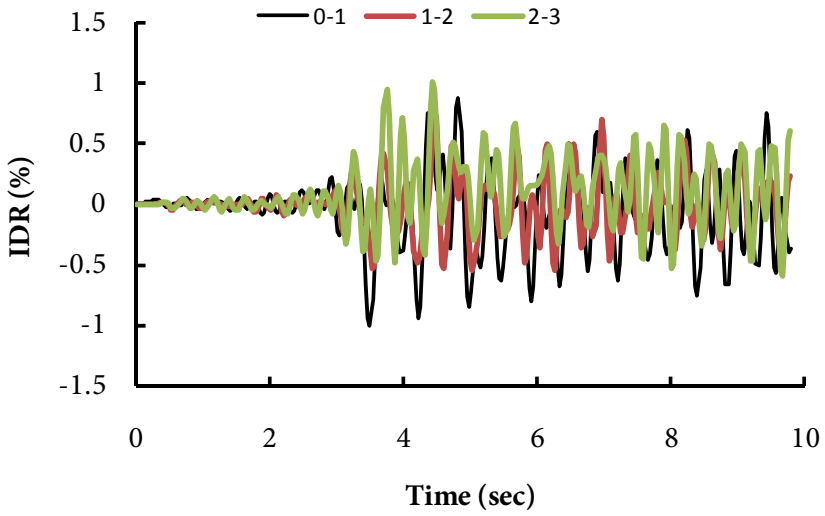

Fig. 7.38 Duzce record - Interstorey drift ratios

In Fig. 7.39 to Fig. 7.42, the results obtained from the Victoria Mexico earthquake excitation for the simple zipper frame are presented. The structure displays the same behavior as in the Duzce record, with the columns between stories 1-2 baring the largest relative displacements.

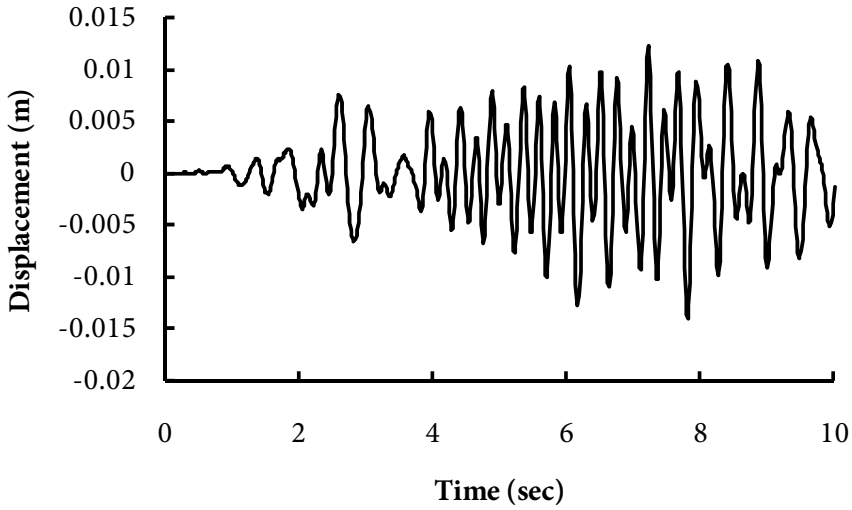

Fig. 7.39 Victoria Mexico record - Longitudinal Displacement – 1st floor

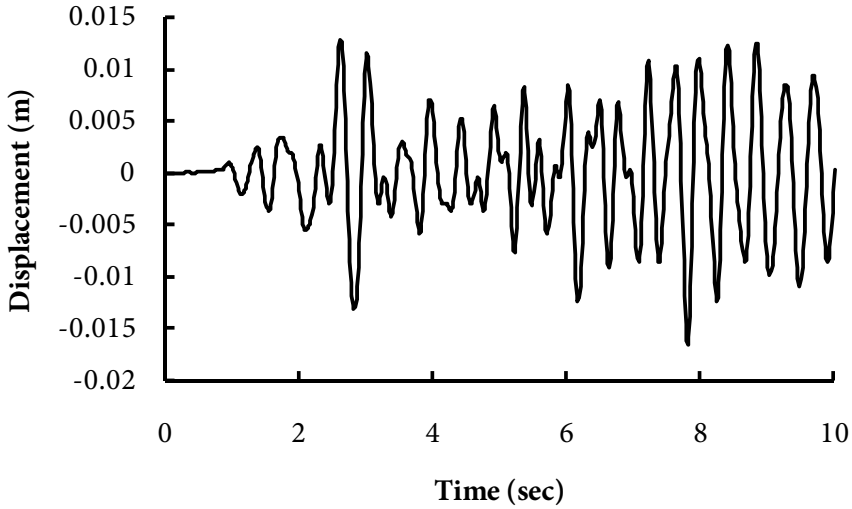

Fig. 7.40 Victoria Mexico record - Longitudinal Displacement – 2nd floor

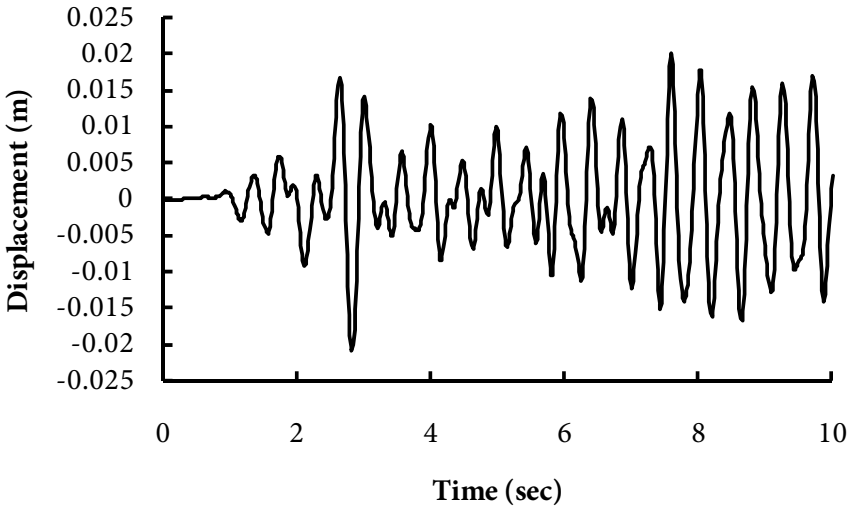

Fig. 7.41 Victoria Mexico record - Longitudinal Displacement – 3rd floor

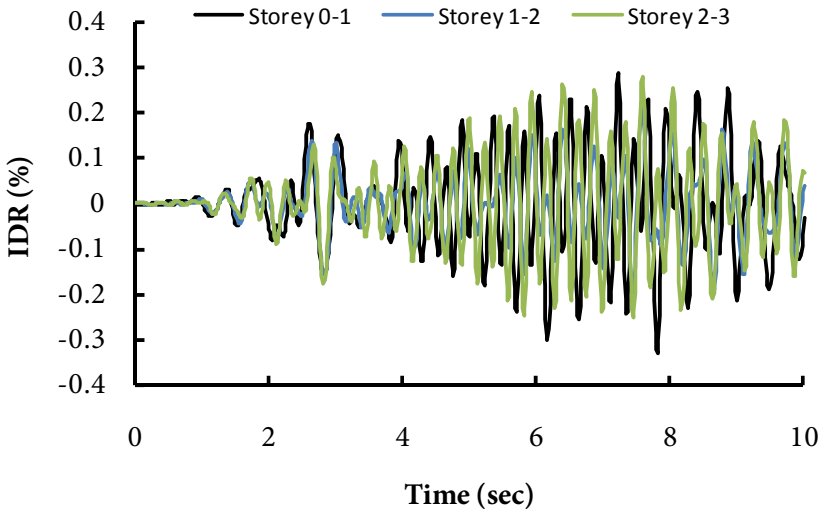

Fig. 7.42 Victoria Mexico record - Interstorey drift ratios

Finally in Fig. 7.43 to Fig. 7.48 the results obtained from the Imperial Valley E05 record are presented.

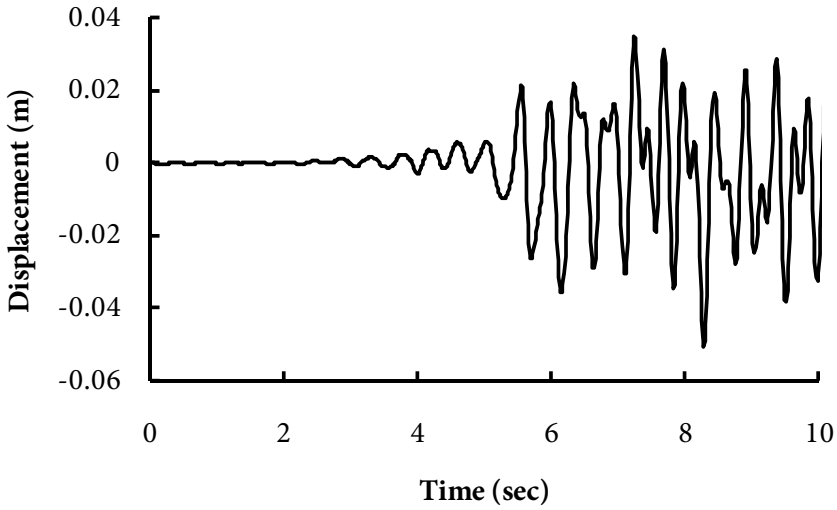

Fig. 7.43 IMPV E05 record - Longitudinal Displacement – 1st floor

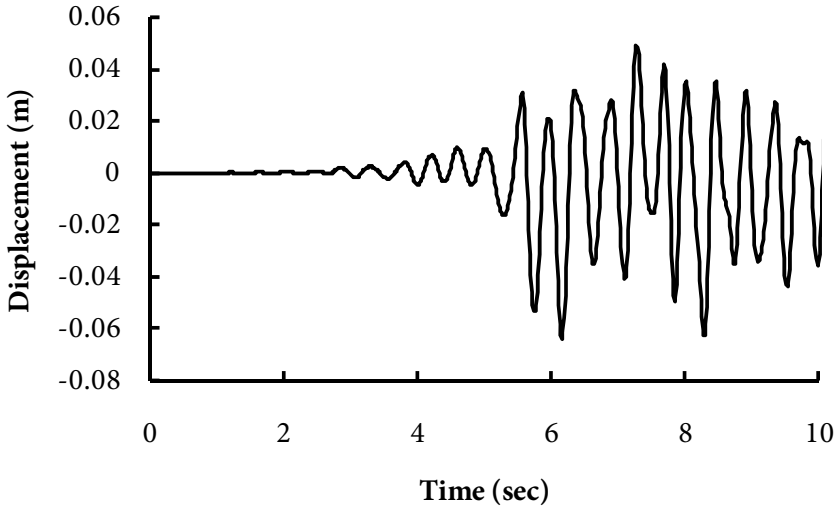

Fig. 7.44 IMPV E05 record - Longitudinal Displacement – 2nd floor

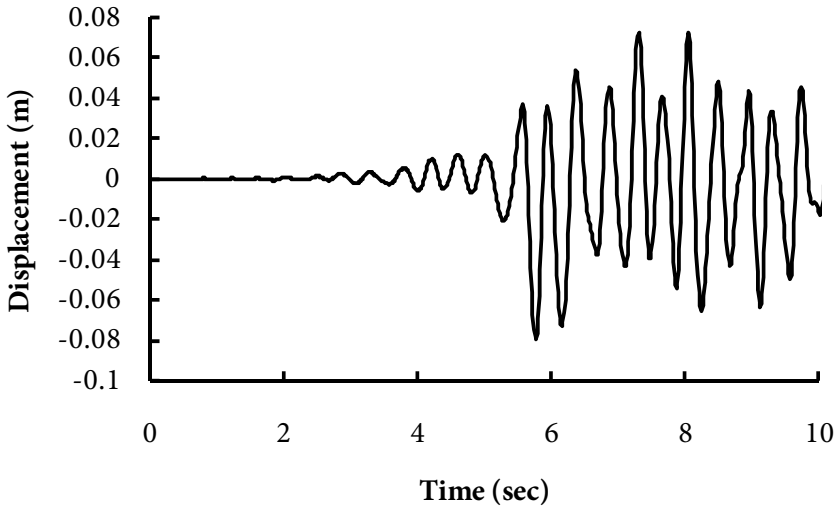

Fig. 7.45 IMPV E05 record - Longitudinal Displacement – 3rd floor

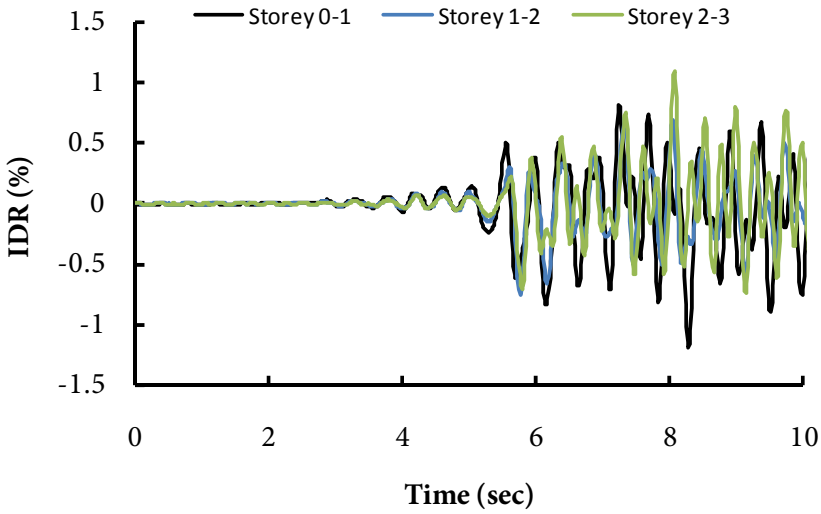

Fig. 7.46 IMPV E05 record - Interstorey drift ratios

The dissipation mechanism predicted by the design is confirmed in both cases. The compression braces successively buckle. Yielding of columns is also observed, in later stages of the loading history. However, the corresponding hysteretic loops are narrow and yielded columns are concentrated on the third floor where the largest values of IDRs are observed. Typical hysteretic loops from a column element at the second and third strorey are presented in Fig. 7.47 and Fig. 7.48 respectively.

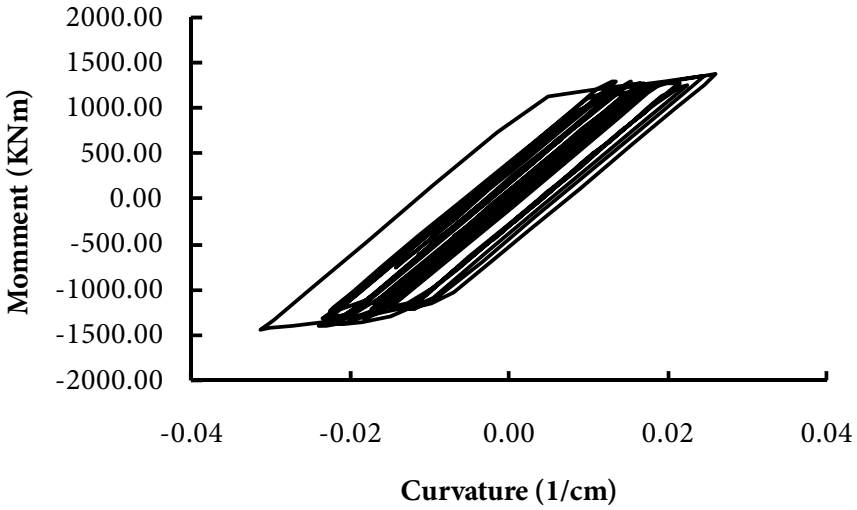

Fig. 7.47 Typical Moment-curvature hysteretic loop 2nd story

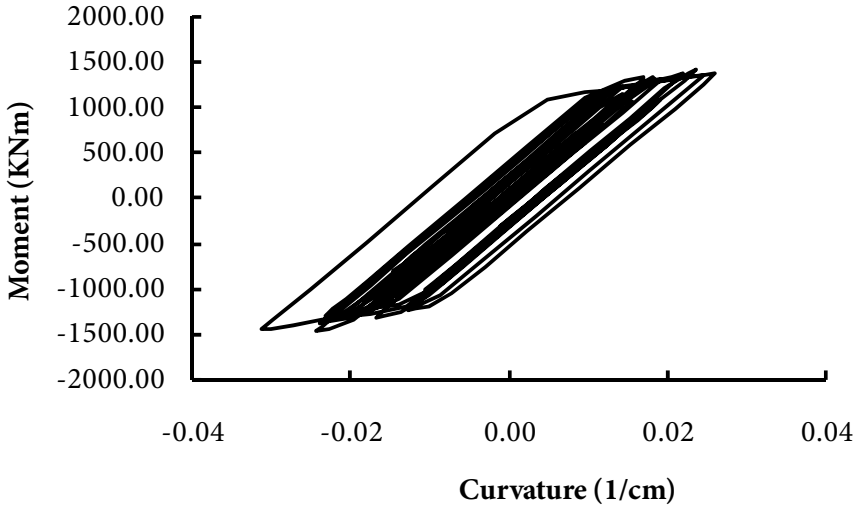

Fig. 7.48 Typical Moment-curvature hysteretic loop 3rd story

A similar behavior is obtained from the analysis of the suspended zipper frame system. Although the displacements are smaller than the simple zipper frame, differences are not significant. In the case of the IMPV E05 record, presented in Fig. 7.49, the differences in the 3rd strory horizontal displacement are less than 1%.

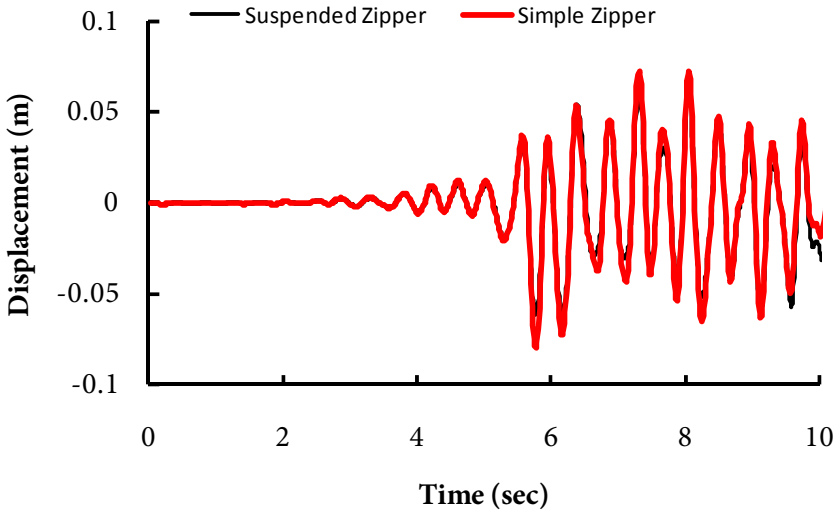

Fig. 7.49 Comparison of third floor horizontal displacements (IMPV E05 record)

The largest deviations were met in the case of the IMPV Brawley motion record. The corresponding time histories are presented in Fig. 7.50.

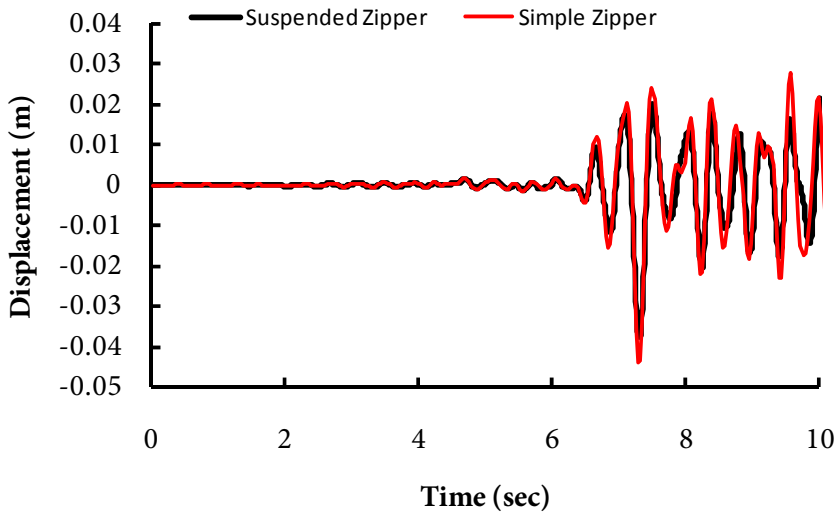

Fig. 7.50 Comparison of third floor horizontal displacements (IMPV Brawley record)

The maximum displacements for the two bracing systems are summarized in Table 7.5. It is evident that the suspended zipper brace system is more efficient since both the absolute values of maximum displacement, as well as the corresponding mean values are smaller compared to the simple zipper brace. However, differences are not striking and further investigation should be made on the applicability of the suspended zipper frame.

Event	Max Floor Displacement (cm)	
[-]	**Zipper Brace**	**Suspended Zipper Brace**
Duzce	8.2	7.8
Brawley Airport	4.7	3.8
El Centro Array #4	7.2	5.7
El Centro Array #5	5.7	6.2
El Centro Array #7	6.2	5.4
Holtville Post Office	7.2	6.3
Chihuahua	2.1	1.8
Mean Values	**5.9**	**5.3**

Table 7.5 Maximum and Mean Floor Displacement Values

Chapter 8

CONCLUSIONS AND FUTURE RESEARCH

8.1 Summary and concluding remarks

In this dissertation, a general form of the Bouc-Wen model is derived in stress-strain form, based on the phenomenological concepts of the classical theory of plasticity. A rate form of the stress tensor is derived that accounts for the full cyclic behavior of the continuum. This rate form is quite general in the sense that it accounts for every combination of yield criteria and hardening laws whereas existing formulations only describe hysteretic behavior with linear kinematic hardening. Based on concepts that stem from the endochronic theory of plasticity, additional smooth operators are derived that account for the cyclic induced stiffness degradation and strength deterioration phenomena observed in materials. The formulation derived depends on total stress components rather than their deviatoric parts, thus yielding a formulation that is easily incorporated in the Finite Element scheme as demonstrated in this work.

The generalized hysteretic stress-strain law developed is implemented on the Finite Element Scheme, yielding a versatile and compact formulation for the nonlinear dynamic analysis of structures. As an example, the triangular plane stress element is reformulated, to incorporate Bouc-Wen hysteretic plasticity. Examples are presented that demonstrate the ability of the proposed formulation to simulate common and complex elastoplastic responses.

Moreover, a family of hysteretic macro-elements is derived for the modeling of skeletal structures under static or dynamic loading. Firstly, a Total Lagrangian three-dimensional hysteretic truss element is presented. Next, a beam element is formulated, starting from a two-dimensional Euler/Bernoulli formulation and concluding to a generalized locking free three-dimensional Timoshenko beam element with torsional warping. The hysteretic law incorporated is based on stress resultant-generalized displacement relations and allows for the simulation of interaction schemes in the stress resultant space.

Finally, a solution approach is proposed for the nonlinear static and dynamic analysis of structures modeled by hysteretic finite elements and macro-elements. The equation of motion for a multi-degree freedom system consisting of both finite elements and macro-elements is defined in terms of total stress components, nodal displacements and element hysteretic deformations. In doing so, all the state matrices, namely the stiffness matrix and the hysteretic matrix of the skeletal substructure and the equilibrium matrix of the finite element substructure remain constant throughout the analysis procedure and need only be evaluated once. Inelasticity is treated at the element level through the incorporation of the evolution equations of the hysteretic parameters.

The formulations presented in this work are verified in terms of computational cost and accuracy through comparison with various commercial and academic FEM codes such as SAP2000, Abaqus, Nastran X, Idarc2D, Hyplas and OpenSees.

8.2 Future research

The following are research directions that further improve the work presented in this dissertation:

1. The hysteretic FEM formulation presented in this work can be extended to shell and three-dimensional finite element formulations, yielding a unified approach in the nonlinear dynamic analysis of structures.
2. Incorporation of numerically derived stress-resultant interaction surfaces in the proposed macro-element formulation.
3. Though cost-ineffective, the fiber based beam element formulation bares advantages in certain cases of combined loading such as bending with torsional and distortional warping in the large displacement regime. The macro-element formulation presented

can be extended to incorporate fiber based beam element schemes by incorporating the stress-strain generalized hysteretic model presented in this work.

4. Further improvement of the generalized stress-strain hysteretic law presented to incorporate damage induced phenomena.

REFERENCES

[1]. Abaqus, Hibbit and Karlson and Sorensen Inc., Theory manual – version 6.5 Edition, 2005.

[2]. Amjad J. A., Zaoyang G. (2001). "Framework for Finite Element Based Large Increment Method for Nonlinear Structural Problems", *Journal of Engineering Mechanics*, Vol. 127, No. 7, pp. 739 – 746.

[3]. Armenakas A. E. (2005). "Advanced Mechanics of Materials and Applied Elasticity", Taylor & Francis, New York.

[4]. Argyris J. H., Boni B., Hindenlang U., Kleiber M. (1982). "Finite element analysis of two- and three-dimensional elasto-plastic frames--the natural approach", *Computer Methods in Applied Mechanics and Engineering*, 35(2), pp. 221-248.

[5]. ASCE. (2007). "Seismic Rehabilitation of Existing Buildings (41-06)".

[6]. Auricchio, F., Fugazza, D., and DesRoches, R. (2008). "Rate-dependent Thermo-mechanical Modelling of Superelastic Shape Memory Alloys for Seismic Applications," *Journal of Intelligent Material Systems and Structures*, Vol 19, No. 1, pp. 47-61.

[7]. Baber, T. T., Yi-Kwei Wen. (1980). "Seismic response of hysteretic degrading structures", *Publ. Turk. Natl. Comm. on Earthquake Eng*., Volume 7, Pages 457-464.

[8]. Baber, T. T., Noori, Mohammad N. (1985). "Random vibration of degrading, pinching systems", *Journal of Engineering Mechanics* 111 (8), pp. 1010-1026.

[9]. Barham, W.S., Aref A.J., Dargush G.F. (2005). "Development of the large increment method for elastic perfectly plastic analysis of plane frame structures under monotonic loading", *International Journal of Solids and Structures*, Vol. 42, pp. 6586 – 6609.

[10]. Barham, W.S., Aref A.J., Dargush G.F. (2008). "On the elastoplastic cyclic analysis of plane beam structures using a flexibility-based finite element approach", *International Journal of Solids and Structures*, Vol. 45, Issues 22-23, pp. 5688-5704.

[11]. Bathe K.J. (2007). Finite Element Procedures, Prentice Hall Engineering, Science, Mathematics, New York.

[12]. Bazant S., Bhat P. (1977). "Prediction of Hysteresis in Reinforced Concrete Members." *ASCE Journal of Structural Engineering*, 103(ST1), pp. 151-167.

[13]. Belytschko T., Liu W. K., Moran B. (2000). "Nonlinear Finite Elements for Continua and Structures", John Wiley & Sons, New York.

[14]. Black, C.J., Makris, N., Aiken, I.D. (2004). "Component testing, seismic evaluation and characterization of buckling-restrained braces," *J. of Struct. Eng.*, ASCE 130(6), pp. 880-894.

[15]. Bitaraf M., Ozbulut O. E., Hurlebaus S., Barroso L. (2010). "Application of semi-active control strategies for seismic protection of buildings with MR dampers", *Engineering Structures*, Volume 32, Issue 10, pp. 3040-3047.

[16]. Bonnet P. A., Williams M. S., Blakeborough A. (2008)**. "**Evaluation of numerical time-integration schemes for real-time hybrid testing**",** Earthquake Engineering & Structural Dynamics, Vol. 37, 13, pp. 1467-1490.

[17]. Bouc, R. (1967). “Forced vibration of mechanical systems with hysteresis”, Proceedings of the Fourth Conference on Non-linear oscillation, Prague, Czechoslovakia.

[18]. Bozorgnia, Y, Bertero, V. (2004). "Earthquake Engineering: From Engineering Seismology to Performance-Based Engineering", CRC Press, New York.

[19]. Brasile S., Casciaro R., Formica G. (2009). “Finite Element Formulation for nonlinear analysis of masonry walls”, Computers & Structures, Vol. 88 , (3-4), pp. 135-143.

[20]. Brokate M., Kenmochi N., Müller I., Rodriguez J. F., Verdi C. (1993). “Phase Transitions and Hysteresis”, Lectures given at the 3rd Session of the Centro Internazionale Matematico Estivo (C.I.M.E) held in Montecatini Terme, Italy, July 13-21, 1993.

[21]. Carpinteri A., Corrado M., Paggi M., Mancini G. (2009). “New Model for the Analysis of Size-Scale Effects on the Ductility of Reinforced Concrete Elements in Bending”, J. Engrg. Mech. 135, pp. 221-229.

[22]. Casciati F. (2006). “Stochastic Dynamics of Hysteretic media”, Probabilistic Methods in Applied Physics, Springer Berlin / Heidelberg, 270-283.

[23]. Chaboche, J.L., (1991). “On some modifications of kinematic hardening to improve the description of ratcheting effects”, Int. J. Plasticity, 7, pp. 661–678.

[24]. Chang Ch. Ch., ShiY. (2010). “Identification of time-varying hysteretic structures using wavelet multi resolution analysis”, International Journal of Non-Linear Mechanics, 45, 21–34.

[25]. Chao S. H. and Loh C. H. (2007). "Inelastic response analysis of reinforced concrete structures using modified force analogy method", Earthquake Engng Struct. Dyn. 2007; 36:1659–1683.

[26]. Charalampakis A.E., Koumousis V.K. (2008a). "Identification of Bouc–Wen hysteretic systems by a hybrid evolutionary algorithm", Journal of Sound and Vibration, Vol. 314, Issues 3-5, pp. 571-585.

[27]. Charalampakis A.E., Koumousis V.K. (2008b). "Ultimate strength analysis of composite sections under biaxial bending and axial load", Advances in Engineering Software 39 (11), pp. 923-936.

[28]. Charalampakis A.E., Koumousis V.K., (2009). "A Bouc Wen Model compatible with plasticity postulates", Journal of Sound and Vibration, Vol. 322, Issues 4-5, pp. 954-968.

[29]. Chatzi E. N., Smyth A. W. (2009). "The unscented Kalman filter and particle filter methods for nonlinear structural system identification with non-collocated heterogeneous sensing", Structural Control and Health Monitoring 16 (1), pp. 99-123.

[30]. Chatzi, E. N., Smyth A. W., Masri S.F. (2010). "Experimental application of on-line parametric identification for nonlinear hysteretic systems with model uncertainty." *Journal of Structural Safety*, Vol. 32, No. 5, pp. 326-337.

[31]. Chen Z., Ge H., and Usami T. (2006). "Hysteretic Model of Stiffened Shear Panel Dampers", *J. Struct. Engrg.*, 132, 478, DOI:10.1061/(ASCE)0733-9445(2006)132:3(478).

[32]. Cherng R. H. and Wen Y. K. (1991). "Stochastic Finite Element Analysis of Non-Linear Plane Trusses", Journal of Non-Linear Mechanics, Vol.26, pp. 835-849.

[33]. Chiang D.-Y. (1999). "The generalized Masing models for deteriorating hysteresis and cyclic plasticity." *Applied Mathematical Modeling*, Volume 23, Issue 11, pp. 847-863.

[34]. Choi S.B., Lee S.K. (2001). "A hysteresis model for the field dependent damping force of a magnetorheological damper", Journal of Sound and Vibration 245(2), 375-383.

[35]. Chopra A. (2006). "Dynamics of Structures." Prentice Hall, New York.

[36]. Cook R. D., Malkus D. S., Plesha M. E., Witt R. J. (2002). "Concepts and applications of finite element analysis", 4ed., John Wiley & Sons, New York.

[37]. Dafalias, Y., Kourousis, K., and Saridis, G. (2008). "Multiplicative AF kinematic hardening in plasticity", International Journal of Solids and Structures, 45(10), pp. 2861-2880.

[38]. Dahl, P. R. (1976). "Solid Friction Damping of Mechanical Vibrations", AIAA Journal, Vol. 14, No. 12, pp. 1675.

[39]. Dede T., Ayvaz Y. (2010). "Plasticity models for concrete material based on different criteria including Bresler-Pister", Materials & Design, 31(1), pp. 278-286.

[40]. Den Hartog J. P. (1999). Strength of Materials, Dover, New York.

[41]. DesRoches R., Leon R., Hess G. (2001). "Seismic design and retrofit using shape-memory alloys", *Earthquake Engineering Frontiers in the New Millenium*, Spencer B. F. and Hu Y. X., eds.

[42]. De Souza RM. (2000). "Force-based finite element for large displacement inelastic analysis of frames." Ph.D. Dissertation, Department of Civil and Environmental Engineering, University of California, Berkeley.

[43]. Der Kiureghian A., Fujimura K. (2009). "Nonlinear stochastic dynamic analysis for performance-based earthquake engineering", *Earthquake Engineering & Structural Dynamics*, Volume 38, Issue 5, Date, pp. 719-738.

[44]. Dobson, S., Noori, M., Hou, Z., Dimentberg, M., Baber, T. (1997). "Modeling and random vibration analysis of SDOF systems with asymmetric hysteresis", International Journal of Non-Linear Mechanics 32 (4), pp. 669-680.

[45]. Dunne F., Petrinic N. (2005). "Introduction to Computational Plasticity", Oxford Press, Oxford.

[46]. EN 1998 Eurocode 8 Earthquake, Part 3: Strengthening and repair of buildings.

[47]. Erlicher S., Point N. (2004). "Thermodynamic admissibility of Bouc Wen type hysterisis models", C. R. Mecanique, Vol. 332, pp. 51-57.

[48]. Erlicher S., Bursi O. S. (2009). "Bouc–Wen-Type Models with Stiffness Degradation: Thermodynamic Analysis and Applications", Journal of Engineering Mechanics, Vol. 134, No. 10, 843 – 855.

[49]. Fardis M. (2010). "Advances in Performance-Based Earthquake Engineering", Springer, Berlin

[50]. Fardis M. N., Filippou F. C., Worner J-D., Bonacci J. F., Pantazopoulou S., Carvalho E. C., Coelho E., Calvi M., Via G., Vintzeleou E. (1996). "RC Frames under Earthquake Loading", Thomas Telford, New York.

[51]. Foliente G. C (1995). Hysteresis modeling of Wood Joints and Structural Systems, Journal of Structural Engineering, 121(6), pp. 1013-1022.

[52]. Formisano A., De Matteis G., Mazzolani F.M. (2010). "Numerical and experimental behaviour of a full-scale RC structure upgraded with steel and aluminium shear panels", *Computers & Structures*, Volume 88, Issues 23-24, Special Issue: Association of Computational Mechanics - United Kingdom, Pages 1348-1360.

[53]. Gerolymos N., Gazetas G. (2005). "Phenomenological model applied to inelastic response of soil-pile interaction systems, *Soils and Foundations*, 45 (4), pp. 119-132.

[54]. Gerolymos N., Gazetas G. (2006). "Development of Winkler model for static and dynamic responseof caisson foundations with soil and interface nonlinearities", Soil Dynamics and Earthquake Engineering, 26, pp. 363 – 376.

[55]. Gerolymos N., Gazetas G. (2007). "A model for grain-crushing-induced landslides—Application to Nikawa, Kobe 1995", Soil Dynamics and Earthquake Engineering, 27(9), pp. 803 – 819.

[56]. Gendy A. S. and Saleeb A. F. (1992). " Generalized Yield Surface Representations in the Elastoplastic three-dimensional analysis of frames", *Computers & Structures*, Vol. 49(2), pp. 351-362.

[57]. Ghobarah, A., and Elfath, H. A. (2001). "Rehabilitation of a reinforced concrete frame using eccentric steel bracing." *Journal of Eng. Struct.*, 23(7), pp. 745–755.

[58]. Grange S., Kotronis P., Mazars J. (2009). "A macro-element to simulate 3D soil–structure interaction considering plasticity and uplift." *International Journal of Solids and Structures*, 46 (2009), pp. 3651–3663.

[59]. Guggenberger J., Grundmann H. (2005). "Stochastic Response of large FEM models with hysteretic behaviour in beam elements", Comp. Methods Appl. Mech. Engrg, Vol, 194, pp. 1739-1756.

[60]. Halmos P. (1974). "Measure Theory in Mathematics", Springer Verlag, Berlin.

[61]. Hashigushi K. (2009). "Elastoplasticity Theory", Springer, Berlin.

[62]. Hassan, T., and Kyriakides, S. (1994). "Ratcheting of cyclically hardening and softening materials I. Uniaxial Behavior", International Journal of Plasticity, 10(2), pp. 149-184.

[63]. Heyman J., Dutton W. E. (1954). "Plastic design of plate girders with unstiffened webs", *Weld. Metal Fabric*, pp. 265–272.

[64]. Hibbitt, Karlsson & Sorensenn, Inc (2000). "Abaqus / Standard User's Manual (Volume I, Version 6.1)." HKS publications, New York.

[65]. Hill R., (1998). "The mathematical theory of plasticity", Clarendon Press, Oxford.

[66]. Hjelle O., Daehlen M. (2006). "Triangulations and Applications", Springer Berlin, 2006.

[67]. Hjelmstad, K. D., and Popov, E. P. (1983). "Cyclic behavior and design of link beams." *J. Struct. Eng*., 109_10_, 2387–2403.

[68]. Hinchberger S.D. (2009). "Simple Single-Surface Failure Criterion for Concrete", *Journal of Engineering Mechanics*, Vol. 135(7), pp. 729-732.

[69]. Huddleston, J. V. (1979). "Nonlinear Analysis of Elastically Constrained Tie-Rods under Transverse Loads. International Journal of Mechanical Sciences 21(10), pp. 623-630.

[70]. Ikhouane F., Rodellar J. (2007). "Systems with hysteresis: Analysis, identification and control using the Bouc-Wen model",John Wiley & Sons, New York.

[71]. Irgens F. (2008). "Continuum Mechanics", Springer-Verlag, Berlin.

[72]. Ismail, M., Rodellar, J., Ikhouane, F. (2010). "An innovative isolation device for aseismic design", *Engineering Structures*, 32 (4), pp. 1168-1183.

[73]. Iu C.K., Bradford M.A., Chen W.F. (2009). "Second-order inelastic analysis of composite framed structures based on the refined plastic hinge method", *Engineering Structures*, 31(3), pp. 799-813.

[74]. Kachanov I.M. (2004). "Fundamentals of the theory of plasticity", Dover Publications, New York.

[75]. Kasai, K., and Popov, E. P. (1986). "General behavior of WF steel shear link beams." *J. Struct. Eng*., 112(2), pp. 362–382.

[76]. Kattan P. I., Voyiadjis G. Z. (2001). "Damage Mechanics with Finite Elements", Spriger, Berlin.

[77]. Khandelwal K., El-Tawil S., Kunnath K. S., and Lew H. S. (2008). "Macromodel-Based Simulation of Progressive Collapse: Steel Frame Structures." *J. Struct. Engrg*., 134(7), pp. 1070-1078.

[78]. Khatib, I., Mahin, S. and Pister, K. (1988). "Seismic Behavior of concentrically braced steel frames." UCB/EERC-88/01, Earthquake Engineering Research Center, University of California, Berkeley, California.

[79]. Kiureghian der A., Fujimura K. (2009). "Nonlinear stochastic dynamic analysis for performance-based earthquake engineering", Earthquake Engineering & Structural Dynamics, Volume 38, Issue 5, pp. 719-738.

[80]. Krajcinovic D. (1996). "Damage Mechanics", North-Holland Series in Applied Mathematics and Mechanics, Elsevier, Amsterdam.

[81]. Kwan A. K. H., He X. G. (2001). "Finite element analysis of effect of concrete confinement on behavior of shear walls", Computers & Structures, 79(19), pp. 1799-1810.

[82]. Lambea J.D. (1973). "Computational Methods in Ordinary Differential Equations" Wiley & Sons, New York.

[83]. Logemann, H., and Mawby, A. (2003). "Extending hysteresis operators to spaces of piecewise continuous functions." Journal of Mathematical Analysis and Applications, 282(1), 107-127.

[84]. Lubliner J. (2008). "Plasticity Theory", Dover, New York.

[85]. Ma F., Zhang H., Bockstedte A., Foliente G.C., Paevere P. (2004). "Parameter analysis of the differential model of hysteresis", Journal of Applied Mechanics ASME, 71,pp. 342–349.

[86]. Macneal R., (1978), "A simple quadrilateral shell element", *Computers & Structures*, *8*(2), 175-183, doi: 10.1016/0045-7949(78)90020-2.

[87]. Mazzolani, F. M. (2008). "Innovative metal systems for seismic upgrading of RC structures." *J. Constr. Steel Res.*, 64(7–8), pp. 882–895.

[88]. Málaga-Chuquitaype C., Elghazouli A. Y., Bento R.**, "**Rigid-plastic models for the seismic design and assessment of steel framed structures**"** Earthquake Engineering &Structural Dynamics, Early View.

[89]. MapleSoft, Maple 13 User Manual. (2007). Maplesoft, New York

[90]. McKenna F, Fenves G. L., Scott MH. (2000). "Open system for earthquake engineering simulation.", Berkeley, CA: University of California, Available from: <http://OpenSees.berkeley.edu>.

[91]. Marsden J. E. and Hughes T. J. R. (1994). "Mathematical Foundations of Elasticity", Dover Publications.

[92]. Mercan O., Ricles J. M. (2007). "Stability and accuracy analysis of outer loop dynamics in real-time pseudodynamic testing of SDOF systems", Earthquake Engineering & Structural Dynamics Volume 36, Issue 11, September 2007, pp. 1523-1543.

[93]. Mazza F., Mazza M. (2010). "Nonlinear analysis of spatial framed structures by a lumped plasticity model based on the Haar–Kàrmàn principle", *Computational Mechanics*, *45*(6), 647-664. doi: 10.1007/s00466-010-0478-0.

[94]. Masing, G. (1926). "Eigenspannungen Und Verfestigung Beim Messing", *Procceedings of the Second International Congress for Applied Mechanics*, Zurich, Switzerland, pp. 332-335 (in German).

[95]. Mohareb, M. (2002). "Plastic interaction relations for pipe sections",*Journal of Engineering Mechanics*, 128 (1), pp. 112-120.

[96]. Mokha A., Constantinou M. C., Reinhorn A. M., Zayas V. A. (1991). Experimental Study of Friction-Pendulum Isolation System, J. Struct. Engrg., 117, pp. 1201-1217.

[97]. Munoz J.J, Bonet J., Huerta A., Peraire J. (2009). "Upper and lower bounds in limit analysis: Adaptive meshing strategies and discontinuous loading", Int. J. *Numer. Meth. Engng*; 77:471–501.

[98]. Naeim F., Skliros K., Reinhorn A. M. (2000). "Influence of hysteretic deteriorations in seismic response of multistory frame buildings",*12th World Congress on Earthquake Engineering (WCEE 2000)*, N. Zealand.

[99]. Nagtegaal J. C., De Jong, J. E. (1981). "Some computational aspects of elastic-plastic large strain analysis", *International Journal for Numerical Methods in Engineering*, vol. 17, pp. 15-41.

[100]. Neto de Souza, EA, Peric D., Owen DRJ., (2008). "Computational Methods for Plasticity Theory and Applications", Willey, West Sussex, UK.

[101]. Neuenhofer A., Filippou F. C. (1998). "Geometrically nonlinear flexibility-based frame finite element." *Journal of Structural Engineering (ASCE)*, 124(6), pp. 704 -711.

[102]. Newman J., Choo B., S. (2003) "Advanced Concrete Technology 2 - Concrete Properties", Butterworth-Heinemann, Oxford.

[103]. Nigam, N. C. (1970). "Yielding in framed structures under dynamic loads." *Journal of the Engineering Mechanics Division, ASCE*, 96(EM5), pp. 687-709.

[104]. Noran – NeiNastran, Noran Engineering (2007). "NEi Nastran Reference Manual Version 9.1", Demand Manuals a division of Trafford Holdings Ltd, New York.

[105]. Orbison J, McGuire W, Abel J. (1982). "Yield surface applications in nonlinear steel frame analysis", Comput. Methods Appl. Mech. Eng.,33, pp. 557–73.

[106]. Mercan O., Ricles J. M. (2007). "Stability and accuracy analysis of outer loop dynamics in real-time pseudo dynamic testing of SDOF systems", Earthquake Engineering & Structural Dynamics Volume 36, Issue 11, September 2007, pp. 1523-1543.

[107]. Ozdemir, H. (1976). "Nonlinear Transient Dynamic Analysis of Yielding Structures", Ph.D. Dissertation, University of California, Berkeley.

[108]. Panoskaltsis, V. P., Polymenakos, L. C., Soldatos, D. (2008). "On large deformation generalized plasticity", *Materials and Structures*, 3(3), 441-457.

[109]. Panoskaltsis, V.P., Bahuguna, S., Soldatos, D. (2004). "On the thermomechanical modeling of shape memory alloys", *International Journal of Non-Linear Mechanics*, 39 (5), pp. 709-722.

[110]. Papachristidis, A., Fragiadakis, M., Papadrakakis, M. (2010). "A 3D fibre beam-column element with shear modelling for the inelastic analysis of steel structures*", Computational Mechanics*, 45 (6), pp. 553-572.

[111]. Papakonstantinou, K. G., Dimizas, P. C., Koumousis, V. K. (2007). "An Inelastic Beam Element with Hysteretic Damping", Shock and Vibration Journal, Special Issue ICED, Vol. 15, nos. 3-4, June 2008, pp. 273-290.

[112]. Papoulia, K.D., Panoskaltsis, V.P., Bahuguna, S., Korovajchuk, I. (2007). "The generalized Kuhn model of linear viscoelasticity", *Mechanics of Time-Dependent Materials*, 11 (3-4), pp. 217-230.

[113]. Park, N.-H., Choi, S., and Kang, Y.-jong. (2005). "Exact distortional behavior and practical distortional analysis of multicell box girders using an expanded method." *Computers & Structures*, 83, 1607-1626.

[114]. Patnaik, S.N., Coroneos, R.M., Hopkins, D.A. (1998). "Recent advances in the method of forces: Integrated force method of structural analysis.", *Advances in Engineering Software*, 29 (3-6), pp. 463-474.

[115]. Pires J. A. (1993). "Stochastic Seismic Response Analysis of Soft Soil Sites", Nuclear Engineering and Design, 160(3), 363-377.

[116]. Piyawat K., Pei J. S. (2009). "Linking Nonlinear System Identification with Nonlinear Dynamic Simulation under Opensees: Some Justifications and Implementations.", *Journal of Engineering Mechanics*, 135, pp. 1214-1226.

[117]. Popov E.P. and Stephen R.M. (1970). "Cyclic Loading of Full-Size Steel Connections", UCB/EERC-70/03.

[118]. Preisach F. (1935). "Über die magnetische Nachwirkung. Zeitschrift für Physik", 94:277-302.

[119]. Priestley M. J. N., Calvi G. M., Kowalsky M. J. (2007). "Displacement Based Seismic Design of Structures", IUSS, Pavia, Italy.

[120]. Radhakrishnan K., Hindmarsh A. C., (1993). "Description and Use of LSODE, the Livermore Solver for Ordinary Differential Equations," LLNL report UCRL-ID-113855.

[121]. Rakowski J. (1990). "The interpretation of the shear locking in beam elements", Computers & Structures, Vol. 37, 5, 1990, pp. 769-776.

[122]. Reddy J.N. (2008). "An introduction to continuum mechanics", Cambridge University Press, Cambridge.

[123]. Ramberg, W., Osgood, W. R. (1943). "Description of stress-strain curves by three parameters", *Technical Note No. 902*, National Advisory Committee For Aeronautics, Washington DC.

[124]. Roeder, C. W., and Popov, E. P. (1977). "Inelastic behavior of eccentric braced frames." Rep. No. UCB/EERC-77/18, Earthquake Engineering Research Center, Univ. of California, Berkeley, Mich.

[125]. Roh H. and Reinhorn A. M. (2010). "Nonlinear Static Analysis of Structures with Rocking Columns." *J. Struct. Engrg*. 136(5), pp. 532-542.

[126]. Roufaiel M. S. L. and Meyer C. (1987). "Analytical Modeling of Hysteretic behavior of R/C frames", ASCE Journal of the Structural Division, 113, pp. 429-444.

[127]. Saiidi M., Sozen M.A. (1981). "Simple Nonlinear Seismic Analysis of Reinforced Concrete Structures", ASCE Journal of the Structural Division, 107, ST5, pp. 937-952.

[128]. Sapountzakis, E. J., and Mokos, V. G. (2003). "Warping shear stresses in nonuniform torsion by BEM." *Computational Mechanics*, 30, pp. 131-142.

[129]. SapountzakisE.J. and MokosV.G. (2004)."Nonuniform torsion of bars of variable cross section", *Computers & Structures*, 82, (9-10), pp 703-715.

[130]. Saritas A., Filippou F. C. (2009). "Inelastic axial-flexure–shear coupling in a mixed formulation beam finite element", *International Journal of Non-Linear Mechanics*, *44*(8), 913-922, doi: 10.1016/j.ijnonlinmec.2009.06.007.

[131]. Shampine, L.F and Gordon, M.K. (1975). "Computer Solution of Ordinary Differential Equations: The Initial Value Problem". W.H. Freeman and Co., San Francisco, CA.

[132]. Initial Value Problem (1975). W.H. Freeman and Co., San Francisco, CA.

[133]. Skordeli M., Bisbos C. (2010). "Limit and shakedown analysis of 3D steel frames via approximate ellipsoidal yield surfaces", *Engineering Structures*, *32*(6), 1556-1567, doi: 10.1016/j.engstruct.2010.02.004.

[134]. Schulz M. and Filippou F.C. (1998). "Generalized Warping Torsion Formulation", *J. Engrg. Mech.* 124, 339.

[135]. Simo J. C., Hjelmstad K. D., Taylor R. L., (1983), "Numerical formulations of elasto-viscoplastic response of beams accounting for the effect of shear", Computer Methods in Applied Mechanics and Engineering, 42, pp. 301-330.

[136]. Simo J. C., Taylor R. L. (1985). "A return mapping algorithm for plane stress elastoplasticity", International Journal for Numerical Methods in Engineering, 22(3), pp. 649-670.

[137]. Simo, J. C., Taylor R. L. (1985). "Consistent tangent operators for rate-independent elastoplasticity", *Computer Methods in Applied Mechanics and Engineering*, 48, pp. 101-118.

[138]. Simo J. C., Hughes T. J. R. (1998). "Computational Inelasticity", Springer, Berlin.

[139]. Sivaselvan M. V., Reinhorn A. M. (2000). Hysteretic Models for deteriorating inelastic structures, Journal of Engineering Mechanics 126 (6), pp. 633-640.

[140]. Sivaselvan M. V., Reinhorn A. M..(2003). "Nonlinear Analysis Towards Collapse Simulation – A dynamic Systems Approach", MCEER Technical Report.

[141]. Skelton R. P. , Maier H. J. , Christ H. -J. (1997). "The Bauschinger effect, Masing model and the Ramberg-Osgood relation for cyclic deformation in metals." *Materials Science and Engineering A*, Volume 238, Issue 2, 15, pp 377-390.

[142]. Song P. F., and Powell, G. H. (1982). "Generalized Plastic Hinge Concepts for 3D Beam-Column Elements" UCB/EERC Rep. No. 82-20, Earthquake Engrg. Res. Center. University of California at Berkeley, California.

[143]. Spacone E., Ciampi V. and Filippou F.C. (1992) "A Beam Element for Seismic Damage Analysis." UCB/EERC 92/07, Earthquake Engineering Research Center, University of California, Berkeley.

[144]. SpaconeE., CiampiV. and FilippouF.C. (1996). "Mixed formulation of nonlinear beam finite element, Computers and Structures"58 (1), pp. 71–83.

[145]. Spillers W. R. (1962). Automated Structural Analysis: An introduction, Pergamon Press Inc., New York.

[146]. Stolarski, H., Belytschko, T. (1983). "Shear and membrane locking in curved C_0 elements", *Computer Methods in Applied Mechanics and Engineering*, 41(3), pp. 279 – 296.

[147]. Symeonov V. K., Sivaselvan M. V., Reinhorn A. M. (2000). "Nonlinear Analysis of Structural Frame Systems by the State Space Approach", *Computer Aided Civil and Infrastructure Engineering*, Vol. 15, pp. 76-89.

[148]. Takeda T. et al. (1970). “R/C response to simulated earthquakes”, *ASCE Journal of the Structural Division*, 96, ST12, pp. 2557-2573.

[149]. Takizawa, H. and Aoyama, H. (1976). "Biaxial effects in modeling earthquake response of RC structures." *Earthquake Engrg. and Struct. Dyn.*,Vol. 4, pp. 523-552.

[150]. Taherizadeh A., Green D.E.,Ghaei A, Yoon J.W. (2010). “A non-associated constitutive model with mixed iso-kinematic hardening for finite element simulation of sheet metal forming”, International Journal of Plasticity, 26, pp. 288-309.

[151]. Thyagarajan, R. S. (1989). “Modeling and analysis of hysteretic structural behavior.” Technical Report: CaltechEERL:1989.EERL-89-03.

[152]. Thyagarajan RS, Iwan WD (1990). "Performance characteristics of a widely used hysteretic model in structural dynamics", *Proceedings of the 4th US National Conference on Earthquake Engineering*, EERI, Palm Springs.

[153]. Triantafyllou S., Koumousis V. (2008). “A beam element formulation for the nonlinear dynamic analysis of structures using the Bouc-Wen hysteretic rule”, 6th GRACM International Congress on Computational Mechanics, Thessaloniki, Greece, 19-21 June.

[154]. Tsopelas, P.C., Roussis, P.C., Constantinou, M.C. (2009). "Nonlinear dynamic analysis of multi-base seismically isolated structures with uplift potential I: Formulation, Earthquake Engineering and Engineering Vibration", 8(3), pp. 421-431.

[155]. Valanis, K.C. (1971). ”A theory of viscoplasticity without a yield surface.” Arch. Mech. Stossowanej, 23(4), 517-551.

[156]. Valanis, K.C., Lee, C.F. (1984). "Endochronic theory of cyclic plasticity with applications." *J. Appl. Mech*., Vol. 51 pp.367–74.

[157]. VallesR. E., Reinhorn A. M., Kunnath S. K., Li C., Madan A. (1996). "IDARC2D Version 4.0: A Computer Program for the Inelastic Damage Analysis of Buildings", Technical Report NCEER – 96 – 0010.

[158]. Valoroso N., Rosati L. (2009). "Consistent derivation of the constitutive algorithm for plane stress isotropic plasticity, Part I: Theorical Formulation", 46(1), pp. 74-91.

[159]. Vamvatsikos D. and Cornell C.A. (2004). "Applied Incremental Dynamic Analysis",*Earthquake Spectra*, 20(2): 523-553

[160]. Visintin A. (2003). "Differential Models of Hysterisis", Springer, New York.

[161]. Volterra, V. (1928). "Sur la Théorie Mathématique des Phénomènes Héréditaires", Journal de Mathématiques Pures et Appliquées, 7(3), 249-298 (in French).

[162]. Voyiadjis G. Z., Kattan P. I. (2005). "Damage Mechanics", Taylor and Francis, New York

[163]. Wen, Y., K. (1976). "Method of random vibration of hysteretic systems", *Journal of Engineering Mechanics Division*, 102, pp. 249-263.

[164]. Wen, Y., K. (1980). "Equivalent linearization for hysteretic systems under random excitation",Journal of Applied Mechanics, Transactions ASME, 47(1), 150-154.

[165]. Wolfram Mathematica, Core Language Manual, Wolfram Documentation Center, http://reference.wolfram.com/mathematica/guide/Mathematica.html.

[166]. Wong, C.W., Ni, Y.Q., Ko, J.M. (1994). "Steady-state oscillations of hysteretic differential model. II: performance analysis."*ASCE J. Eng. Mech.*, 120(11), pp. 2299-2325.

[167]. Wong K., Yang R. (1999). "Inelastic Dynamic Response of Structures Using Force Analogy Method", Journal of Engineering Mechanics, Vol. 125, No. 10.

[168]. Wriggers P. (2008). "Nonlinear Finite Element Methods", Springer-Verlag, Berlin.

[169]. Xu, J., and Dolan, J. D. (2009). "Development of a nailed wood joint element in ABAQUS." *J. Struct. Eng.*, 135, 8, pp. 968–976.

[170]. Yang T.Y., Moehle J. P. and Stojadinovic B. (2009). "Performance Evaluation of Innovative Steel Braced Frames", PEER 2009/113.

[171]. Yunhua L. (1998). "Explanation and elimination of shear locking and membrane locking with field consistence approach", Comput. Methods Appl. Mech. Engrg., 162, pp. 249-269.

[172]. Zhao. Y. (1993). "Modeling of inelastic cyclic behavior of members, connections and joint panels of steel frames." PhD thesis. School of Civ. and Envir. Engrg., Cornell University. Ithaca, N.Y.

[173]. Zhang C., Liu X. (1997). "A large increment method for material nonlinearity problems", Advances in Structural Engineering, 1(2), pp. 99–109.

[174]. Zhang H., Kuang, J. S. (2008). "Eight-node membrane element with drilling degrees of freedom for analysis of in-plane stiffness of thick floor plates", Int. J. Numer. Meth. Engng.; 76:2117–2136.

[175]. Zhang Y. (1993). "Finite Element Modeling of Tornado Missile on Reinforced Concrete Wall Panels", Phd dissertation submitted to the graduate faculty of Texas Tech University.

[176]. Zienkiewicz O. C., Taylor R. L. (2005). "The Finite Element Method", Elsevier Butterworth-Heinemann, Oxford.

[177]. ΟΑΣΠ. (2010)., «Κανονισμός Επεμβάσεων (ΚΑΝ.ΕΠΕ.)», ΟΑΣΠ, Αθήνα. (in greek).